Development of Catalytic Reactor Designs for Enhanced CO Oxidation

A Thesis submitted for the degree of Doctor of Philosophy
in the University of London

by

Layla Kim Doory
B.Sc. (Chemical Engineering)

Ramsay Memorial Laboratory
of Chemical Engineering,
University College London,
Torrington Place,
London, WC1 7JE.

ABSTRACT

The catalytic removal of pollutants including nitrogen oxides (NOx), hydrocarbons (HC's) and carbon monoxide (CO) in the exhaust of automobiles is generally performed by using monolithic supports coated with noble metal catalysts, notably platinum and rhodium (Pt/Rh) adsorbed onto a washcoat.

This is typically achieved to within 90-98% conversion efficiency for average entry conditions ($50<Re<400$ at actual conditions), with pressure drops not exceeding 1.25-2 kN/m^2.

The monolith is a honeycomb structure, essentially composed of many parallel channels of square cross section. This therefore acts as a high surface area reactor. One of its drawbacks lies in the amount of precious metal requirements. With the increasing demand and price of these it is likely that in the future they may contribute to the cost of manufacture even more significantly.

Detailed analysis shows that the overall rate of reaction of the monolith reactor is usually mass transfer rather than kinetically limited. Thus any boost in the mass transfer rate should increase conversion. Conversely for there to be any reduction in overall surface area or precious metal content there would have to be an increase in mass transfer rate.

The effect of increasing mass transfer was studied by two methods namely by axially segmenting the ceramic monolith core sample (consisting of 62 $cells/cm^2$ of 1.04 mm channels) and secondly by inserting static mixers into a catalyst coated pipe (ie."Active Transport Catalytic Reactor" (ATCR)).

This was carried out for carbon monoxide oxidation over a commercially prepared catalyst supplied by Johnson Matthey. The intrinsic kinetics of this reaction were determined experimentally in a differential reactor.

Conversions and pressure drops were measured for each system for varying Reynolds numbers from 73-440 (S.T.P.) in the channel and 160-2140 (S.T.P.) in the pipe, under stoichiometric reactant concentrations, and for steady state fully warmed up reactor conditions ranging from 250°C to 400°C.

A one dimensional model is presented and its predictions compared to the experimental data for conversion and outlet gas temperature.

Good agreement between experimental and theoretical data for the ATCR was found using the one-dimensional model for the conditions investigated. Also the model was found to be sufficiently accurate in predicting

monolith conversions (ie. less than 10% difference between experiment and theory) and exit gas temperatures (ie. average of 4% difference) for high temperatures of 371°C and above.

Pressure drops were also successfully predicted for both segmented monoliths as well as ATCR systems.

Monolith segmentation was found to be successful in both enhancing CO oxidation as well as reducing the total catalyst requirements with the result that up to 30% saving of catalyst was possible.

A simple optimization process using the theoretical data for the ATCR showed that up to 65% saving in reactor surface area (and hence catalyst requirements) is possible. Thus the novel idea of carrying out heterogeneous reactions within an ATCR shows promising results and indeed there is much scope for future research and possible applications.

ACKNOWLEDGEMENTS

I would like to extend my thanks to the following:

Dr. S. P. Waldram for his supervision throughout this project and for his help in reading my thesis.

Dr. U. Ullah for his kind help and for the use of the research facilities.

Johnson Matthey for their help in supplying both the monolith cores as well as the catalyst coated tubes.

SERC for the grant awarded to Dr. S. P. Waldram to support this reseach project.

All the technicians for their assistance and help in building of the equipment, in particular, Mr D. F. Montgomory, Mr K. W. Wheatley, Mr M.A Town, Mr J. S. Graham, Mr. M. Vale and Mr P. I. Punyer.

Special thanks go to all my friends and colleagues within and out of the department who gave me constant support and encouragement. In particular I would like to thank Dr. L. Al-Dhahir for his kind and informative help in reading my thesis as well as the long and fruitful discussions throughout this project.

Last but by no means least I would like to thank my parents for financing my education and for their continual love and support which they have provided throughout my period of study.

To my loving father

CONTENTS

Nomenclature

A	Pre-exponential factor (kmol/m^2.s)
a	order of reaction wrt CO eqn. 5.7
A'	constant defined in eqn. 2.27
A_{Obs}	observed pre-exponential factor (kmol/m^2.s)
B	pre-adsorption factor
B'	constant defined in eqn. 2.27
C	concentration (kmol/m^3)
c_p	specific heat capacity (kJ/kmol K) or (J/kg K)
C_T	total inlet concentration (kmol/m^3)
[CO]	concentration of CO (mol. fract.)
d	hydraulic diameter of pipe or channel (m)
d_h	hydraulic diameter of pipe with mixer inserts (m)
D	constant depending on channel surface roughness , in eqn. 2.8
d_E	diameter of the element
D_i	binary diffusivity of component i in nitrogen (m^2/s)
E_a	energy of adsorption (kJ/kmol)
E_d	energy of diffusion (kJ/kmol)
E_{Obs}	observed activation energy (kJ/kmol)
E_r	activation energy (kJ/kmol)
f	Moody friction factor eqn. 2.17
F	flowrate (m^3/s)
F_t	total flowrate (L/min)
h	heat transfer coefficient (W/m^2 K)
ΔH_r	heat of reaction (kJ/kmol)
K	ratio of pressure drops with and without mixer eqn. 2.28
k_g	thermal conductivity of gas (W/m K)

k_m	mass transfer coefficient (m/s)
k_a	adsorption constant
k_r	rate constant (kmol/m^2.s)
k_s	thermal conductivity of the solid (W/mK)
L	length of reactor (m)
L_D	re-development length (m)
Le	entry length (m)
L_E	length of an element (m)
L_s	length of each monolith segment (m)
L_T	overall length of catalyst (m)
m_{CO}	CO molar flowrate (kmol/s)
m_T	total molar flowrate (kmol/s)
N	total number of segments
n	total number of data points eqn. 5.9
N_E	total number of elements
Nu	Nusselt number [h d / k_g]
$[O_2]$	concentration of O_2 (mol. fract.)
P	pressure (N/m^2)
ΔP	pressure drop (N/m^2)
Pe	solid phase Peclet number for heat transfer ($L \rho u c_p / k_s)(\phi /(1-\phi)$)
Pr	Prandtl number [$c_p \mu / k_g$]
Q_{exp},Q_{ad}	heat release, experimental, adiabatic (Watts)
Q_{loss}	heat loss (Watts)
r	radial position (m)
$-r_{CO}$	reaction rate (kmol/m^{2}s)
r_i	experimentally measured ith data point (refer to eqn.5.9)
r_i^*	theoretically predicted ith data point (refer to eqn.5.9)
R	universal gas constant (= 8.3143 kJ/ kmol.K)
R*	residual (refer to eqn.5.9)
R_h	hydraulic radius of tube (m)
Re	Reynolds number [ρ u d/ μ]

S	surface to volume ratio (m^{-1})
S_A	catalyst external surface area (m^2)
Sc	Schmidt Number [$\mu/\rho D_i$]
Sh	Sherwood number [$k_m d/ D_i$]
Sh_i	Sherwood number due to reaction (refer to eqn.2.13)
Sh_m	mass transfer limited Sherwood number (refer to eqn. 2.13)
Sh_T	overall Sherwood number (refer to eqn. 2.13)
Sh^{∞}_m	Sherwood number when the reaction is infinitely fast (refer to eqn. 2.13)
T	temperature in the gas phase (°C or K)
ΔT	temperature rise in the gas phase (°C or K)
$\bar{T}$	mixing cup temperature (°C or K)
T_S	temperature on the surface (°C or K)
u	velocity (m/s)
X	conversion (%)
$X_{N\,E}$	conversion for the ATCR with N_E elements (%) (refer to eqn. 7.7)
$X_{N=N}$	conversion for the monolith with N segments (%) (refer to eqn. 6.4)
z	axial distance (m)

Greek Symbols

α	shape factor defined by eqn. 2.8
β	limiting friction factor defined by eqn. 2.18
η	effectiveness factor (refer to eqn. 5.3)
θ	corrective factor in eqn. 2.13
λ_{ATCR}	enhancement factor for the ATCR (refer to eqn. 7.7)
λ_{Mon}	enhancement factor for the monolith (refer to eqn. 6.4)
μ	viscosity (kg/m s)
ρ	density (kg/m^3)
ϕ	void fraction
ψ	constant in equation 8.12
ω	constant in equation 8.12

Subscipts

c	entrance contraction
CO	carbon monoxide
e	exit expansion
exp	experimental
ET	empty tube
f	frictional
G	gas phase
in	entering the reactor
out	exiting the reactor
KM	Kenics mixer
MIX	mixer
obs	observed
S	surface
Slz	Sulzer mixer
SM	static mixer
STP	standard temperature and pressure
T	total
w	wall

CHAPTER 1

INTRODUCTION

1.1 Introduction

Sir Humphrey Davy's (Davy, 1840) discovery that platinum wires could induce combustion of fuel-air mixtures "without flames", was the beginning of a wealth of research on catalysis. There has been widespread use of this process in such industries as catalytic fume abatement reactors, acid tail gas reactors and in automobile catalytic converters where the ability to burn combustibles at low temperatures and concentrations in the presence of comparably low concentrations of oxygen is the order of the day. Interest has also grown in high temperature operations such as gas turbines where temperatures of 900-1700°C are common (Ahn, 1983; Pfefferle et al., 1987).

Mounting concern over environmental pollution levels has led to stringent control limits, particularly in the field of auto exhaust emissions. The three major pollutants of the auto emission exhaust are hydrocarbons (HC), nitrogen oxides (NO_x) and carbon monoxide (CO). These are produced in the engine of the car as waste products or from unburnt fuel. Traces of water, hydrogen and sulphur compounds are also present.

Due to the toxicity of the main pollutants, efforts were first made in California in the early 50's to reduce these down to acceptable levels. Initially it was possible to cut down on these by engine redesign and modification of the carburation and ignition of the automobile, in order to reduce the amount of pollutants entering the exhaust. However as governmental emission standards were tightened (refer to Appendix A) an alternative approach was required.

The exhaust gas may be treated thermally (ie. homogeneous oxidation in the gas phase) or catalytically. Carbon monoxide and hydrocarbons need to be oxidized to carbon dioxide and water. This can be achieved by either process, however in the case of nitrogen oxides (NO_x) catalytic processes (ie. reduction by CO or HC's and hydrogen) are required in order to reduce them to nitrogen.

Recent developments led to all three components being treated on the same catalyst, this is termed "Three Way Catalysis". The most effective catalysts are the noble metals, in particular platinum and rhodium on γ-Al_2O_3.

The main concern for auto exhaust treatment is effective reaction with the least pressure drop, since this directly effects engine performance. Much research was undertaken to develop and test various catalytic surfaces as well as support systems. In an effort to reduce pressure drop the industry moved towards a honeycomb design. This provides a large catalyst surface area at low pressure drops. The catalyst is supported on a ceramic honeycomb, called a monolith. This consists of a number of parallel channels coated with a washcoat impregnated with the noble metal catalyst. As with any industry a major concern is total cost. Indeed the major part of the total cost is determined by the precious metal costs.

With the increasing demand for precious metals it is likely that the price will be driven up. Therefore the cost of manufacture of the converters is predicted to rise, since in 1991 up to 68% of the total cost is spent on precious metals alone (refer to section 2.4.2 in chapter 2). Therefore in any determined effort to reduce costs, the reduction in noble metal requirements must be a major factor. Indeed this has been the subject of much research, in areas such as catalyst distribution, surface coverage, enhancing factors including addition of cerium to the catalyst, and in support configuration (for further details refer to chapter 2).

Substantial investigation has been carried out to find new catalysts for example Vanadium oxide, with limited success, however, due to the many advantages attributed to the noble metal catalysts (refer to section 2.4.3 in chapter 2).

Although the catalyst "activity" has attracted much attention, the efficiency of the whole system has not. In fact the limiting factors concerning the operation of present commercial honeycomb converters is not catalyst activity after light-off (ie. the point at which the reaction becomes self sustaining) but the mass transfer limitation of reactants from the bulk gas to the active sites of the catalyst.

Steady state reaction temperatures are seldom less than 400°C, and at such conditions the reaction is usually mass transfer limited. The flow through the channels of the converter is laminar with Reynold's numbers varying from 50-400 (at operating conditions). The reactants are transported to the catalytic wall by diffusion described in terms of the mass transfer coefficient. This is a function of the Reynolds number, the Schmidt number, and the diameter to length ratio of the channel.

One method of reducing the amount of catalyst required would be to enhance the efficiency of the reactor by decreasing the limiting factors (ie.

enhancing mass transfer). This can be achieved by either segmenting the current monolith system so as to disrupt developing boundary layers or by adopting an alternative configuration in order to promote mixing. An alternative design is the "Active Transport Catalytic Reactor" (ATCR). This is a catalytic wall coated tube into which are inserted static mixing devices which use the energy of the flowing medium to create mixing. However, there is a compromise to be made between increased mass transfer efficiency and increased pressure drop.

An ideal requirement would be to provide a reactor which can deal with the pollution aspect at low pressure drops and at reduced surface area, (and therefore noble metal content), by enhancing heat and mass transfer within the reactor.

The channel within a monolith may be thought of as a tubular reactor. Thus by segmenting the monolith axially, the effects of induced entry length can be tested on the overall performance of the reactor.

1.2 Objectives of this study

The aims of this study are to investigate the effects of enhancing mass and heat transfer coefficients for the oxidation of carbon monoxide in tubular reactors coated with Al_2O_3 impregnated with a Pt/Rh catalyst.

Experiments were carried out using two sets of apparatus. In a preliminary study using the first equipment set-up (chapter 3), the axial and radial temperature profiles within a monolith reactor at operating conditions typical of an auto-exhaust were determined with the aim of obtaining a detailed picture of the monolith operating conditions. The remainder of the study was performed using the second apparatus (chapter 4).

The experiments were conducted in three parts:

(i) the intrinsic kinetics of CO oxidation over a commercially prepared monolithic catalyst (supplied by Johnson Matthey) were determined in a differential reactor (chapter 5),

(ii) the conversions and pressure drops of integral and segmented monoliths for varying inlet conditions were found (chapter 6),

(iii) an investigation of the ATCR under similar conditions to the monolith (chapter 7) was performed .

Finally a one dimensional model is presented (chapter 8) and compared to the experimental data for the monolith as well as the ATCR. Also experimental and theoretical pressure drops are compared for both the monolith and ATCR. A simplified optimization procedure is then carried in order to minimize the catalyst surface area of the ATCR compared to the monolith under similar operating conditions and for similar outlet conversions without exceeding the pressure drop of the monolith.

CHAPTER 2

LITERATURE SURVEY

2.1 Introduction

The first catalytic converter was used in 1975, and was of a dual bed type. This consisted of two packed beds coated with catalyst enclosed in a metal casing and placed between the engine and the muffler. Catalytic converters were used in conjunction with engine re-design as well as fuel modifications. Thus lead was removed from gasoline, since this caused serious poisoning of the catalyst (Miyoshi, 1985) and environmental effects for example brain damage in children. The engine was operated rich (ie high fuel to air ratio) to catalyze the reduction of the nitrogen oxides (NO_x) in the first bed followed by air addition to the exhaust and oxidation of CO and HC over a second oxidation catalyst. However, this process had a considerable fuel economy penalty.

A considerable improvement was possible with the development of the Three-Way Catalyst (TWC) in which a whole new engine fuel management control system was required to meet the operating needs of the catalyst. The name three-way as it suggests comes from the fact that all three components, CO, HC and NO_x are simultaneously treated in one catalyst system.

Three-way catalysts show a maximum operating performance at the stoichiometric air-to-fuel ratio (A/F) of 14.7:1. Figure 2.1 shows the optimum window of operation. The percentage conversion is shown as a function of A/F. The stoichiometric balanced composition is within the shaded area. Engines are therefore designed to control the converter at this ratio giving a small window of operation. Sufficient oxygen must be present in a stoichiometric sense to oxidize the pollutants. This may be provided by a pump that introduces air into the exhaust manifold before the catalyst, or by calibrating the vehicle to run with excess oxygen.

Automotive catalytic converters are required to deal with a wide variation in operating conditions, including cold start operation ie. when the catalyst starts off cold. Space velocities range in general from 20,000-100,000 hr^{-1} at NTP, and temperatures range from cold start up to about 600°C.

However, temperatures as high as 900°C are possible depending on the A/F ratio and flow conditions. Therefore the catalyst is required to deal with temperature extremes, air fuel ratio changes and gas velocity variation.

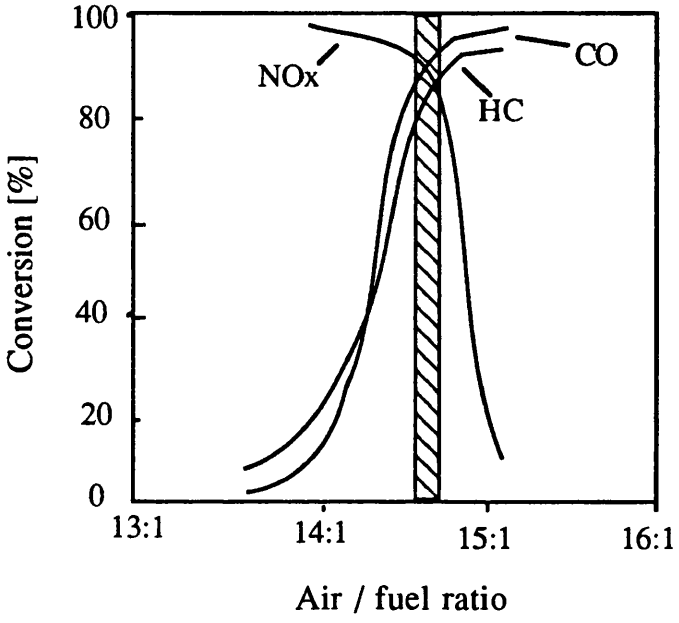

Figure 2.1 Optimum operating window for catalytic converter (Taylor, 1990)

The performance of a catalytic converter is a function of the following design parameters:

a) Type of Support
b) Type of Catalyst
c) Washcoat

Each of these topics has received much reseach and interest since they affect the overall performance of the converter. However, they do not necessarily act independently and indeed in some cases are interdependent.

The present work is concerned with the experimental testing of alternative catalytic reactor systems, as a result of varying catagory a) above.

In this review, the above topics will be discussed, with particular attention given to the monolith converter since this is the dominant technology. Hence, the review is particularly general with the view to giving the reader an

insight into the possible variables which go into designing a particular support system and the effects of varying these on the overall converter performance. A review of the literature concerning the kinetics of CO oxidation as well as the possible models for the monolith converter is also presented.

A novel alternative to the monolith is to use static mixing devices in conjunction with the heterogeneous reactions. Since there is no published information dealing with this subject, it is not possible to review this aspect of the work. However, information concerning Nusselt and Sherwood numbers as well as pressure drops are presented for specific mixer designs used in industry.

2.2 Support Design

2.2.1 Types of support

The main aim of a support system is obviously to provide a surface for the application of the catalyst to provide easy access for the reactants. In the case of auto-exhaust treatment, the catalyst-support system is required to deal with wide and varied operating conditions, and therefore should be able to withstand the wear and tear that may occur as a result.

Some important design qualities when deciding on a support for use in the auto-industry are:

i) Low support pressure drop,
ii) Good catalyst adhesion to the support walls,
iii) High support tensile strength with resistance to thermal degradation and shock fracture,
iv) Good attrition resistance to vibrations and fluctuating operating conditions,
v) Low cost of manufacture.

In the early stages, the fixed bed pelleted catalysts were the dominant technology. However, an alternative, based on the honeycomb structure, later emerged. This honeycomb or monolith as it is now called was invented in 1949 by Eugene Houdry and represented a significant advance in technology. It is

commonly composed of extruded cordierite ($2MgO.2Al_2O_3.5SiO_2$) to form a thin walled honeycomb design.

Both systems have served well, however a move towards the monolithic type of converter has occured more recently since it is more adaptable to recent designs of smaller and lighter units (Howitt, 1987). A comparison of the two types is presented in section 2.2.2. Many other configurations such as the use of metalor ceramic fibres coated with catalyst have been proposed. Another support material proposed by Leak et al. (1968), is obtained by depositing high surface area alumina on a porous metal mesh such as stainless steel wool.

Other designs have been studied including a ceramic foam variety from Champion Spark Plug. Also 0.05 mm thick ferritic stainless foils have been used in Europe for light-off catalysts situated close to the exhaust manifold for use during warm-up of the main converter (Church et al., 1989).

Many of the supports mentioned above are notable for their high surface area to volume ratio, with little attention being paid to reducing the overall catalyst surface area and hence catalyst content.

Novel catalytic converter systems are continually being investigated, with the intention of improving performances and reducing the overall pressure drop and some with the aim of reducing the overall catalyst surface area, these are discussed further in section 2.5 of this chapter.

2.2.2 Comparison of pellet and honeycomb converters

The main difference between the two systems is the extent to which mixing occurs. The gas flow in pellet beds is turbulent and is thus more advantageous in terms of mass transfer than within honeycombs, where the flow is laminar. However, an increase in turbulence usually means a corresponding increase in pressure drop across the bed. In general pressure drops for the honeycomb converter are lower than for the pelleted beds.

Pellet beds typically weigh about twice as much as the honeycomb converters and have a severe problem of pellet attrition. The latter effect is due to pellet vibration during use in which significant pellet loss may occur (Weaver, 1969). This tends to lead to by-pass of exhaust gas through voids formed in the pellet bed. Also attrition within pellet beds leads to fines and

hence to large pressure drops. However, the replacement of pellets in a pellet catalytic converter is more readily accomplished than the replacement the of honeycomb converter for instance if poisoning occurs (Kummer, 1980).

Due to durability problems, pelleted beds were phased out in automobile systems until only 5% were being used by the late 80's (Taylor, 1990). Honeycomb structures are preferred since they provide more mass transfer per unit pressure drop than pellet catalyst beds of the same total cross-sectional area (Pfefferle et al.,1987).

2.3 The Monolith

2.3.1 Description

The present honeycomb structures used by many automobile manufacturers, for example Volkswagon and Jaguar, are ceramic. Figure 2.2 is a photograph of a typical monolith. The internal channel dimension is approximately 1 mm. In general the cell densities range from 62/ cm^2 to 31/cm^2 of front face separated from one another by thin (0.15-0.3 mm), porous (~50% porous, 2-10 μm pore diameter) walls (Bagley et al., 1973; Kummer, 1980). The channel shapes can be either square, triangular, hexagonal, or sinusoidal.

Ceramic honeycombs can be produced in a variety of ways, but are today principally produced by an extrusion method (U.S. Patent, Corning Glass Works, 1975).

When in use, honeycombs are held tightly in an alloy steel canister by means of a compressed alloy steel mesh (usually Inconel) and the typical overall diameter and length of the monolith are from 2 to 10 cm and 5-23 cm respectively (Kuo et al., 1971; Wei, 1975).

2.3.2 Monolith Variations

Within the monolith there is generally laminar flow usually with Reynolds numbers ranging from 50-400 at operating conditions. Therefore

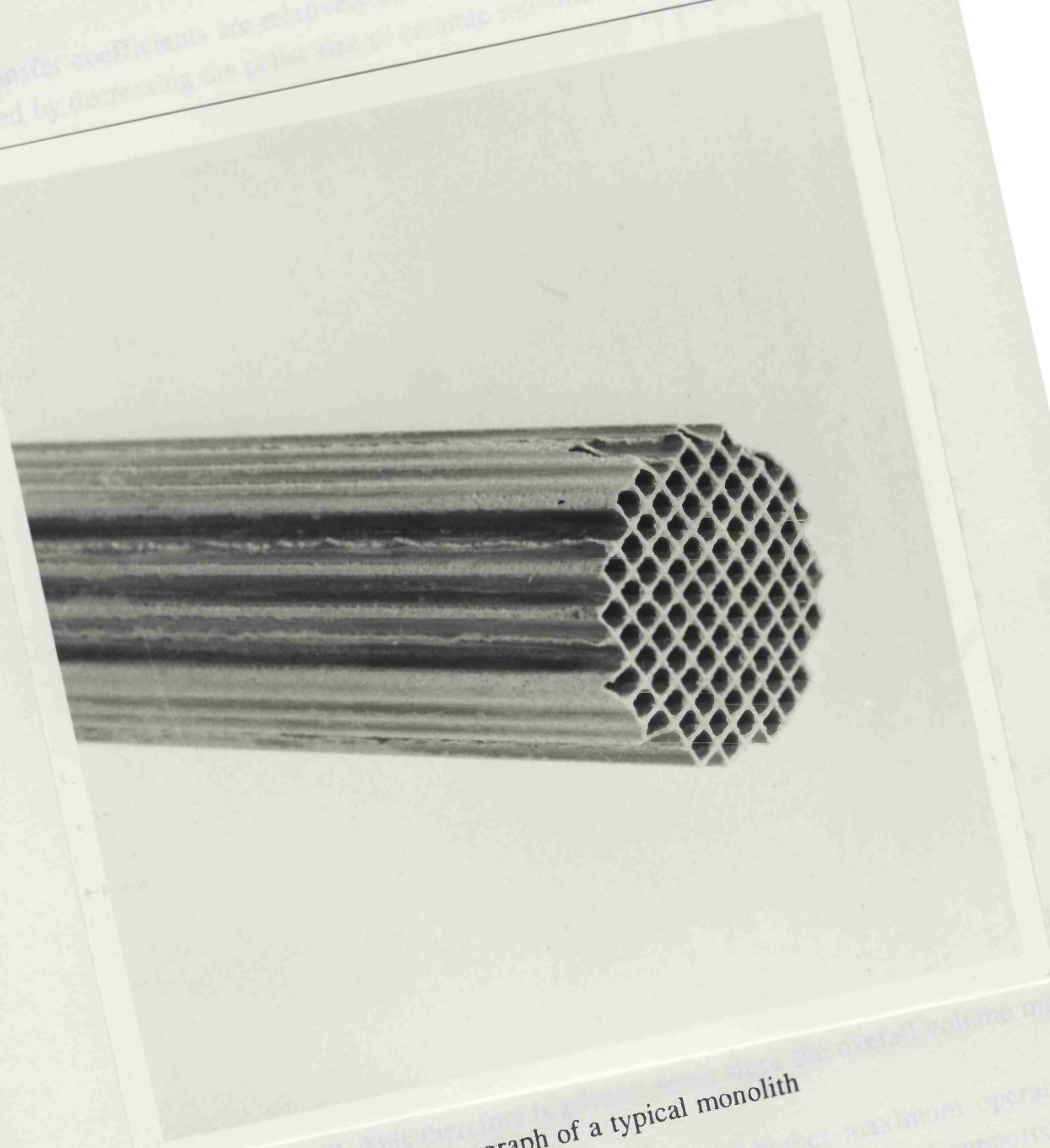

Fig. 2.2 Photograph of a typical monolith

mass transfer coefficients are relatively small. Until now, conversion could be increased by decreasing the pellet size or ceramic monolith channel diameter to increase the catalyst surface area, at the expense of greatly increasing the pressure drop (Pfererle et al., 1987).

Much work has been carried out on improving the performance of the monolith, to find the best material of construction (Nonnenmann, 1985; Platinum, 1990), best channel shape (Hegedus ,1973; Heck et al., 1974; Young and Finlayson, 1976b), and catalyst to be used (see section 2.4).

2.3.2.1 Materials of construction

Monoliths are either constructed from metal or ceramics. Because of their low thermal mass, metal monoliths have the advantage of fast warm-up to the minimum effective operating temperature of 250°C and therefore are more advantageous during the cold start. Effective light-off is critical since most of the pollution during any test cycle occurs at the cold start or shortly thereafter. Comparisons of ceramic versus metallic structures have been widely quoted (Nonnenmann, 1985; Hawker et al., 1988).

An important feature in metallic supports lies in the thin walls around the channels. This results in a back pressure up to 60% lower than for the ceramic system for the same overall diameters and typical operating conditions (Nonnenmann,1985).

Metallic supports are also advantageous because of their relatively high thermal conductivity which prevents overheating at local hot spots.

Metal type monoliths combine the catalyst support and surrounding shell into a single unit negating the requirement of any padding between the catalyst support and shell. This therefore is advantageous since the overall volume may be reduced.

Ceramic supports have the advantage of higher maximum operating temperatures (1400-1650°C) (Krill et al., 1980), whereas metal supports are limited to lower maximum operating temperatures (1350°C).

The effectiveness and reliability of a metallic catalyst depends largely on good adhesion of the washcoat to the metal surface. This has been tackled by companies such as Harwell and Sandik in which they used their expertise to develop a metallic substrate onto which the catalyst can be bonded.

Harwell's metallic substrate is an iron-chromium alloy called Fecralloy. This is composed of 15.5 % chromium, 4.47 % aluminium, 0.26 % yttrium, 0.27 % cesium and the balance is iron. Thus in a similar fashion to the monolith, the surface is then coated with alumina oxide impregnated with catalyst. The aluminium and yttrium provide bonding points between the alumina coating and the matrix. Although these metallic substrates have been used successfully, there is still a need to improve the metallic adhesion qualities, as was discovered in the present experimental study.

Production versions of metallic substrates consist of flat and corrugated foils of thickness ranging from 0.04 to 0.05 mm which are alternate and are rolled corresponding to the specified length of the substrate. Rolling is done in either a spiral or S-shape. Metallic supports are used by some car manufacturers for example Porsche and Mercedes-Benz. Although the metallic honeycombs have many advantages they are not as common as their ceramic counterpart due to their higher manufacturing cost. The advantages of the ceramic honeycomb were described in section 2.2.2.

2.3.2.2 Channel shape and size

The channel size and shape are important factors in the design of monolith support systems, not only because they determine the overall surface to volume ratio, but in turn determine the light-off characteristics as well as the Sherwood and Nusselt numbers.

Hegedus (1973) suggested that some shapes are better than others in reducing mass transfer limitations. Table 2.1 shows the limiting Sherwood numbers for various geometries. Hegedus in a theoretical study for completely mass transfer limited conditions suggested that the length of the monolith required for a given conversion decreases with increasing limiting Sherwood number. He also found that channels which were elongated rectangles in shape gave the shortest monoliths (highest mass transfer), followed by hexagons or

Table 2.1 Limiting Sherwood numbers and Moody friction factors for fully developed laminar flows in variously shaped straight ducts with zero surface concentration. Shah and London (1971)

Channel shape	Limiting Sherwood number, (α)	Limiting friction factor, $\beta = f \times Re$
Circle	3.66	64.0
Parallel plate	7.54	96.0
Square	2.976	56.92
Rectangle #	4.439	72.93
Triangle	2.47	53.33
Sinusoidal †	2.47	52.4
Hexagon	≈3.66	60.216
Ellipse	3.742	77.092

length to side ratio =4

† aspect ratio = 1

cylinders, squares, and equilateral triangles. Hegedus demonstrated that there is a direct link between increased mass transfer coefficients and shorter length in straight ducts of fixed hydraulic radius and for completely mass transfer limited situations. The effect of channel geometry on the performance of honeycomb-type catalysts was also calculated by Johnson and Chang (1974) and Heck et. al. (1974). These studies deal with the limiting case of infinite reaction rate.

Young and Finlayson (1976b), in a purely theoretical paper, studied the effects of channel shape on conversion for the less severe case than the limiting case. They suggested that due to the poorer heat transfer in the square geometry as compared to the circular, more heat accumulates at the wall, which increases the reaction rate and causes the reaction to light off nearer the inlet. From their studies they concluded that there is a trade off in the performance of the various cell geometries in that converters with poor heat transferring properties light off earlier, however they may have good or bad mass transfer characteristics, therefore affecting the performance in terms of final conversion.

Socha et al. (1989) performed some experimental investigations on the conversions of NO_x, CO and HC's for different channel sizes or densities (ie. 31, 62, 93 cell/cm^2) at a fixed catalyst loading and frontal area. They found that as the cell density increased the conversions of CO, NO_x and HC also increased. The results suggest that the total surface area of the monolith which is directly related to the cell density is a dominant design factor. This is because with higher cell density, the reduced diffusion distance is a factor. Total surface area influences performance because mass transfer of the exhaust gases to the wall surface is limiting the extent of the catalytic reaction under mass transfer limited situations (Socha, 1989).

The work of Day et al. (1988) showed that cell density had a significant influence on light-off with the higher cell densities giving faster light-off.

It follows therefore that increased cell density, or smaller diameter channels, are more advantageous because they provide a higher surface to volume ratio. However, there is a corresponding increase in pressure drop. Therefore there is a compromise to be made in the choice of channel size.

2.4 Types of Catalyst

2.4.1 Noble-metal catalysts

Noble metals have been found to be the most successful class of active ingredients for both oxidation and reduction. The most commonly used noble metals are platinum, palladium and rhodium.

Platinum (Pt) and palladium (Pd) are used for their high activity in oxidizing carbon monoxide and hydrocarbons, whereas rhodium (Rh) is beneficial for its reduction capabilities of the nitrogen oxides. Although both Pt and Pd reduce NO_x if the feed-gases are net reducing there is often a significant amount of NO_x which is reduced all the way to ammonia (NH_3) (Taylor, 1975; Schlatter and Taylor, 1977). Rh, however, is effective in reducing NO_x directly to nitrogen and oxygen without the formation of the unwanted by-product NH_3 for an air/fuel ratio near stoichiometry as well as having good oxidation properties (Church et al., 1989).

The noble metals are applied to a washcoat (usually Al_2O_3) by impregnating them by a dip or injection process with a solution containing the noble-metal compounds (e.g. H_2PtCl_6 and H_2PdCl_4). By passing H_2S through the honeycomb, one can fix the noble metal on the alumina surface as a colloidal sulphide precipitate, and produce a relatively constant noble-metal concentration in the axial direction, independent of the subsequent drying process (Summers et al., 1978).

In an oxidizing atmosphere the noble metals can disperse as oxides on the Al_2O_3 surface at temperatures below the decomposition temperature of the oxides (PtO_2, 585°C; PdO, 790°C), or even at higher temperatures if the complex between the noble-metal oxide and the support surface possesses sufficient stability. This dispersion is similar to that seen for base-metal oxides (Kummer, 1980).

At high temperatures PtO_2, interacts less strongly with a γAl_2O_3 surface, so that at temperatures greater than 600°C in an oxidizing atmosphere, the Pt dispersed-phase decreases and the metallic crystalline Pt phase increases. The dispersed phase is highly ionic in character, and can exist only to the extent of covering a few percent of the alumina surface area. If excess Pt is used, small metallic crystallites of the metal will form. The stability of this ionic dispersion is a function of the support used. This is discussed further in Kummer (1980).

Obviously the extent of catalyst used is determined by the loadings as well as the corresponding support surface area. Catalyst loadings have been found to be important in determining light-off.

Experimental studies have been performed indicating that as the noble metal loading is raised the light-off and also the extent of conversion is improved (Schlatter, 1977; Williamson, 1988; Day et al., 1988; Socha, 1989). Thus Day et al. (1988) found that increasing the Pt and Rh loadings from 0.1 wt% and 0.01 wt% respectively to 0.2 wt% to 0.02 wt% respectively, resulted in improved light-off performances for CO, NO_x and HC's. However, interestingly Socha (1989) found that in the mass transfer limited regime increasing the total volume of the converter for a fixed noble metal loading per converter gave increased conversions. Socha et al. (1989) concluded that cell density and total converter volume have a greater impact on the overall conversion than precious metal loadings in a fully warmed up reactor. Therefore, under mass transfer limiting conditions Socha et al. (1989) suggested that dispersing the catalyst over a larger surface area is more advantageous for all the cell densities tested. However, in cold start operation noble metal loadings become important since the kinetics controls the extent of reaction, and therefore the number of active sites becomes important. Therefore, in any reactor development it is important that the catalyst loading is sufficient to achieve effective light-off.

In general, the noble metal content of the auto catalyst consists of Rh and Pt. The noble-metal concentrations on the honeycomb used in practice are between 1 and 2 g/L of honeycomb volume, with a Pt/Rh ratio of 5 on a weight basis. More recently however, the major catalyst companies are researching the possibilities of using Palladium only. If they are successful this would lead to significant cost savings in pgm. The resurgence of interest in Pd is further discussed in a review by Summers et al.(1988).

2.4.2 Demand and supply of precious metals

The demand for precious metals such as Platinum, Palladium and Rhodium has grown steadily as governmental emission standards for car exhausts have become more stringent. This is due to the success of these metals

in meeting the required standards. However, the tighter measures in the USA have meant stricter standards on NO_x emissions. Thus precious metal substitutions such as that from Pd to Rh were required, and the proportion of cars fitted with three way catalysts employing a Pt/Rh ratio of 5:1 has risen. In addition, higher loadings of precious group metals (pgm) in some catalysts are already being employed by some automakers in response to the increased tightening of standards and durability requirements in California.

The continuing demand for new cars suggests that the demand for precious group metals in the auto industry is likely to increase. This trend, however, fluctuates from year to year depending on the economic situation presiding at that time, and therefore as in the case of the year 1990/1991 car sales fell in many countries. However, total world demand for noble metals for use in the autocatalyst industry continued to rise due to the reasons mentioned above. This together with need for increased precious metal supplies in other industries for pollution combating systems as well as the jewellery trade, electrical and glass industries has led to an ever increasing demand.

Competition from other sources has meant that industries have become very prudent in their use of precious metals and in some cases have attempted to cut back, especially in the glass industry.

At present the supply is able to compete with the demand and Johnson Matthey (Platinum,1991) foresee a levelling-off of car demand and therefore in autocatalysts demand by 1993. However, as Eastern-Europe and the third world become more aware of the problems posed by pollution it is likely that demand will rise sharply in the future. Therefore an increase in Pt/Rh prices is likely. However, recycling of spent auto-catalyst converters is possible and in fact is already viable in the US and Japan and in some European countries. This is likely to be necessary if demand and supply quotas are to be met. The recovery of precious group metals from spent catalytic converters is discussed further by Musco (1982). The split for Pt and Rh in various industries are shown in figures. 2.3 and 2.4 respectively. It can be seen that catalytic converters accounted for 36% of the platinum demand and 84% of the rhodium demand in 1990, this represented a significant fraction of western world demand.

The total world demand for Pt and Rh are shown in figure 2.5 (taken from Platinum 1990, 1991).

Fig. 2.3 Platinum Demand in the Western World 1990

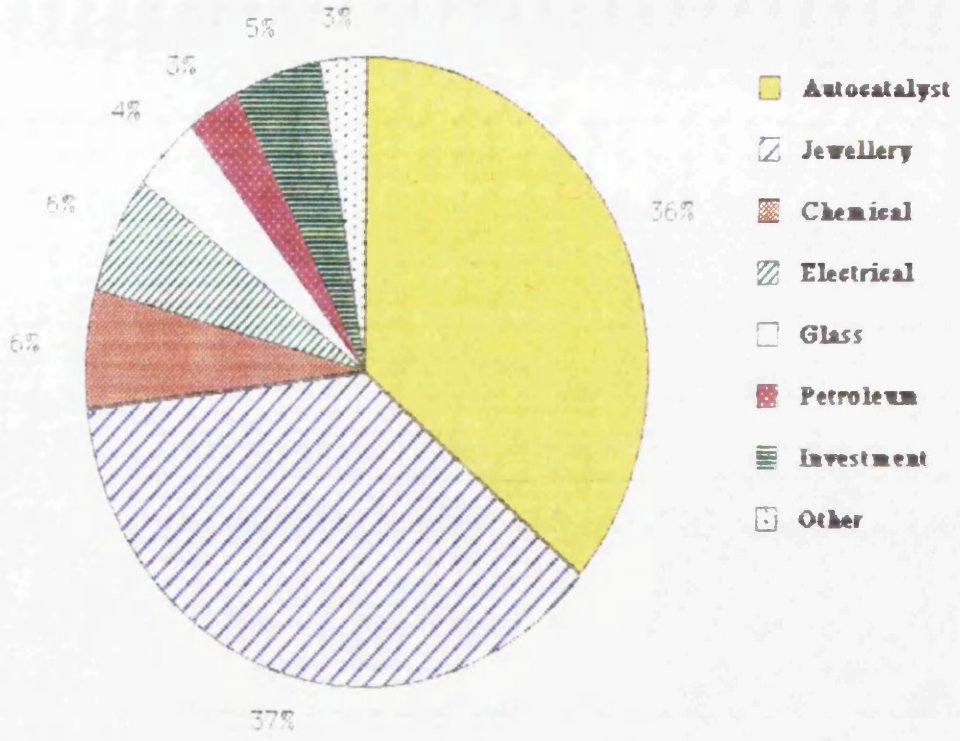

Total demand=3,660,000 oz (Platinum, 1991)

Fig. 2.4 Rhodium Demand in the Western World 1990

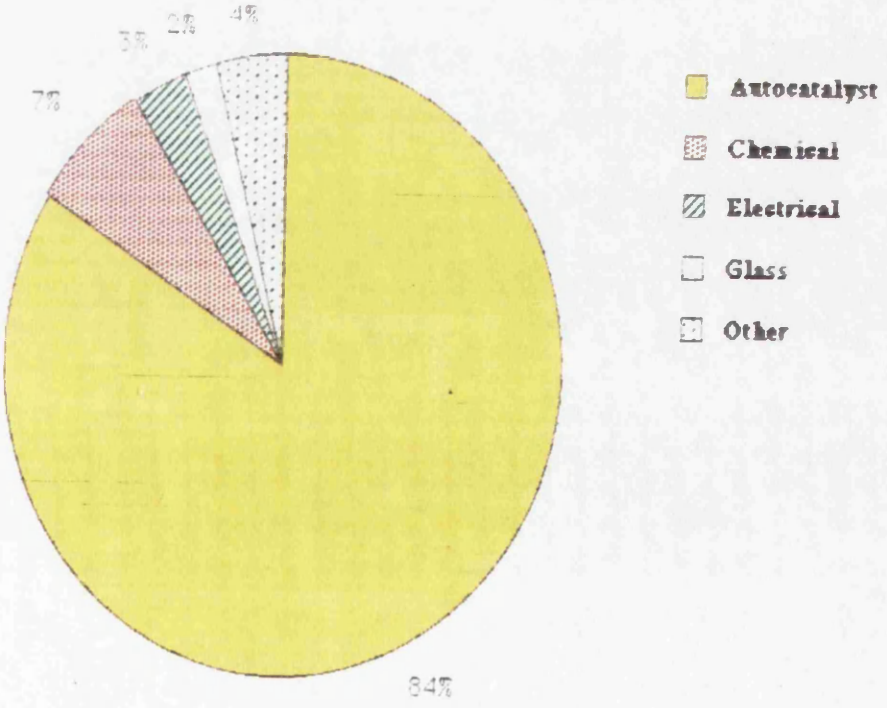

Total demand=392,000 oz (Platinum, 1991)

Fig. 2.5 Platinum and Rhodium World Demand

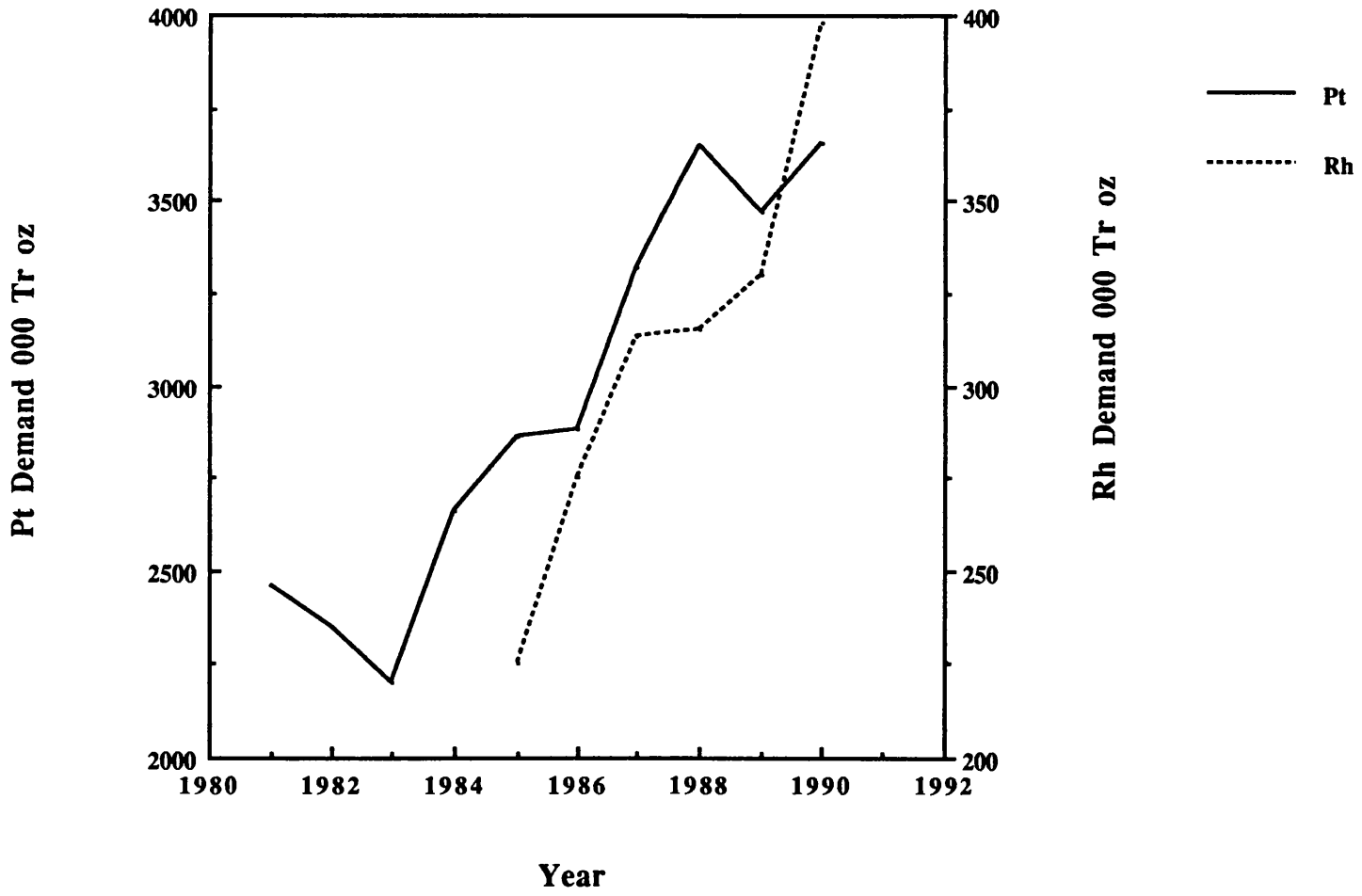

The price of rhodium fluctuates considerably due to its rarity in the world it being 15-20 times more scarce that Pt. However with new mines emerging in the world it is hoped that supply will increase though recent new mines have been disappointing in that little or no Rh has been found.

The breakdown cost of manufacture of the catalytic converter is given in Groenendal (1987) for 1985. If the current prices of precious metals are taken into account, and it is assumed that there is 10% inflation per year for each category, then an estimate of the current catalytic converter price can be found. This is given in figure 2.6 for a 1.3 L 3-way catalyst, where the category "materials" consists of honeycomb, washcoat and base metal costs. Rhodium is by far the largest cost component covering 50%, with approximately 68% (1991) of the total cost of the converter being precious metal costs.

2.4.3 Base metal catalysts

Due to the high expense attributed to noble metals, investigations proceeded in search of less expensive alternatives namely in the form of base metals.

Much of the early work with catalytic converters concerning the use of base-metal catalysts had limited success. A very large number of base metal oxides and mixtures of oxides were considered, especially the oxides of nickel, chromium, manganese, cobalt, vanadium, cesium, copper and iron.

Saturated hydrocarbons constitute about 20-30% of exhaust hydrocarbons and are the most difficult to oxidize. Base-metal oxide catalysts (particularly CuO or Co_3O_4) show similar activities per unit surface area to those of noble-metal catalysts for the oxidation of CO, however they are less active in oxidizing hydrocarbons, particularly saturated hydrocarbons. Thus because of their lower intrinsic activity, base-metal oxide catalysts are best employed as large pellet beds, or as large honeycomb structures (Kummer, 1980).

There are no catalysts today composed only of base metals since noble metals are more advantageous for the following reasons:

Fig. 2.6 Typical cost make-up of a European 3-way catalyst

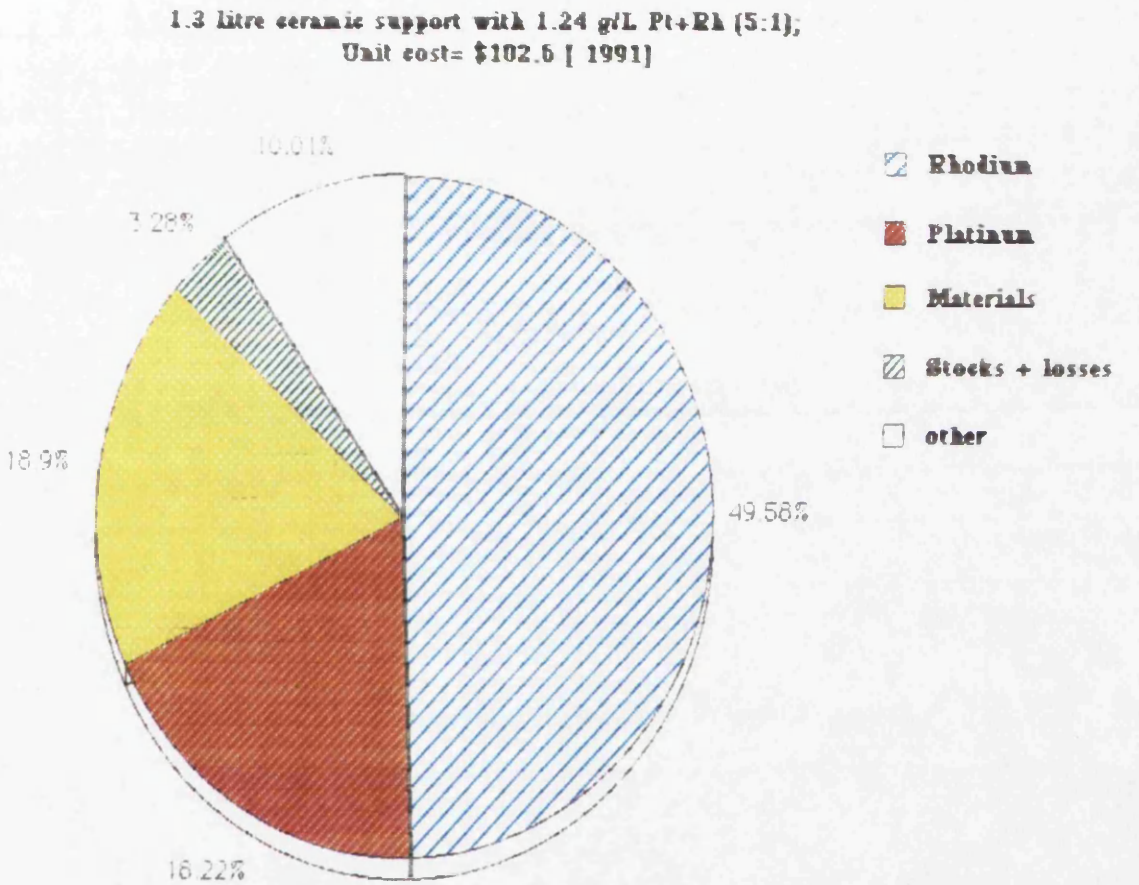

(1) base metal oxides have a lower specific activity for hydrocarbon oxidation than noble metals
(2) noble metals are much less deactivated by the sulphur in the fuel at temperatures of around 500°C than are base-metal oxides;
(3) base metal oxides can suffer from significant sintering at temperatures of 900°C and above.

However, at low temperatures noble metals are found to be less active than base metal catalysts (Schlatter et al., 1973) and therefore it is preferable to use noble metal catalysts in conjunction with base metal catalysts for the optimum performance.

2.4.4 The washcoat

Pure noble metals sinter rapidly at temperatures of 500-900°C prevailing in auto-exhaust catalysts. Since catalytic behaviour is manifested exclusively by surface atoms, the noble metals should be dispersed as finely as possible on a washcoat (usually Al_2O_3) in order to make the most effective use of this expensive material as well as to prevent particle-to-particle metal contact, and consequently reduce sintering. Thus the main goal of a washcoat system is to provide a base for the noble metal dispersions and prevent interactions between the metals to form alloys or interaction of the metals with the support material and thus reduce catalyst sintering upon exposure to high temperatures. Also noble metals suffer from deactivation by lead, sulfur and phosphorous compounds (Williamson et al., 1979; Miyoshi, 1985). The washcoat plays an important role in behaving as a poison sink. Indeed the higher the surface area the better the catalyst will resist the effects of poisons. The washcoat as well as the underlying support have a key role in determining the activity and durability of the catalyst system. The overall stability of the catalyst is to a large extent dependent upon that of the washcoat in terms of surface area and adhesion. The choice of washcoat also determines the mechanical as well as the thermal durability of the substrate, consequently coated monoliths have a lower mechanical and thermal shock resistance than uncoated monoliths and therefore

this has led to the development of new washcoat formulations (Gulati et al., 1989).

Washcoats generally contain mixtures of stabilisers, promoters and alumina. The aluminas are chosen for their inherent stability and form the bulk of the washcoat, frequently in excess of 90%. Dispersing agents are used to provide the necessary surface tension and flow properties required to allow penetration of the channels and achieve a uniform coating of the walls.

The effect of washcoat loading and distribution within the channel has long been debated. Thus high loading and even distributions in square channels give rise to circular shaped cells (refer to figure 3.5b in chapter 3) which may effect the performance of the catalyst (ie. light-off) as well as the overall pressure drop. However, Williamson et al. (1988) showed that on increasing the washcoat loading the overall conversion can be improved at 450°C. Therefore increased washcoat loading is beneficial. However, in practice it is generally limited with the result that the washcoat is concentrated within the corners of the cell with relatively little material on the walls in order to reduce pressure drop. For further details on the effects of washcoat type and loading see Cooper et al. (1987).

A tight control in the washcoat preparation and its application is required to prevent premature failure due to adhesion problems and delamination. Although there is little detail available on the commercial processes involved in washcoat applications, in particular with regard to metallic supports, in general it is well known that the coating is fixed by calcination at elevated temperatures (Cooper et al., 1987).

2.4.5 Promoters and stabilizers

The gamma-alumina washcoat is inherently stable, however at elevated temperatures it slowly converts to the delta-, theta- and alpha-phases with a resulting loss in surface area. Therefore stabilizers are usually added to retard this process. A number of alkaline and rare earth oxides are able to enhance the stability of alumina (Gaugin et al., 1975). Thus the use of promoters has been

extensively studied in particular cerium (Ce) and nickel (Ni) (Cooper and Keck, 1980; Kim, 1982; Su et. al., 1985; Cooper et al. ,1987; Harrison et al., 1988) as well as Barium (Ba). However, increasing concern regarding the environmental impact of nickel has resulted in the decline of its usage. Cerium (Ce) is used for temperatures up to 1000°C and barium (Ba) for temperatures above this.

Not only do promoters stabilize the washcoat but are also found to be useful in enhancing the activity and stability of noble metal catalysts (Summers et al., 1979).

Rhodium is the most effective of the noble metal catalysts in reducing the oxides of nitrogen to harmless nitrogen, however, it is extremely sensitive to deactivation by exposure to high temperature lean operation. Cerium is found to block or retard the deactivation process of Rh at high temperatures which therefore results in improved CO performance under oxidizing conditions for all equivalence ratios. However best results are found during fuel rich operation. This is probably due to cerium's ability to store oxygen at low partial pressures, and therefore during rich fuel excursions it is able to give up this stored oxygen for the purpose of CO and HC oxidation. The beneficial effects of Ce on improving the stoichiometric performance of Pt/Rh TWC's are given in Williamson et al. (1988). Cerium favourably alters the reaction kinetics of CO oxidation. Depending on the CO/O_2 ratio, there is a decrease in the apparent activation energy and CO inhibition with Ce. Therefore there is improved low-temperature performance as the Ce content in the catalyst is increased, especially in a reducing environment.

The extent to which the Ce is effective depends upon its loading (Harrison et al., 1988; Summers et al., 1979). Williamson et al. (1988) found that there were significant improvements in the conversion of CO and NO_x with increased loadings. However, further increase in loadings produced a plateau in conversion indicating the limit to which increasing Ce loadings are beneficial. Under fuel lean conditions increased Ce loadings enhance NO_x activity (Yao et al., 1977; Yao et al., 1980). However, under fuel rich operation NO_x and HC performances decrease as a result of Rh-Ce interactions (Williamson, 1988). Therefore, it is necessary to optimize promoter loadings. A good review of the types of deactivation experienced within catalyst support systems is given by Carol et al. (1989).

Cerium, usually as its oxide ceria, is used very widely in present three way catalysts and is added at a loading of 2-30 wt% to the alumina washcoat

(Taylor,1990). For further information on the promotion of metals by ceria and its other advantages consult Harrison et al. (1988).

2.5 Alternative Reactor Configurations

The two processes which limit the rate of conversion of any reactive species are first the mass transport or diffusion from the flow passage feedstream to the porous washcoat surface, and second the rate of reaction at the site. For normal operating conditions of the car exhaust, the flow within the monolith is laminar and therefore the mass transfer coefficients are very low. The reactions occuring are exothermic and temperatures are usually high enough for the reaction not to be in the intrinsically reaction rate limited regime. Therefore under normal conditions the reaction is in the mass transfer limited regime.

In an attempt to enhance the mass transfer within the monolith channels Wendeland (1980) performed experiments on segmented monoliths for the oxidation of CO and hydrocarbons. The monolith segments were separated and rotated in order to increase the flow disturbance between each slice. Mass and heat transfer rates are higher in the entrance regions compared to the fully developed regions of the channels due to the disruption and subsequent redevelopment of the boundary layers. His results using a test-stand engine and a laboratory coated platinum supported square channelled monolith showed improvements compared to the integral (one piece) monolith. Thus at a temperature of 550°C and a flowrate of 0.04 kg/s he found that a four-segmented monolith gave improved efficiencies of 6% for CO and 12.3% for the HC's when they were oxidized. This represents a residual or unconverted fraction of 44% for CO and 33% for HC. Wendeland's results clearly indicate that by disrupting the flow in a mass transfer limited situation improvements in the overall conversion performance are possible. The effects of interspacing separation on the overall conversion was also investigated. The results showed that the performance in terms of conversion was not affected significantly by varying interspacing for the conditions tested in the study. Wendeland's work however, does not investigate the effects of segmentation on the overall reactor pressure drop.

In the present study, the effects of segmentation on both the conversion and pressure drop for the oxidation of CO were investigated. Some of the results are summerized in Doory et al.(1990).

Kesselrig (1980) proposed using three bed segments in series with different cell sizes for converters requiring high throughput. The first segment had the largest channel size cells and the last segment had the smallest cell size. The larger cells were placed first to prevent quenching (ie. when the reaction temperature falls below the critical value needed to sustain the heterogeneous reaction) and also to preheat the gases for entry into the second graded bed. The aim in the second unit was to maximize the heat transfer from the solid to the gas phase and therefore pre-heat the gases sufficiently to light-off the homogeneous reactions in the third unit. This work however was for high temperature combusters having high throughputs of between 140,000 to 850,000 hr^{-1} (over 1200°C) in which homogeneous reactions are predicted to occur. However, the experimental results showed high improvements in the reduction of HC's at temperatures as low as 350°C in fuel rich conditions compared to the single cell size arrangement.

New metal support designs have been proposed by Sueddeutsche Kuehlerfabrik Behr under the names Metalit-S and Metalit-SQ (Nonnenmann, 1989). These are fundamentally similar to the monolith except that flow is encouraged to redevelop at interruptions or slots in the channel geometry. Also fissures in the channel walls allow internal gas flow radially throughout the monolith cross-section in an attempt to eliminate concentration and temperature gradients across the diameter of the monolith. Experimental investigations (Nonnenmann, 1989) showed improved light-off characteristics compared to conventional type metal support with continuous walls (62 cells/cm^2). Also it was possible to reduce the number of cells from 62 to 31 / cm^2 which corresponded to a 27% saving of support material and therefore consequently a reduction in cost. This type of support therefore shows promising applications in the auto-industry, however, as discussed in section 2.3.2.1, as with other metallic supports the cost of manufacture is perhaps a limiting factor in its general use.

A novel pellet geometry called the minilith was investigated by Pereira (1984). This is a cross between a pellet and a monolith, and provides a high surface to volume ratio, and produces turbulent characteristics but with relatively low backpressure. Various sized pellets as well as spoked extrudates

were compared with the minilith for conversion and pressure drop and it was found that the minilith was best. His studies showed promising results in terms of backpressure when compared with spherical pellets or the monolith. Also from the theoretical predictions the conversion of the minilith gave better performance than either spherical or cylindrical pellets. However, investigations are required to test the vibrational resistance of the novel pellet geometries, since this is a major disadvantage in the use of pellets for use in converters as discussed in section 2.2.2.

Bensalem et al. (1982) suggested using a two chamber tubular reactor. The first part contains small diameter channels with catalytic walls, and the final portion is a larger diameter tube with no catalyst. This was predicted to be more efficient than constant cross section channels at high temperature although less catalyst was used. This geometry however is only appropriate for turbulent and high temperature operation greater than 527°C when homogeneous reactions are predicted to occur.

Static mixers have been used in homogenization, as well as heat and mass transfer processes, including adsorption, extraction and solution and also as homogeneous chemical reactors (Weyermuller,1969; Bor, 1971; Jagadeesh and Satyanarayana, 1972; Kemblowski and Pustelnik,1974; Chen, 1975; Tauscher,1976; Erdman, 1977; Nauman, 1979; Pahl et al., 1982). These consist of mixing elements placed inside a tube. All of the work concerning chemical reactors using static mixing elements is for homogeneous reactions. An unconventional use is in heterogeneous catalysis applications. This process is investigated in the present work. The reactor is termed the "Active Transport Catalytic Reactor" (ATCR) and consists of a catalytically coated tube filled with static mixer inserts (Doory el al., 1991).

Two important mixer types are the Kenics and the Sulzer mixers shown in figure 7.1, chapter 7. The appeal of such mixers is their capacity to enhance mass and heat transfer coefficients compared to the empty tube, however, this leads to a corresponding penalty in terms of pressure drop.

2.6 Kinetics of Heterogeneous CO Oxidation

2.6.1 Historical background

The oxidation of carbon monoxide over platinum group metals has been widely studied. However, the conclusions regarding the mechanisms and rate equations are somewhat conflicting. These are probably due to the frequent observations of hysteresis associated with steady state multiplicity, self-sustained oscillations in the reaction and to the fact that there is no generally accepted theoretical explanation for them, even though a large number of studies have addressed the subject. There is general agreement however, in the qualitative trends in the behaviour of the kinetics regarding the changing order with respect to CO concentration. The order varies from positive to negative order with respect to CO as its concentration increases (Hegedus ,1977; Voltz ,1973; McCarthy et al., 1975). Therefore the reaction appears to be inhibited by CO at higher concentration, usually above approximately 0.4% (vol).

Two types of mechanisms have been proposed to fit the experimental data depending on the conditions. These are:

1) The Eley-Rideal mechanism:- where one reactant is adsorbed firmly on the catalyst surface while the other strikes the adsorbate from the gas phase. This is described by:

$$CO\ (gas) + PtO^{*} \leftrightarrow Pt + CO_2\ (gas) \qquad (2.1)$$

$$PtCO^{*} + O_2\ (gas) \leftrightarrow PtO^{*} + CO_2\ (gas) \qquad (2.2)$$

In this case a gaseous molecule of CO or a species loosely bound on the surface, attacks a chemisorbed oxygen atom on the surface to form a bond.

2) The Langmuir-Hinshelwood mechanism:- where both reactants have to be adsorbed on the catalyst surface in order to form the reaction product:

$$PtCO^{*} + PtO^{*} \rightarrow CO_{2}\,(gas) \qquad (2.3)$$

Much of the kinetic work which has been performed was done using platinum catalysts with few studies directly concerned with rhodium. Due to the large amount of work in this field there are many reviews in the literature including Engel and Ertl (1980) Razon et al. (1986) and Lindstrom et al. (1984).

One of the first studies was performed by Langmuir (1922) using a platinum wire catalyst. The results showed that at low temperatures the reaction was inhibited by CO and enhanced by oxygen. This was confirmed later by various workers (Sklyarov, et al.,1969; Su and Shishu, 1972). Above 371°C, however, the reaction is not strongly inhibited by CO. This is expected since there is reduced chemisorption of CO at higher temperatures where diffusion seems to be the controlling factor (Langmuir, 1922; Solov'eva, 1960; Su and Shishu, 1972). Regarding the mechanism, he postulated that the oxidation involved the reaction of adsorbed atomic oxygen and CO in the gas phase. This is the so called Eley-Rideal mechanism as described above by condition 1. Sklyarov et al. (1969), proposed the interaction of chemisorbed molecular O_2 with CO in the gas phase.

Shishu et al. (1974) made a comprehensive investigation of CO oxidation on a monolithic platinum catalyst in a differential flow reactor at atmospheric pressure and for a temperature range of 232-427°C for a synthetic gas make-up similar to those in engine exhaust gases. Asymmetric behaviour was found to occur which means that pre-adsorbed CO inhibits the adsorption of oxygen, whereas the reverse is not the case. Shishu developed rate equations based on the dual-site mechanism in which the surface reaction between adjacently adsorbed CO and O_2 molecules was rate controlling.

There is no general agreement as to the correct mechanism and indeed experimental results by several investigators (Bonzel and Ku ,1972; Lindstrom, 1984) tend to indicate that the basic mechanism of this reaction may not be unique and depends on experimental conditions.

Pacia et al. (1976) proposed that, depending on the experimental conditions, the two possible mechanisms exist and may compete. Previous experimental evidence using thermal desorption and reactivity experiments, performed by Winterbottom (1973) reached the same conclusion. Thus Pracia et al. (1975) proposed that the Langmuir-Hinshelwood mechanism is the major reaction at high temperature above 300°C, with competition occurring at temperatures below this. In their study, Pacia at al. (1976) postulated that in the low temperature range the Eley-Rideal mechanism may well be dominant at pressures around 1 torr but is negligible for CO pressures $< 3 \times 10^{-8}$ torr. Within the literature therefore there seems to be some agreement that at higher temperatures and low reactant pressure the reaction proceeds via the Langmuir Hinshelwood mechanism between adsorbed CO and adsorbed atomic oxygen, whereas controversy exits at low pressure and low temperature.

Normally the Langmuir-Hinshelwood, or the power law equation, are used to model the experimental kinetic data (Shishu et al., 1974). However for low CO concentrations the power law model breaks down and the L-H is used.

The most widely accepted model is that of Voltz (1973). A comprehensive study investigating the kinetics of CO oxidation on a platinum-alumina catalyst using a synthetic gas mixture, similar to conditions in a car exhaust, between 204 and 371°C was performed. Voltz's model is based on the dual-site bimolecular Langmuir Hinshelwood reaction. Voltz's work was generally consistent with other workers in that both the enhancement of oxidation by O_2 and inhibition by CO agree with previously published results for both supported platinum catalysts and platinum wires and films. The results showed that an increase in the concentration of CO from 0.7 to 4 % sharply decreases the conversion of CO. Propylene and nitrogen oxide were also found to have an inhibiting effect on the oxidation of CO. Voltz determined the reaction rates to be free of both inter and intraparticle diffusion effects at 204 and 288°C, since the outside active layer was a very small fraction of the particle diameter and made diffusion paths very short. By making some simplifying assumptions regarding the reaction mechanism, the effectiveness factor was calculated to be essentially unity.

The study of Voltz does not necessarily indicate that the reaction model presented describes the true mechanism. However, the rate model did

satisfactorily fit the experimental data and included all the combined effects of important species found in automobile exhaust.

There are few reports of models for CO oxidation on Rh (Campbell et al., 1978; Oh et al., 1986). However, the general conclusions are that Rh behaves similarly to Pt except that it is more active for low temperature CO oxidation (Cho et al., 1989), however the reasons for this are still under investigation.

2.6.2 Multiplicities, hysteresis and self-sustained oscillations

Negative order reactions, when coupled with intra pellet diffusion resistances, have been predicted to give rise to peculiar phenomena, such as isothermal effectiveness factors (ratio of actual reaction rate within a pore to the rate of reaction if not slowed by pore diffusion) above unity and multiple solutions.

Multiple steady states for CO oxidation in a single, isothermal, porous Pt-alumina catalyst was first observed by Beusch et al. (1972). They suggested that the multiplicities were caused by the interactions between kinetics and chemisorption rates, and not by any diffusion-reaction mechanism.

As well as multiplicities, oscillations have also been observed. Many different forms and magnitudes of oscillations are reported with no quantitative agreement but a surprising amount of similarity in the shapes of the oscillatory waveforms. McCarthy et al. (1975) studied CO oscillations on pellets coated with Pt (0.035 %) catalysts on Al_2O_3. Self-oscillations were observed with a period of 20 s under excess oxygen in a mixture of 0.08 to 0.3 % CO. Self-oscillations with periods of several minutes were observed by Beuch et al. (1972) for pelleted catalyst (Pt 0.3 %) on Al_2O_3 for 1 % CO.

As to the cause, the influence of mixing has always been a matter of some controversy. Diffusional and hydrodynamic effects were among the first explanations proposed for observed multiplicities and oscillations (eg. Elnashaie et al., 1973; Hegedus, 1977) , and many still accept this explanation. According to Voltz et al. (1973) and Wei and Becker (1975) multiple solutions for CO oxidation in porous catalysts pellets were predicted as a result of diffusion-

reaction interactions, however from their calculations this should occur for CO concentrations larger than 10%.

However, oscillations have been observed in systems where great care has been taken to eliminate transport resistances. There is as yet no complete agreement as to the degree to which they are eliminated, but many accept that diffusional resistances seem not to play a vital role in the qualitative behaviour of the reaction. However, they have a role in quantitative effects, and the nature of the waveforms may be affected qualitatively by them. MacCarthy et al. (1975) suggested that this was due to competing mechanisms or of the mechanism for oxygen attack on chemisorbed CO. Switching of CO complex on the surface has been proposed as a possible explanation (Hugo and Jakubith, 1972).

This was supported in a study by Lindstrom (1984) in which he performed extensive experiments and came to the conclusion that the oscillatory behaviour is the result of inherent surface mechanistic causes and not extraneous external/internal mass and heat transport limitations.The conclusions are still far from agreed upon and more work is continuing in this area.

It would seem that much of the data reported for multiple steady states and self sustained oscillations, reviewed by Engel and Ertl (1980), are for low temperature operation below 300°C, with very little above this temperature. However Edelbock and Lintz (1982) reported observing "hard" oscillations for their studies at 350°C. Their experimental studies for the oxidation of CO (in excess) on polycrystaline Pt were performed under atmospheric pressure for mole fractions of CO in the range 0.0025-0.02 . They suggest that there was no mass transfer limitation, however catalyst pretreatment was not discussed nor the levels of impurities. The conclusions were that their observations were due to the transition of the reaction from ignition to extinction (due to external noise for extremely sensitive reactions).

Other possible explanations put forward are as a result of impurities either in the gas stream or in the catalyst. Again, there has been much work in this field. Razon et al. (1987) conducted their own experiments and discovered that small amounts of impurities on the catalyst surface do affect the experiment. Also Lamb et al. (1977) reported oscillations induced by impurities in the gas stream. However, these effects are still largely unexplained. It must be noted that in many cases the past history of the catalyst had not been well documented.

The latest explanations deal in terms of the competing mechanisms at the surface depending on the operating conditions occurring rather than impurites . However, these may also contribute to the effects of the observed oscillations and multiple steady states.

Other explanations have also been reported and these are reviewed in Sheintuch and Schmitz (1977), Slin'ko and Slin'ko (1978), and Razon and Schmitz (1987). It seems that the conclusions drawn are that although much work has been performed, there seems to be little agreement between experimental results as well as theory put forward to explain these. The results depend very much on catalyst pretreatment, working conditions, and impurities in the gas as well as the catalyst. Therefore only trends in experimental results can be concluded.

The above observations indicate that the oxidation of CO may not be a straightforward reaction. This was taken into consideration during the kinetic experiments, described in chapter 5.

2.6.3 The kinetic equation

As previously mentioned, it is generally accepted that the model presented by Voltz et al. (1973) is representative of the experimental results. This model is of the Langmuir-Hinshelwood type where surface reactants are adsorbed on neighbouring sites. The rate of such a reaction is proportional to the probability that each reacting species is adsorbed on neighbouring sites which is proportional to the fraction of surface covered by each species. However as the number of sites are taken up then there is less chance for a molecule to be adsorbed on to the surface of the catalyst. Thus the reactants become self inhibiting. This is indicated by the presence of the concentration terms of each species in the denominator. However it has been observed that for the oxidation of CO on noble metals CO is more strongly adsorbed and therefore the inhibition effect of oxygen becomes relatively insignificant. The equation then takes the form of Voltz's equation which for the oxidation of CO is given by :

$$-r_{CO} = \frac{k_r [CO] [O_2]}{(1 + k_a [CO])^2} \qquad (2.4)$$

where k_r is a rate constant and k_a is the adsorption constant. The denominator is a resistance term which includes the inhibition effects of CO, due to its chemisorption, on the reaction rate. This represents a rate equation which correspond to a reaction mechanism with the surface reaction of adsorbed CO molecules with adsorbed O_2 molecules as the rate-controlling steps (dual-site mechanism). This type of mechanism is consistent with the results from a detailed kinetic study of CO oxidation over a platinum catalyst by Shishu et al. (1974).

The kinetic parameters depend on temperature according to the Arrhenius equations:

$$k_r = A \exp\left(-\frac{E_r}{RT_s}\right) \qquad (2.5)$$

$$k_a = B \exp\left(-\frac{E_a}{RT_s}\right) \qquad (2.6)$$

The adsorption constants decrease with increasing temperature, which means that the inhibition effects decrease with increasing temperature.

2.7 The Overall Reaction Rate

The overall reaction rate is determined by the intrinsic kinetics as well as the mass transfer to the surface of the catalyst. A general diagram showing the overall rate as it varies with the bulk gas temperature is given in figure 2.7. At low temperatures the overall reaction rate is determined by the intrinsic kinetics of the reaction (this varies exponentially with increase in absolute temperature)

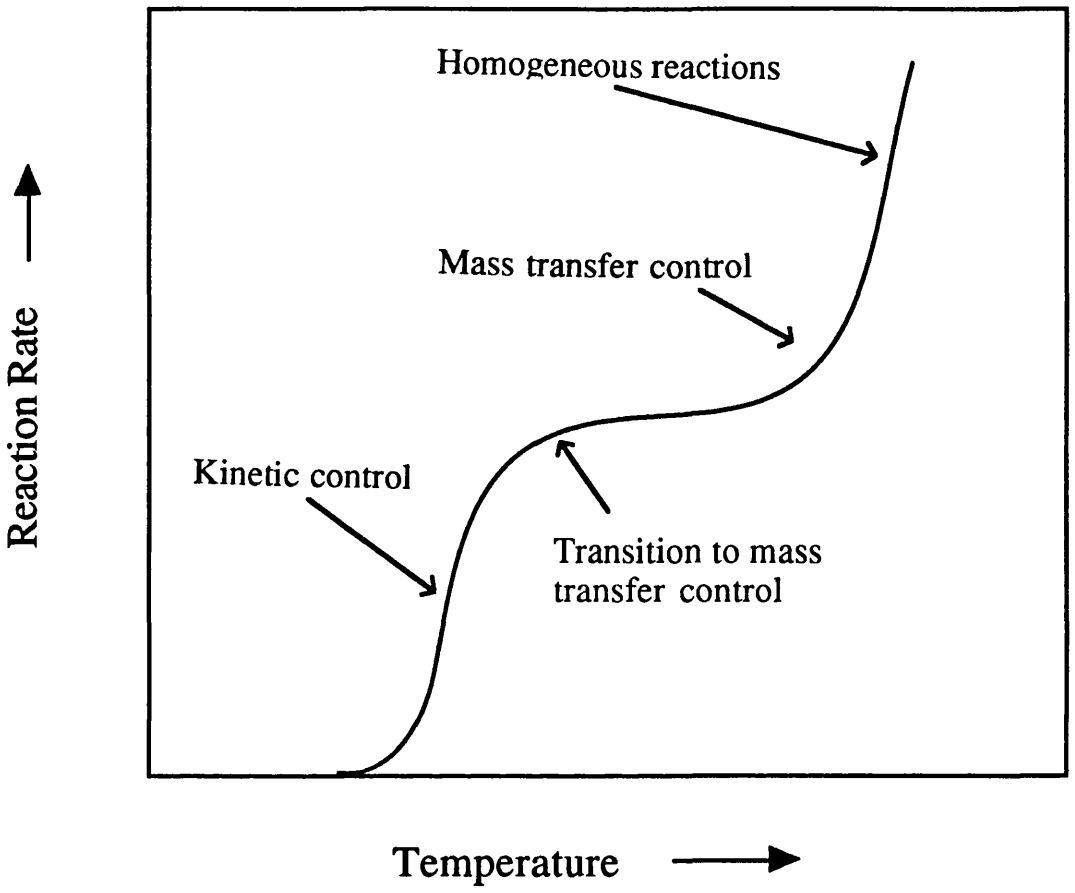

Figure 2.7 Reaction rate versus temperature in a typical monolithic reactor

until the heat generated at the catalyst surface exceeds that which is lost to the gas; at this point the reaction lights-off (ignites). As the temperature is increased further the surface reaction continues to increase until the rate at which reactants are transported from the bulk stream to the catalytic surface becomes the limiting step. The reaction is then mass transfer limited. The diffusion rate or mass transfer coefficient is not markedly affected by temperature, and thus further increase in temperature has limited influence on the overall reaction rate and hence the conversion. It is thought that the hot catalytic surface heats at least a portion of the boundary gas layer and if the gas temperature is high enough this triggers off a homogeneous gas phase reaction near to the surface and eventually throughout the whole tube. The reaction then becomes independent of mass transfer and again increases exponentially with increase in temperature.

In between these regimes, there are intermediate regions in which the reaction is both mass transfer and catalytically limited or mass and homogeneously reaction rate limited at the same time.

For normal positive order reactions as the concentration of reactant increases so does the rate, however for negative order reactions or LH type reactions the reverse can be true, ie as reactant concentration increases the reaction rate decreases for certain ranges of concentration. Wei (1975) demonstrated that the performance of reactions with this type of kinetics may benefit with increased backmixing and therefore the recycle and CSTR type of reactors are superior in performance to the piston flow reactor for L-H type kinetics.

2.8 Laminar Profile Within a Tubular Reactor

Typical Reynolds numbers within the channels of the monolith range from 50 to 400 at operating conditions and therefore the flow is well within the laminar regime. At the entrance of the passage the flow is developing as shown in figure 2.8. The flow eventually becomes fully developed to give a

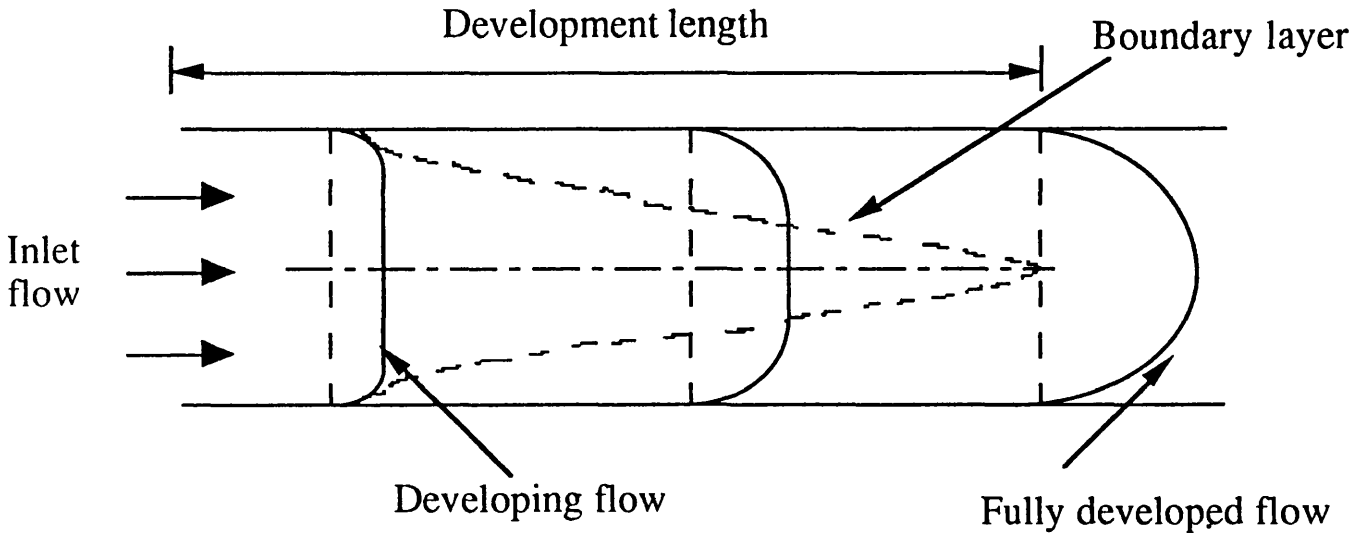

Figure 2.8 Flow development for laminar flow in a tube

parabolic profile. Therefore at the channel entrance mass and heat transfer coefficients are higher because the boundary layer has still not fully developed.

The flow at the entrance can be assumed to be plug flow, however as the flow develops this assumption will not be valid. The influence of a developing profile or indeed the effect of assuming complete plug flow within a tubular reactor can be determined by knowledge of the entry lengths. These can be found using Langhaar's analysis (1942) for laminar flow within circular tubes to yield:

$$Le / d = 0.0575\ Re \qquad (2.7)$$

where Le is the development length for centre-line velocity to reach 99% of its fully-developed value.

Figure 2.9 is a plot of entry lengths as a function of diameter to length ratio (d/L) for varying Reynolds numbers. This shows that the smaller the ratio of d/L then the lower is the entry length effect, for constant Reynolds numbers. When the Reynolds number is increased, the effect is to lengthen the entrance region for enhanced Sherwood and Nusselt numbers.

Typically for a 1 mm diameter by 15 cm long channel, the ratio d/L=0.0067, which for the Re range of 50-400, in figure 2.9 corresponds to an Le/L ratio of 2-15%. Thus for a typical monolith converter the effect of entry length is negligible. However, by segmenting the monolith, the flow can be encouraged to redevelop increasing the entry length region significantly. Hence, for example, if the 15 cm long monolith is sliced into 1 cm slices, the total entry length region at a Reynolds number of 200 can be increased from 8 % for the integral core to 115 % (ie. the calculated entry length exceeds the combined length of the segments by 15% so that the boundary layer never fully develops) for the segmented core. This indicates the obvious potential of enhancing mass transfer by segmentation.

Fig. 2.9 Entry length as a function of d/L

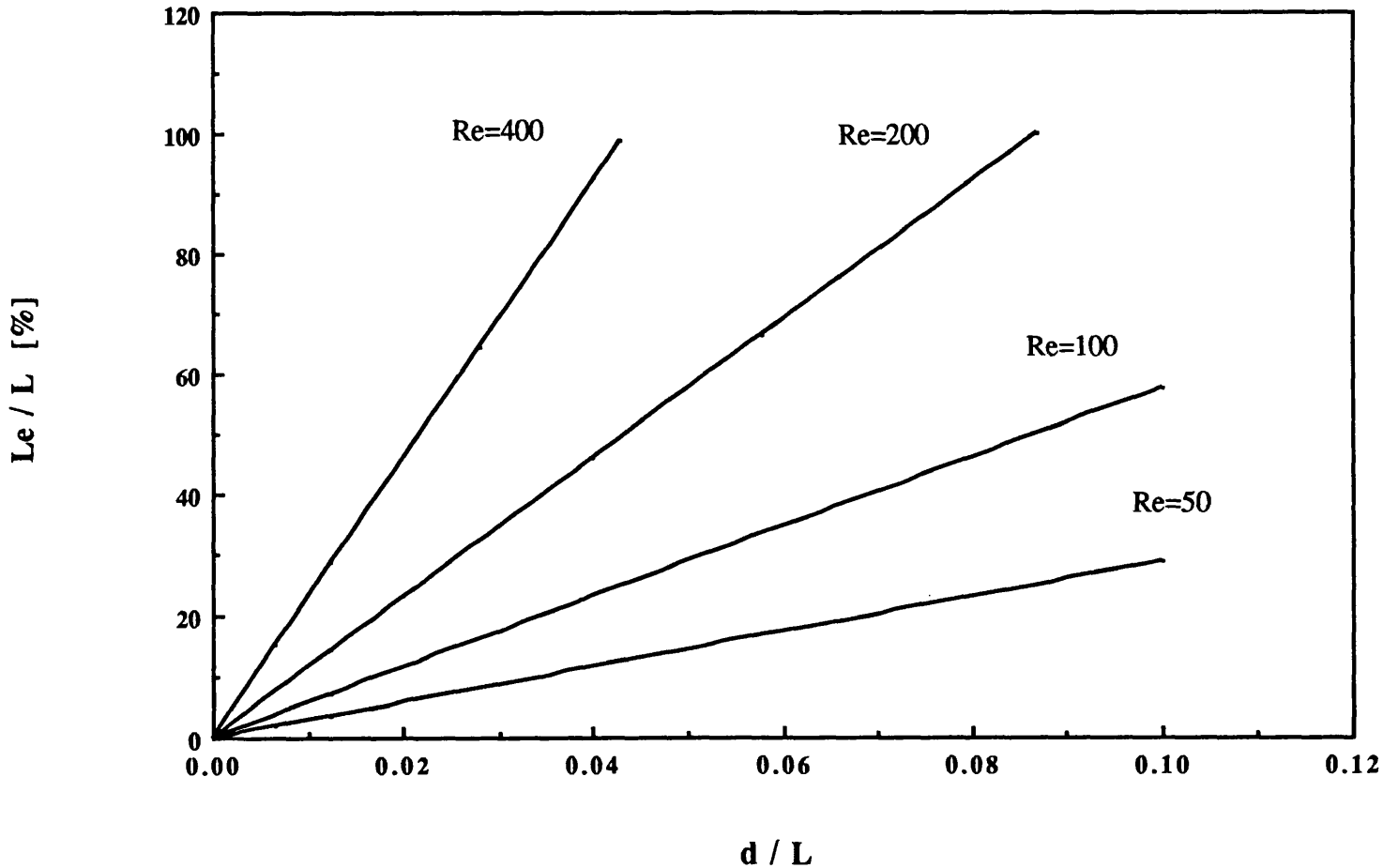

2.9 Reviews of Mathematical Models

2.9.1 Introduction

In developing any heterogeneous model, the following processes should be taken into account:

a) the diffusion of the reactants to the catalytic surface and diffusion within the porous solid,
b) reaction of these at the catalytic sites,
c) the transfer of the heat of reaction away from the catalyst , by conduction in the wall or by convection and conduction back to the bulk of the fluid,
d) the diffusion of reaction products back to the bulk fluids where they are carried downstream.

These fundamental processes take place for all heterogeneous reactor systems and the differences between each type of reactor system depends on the magnitudes of the characteristics described ie. diffusion, conduction, surface reaction and heat transfer. Radiation and heat loss terms may also be added in high temperature situations.

The monolith reactor consists of a number of parallel passages coated with a washcoat impregnated with catalyst. The channels may be thought of as hollow tubular reactors.

If the flow characteristics within each channel are identical as is the case in an ideal adiabatic system, then the reactor can be modelled as a single channel, with the overall moles converted being the summation of each of the individual tubular reactor. This assumption has dominated much of the modelling that has been done.

Modelling of monolith type reactors has been studied to varying degrees of complexity. In general there are two types of steady state models:

a) one-dimensional
b) two-dimensional

Three dimensional modelling has been pursued (Young and Finlayson, 1976) however due to its complexity it is not preferred.

The one-dimensional model assumes that the dependent variables are a function of only one space variable, the axial distance z. All the fluid properties are therefore assumed to be constant over the cross-section. This represents plug flow in which it is assumed that the resistances to heat and mass transfer are "lumped" at the channel wall, through the use of heat and mass transfer coefficients respectively.

The two-dimensional model as the name suggests considers both radial and the axial variation of the dependent variables, namely concentration and temperature, within the tubular reactor.

There has been much controversy as to the best model to choose. The complexity of each of these models has been varied by many workers and these will be discussed in the next section. However, the extent to which these additional complexities become important depend to a large extent on the reactor and conditions at which it operates.

Although there has been much theoretical work, and indeed much experimental work, there has been little in the way of comparison between the two in the literature. However, some of the experimental work which is compared to theory is decribed below.

Transient models are usually important in practical situations since the effectiveness of the catalytic converter immediately after a cold start is critical as a large portion of the emissions occurs in this initial period. Thus a converter that can warm up quickly has a decided advantage and not surprisingly most of the modelling efforts in transient behaviour are in the automobile exhaust clean-up field. However it is also of interest to stationary gas applications because of the excessive thermal stress and shocks which can affect the combustor during ignition/ shut-down operation. In severe cases these can result in monolith failures (DeCorso et al., 1978). However, this area will not be dwelt upon in this work since our concern is mainly with steady state operation. For more information refer to Ahn (1983).

In attempting to model alternative reactor systems (for example the ATCR) a measure of the extent of mixedness is required. The simplest approach would be to apply a one dimensional model requiring Sherwood and Nusselt numbers. These would need to be found from experiment for the particular system in question.

Two well known mixers which may be used in the ATCR described in section 2.6 are the Kenics and the Sulzer mixers. A review of the literature concerning these, in particular regarding the pressure drop across the reactor,

which is of major concern in exhaust systems, is given in sections 2.9.4, and 2.9.5.

2.9.2 Monolith Models

2.9.2.1 Low temperature operation

Prior to 1973 little work was done on the modelling of monoliths. Much work, however, was performed on two-stage catalytic converters (these usually being in the form of packed beds). In much of the earlier theoretical work concerning monoliths, adiabatic reactor operation was assumed and modelling was performed on a single channel basis, with this being assumed to be representative of the whole monolith system.

Hegedus (1973) formulated a simple one dimensional (plug flow) model, assuming isothermality and complete mass transfer limitation. For the latter to be true the kinetics are assumed to be infinitely fast with the concentration of reactants at the wall being equal to zero. Hegedus stated that even for nonisothermal or adiabatic systems, a reasonable approximation of their behaviour can be constructed by an isothermal treatment if they are mass transfer controlled. Thus for these systems the parameters are nearly independent of temperature changes and were therefore assumed constant. This very simple model was based on a single channel, neglecting longitudinal dispersion in the porous solid, dispersion in the fluid, assuming steady state and isothermal behaviour. The model also assumed that the velocity profile was uniform across the radius of the duct. For a typical monolith, operating well within the laminar region, a distorted parabolic profile would be more appropriate. However, for the purpose of his report, Hegedus described the error introduced by this assumption as minimal.

The model, described by Hegedus (1973), is oversimplified since isothermality and complete mass transfer limitation are assumed. In real situations the reactions can be either mass transfer limited or reaction rate limited or both depending on the operating conditions.

In his model Hegedus made use of one of the most widely used mass transfer correlations, that of Hawthorn (1973). Hawthorn produced correlations for both Sherwood and Nusselt numbers in variously shaped straight ducts by combining numerical solutions for developing laminar flows in smooth circular

tubes with analytical solutions of fully developed laminar flow situations. Hawthorn's work was based on the data of Kays and London (1964) for heat transfer in pipes, and only by analogy was able to describe mass transfer. The relations are:

$$Sh = \alpha \left(1 + D\ Re\ Sc\ \frac{d}{L} \right)^{0.45} \qquad (2.8)$$

$$Nu = \alpha \left(1 + D\ Re\ Pr\ \frac{d}{L} \right)^{0.45} \qquad (2.9)$$

where α is the limiting Sherwood number for fully developed laminar flow and depends on the shape of the channel, D is a constant which depends on the surface roughness of the ducts wall (taken to equal 0.095), d is the hydraulic diameter (defined here as four times the flow cross section, divided by the wetted perimeter), L is the uninterrupted length of the reactor, and Re and Sc represent the Reynolds and Schmidt numbers respectively with their usual definitions. Table 2.1 in section 2.3.2.2 presents a list of the values of α for the variously shaped ducts.

Votruba et al. (1975a) established an adiabatic one dimensional model for a first order reaction, using the lumped parameters of Hawthorn. Axial heat conduction in the solid phase was also included. When conduction is neglected in monolith models, the front part of the channel is not affected by light-off further down the channel. However, in reality conduction and radiation in the walls tend to heat the front part of the channel and therefore lead to the light-off (ignition) point moving closer to the entrance of the channel. Longitudinal heat conduction in the monolith wall can therefore influence the performance of a monolith reactor by promoting early ignition. The ignition of the catalytic reactor is characterized by a sharp increase in wall temperature. The study of Votruba et al. (1975a) showed that heat conduction in the solid phase is important for honeycomb structures with the Peclet number (Pe)<200, where Pe is defined as the ratio of heat transfer by convection in the gas phase to the heat conduction in the solid phase. Therefore for higher Peclet numbers heat conduction can be neglected and the proposed model reduces to a simple two-phase piston-flow model.

The magnitude of the thermal conductivity and fractional open area determines the size of Peclet number. In typical ceramic converters Peclet numbers exceed 200 and therefore the conduction in the solid phase is of minor importance and may be neglected. This was established by many workers including Votruba et al. (1974) and Young and Finlayson (1976a & b).

Votruba et al. (1975b) proposed alternative correlations for Sherwood and Nusselt numbers to those proposed by Hawthorn (1973). These were based on evaporation experiments in monoliths using water and some hydrocarbons. The experiments consisted of the vaporisation of the water and hydrocarbons from the porous surface of monolith structures. This was carried out by weighing the monolith structure (initially saturated with the test liquid) continuously while a known supply of air was introduced to provide constant drying. The extent of evaporation in a given time determined the mass and heat transfer coefficients. Experiments were repeated for monolith channels sizes ranging from 1 to 10 mm in diameter. The experimental data were subject to an 8.6% tolerance for Sherwood number data and 14.3 % for Nusselt number data. The results were correlated for data lying between $3<Re<480$ and $0.57<Sc<3.3$ and for a Prandtl number of (Pr) 0.74 giving:

$$Sh = 0.705 \left(Re \frac{d}{L} \right)^{0.43} Sc^{0.56} \qquad (2.10)$$

$$Nu = 0.571 \left(Re \frac{d}{L} \right)^{0.67} \qquad (2.11)$$

Votruba et al. (1975b), however, do not specify the shape of the channel used in the study, or indeed the effect of channel shape on the above the correlations.

Both Hawthorn and Votruba's equations were established for non reacting conditions.

In a preliminary study Young and Finlayson (1974), showed that there is a significant difference between a one-dimensional model, where only axial gradients are considered, and a two-dimensional model, where both axial and radial gradients are considered.

Using their two-dimensional model they calculated Nusselt and Sherwood numbers along the channel length during reaction. Thus for Nusselt

number for example this was calculated from the temperature gradient at the wall generated from the two dimensional model:

$$Nu = \frac{2\,(\delta T/\delta r)\Big|_{r=R_h}}{T_S - \bar{T}} \qquad (2.12)$$

where $\bar{T}$ is the mixing cup temperature of the fluid and R_h is the hydraulic tube radius. The Sh can be found in an analogous way. The resulting profiles are shown in figure 2.10. Thus Young and Finlayson showed that there is an unusual behaviour in the presence of rapid reactions. At the entrance of the channel both the Nu and Sh numbers drop as the flow starts to develop, however there is a sharp rise in both the Nu and Sh numbers at the light-off point to produce a discontinuity after which there is a new entrance region. This unusual behaviour was confirmed by Heck and Wei (1975). Therefore catalytic wall reactions in the channels of a catalytic converter can influence the Nu and Sh and hence the heat and mass transfer coefficients respectively especially at light-off.

Heck et al. (1974) measured the transient warm-up of a number of monolithic catalyst supports and compared these with various models. The experiments were performed in order to measure temperature profiles for transient operation under nonreacting conditions for inlet gas temperatures of 304°C and 343°C. The Nusselt number was found to be very high at the entrance but rapidly declined to an asymptotic value a few diameters downstream.They also discovered that the entrance region of developing thermal boundary layer was longer than expected, possibly because of entrance turbulence.

One of the most detailed studies was conducted by Young and Finlayson (1976a, 1976b, 1979), in which one, two and three dimensional models were tested both including and excluding axial conduction in the walls. In particular the assumptions of Hegedus (1973) and Votruba et al. (1975a) for constant heat and mass transfer coefficients were tested to find their limitations, since the calculations of Young and Finlayson (1974) suggested that the assumptions may not always be valid. All the models studied by Young and Finlayson embodied the assumption that the velocity profile of the fluid was fully developed throughout the converter, since a detailed analysis revealed that the effect of the

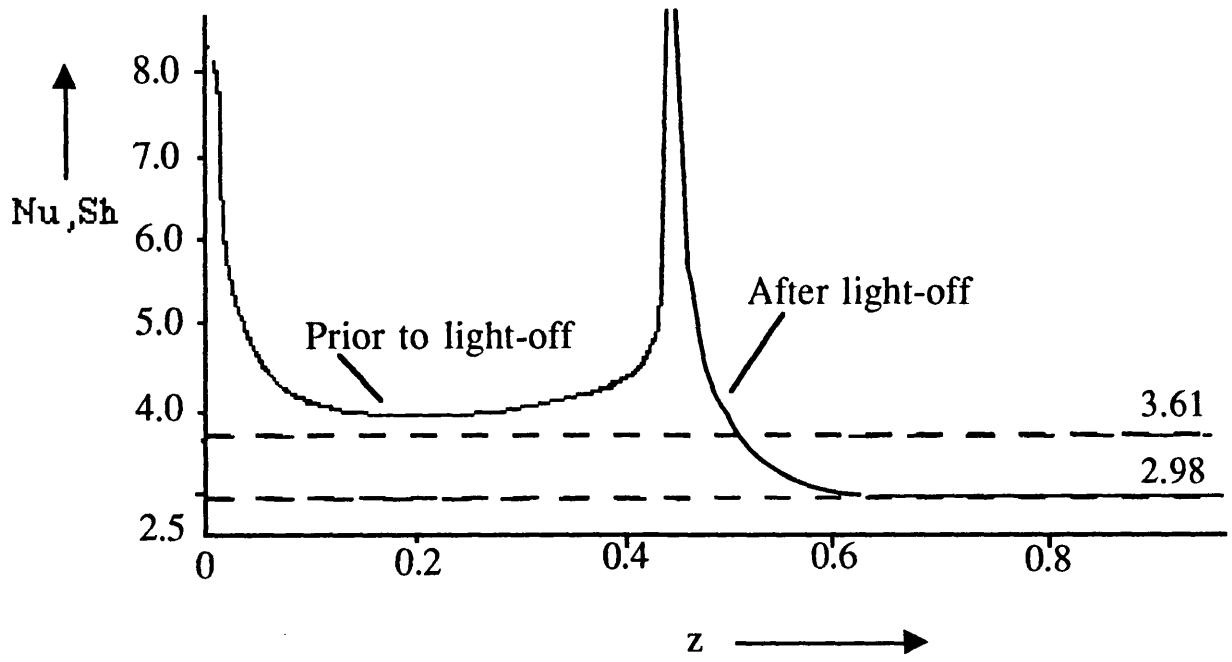

Figure 2.10 Nusselt and Sherwood profiles along a monolith channel during reaction (Sh=Nu), Young and Finlayson (1974)

velocity profile developing near the inlet is small (only 7%, Young and Finlayson (1976a)). They concluded that the simple one dimensional model using lumped parameters was not adequate for the following reasons:

i) The flow within the channels of the monolith in auto-catalytic devices is laminar, and therefore the plug flow assumption is an oversimplification.This was found to predict premature light-off and could lead to overestimates in exit conversion,

ii) Non-reacting correlations may not be sufficiently accurate due to the discontinuities observed in both the Nusselt and Sherwood numbers during reaction (figure 2.10).

Therefore, in their judgement the more complex and hence computationally more time consuming two-dimensional model should be used for the monolith catalyst. They also concluded as did Votruba (1975a) that axial conduction in the solid is sometimes important, ie. when Pe<200.

The main difference between the predictions of the one and two dimensional models is due to the discontinuities in the Nusselt and Sherwood numbers at light-off (refer to figure 2.10) not being accounted for in the one dimensional model. Thus far, there are no correlations for Nusselt and Sherwood numbers in the literature which take account of these exothermic effects .

Heck et al. (1976) compared steady state one and two dimensional models. In their models, axial conduction in the solid and in the gas were neglected and the reaction was assumed to take place on the monolith surface, with no reaction occurring within the pores. In their solution method they took account of the discontinuities at light-off (refer to figure 2.10) by using the analytical solutions of Grigull and Tratz (1965) to estimate the Nusselt and Sherwood numbers for constant wall flux prior to light-off and constant wall temperature after light-off. Their predictions of concentration and temperature profiles for the one and two dimensional models were found to be very close. Thus they concluded that the simpler and less time consuming one-dimensional model is adequate for predicting monolith behaviour.

Kelly et al. (1977), in a one dimensional model, attempted to allow for the effects of wall temperature variation on heat and mass transfer coefficients

by expressing the Nusselt and Sherwood numbers as a function of axial distance, wall temperature, initial gas temperature and initial flow rates. Their model, however, describes high temperature operation and includes homogeneous reaction which is less applicable to the lower temperatures experienced in clean-up devices in the auto-industry.

Houzelot and Villermaux (1976,1977) determined asymptotic values for Sh for fully developed laminar flow in an annular cylindrical reactor in which a first order heterogeneous reaction (the decomposition of ozone) was taking place. Limiting values of Sh were numerically determined and represented by semi-empirical expressions. The additivity relationship of mass transfer resistances in series were applied for the diffusional and chemical contributions to the overall resistance. Experiment and theory was found to be in excellent agreement. The equation is as follows:

$$\frac{1}{Sh_T} = \frac{1}{Sh_m} + \frac{1}{Sh_i} = \frac{1}{Sh^{\infty}_m} + \frac{\theta}{Sh_i} \qquad (2.13)$$

where Sh_T is the overall Sherwood number, Sh_m is the mass transfer limited Sherwood number, Sh_i is the Sherwood due to the reaction, Sh^{∞}_m is the Sherwood number when the chemical reaction is infinitely fast, and θ is the corrective factor.

This is however of limited use and would require extension if it were to describe the variable mass and heat transfer coefficient near the entrance and light off regions of the reactor.

Sundaram and Froment (1979,1980) derived the local Nu for laminar flow and in the absence of reaction from a large number of two dimensional simulations:

$$Nu = 3.655 + 0.145\, z^{-0.778} \exp(-7.158\, z) \qquad (2.14)$$

They proceeded to describe Nu for endothermic reacting conditions, however were unable to do the same for exothermic reactions due to the discontinuity in the Sherwood and Nusselt numbers (refer to figure 2.10) described by Young and Finlayson (1974).

Bennett et al. (1990) performed an experimental investigation and established the following correlation for Sherwood numbers in a monolith for non reacting conditions:

$$Sh = 0.0767 \left(1 + Re\ Sc\ \frac{d}{L} \right)^{0.829} \qquad (2.15)$$

It is envisaged that if light-off occurs at the entrance to the channel the discontinuities predicted at light-off (figure 2.10) shift to the entrance with the result that these overlap the developing profile at the entrance. Thereafter, the flow should develop in the usual way, and therefore the Nu and Sh described for non reacting conditions may be appropriate, with the result that the one dimensional model using known correlations for non-reacting conditions may approach the two dimensional model.

Table 2.2 summarizes the Nu and Sh correlations in pipes and channels with constant wall temperature.

Stevens and Ziegler (1977) developed a plug flow model based on the same assumptions as Votruba (1975a), but included the effects of velocity variation on conversion by means of a momentum balance for the gas phase. The change in gas phase temperature is the major cause of velocity change whereas pressure drop is primarily affected by the frictional losses. In determining velocity and gas phase temperature profiles constant pressure was assumed to be sufficient. Stevens and Ziegler found that neglecting the effects of velocity change with conversion in plug flow solid catalysed reactions can lead to a significant over-estimation of conversion. Therefore they suggest including the momentum balance. However for practical situations with low pressure drop, velocity rises can be taken as essentially proportional to the rise in the absolute temperature. This approach however, is perhaps more acceptable for high temperature situations (above 700°C), where homogeneous reactions are predicted to occur and the effects of property variations may be significant.

England et al. (1987) conducted experiments using diagnostic laser techniques in a catalyst coated tubular wall reactor for weak CO-air mixtures at temperatures near 225°C, to measure velocity and concentration profiles along the length of the reactor. Lasar Doppler Anemometry (LDA) was employed to

Table 2.2 Sherwood and Nusselt numbers for laminar flow in non-reacting tubes

Authors	Sherwood and Nusselt numbers
Hawthorn (1973)	$Sh = \alpha (1 + D\ Re\ Sc \frac{d}{L})^{0.45}$ $Nu = \alpha (1 + D\ Re\ Pr \frac{d}{L})^{0.45}$
Votruba (1975b)	$Sh = 0.705 (Re \frac{d}{L})^{0.43} Sc^{0.56}$ $Nu = 0.571 (Re \frac{d}{L})^{0.67}$
Sundaram and Froment (1979)	$Nu = 3.655 + 0.145\ z^{-0.778} \exp (- 7.158\ z)$
Bennett et al. (1990)	$Sh = 0.0767 (1 + Re\ Sc \frac{d}{L})^{0.829}$
Seider Tate (1936)	$Nu = 1.86 (Re\ Pr \frac{d}{L})^{1/3}$

obtain velocity profiles and Coherent Anti-Stokes Raman Spectroscopy (CARS) was used to measure the concentration of CO_2 at various points along the axis of the reactor. The tube was 1 cm diameter and 15 cm long. Experiments were carried out for flow rates ranging from 75-500 cm^3/min giving on average a Reynolds number at experimental conditions of 13, which is well within the laminar regime. A simple two dimensional model and plug flow model were compared to the data. Since low temperatures were used it was assumed that mass transfer limitation was negligible compared to the intrinsic kinetics. They found good agreement using the two-dimensional model and errors of 15% between the experimental exit conversions and the plug flow model. This may not be surprising, since at low temperatures when the mass transfer limitation is negligible, the errors which may be associated with the Sherwood and Nusselt numbers, for non-reacting conditions, are eliminated.

Hlavecek et al. (1976) describe a model similar to Votruba et al. (1975a), but include radiation effects. They assumed that the reaction took place adiabatically and that the inlet stream was equally divided between each passageway. In their model pore diffusion and axial heat and mass dispersion were neglected. However axial heat conductivity of the solid as well as the radiation effects were considered in their one dimensional model. They experimentally observed a strong autothermal pre-heating caused by radiation. However, they concluded that addition of the radiation term is justified only for temperatures greater than 427°C.

Sinkule and Hlavacek (1978) also extended the model of Votruba (1975a) to include a radiation term. Their model predicted a cooling effect in the solid phase at the entrance and exit of the channel in comparison with a non-radiative model, thus causing a slight shift in the reaction zone and therefore predicting slightly lower values in conversion along the passage. Indeed the effects on the conversion profiles were slight and could be taken as negligible.

Lee and Aris (1977) solved a two dimensional radiation model. They found that the peaks of the Nu and Sh at the reactor entrance and ignition zone were further broadened by radiation. They approximated the effect of radiation in terms of an equivalent thermal conductivity because of the severe computational difficulty involved in solving the radiation model. However, this approximation was not successful, since the predictions were very similar to that of the non-radiation model.

The earlier models implicitly assumed adiabatic reactor operation, neglecting the thermal interactions among adjacent channels and did not consider the radially nonuniform velocity profiles observed in automotive converters. However, in the real situation the flowrate in each channel of the monolith is a strong function of the channels radial position. Lemme and Givens (1974) experimentally measured the radial velocity profiles across the monolith and found that the velocities are much higher in the channels near the centre of the reactor than for channels at the periphery as seen in figure 2.11. This leads to significant radial temperature and concentration gradients, which may severely degrade the performance of the reactor.

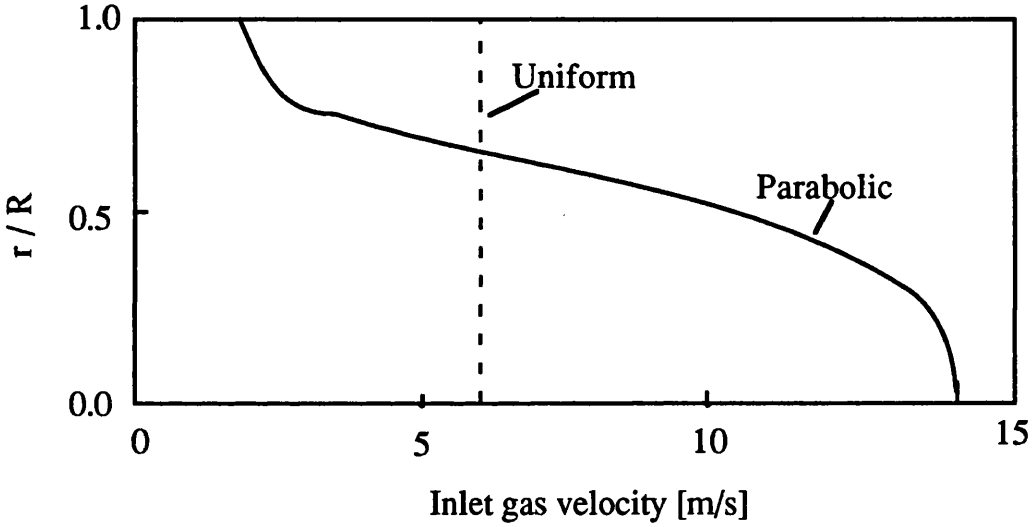

Figure 2.11 Experimentally measured (Howitt and Sekella, 1974) parabolic flow profile across a monolith catalytic converter.

Zygourakis (1989) studied the effects of radially non uniform flow distributions as well as the effects of heat losses in the adiabatic transient operation of monolithic catalysts. The investigation was concerned with the light-off behaviour of fresh and deactivated converters. He solved an axisymmetric two-dimensional model that considered both axial and radial conduction of heat in the substrate, heat transfer between solid and fluid, and chemical reactions occurring in the catalyst layer. His model also included radial thermal conductivities in the monolith walls which were obtained via an equivalent continuum approach. The model included a two dimensional equation in the solid phase but a one dimensional equation for the fluid phase. The effect of developing laminar flow near the entrance of the channels was

accounted for in the Sherwood and Nusselt numbers by varying these with axial distance according to Dennis et al. (1959) series expansion. He concluded that flow nonuniformities may adversely affect the local balance between heat generation and heat convection rates, leading to severe degradation of light-off performance. Model predictions also showed that ambient heat losses only slightly retarded the light-off process, but they could significantly decrease the steady-state conversions. Zygourakis therefore concluded that flow maldistribution effects as well as ambient heat losses should be included in any detailed model as well as developing flow in the channels and diffusional limitations in the catalytic layers and radiation effects as well as the problem of the fluid flow in the expanding conical section before the reactor. Table 2.3 summarizes the heterogeneous models for the monolith.

2.9.2.2 High temperature operation

There has been much work performed in modelling high temperature reactors, usually for afterburners in which temperatures in excess of 427°C are common and therefore include homogeneous reactions. Some of these models will be described for completeness.

Cerkanowicz et al. (1977) based their model on Votruba's (1975) but included homogeneous reactions and allowed for velocity variation caused by temperature variation in the monolith channel. Fluid and transport property variations caused by a large temperature rise can have a significant influence on reactor performance. The model however only incorporated density variation as a function of temperature and neglected other properties including specific heat capacity, viscosity, thermal conductivity and mass diffusivity. These are all functions of temperature and in a high temperature situation would need to be incorporated.

Ahn (1983) extended the model of Cerkanowicz et al. (1977) to include the effects of radiation and to account for the variation in heat and mass transfer coefficients as a result of changes in Reynolds numbers due to changes in gas physical properties along the length of the channel. This was performed for both transient and steady state operation. Ahn found that the radiation and conduction terms significantly affect temperature profiles, however they have

Table 2.3 Heterogeneous monolith models

Authors	Dimension of model	Transient / Steady-state	Complexity of channel arrangement	Heat and mass transfer properties	Fluid properties	Axial conduction in the wall	Radiation effects
Hegedus (1973)	1-D	SS	Single channel	Lumped (constant)	Constant	None	None
Young and Finlayson (1974)	1-D	SS	Single channel	Lumped (constant)	Constant	Yes / No	None
Young and Finlayson (1974)	2-D	Transient and SS	Single channel	Distributed	Constant	Yes / No	None
Votruba et al. (1975a)	1-D	SS	Single channel	Lumped (constant)	Constant	Yes	None
Young and Finlayson (1976)	1-D	SS	Single channel	Lumped (constant)	Constant	Yes / No	None
Young and Finlayson (1976)	2-D and 3-D	SS	single channel	Distributed	Constant	Yes / No	None
Heck et al. (1976)	1-D	SS	Single channel	Lumped (variable)	Constant	None	None

Table 2.3 Contd.

Authors	Dimension of model	Transient / Steady-state	Complexity of channel arrangement	Heat and mass transfer properties	Fluid properties	Axial conduction in the wall	Radiation effects
Heck et al. (1976)	2-D	SS	Single channel	Distributed	Constant	None	None
Hlavacek et al. (1976)	1-D	SS	Single channel	Lumped (constant)	Constant	Yes	Yes / No
Stevens and Ziegler (1977)	1-D	SS	Single channel	Lumped (constant)	Constant	Yes	None
Lee and Aris (1977)	2-D	SS	Single channel	Distributed	Constant	Yes	Yes
Sinkule et al. (1978)	1-D	SS	Single channel	Lumped (constant)	Constant	Yes	Yes
England et al. (1987)	2-D	SS	Single channel	Distributed	Constant	None	None
Zygourakis (1989)	1-D fluid phase; 2-D solid phase	Transient	Thermal interaction	Lumped (variable)	Constant	Yes and radial	None

SS-Steady state
1-D one dimensional model
2-D two dimensional model

little influence on overall conversion. This result is similar to that predicted by Sinkule and Hlavacek (1978).

Albow and Wise (1979) developed a one dimensional model which included both homogeneous and heterogeneous reactions. In this work, catalysed combustion was examined by means of a simplified model which included heat transfer by convection from the tube wall to the gas, by conduction to the surroundings, and by conduction along the tube wall. Transfer coefficients were taken to be constant. Also conduction to the surroundings was assumed to be negligible for ducts in the interior of the monolith where uniform conditions prevail (DeCorso et al., 1977). They assumed ducts near the periphery of the monolith were subject to heat transfer through the duct wall. Heat conduction along the tube wall was found to be important only near the duct entry where temperature gradients are high. Their model compared satisfactorily with the experimental data of Hegedus (1975) when the effect of heat loss from the reactor to the environment was taken into account.

Bensalem et al. (1982) in a purely theoretical study described a one dimensional model for homogeneous and heterogeneous reactions for steady state and plug flow conditions. The model was tested for both laminar and turbulent flow operation. The results however, were mainly concerned with turbulent conditions which are not applicable to the auto-industry.

Phang (1984) developed a two dimensional steady state model under adiabatic conditions which accounted for developing flow and incorporated variable fluid properties. In his approach, Phang compared his model to the plug flow and two-dimensional models with constant properties. Phang's work is significant since he also compared his models directly to experimental data for the oxidation of propane. Overall agreement between experiment and his predicted two dimensional model for exit propane concentrations were ±15%, whereas his plug flow approach predicted ±40% error. He concluded that the high error experienced with the plug flow model was due to the fact that laminar flow is predicted to occur in the channels of the monolith and therefore plug flow assumptions are oversimplified. Also the plug flow model was found to be very sensitive to the choice of Nusselt and Sherwood numbers, and therefore any error in these would affect the final result. It should be noted however, that Phang's work was conducted for high temperature operation

where homogeneous reactions are predicted to occur therefore his findings may not be relevant to low temperature situations.

Crumpton (1988) developed a multi-channel non-adiabatic model, in which the substrate was thought of as being in a ring structure. Mass and energy balances were derived over a discrete section of the reconfigured monolith, in the form of a one dimensional flow equation in the fluid phase. The effects of axial conduction in the solid phase as well as radiation effects were also tested. The predictions were compared to the experimental data of Bennett (1988) and Phang (1984) for the oxidation of propane at inlet bulk gas temperatures of 250-500°C. In general, Crumpton's model tended to overpredict conversions, however the qualitative trends seemed to follow the experiment data. Also Crumpton found that the inclusion of radiation terms were only necessary for monolith operation above 700°C.

The high temperature models are summarized in table 2.4.

2.9.2.3 Multiple steady states

For a highly exothermic reaction taking place in a reactor it is possible for there to be more than one steady state for a given set of inlet conditions (feed temperature, concentration, and flow rate). This is known as multiplicity and is a function of the extent of heat generated from the reaction and the heat removed. This is interesting for catalyst converter design since the transition from an upper steady state where the conversion is near completion, to a lower steady state where the conversion is low, can lead to a large decrease in combustion efficiency.

The appearance of multiple steady states was confirmed experimentally by Hlavacek (1976) for CO oxidation using a monolith. A number of catalysts was tested including Pt, Pd, CuO, MnO_2 etc. Their results showed that for $Pe<900$ multiple steady states exist with only two solutions being stable in the temperature range of 130-200°C and for CO concentrations as low as 1% for Pt.

Many of the models described in the previous section are capable of predicting multiple steady states (Votruba, 1974; Young and Finlayson, 1976; Bensalem, 1982; Lee and Aris, 1977).

Table 2.4 Summary of heterogeneous / homogeneous monolith models

Authors	Dimension of model	Transient / Steady-state	Complexity of channel arrangement	Heat and mass transfer properties	Fluid properties	Axial conduction in the wall	Radiation effects
Kelly et al. (1977)	1-D	SS	Single channel	Lumped [fn [T]]	Variable	Yes	Yes
Cerkanowicz (1977)	1-D	SS	Single channel	Lumped	Variable	Yes	None
Albow and Wise (1979)	1-D	SS	Peripheral and central	Lumped (constant)	Constant	None	None
Bensalem and Ernst (1982)	1-D	SS	Single channel	Lumped (constant)	Variable	None	None
Ahn (1983)	1-D	Transient and SS	Single channel	Lumped [fn (T)]	Variable	Yes	Yes
Phang (1984)	2-D	SS	Single channel	Distributed	Variable	Yes	None
Crumpton (1988)	1-D fluid phase; 2-D solid phase	SS	Thermal interaction	Lumped [fn(T)]	Variable	Yes and radial	Yes

SS-Steady state
1-D one dimensional model
2-D two dimensional model

Indeed the one dimensional models may give rise to an infinite number of steady states, whereas the two dimensional model gives rise to a unique solution. Young and Finlayson (1974) showed in their comparison of one and two dimensional models that the lower steady state profiles of solid and gas temperatures of the one-dimensional model occur when the monolith is heated from an initial low temperature, while the higher steady state profiles are reached when the converter is cooled from an initial high temperature. For intermediate initial temperatures the final steady state may lie between those. The unique profiles for the two-dimensional model are closest to the lower steady state of the one-dimensional model. Therefore they concluded that the two dimensional model is a more realistic model of the monolith. However, if the plug-flow two phase model is perturbed by a small axial conductivity term the infinite number of solutions collapses to three. This is in agreement with their experimental observations (two solutions are stable).

Bensalem et al. (1982) described the transition between the reaction limited region (multi-solution domain) and a mass transfer controlled region (unique solution) by a sharp increase in the wall temperature which characterizes light-off. In his study two physical steady states were predicted. Fuel-air ratio and inlet temperature effects on the catalytic light-off were studied at laminar and turbulent conditions.

CO oxidation has been known to produce unusual behaviours as discussed in section 2.6.2, with no conclusive explanation for these. However, multiple steady states cannot occur in completely mass transfer limited conditions. The present work is concerned mainly with the latter condition.

2.9.2.4 Summary

The following conclusions may be drawn from the discussions above:

1) For ceramic honeycomb converters the Peclet number exceeds 200 and therefore axial heat conduction in the solid phase may be neglected (Votruba et al., 1976),
2) The temperature rises (typically given by Votruba et al.,1975a) in monoliths used in the auto industry are not large enough to initiate gas-phase reactions. Hence, the exclusion of homogeneous reactions is justified as in the models by (Heck et al., 1976; Young and Finlayson, 1976a, etc),

3) It is generally assumed that the fluid properties are constant since the temperature rise is relatively small for low temperature operation ie. no homeogeneous reactions taking place (table2.3),

4) Radiation effects cause the channel solid temperature at the inlet and exit to be reduced and may effect light off, however it is not predicted to be significant for temperatures below 427°C, and therefore for temperatures below this radiation may be neglected (Hlavacek et al.,1976),

5) Pressure drops across monolith reactors are low and therefore the reactor may essentially be thought of as isobaric (Stevens and Ziegler, 1977; Phang, 1984),

6) The adequacy of the one dimensional compared to the two dimensional model is somewhat contradictory in the literature and to a large extent depends on the choice of mass and heat transfer coefficients needed to solve the simpler one dimensional model. However for low temperature operation when mass transfer is not the limiting step the simple plug flow model was found to be adequate (England et al., 1987).

7) The flowrates within the channels of a typical monolith in the auto-industry is well within the laminar regime, with most of the flow being fully developed. Hence, entry length effects are generally insignificant (section 2.9). Consequently, the plug flow assumption may be an over-simplification and indeed may lead to over estimation in conversion (Young and Finlayson, 1976).

8) Thermal interactions and flow maldistributions within monolithic reactors may be important (Crumpton, 1988; Zygourakis, 1989) however these will be neglected in the present approach.

In general, the two dimensional model approach is perhaps more accurate (Young and Finlayson, 1976) however many workers prefer to use the simpler one dimensional approach due to the relative ease in its solution compared to two dimensional models. The work of Heck et al. (1976) indicates that there is little difference between the one and two dimensional models provided the Nusselt and Sherwood numbers are defined correctly.

During actual conditions, the reactor is more likely to be operating in the mass transfer limited regime, therefore if a plug flow model is to be adopted the mass and heat transfer coefficients need to be adequately described under reacting conditions. These coefficients behave unusually at light-off (Young and Finlayson, 1974). Therefore, Hawthorn and other correlations determined under non-reacting conditions may not be suitable. However, if

light-off occurs at the beginning of the reactor a simple Hawthorn or indeed Votruba type correlation for the prediction of Sherwood and Nusselt numbers may be acceptable at reactor conditions. Indeed, Kock (1973) studied mass transport in monoliths for ethylene oxidation and found good agreement between his data and fully developed laminar flow theory when the temperature was high enough for the reaction to be completely mass transfer limited. Some of the correlations for developing flow developed under non reacting conditions will be tested and used in the modelling processes in chapter 8.

The extent to which entry lengths influence flow within a channel or pipe depends on the Reynolds number and diameter of the tube (refer to equation 2.8). Therefore, for small long channels at low Reynolds numbers the entry lengths are short and the flow may be fully developed. However, for larger diameter tubes at the same Reynolds numbers, the entry lengths may become significant. At the immediate entrance to the pipe, there is a flat velocity profile (ie. plug flow). With increasing entry length, this flat velocity profile will be maintained over a larger axial distance, and therefore plug flow may be approximated along more of the pipe. The present study deals with both a relatively large diameter tube as well as the smaller diameter channel. Although in the case of the monolith, fully developed flow is more characteristic, it is envisaged that a one dimensional model will be sufficient as a first approximation as discussed in chapter 8, and will serve as a much better approximation in the case of the larger diameter tubular reactor.

2.9.3 Pressure drop in the monolith

The pressure drop within the catalytic converter is important because of its effect on engine performance. A pressure of 12-20 cm H_2O (1.2-2 kN/m^2) across the converter bed is regarded as the upper limit of acceptability (Wie, 1975).

Essentially, the pressure drop in the monolith converter occurs as a result of "pipe flow losses" in the substrate channels as well as "entrance and exit losses" due to abrupt changes in cross section and is described by Votruba et. al. (1974) as:

$$\Delta P = \Delta P_c + \Delta P_e + \Delta P_f \qquad (2.16)$$

The extent to which the contraction and expansion effects become important depends to a large extent on the ratio of L/d. Thus for a monolith unit 15 cm long under typical operating conditions the ΔP_c and ΔP_e components are negligible in comparison to the frictional losses and may be eliminated from equation 2.16 (Votruba et. al.,1974).

Hegedus (1973) and Votruba (1974) used a simple formula for a conduit, of hydraulic diameter, d, to approximate the frictional pressure drop:

$$\Delta P = f \frac{L}{2 d} (\rho u^2) \qquad (2.17)$$

where f is the length mean value of the friction factor (i.e. Moody's friction factor (1944)). Moody's friction factors are determined for fully developed steady flows and are given for various channel shapes in table 2.1 (p.13).

Friction factor correlations for developing flow within the channels were determined by Hawthorn (1973):

$$f = \frac{\beta}{Re} (1 + 0.0445 \, Re \, \frac{d}{L})^{0.5} \qquad (2.18)$$

where β corresponds to the limiting Moody friction factor for fully developed flow given in table 2.1 for variously shaped ducts.

In the case of segmented monolith systems, Votruba et. al. (1974) described the monolith catalyst structure as essentially a plate containing multiple sharp-edged holes. In an experimental investigation Votruba et. al. (1974) measured pressure drops for monolith segments in series for monolithic structures having the values of L/d in the range 3.75-37.6 and spacings of 0, 10 and 20 mm. The data were correlated for the friction factor by means of a Muhle (1972) type equation for sieve trays. Thus for non-zero spacing, the friction factor was correlated according to:

$$f = N [\frac{64}{Re} \frac{d}{L} + 1.75 (1 - \phi)] \qquad (2.19)$$

where N is the number of monolithic segments and ϕ is the empty cross-section of monolithic matrix, and the value 64 corresponds to the limiting friction factor for a cylindrical channel (ie. β given in table 2.1 for variously shaped ducts). The right hand term (ie. $1.75(1 - \phi)$) in equation 2.19 corresponds to the entrance and expansion losses term, and the left hand term (ie.(64 d/Re L)) corresponds to the fully developed friction term. According to Votruba et al.

(1974), developing flow within the segments was found to be insignificant compared to the entrance and expansion losses, and therefore was not considered in equation 2.19.

2.9.4 The tubular flow reactor with static mixing elements

Since the early 70's, once the advantages of static mixer units began to be realized (especially in the heat exchanger mode), much work has been performed on a variety of configurations.

Two well known designs emerged on the market, these being the Kenics and the Sulzer mixers. Many other mixer designs have since emerged, for example the Ross (Genetti et al., 1982), and the Helax mixers (Kabatek et al., 1989). These devices are static and use the energy of the flowing fluid to promote mixing throughout the cross section of the duct. The Kenics mixer divides and recombines the flow stream reducing the striation thickness by a factor of two or more for each elemental unit of the mixer, and therefore a series combination of these elements can approach homogeneity on a molecular scale (Nauman, 1979). The Sulzer mixer cuts and divides the flow in a reproducible fashion.

Obviously the advantages of these mixers lies in their ability to mix the fluid and therefore increase the mass and heat transfer coefficients radially as well as axially to varying extents depending on the particular designs of the element.

Usually experimental and theoretical data for these well known mixers come in the form of bulletins or research reports dealing mostly with pressure drops and homogenization performance. However, there is only very limited work on the use of static mixers as reactors and in particular there is no published literature concerning the use of these devices in heterogeneous reaction situations. Also, there is no theoretical treatment available in the literature in the case of reacting systems, due to the complicated three dimensional nature of the flow in the mixers. However, there have been some residence time distribution experiments (Nigam et al., 1980, 1985; Kemblowski et al., 1988) and work involved in determining Nusselt and Sherwood numbers. For heterogeneous reactions the residence time distribution work is of limited use, however the Nusselt and Sherwood numbers are useful in determining conversion in static mixer reactors for the simple plug flow approach.

One of the first investigations in which static mixers were used to promote reaction was carried out by Bor (1971), in which he discussed the application of the then new technology for the design of improved plug flow reactors. He proposed using the static mixing devices to promote uniform temperature and concentration profiles across the reactor, in order to achieve ideal behaviour as in plug flow, at low axial velocities when the flow is laminar.

A preliminary investigation was undertaken by Jagadeesh and Satyanarayana on helical tapes (1972) in which the tube was taken to be a reactor. The reaction investigated was the saponification reaction of ethyl acetate and sodium hydroxide. Flowrates of 600-3,200 ml/min were used for the conversion studies and the Reynolds number range covered was 300-6000. The dispersion number, which is characteristic of backmixing during flow, was found to be of the order of 0.01, compared to 0.066 for the empty tube. The conclusion drawn was that even at low flow rates, the flow profile was closer to that of plug flow than in an empty tube.

The starting point in deriving the Sherwood and Nusselt number correlations in the early stages came from the Seider-Tate equation (1936) for the empty tube for fully developed laminar flow:

$$Nu = 1.86 \left(Re\ Pr \frac{d}{L} \right)^{1/3} \qquad (2.20)$$

where d is the diameter of the pipe, and L is the length of the pipe.

Significant improvements in forced convection for heat transfer in tubes fitted with Kenics mixer elements were reported by Grace (1971) for laminar and turbulent flow conditions. Grace suggested that for laminar flow the heat transfer performance of the mixer may be predicted using the equation:

$$Nu = 3.65 + 3.8 \left(Re\ Pr \frac{d}{L} \right)^{1/3} \qquad (2.21)$$

where Re is the Reynolds number evaluated at the bore diameter of the tube as the characteristic length dimension. The experimental scatter in supporting equation 2.21 is ±50%. Details of the fluid used and the nature of the thermal boundary conditions imposed on the tests were not presented. Further, the number and aspect ratio (aspect ratio is the length to diameter ratio of the

element) of the elements used were not quoted. However, a paper by Morris and Benyon (1976) suggests that it is probable that the heat transfer results of Grace were for elements having an aspect ratio of about 1.5.

A paper by Morris and Mission (1974) presents work performed on transfer of Naphthalene from the tube surface to air flowing in the tube for laminar conditions, and using elements with an aspect ratio of 2.5. The following equation is given for the mean Sherwood number:

$$Sh = 1.86\,(1 + 0.32\,N_E)\left(Re_h\,Sc\,\frac{d_h}{L}\right)^{1/3} \qquad (2.22)$$

where Re_h is based on the effective or hydraulic diameter of the pipe with inserts d_h, L is the length of the test section, and N_E is the number of mixer inserts. The equation was developed for 0 to 10 elements and for a Reynolds number between 508 and 1594 for the experimental data to give an error within ±15%.

The Kenics mixer manual (1988) gives a correlation for the laminar regime Re<2000 as:

$$Nu = 4.65\,(Re\,Pr\,\frac{d}{L})^{\frac{1}{3}} \qquad (2.23)$$

It is not stated but this and all the correlations given in this section are most probably determined for the static mixers placed end to end. For laminar flow, the Nusselt number obtained for the Kenics mixer is 2.5 to 3 times the empty tube Nusselt number, thus the conservative Kenics Nusselt is:

$$Nu_{KM} = 2.5\,Nu_{ET} \quad \text{(laminar flow)} \qquad (2.24)$$

Thus the Kenics mixer is predicted to enhance the overall heat transfer by 250 to 300% compared to an empty pipe.

Correlations for the Sulzer mixer seem to be even more sketchy. However, a correlation is put forward by the makers of the SMX Sulzer (1987):

$$Nu_{Slz} = 2.6\,(Re\ Pr)^{0.35}\left(\frac{Pr}{Pr_w}\right)^{0.14} \qquad (2.25)$$

where Pr_w is the pipe wall Prandtl number.

A comparison of the Sherwood and Nusselt numbers for the Kenics and Nusselt number for the Sulzer is given in table 2.5. It can be seen that these are described for different conditions of operation and indeed in some cases the conditions are not given. It should be noted that nowhere in the the literature are Nusselt and Sherwood numbers related to mixer spacing. This is probably because typically these mixing devices are used by placing them end to end and therefore in the conventional mode of operation spacing is not a factor. However, in the present context the spacing of the mixers is taken into consideration, as discussed in chapter 8.

The Active Transport Catalytic Reactor (ATCR) consists of a metal tube coated with catalyst with mixing elements inserted into this. Nauman (1979) suggested that in order to maximize the driving potential for heat transfer, flow inverters could be used to interchange material between the centerline and the walls. A star and orifice type flow inverter was designed in the Chemical Engineering Department (U.C.L), described in further detail in chapter 7. Although the ATCR helps in improving mass transfer to the walls of the reactor it also experiences an axial pressure decrease due to friction with the walls as well as the elements of the static mixer.

An interesting study was carried out by Nauman (1982), in which he used residence time distributions (Nauman, 1979) to model a first order reaction to determine reaction yields for flow inverters. In the approximate analysis, the actual mixing process was treated as though it were confined to a few isolated planes. The overall reactor was modelled as an open tube with velocity, temperature, and composition profiles which were undisturbed except at the mixing planes where complete mixing in the radial direction was assumed. This assumption may be reasonable in the case of flow inversion where the maximum extent of mixing occurs. This work however, is of limited

Table 2.5 Comparison of Nusselt and Sherwood numbers for the Kenics and Sulzer mixers

Mixer type	Nu or Sh	Re range	N_E range	Aspect Ratio	Author
Kenics	$Nu = 3.65 + 3.8\,(Re\,Pr\,\frac{d}{L})^{1/3}$	Re < 2000	—	1.5	Grace (1971)
Kenics	$Sh = 1.86\,(1 + 0.32\,N_E)\left(Re_h\,Sc\,\frac{d_h}{L}\right)^{1/3}$	508-1594	0-10	2.5	Morris et al. (1974)
Kenics	$Nu = 4.65\,(Re\,Pr\,\frac{d}{L})^{\frac{1}{3}}$	Re < 2000	$N_E > 20$	1.5-2	Kenics Manual (1988)
Sulzer SMX	$Nu_{Slz} = 2.6\,(Re\,Pr)^{0.35}\left(\frac{Pr}{Pr_w}\right)^{0.14}$	Re < 2000	—	—	Sulzer Manual (1987)

use since the use of residence time distributions in order to model reaction yields is restricted to first order homogeneous reactions and therefore cannot be used for heterogeneous reaction systems.

Dudukovic et al. (1979) performed experiments using disks placed coaxially in a cylindrical 6 cm diameter tube. The local mass transfer coefficients were measured using the adsorption method of Koncar-Djurdjevic (1949, 1977) as well as pressure drops. They discovered that when two disks were placed close to each other they behaved essentially as one in terms of Sherwood number, as shown in figure 2.11a. As the distance between the disks is increased as shown in figure 2.11b it can be seen that the first disk forms its own wake but its effective length is affected by the presence of the second. For increased distances each disk behaves independently. Experiments were performed for a Reynolds number of 47,400, however Dudukovic suggested that the same phenomena would be present for the characteristic distances at different Reynolds numbers and different ratios of objects and tube diameters, although the local Sherwood number would differ. These results describe the phenomenon of "redevelopment" after a disturbance and suggest that there is an optimum distance at which to separate the disturbances for there to be the highest overall Sherwood number for the lowest pressure drop.

2.9.5 Pressure drop across the tubular and static mixer reactors

The main purpose of static mixers are obviously to disturb the flow and improve mixing. However, in reality this is often accompanied by an increase in drag across the mixing device with the result that there is increased pressure drop. The latter effect may become important in areas such as polymer engineering and bioengineering, when the pressure drop may need to minimized. Pressure drops in static mixing devices depend on the configuration of the elements. There has been a considerable amount of research involving mixer design to achieve maximum mixer efficiency with the least pressure drop.

Smithberg and Landis (1964) observed that the frictional losses in a continuous twisted tape were due to the axial flow losses, tangential flow losses, and vortex losses as well as the abrupt changes in the velocity vector at adjacent elements.

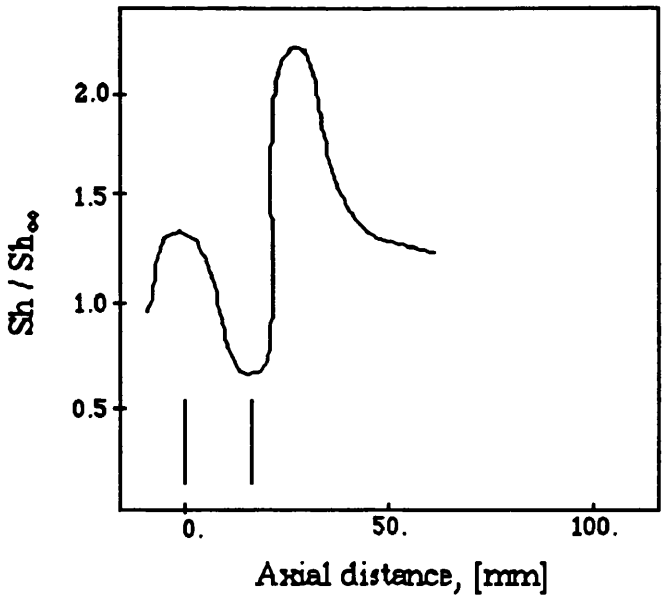

(a)

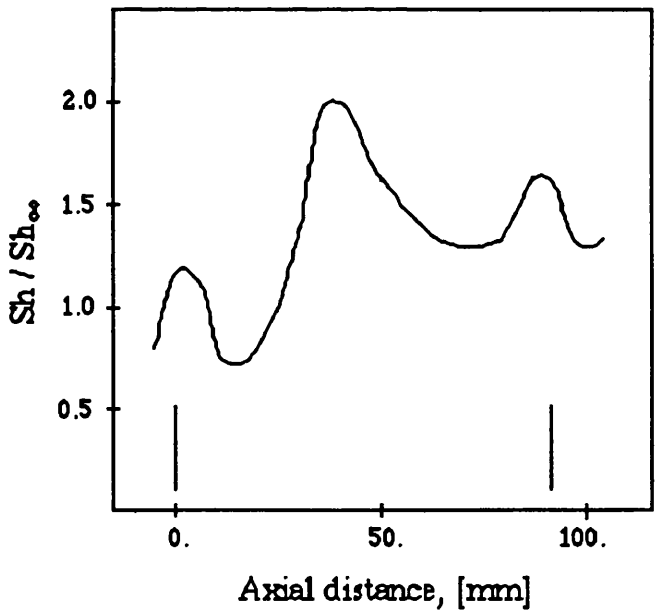

(b)

Figure 2.11 Local Sherwood number as a function of distance for a) small separation between discs, b) large disc separation (Dudukovic et al., 1979)

There are two methods of expressing pressure drop within a mixing device. The first is similar to that for an empty pipe :

$$\Delta P_{Mix} = f_{SM} \frac{\rho u^2}{2} N_E \frac{L_E}{d} \qquad (2.26)$$

where f_{SM} is the friction factor dependant on the mixer geometry as well as the aspect ratio (L_E/d), L_E is the length of a mixing element, and N_E is the total number of mixers in series. The friction factor or Newton number can be expressed as:

$$f_{SM} = A' + \frac{B'}{Re} \qquad (2.27)$$

where A' and B' are constants depending on the type of mixer used, and the Re is based on the empty pipe diameter.

The second method is in terms of a factor K (where K is the pressure drop across the mixer/the pressure drop over the empty tube) which is a function of the geometry of the mixer, the ratio L_E/d as well the Re. Thus:

$$\Delta P_{Mix} = \Delta P_{ET} K \qquad (2.28)$$

where ΔP_{ET} is the empty tube pressure drop when no mixers are present.

Much work has been performed in determining the friction factors and K factors for the various mixer types. However much of it is for limited and narrow Re ranges and mixer aspect ratios.

Table 2.6 gives a summary of the various friction factors for the Kenics and Sulzer mixers for laminar flow in tubes found in the literature. Table 2.7 gives a summary of the K factors for the Kenics mixers.

Table 2.6 Comparison of drag coefficient correlations for Kenics and Sulzer mixers

Mixer type	L_E / d	f_{SM}	Re range	N_E range	Authors
Kenics	1.5	$2 + 460/Re$	0.1-1000	—	Wilkinson et. al. (1977)
	2.0	1.35+342/Re	0.01-10,000	12-24	Sir (1980)
	2.5	$12.6\ Re_h^{-0.5}$	Re < 2000	2-10	Morris and Misson (1974)
Sulzer SMX		62.27+1195/Re	0.2-20	—	Prikop (1982)
		5.1 + 1100/Re	Re < 2000	—	Sulzer Manual (1987)

Table 2.7 K factors for different flow ranges for the Kenics mixer

Mixer type	L_E / d	K	Re range	N_E range	Authors
Kenics	1.5	$K = 3.24\ (1.5 + 0.21\sqrt{Re})$	Re < 2000	—	Grace (1971)
Kenics	3.15	$K=2.03\ Re^{3/8}$	10-1000	21	Genetti (1982)
Kenics	2.0	$K=5.34+0.0211Re$	0.01-10000	12-24	Sir and Lecjaks (1982)

CHAPTER 3

PRELIMINARY EXPERIMENTAL SET-UP AND INVESTIGATION

3.1 Introduction

Experimental work began with an initial experimental set-up designed to investigate the axial and radial temperature profiles within a monolith reactor during the oxidation of carbon monoxide.

The monolith cores were supplied by Johnson Matthey Ltd., and carbon monoxide and oxygen concentrations were in the ratio of 1 % and 2 % (vol %) respectively, for an inlet temperature of 400°C and a Reynolds number range of 44-101 (at 400°C).

The purpose of this chapter is to describe the apparatus and the experimental procedures, as well as the results.

3.2.1 Apparatus

On embarking upon the project, the objective was to keep the apparatus as simple as possible, bearing in mind the requirements of the work. A photograph of the arrangement is shown in figure 3.1, and a schematic diagram of the apparatus is shown in figure 3.2.

Essentially, the process involved supplying a synthetic gas made-up of carbon monoxide, oxygen and nitrogen in known proportions, preheating this to a required temperature and then reacting over the monolith.

The experimental test section consisted of a 15 cm by 1.5 cm Fecralloy tube into which the monolith core could be inserted. This was built in a fume cupboard for safety reasons. The gases passed through flow controllers supplied by Platon Ltd. for nitrogen control (type MNAH), and Brooks Ltd. for carbon monoxide (type 8744-0.05 to 24 L/hr air) and oxygen (type 8944-440 to 2200 L/hr) control respectivly. The flowrates were measured using rotameters with pressure gauges at the outlet, for calibration purposes. Calibration charts were supplied for air at standard operating conditions. In order to measure the flowrate for carbon monoxide for example, the rotameter reading as well as the pressure gauge readings were noted at actual conditions and using the

Fig. 3.1 Photograph of the preliminary experimental set-up

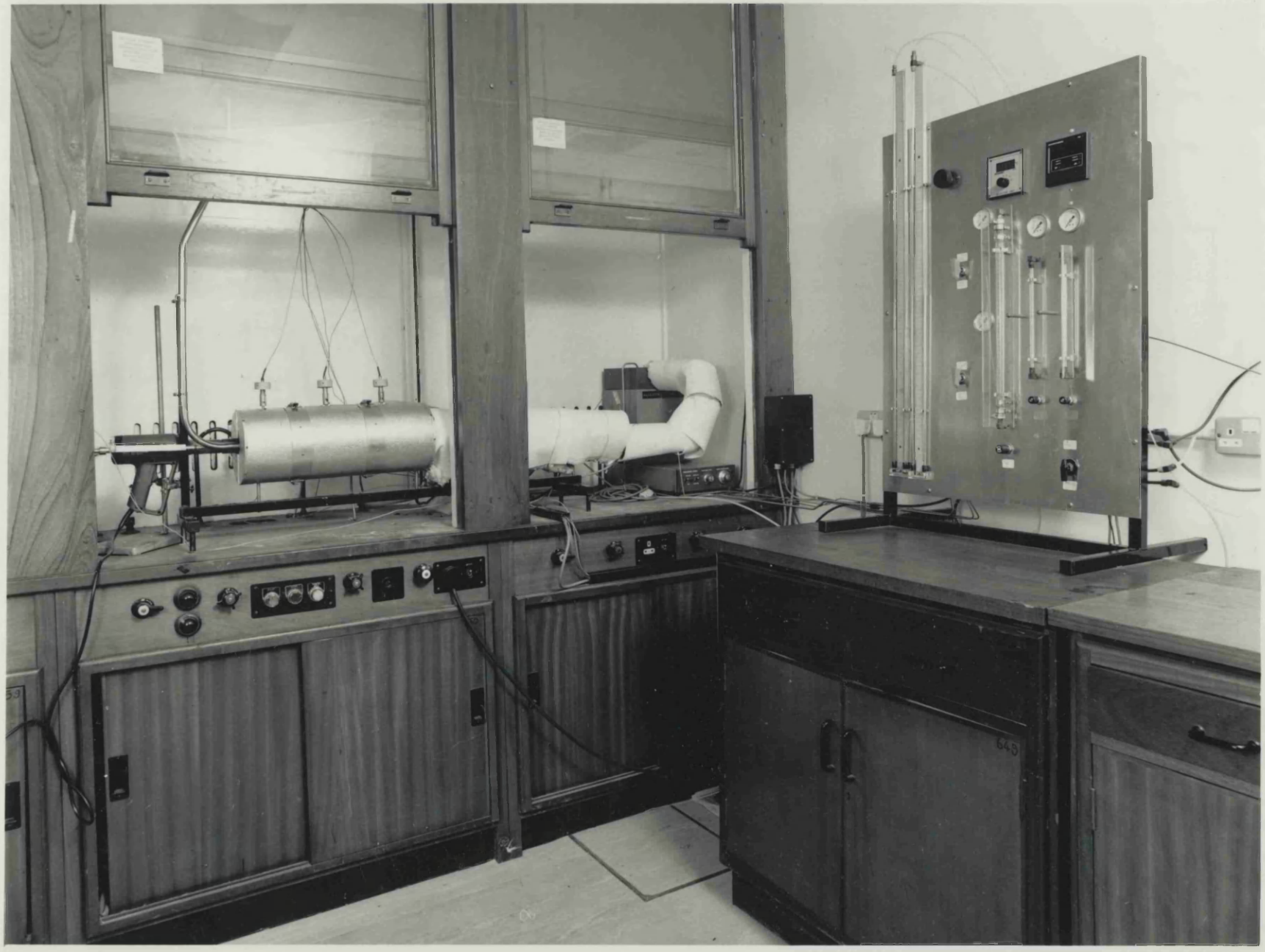

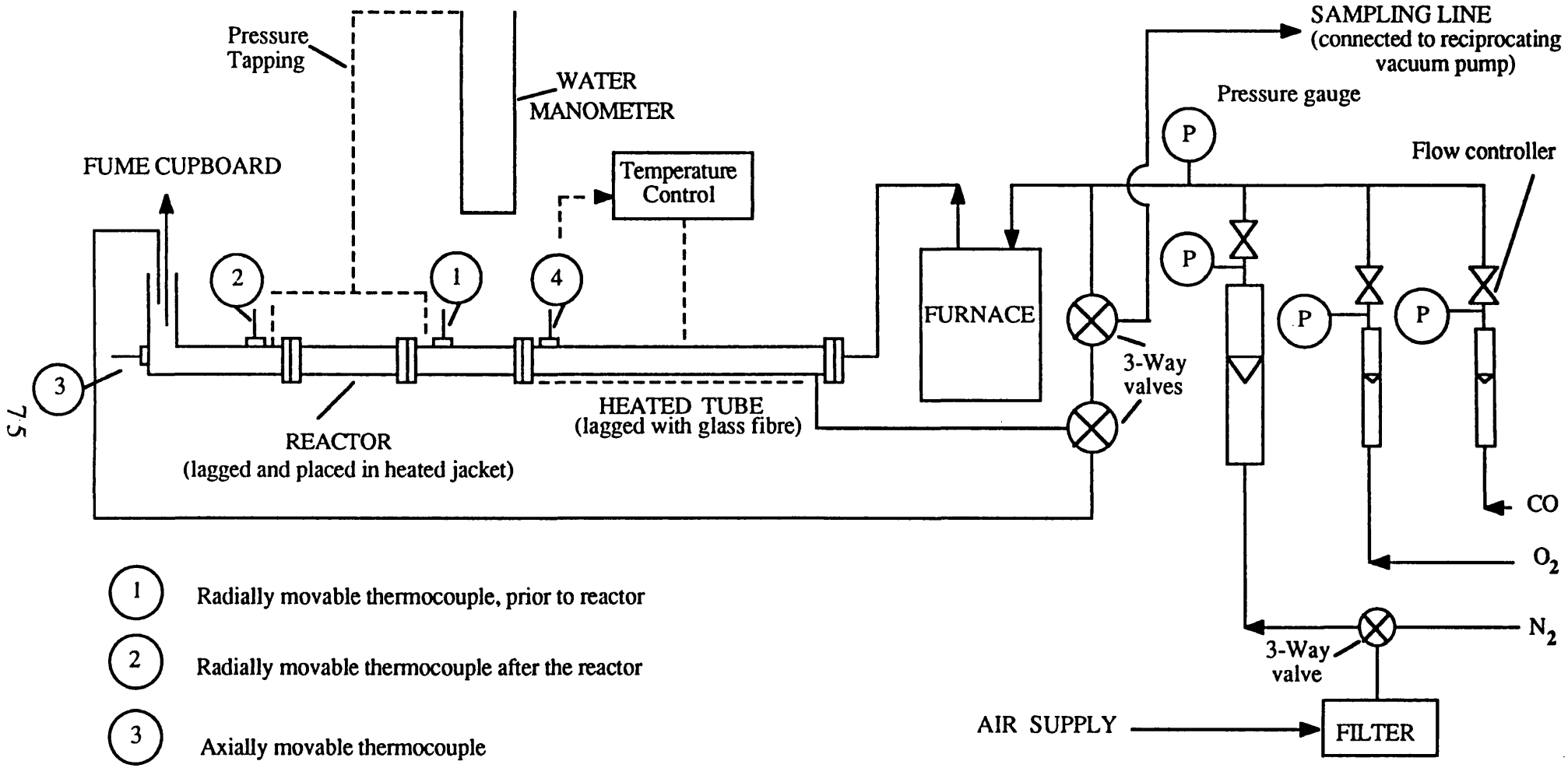

Fig. 3.2 Preliminary experimental setup (not to scale)

calibration charts for air the flowrate of CO gas at STP was calculated using equation 3.1 (Brooks manual, 1986):

$$(F_{CO})_{STP} = (F_{Air})_{STP}\sqrt{\frac{(\rho_{Air})_{STP}\, T_{STP}\, P_{Actual}}{(\rho_{CO})_{STP}\, T_{Actual}\, P_{STP}}} \qquad (3.1)$$

In order to conserve bottled nitrogen gas, preheating was performed using air as this could be supplied on tap. However, prior to its entry to the equipment it was first cleaned by removing any impurities including oil and water using a particulate filter.

The pre-heater consisted of a furnace and a 91 cm pipe of internal diameter 1.5 cm wrapped with a heating tape connected to a feedback controller (microprocessor based 3-term controller, type 810, by Eurotherm), in order to regulate the temperature of the gases entering the reactor. The flexible heating tape was supplied by Electrothermal Engineering limited (type HC 105) and had an outside diameter of 5 mm. It was 4.88 m in length and provided 960 watts with a surface loading of up to 4 W/cm^2.

The thermocouples consisted of 0.5 mm diameter stainless steel sheathed chromel-alumel (type K) elements supplied by Labfacility Ltd. These were placed in various locations as shown in figure 3.2. Three were arranged to traverse radially across the diameter of the pipe. One was placed after the pre-heater, to control the inlet temperature of the gases, and the others at the entrance and at the exit of the reactor. An axially traversing thermocouple was passed through a central channel within the monolith, to measure the temperature along its length.

A detailed diagram of a radially traversing thermocouple is given in figure 3.3. Obviously, during operation, the reactor runs very hot at around 400°C. Hence each of the rotating scales of the traversing thermocouple was encased in a Sindanyo (concrete asbestos) sheath of approximatly 5 cm thickness, in order to reduce the heat transfer from the metallic sheath to the experimenter. In reality, even this was found to be inadequate, and hence thick leather gloves were also required.

It was first envisaged that lagging the reactor test section would be enough to limit heat losses to the surroundings to within 10°C. However, on experimentation it was found that with lagging (7 cm thick) alone, a temperature loss of up to 100°C resulted along the length of the reactor. Therefore, in an attempt to limit this heat loss a heated jacket, which consisted

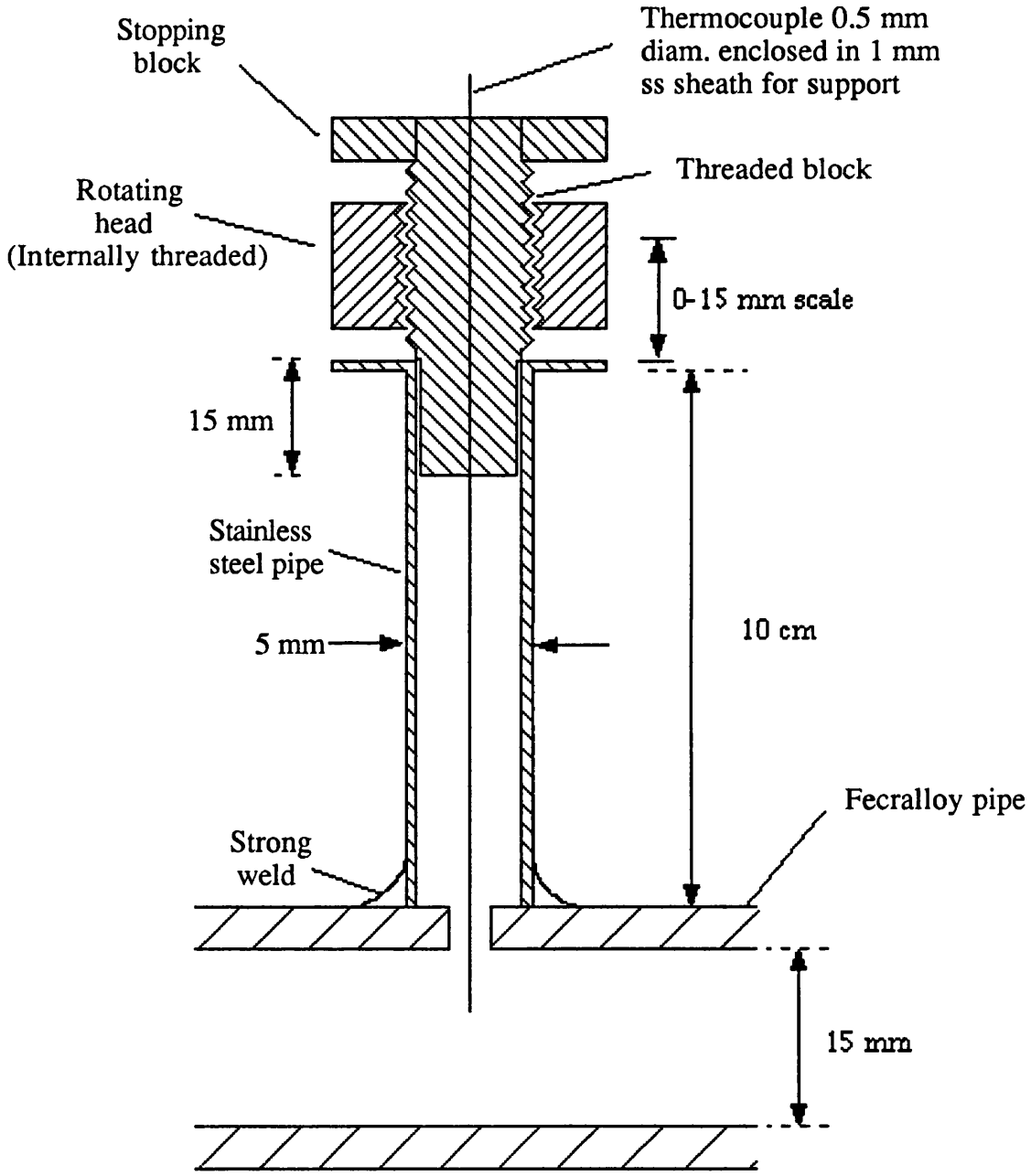

Fig. 3.3 Thermocouple design (not to scale)

of a metal cover lagged with high temperature glass fibre insulation, heated at one side with an air gun (Bosch type PHG 560E, for air flowrate of 500 L/min and outlet temperature of 100-560°C) was used. The jacket allowed easy access to the traversing thermocouples as indicated in figure 3.1.

Figure 3.4 shows a detailed section through the reactor and end pipe giving the dimensions as well as indicating the location of the heated jacket.

The calibration of the thermocouples was tested by inserting them into ice at zero °C and in pure boiling glycerol at a temperature of 290°C. In all cases the thermocouple calibration was found to be accurate to within ± 1-3°C.

Pressure drops were measured using a water manometer connected to the inlet and outlet of the reactor.

A CO detector alarm described in further detail in chapter 4 (table 4.1) was used to detect any leakage of this toxic gas.

3.2.2 Gas analysis

Initially a Perkin-Elmer gas chromatograph was used. It was fitted with two columns including a silica gel column for the separation of carbon monoxide and carbon dioxide and a molecular sieve column to separate oxygen and nitrogen in the outlet gases. Helium gas was used as the carrier. A four port column switching valve (of the GSV series by Negretti and Zambra Ltd.) was used for the sampling and separation processes. The latter was achieved by passing the sample through the columns which were placed in series, with the half meter silica gel first followed by a two meter 5 Å molecular sieve. The columns were connected to the four port valve so that the molecular sieve column could either be switched in or out of the carrier gas path. At normal temperatures silica gel can separate carbon monoxide and carbon dioxide by preferentially adsorbing these to varying extents. The gases nitrogen, oxygen and carbon monoxide were allowed to exit the first column and enter the second, at which time the valve was switched over and the gas chromatograph temperature raised to 160°C so that CO_2 could be eluted and the successive quantitative analysis could proceed. The valve was then switched over for the elution of the rest of the samples, ie CO, oxygen and nitrogen.

At the start of the experimentation, integration of the chromatograph peaks was performed with an apple computer using a program called "Chromatochart". This however proved to be inadequate since the integration

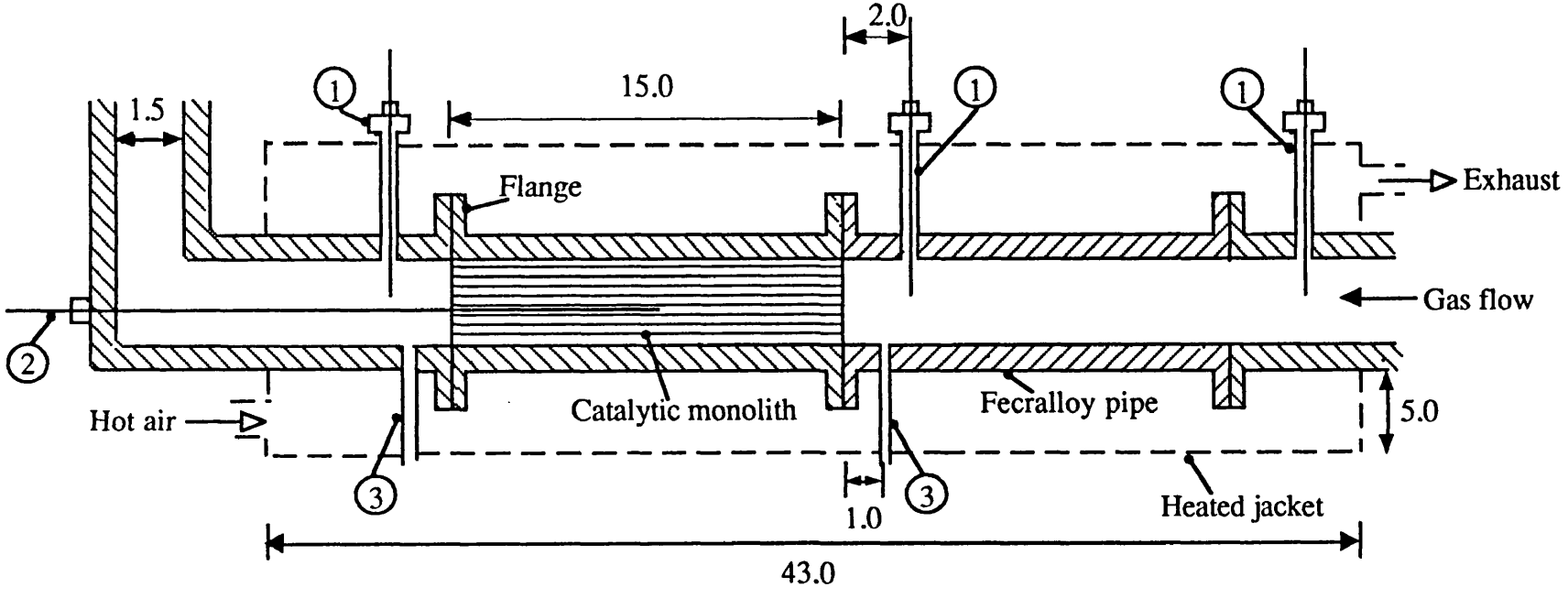

All dimensions are given in cm

① Radially movable thermocouple

② Axially movable thermocouple

③ Pressure tapping

Figure 3.4 Section through reactor and end pipe (Not to scale)

process was unreliable. Therefore a number of alternative techniques were attempted. These included using a digitizer to measure the area under the curve produced on a chart recorder, weighing the paper corresponding to areas under the curve, and by passing the sample through a continuous flow infrared detector.

A comparison was made between the various methods shown in table 3.1. The Chromatochart package gave unreliable results with errors of up 75 %. This was due to the wide variation in gas concentrations (i.e. nitrogen 98 %, CO 1 % and oxygen 2 %) and therefore the program was unable to resolve the peak areas. Hence this method was not up to the required accuracy standards. The weighing technique and digitizer methods although acceptable were cumbersome. Finally it was decided to abandon the gas chromatograph analysis due to the inadequacies of the integration techniques in favour of the continuous flow infrared detector. This is discussed in further detail in section 4.2.6 of chapter 4.

3.3 Monolith Channel Size and Geometry

The size of the channels was measured using two techniques:

i) Enlarging a photograph of the monolith cross section with a scale along its length. The size of the channel could be measured directly.
ii) Using a traversing microscope.

The most accurate method was found using the latter approach. The actual hydraulic diameter of a channel was found by averaging the length measured for the random selection of 25 channels. From these data the average hydraulic diameter of a channel was found to be 1.04 mm $\pm$ 0.02.

Channel shape is important since it effects the calculation of the following:

(i) external catalyst surface area,
(ii) the voidage, for fixed number of cells per unit surface area, which in turn effects the calculation of velocity within the channels,
(iii) friction factors, which are a function of channel shape and size (refer to table 2.1)

Table 3.1 Comparison of various techniques to establish the inlet composition of reactants.

Substance	Rotameter Input Comp. (%)	Weighed Sample		Digitizer Sample		Chromato-chart Sample		Infra-red Detector Sample	
		Comp. %	% error	Comp. %	% error	Comp. %	% error	Comp. %	% error
N_2	97.2	97.6	0.41	97.5	0.3	98.5	1.33	–	–
O_2	1.89	1.55	8.0	1.76	6.9	0.46	75.7	–	–
CO	0.93	0.86	7.5	0.84	9.7	1.09	17.2	0.93	0.0
N_2	97.0	97.2	0.2	97.2	0.2	96.9	0.1	–	–
O_2	2.02	1.80	10.9	1.77	12.4	2.04	1.0	–	–
CO	1.02	1.03	1.0	1.04	1.96	1.01	0.98	1.01	1.0
N_2	96.9	97.1	0.2	97.1	0.2	98.0	1.1	–	–
O_2	2.02	1.79	11.4	1.79	11.4	1.5	25.7	–	–
CO	1.02	1.07	5.0	1.07	5.9	0.82	19.6	0.98	3.9

(vi) Nusselt and Sherwood numbers according to Hawthorn (refer to table 2.2)

The original shape of the support channel used in this study is square, however on coating with γ-alumina, the edges may become rounded, and some channels look circular. Indeed this can be seen in figure 3.5 (a and b) using an electron microscope, where both shapes are observed on the catalyst coated support. For fixed channel size and cell density, the calculation of voidage may alter by as much as 25 % between a square and circular channel shape. On average however, the shapes of the monolith support cells appear square with rounded corners. This produces an average error of 8 % in the calculation of voidage for a square compared to a square channel with rounded corners. However, this error is insignificant if it is compared to the error in the calculation of the voidage associated with the uncertainty in the channel size ie. 18 %. Therefore for the purposes of this work, the channel shape was assumed to be square, and hence all calculations of surface area, etc. of the catalyst will assume this shape.

3.4 Procedures

Prior to all experimental work the extraction fan and fume cupboards were switched on as well as the CO detector alarm. These were carried out in accordance with safety procedures for toxic gases:

1) Leak check and purge equipment with dry inert gas before use.
2) Containers should be in open air as well as in a forced ventilated room.
3) All equipment where there is a possibility of electrostatic charge should be earthed.
4) Low concentrations of carbon monoxide are fatal (as low as 4000 ppm) therefore a CO detector alarm for concentrations in the range 0-250 ppm is required.

Prior to experimental investigations, the monolith required pre-treatment as discussed in chapter 4 (section 4.3). This was in order to acquire constant catalytic activity throughout the experimental testing.

At the start of the experiment, air was passed through the apparatus and the furnace as well as the heating tape were switched on to allow for the warm

(a)

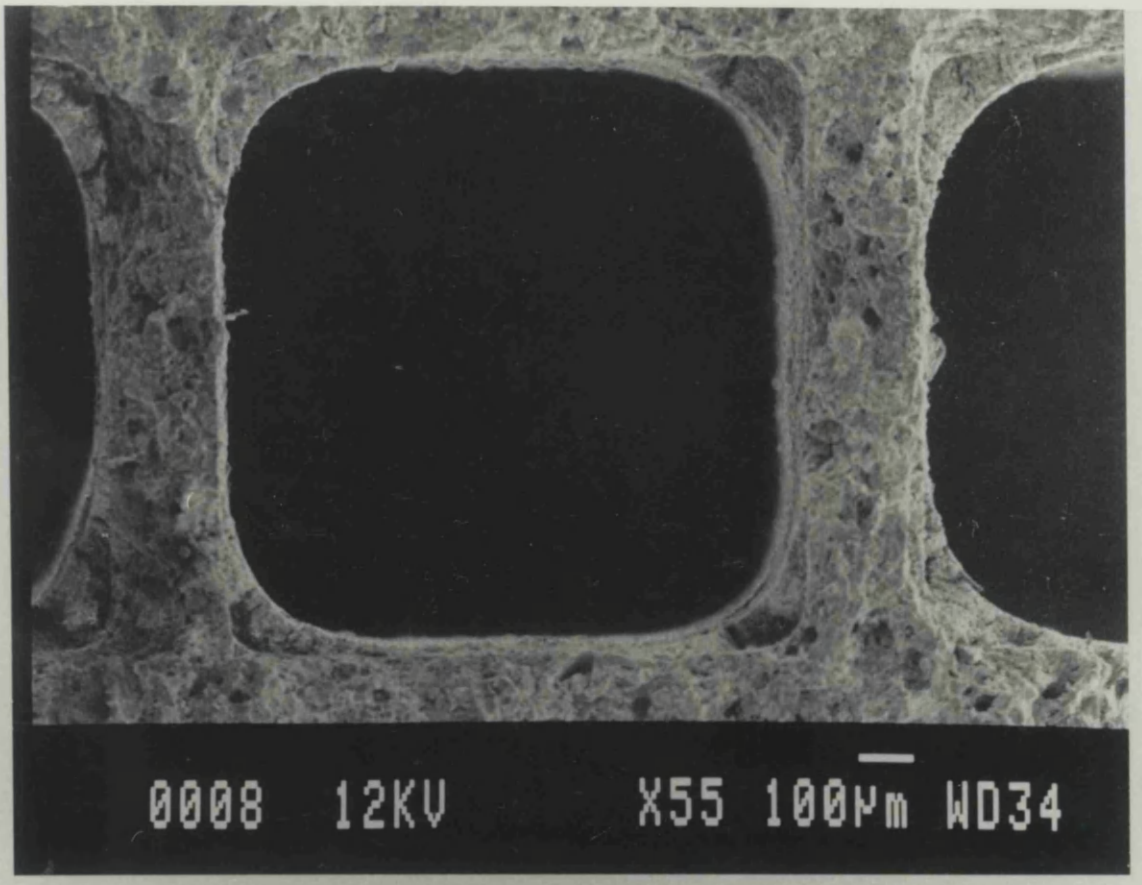

Fig. 3.5 Photograph of channel shapes within a monolith sample
a) square shape with rounded corners, b) cylindrical shape

(b)

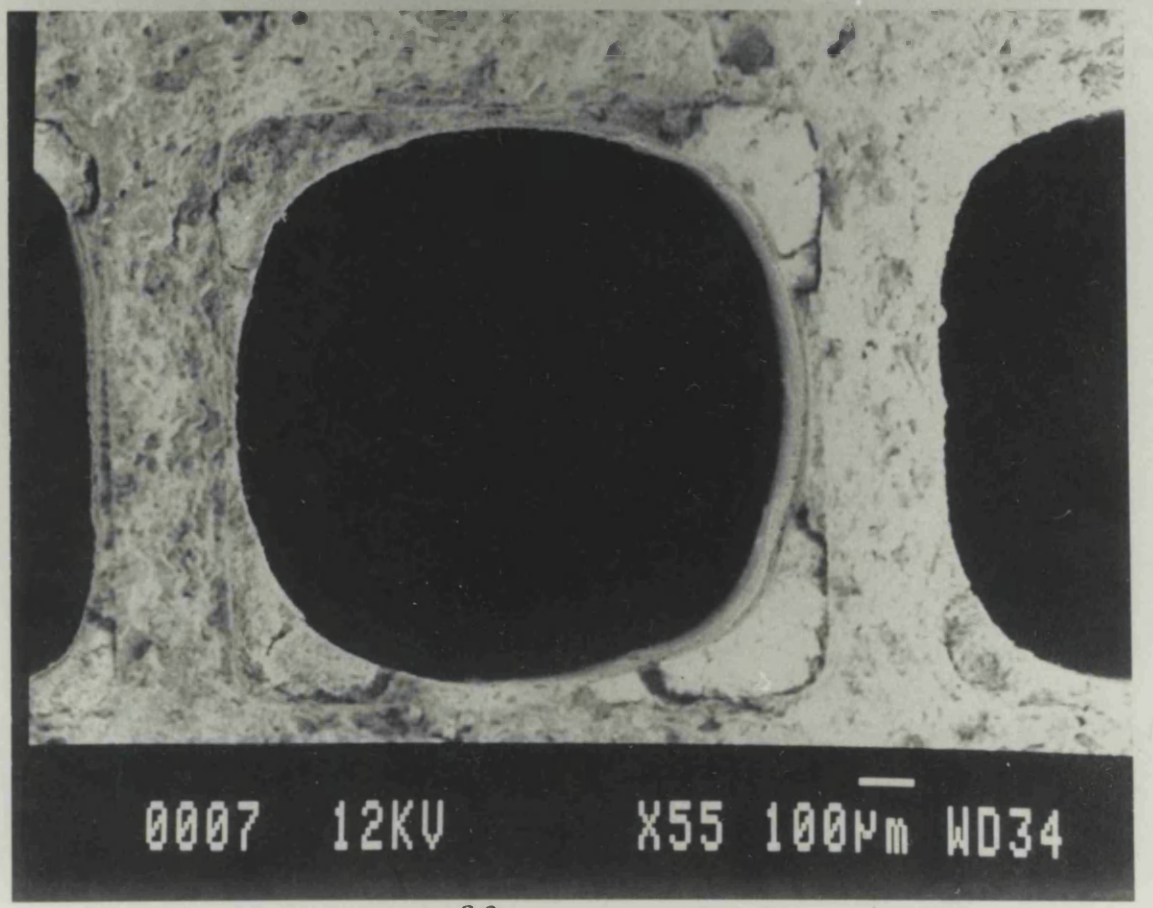

up of the reactor to 400°C. Once a steady state temperature had been reached, usually after approximately half an hour, the CO and oxygen flow rates were set. A constant proportion of the three gases CO, O_2 and N_2 in the ratio of 1 %, 2 % and 97 % (by vol) respectively was always used. These were set using the flow controllers and the corresponding flow was measured using rotameters.

3.5 Results and Discussion

The monolith tested in this study consisted of a 15 cm long core sample of diameter 1.45 cm. Further details of the monolith properties are presented in table B.1 in appendix B.

Prior to reaction, air at 400°C was passed in order to heat the monolith system. Figure 3.6 is a typical plot of the radial temperature profile across the diameter of the tube both before and after the reactor, for an air flowrate of 16.24 L/min (STP) at steady state non-reacting conditions. The heating tape was set to control at 400°C using thermocouple 4, in figure 3.2, at the centre of the tube. The reactor exterior surface temperature was also measured and corresponded to the heating jacket temperature. This was set at 400°C, and controlled to within ±5°C of this value. It can be seen in figure 3.6 that the inlet radial temperature is controlling to within ±5°C of this set value, with a definite loss of temperature at the top of the pipe near the thermocouple shaft. Thus the thermocouple is acting as a heat sink directing heat losses along its shaft to the surroundings ie. the laboratory air. The exiting radial profile, however is more uniform although an average of 3°C lower than the inlet temperature.

Figure 3.7 shows the axial profile along a central channel of the monolith for the same non reacting conditions as in figure 3.6. Since the thermocouple may have been touching the walls of the channel it could be assumed that it measured the monolith channel surface temperature.

In figure 3.7 the axial temperature seems to be isothermal on average to within 5°C of the controlling temperature (ie. 400°C). In general, the exit temperature reading of the axial thermocouple should read approximately the same as the centre line pipe reading of the radial exit thermocouple for non reacting conditions. However in practice it reads approximately 5°C higher. This is probably due to the fact that the radial thermocouple is 2 cm away from the exit of the monolith and therefore some loss of heat to the surroundings is

Fig. 3.6 Radial air temperature profile,upstream and downstream of monolith, prior to reaction

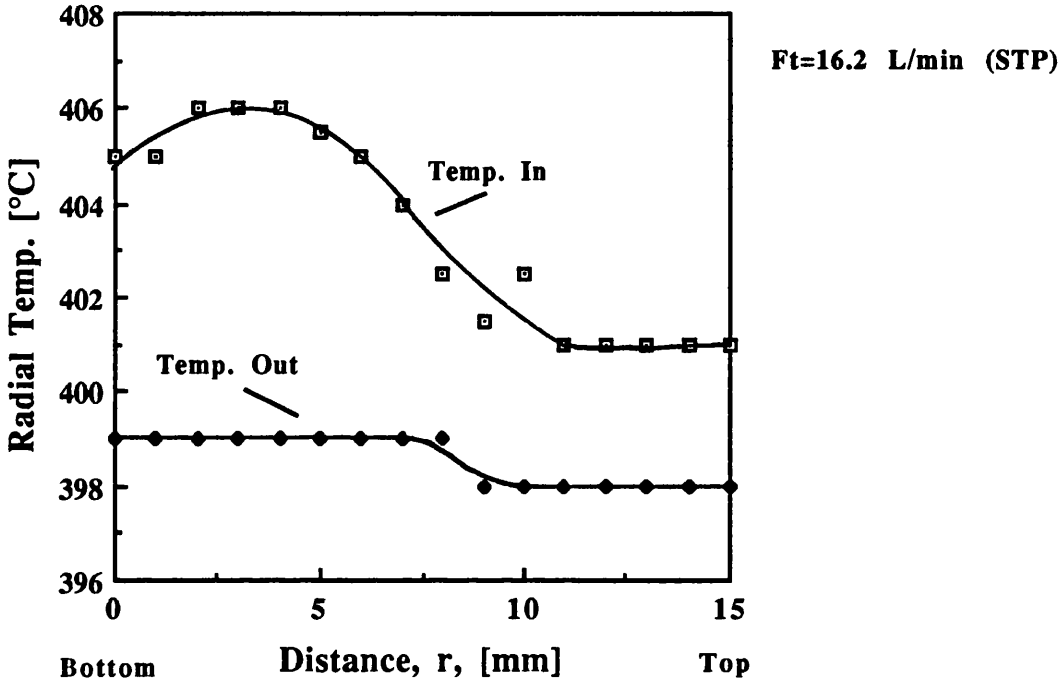

Fig. 3.7 Axial temperature along monolith channel, prior to reaction for Ft=16.2 L/min (STP)

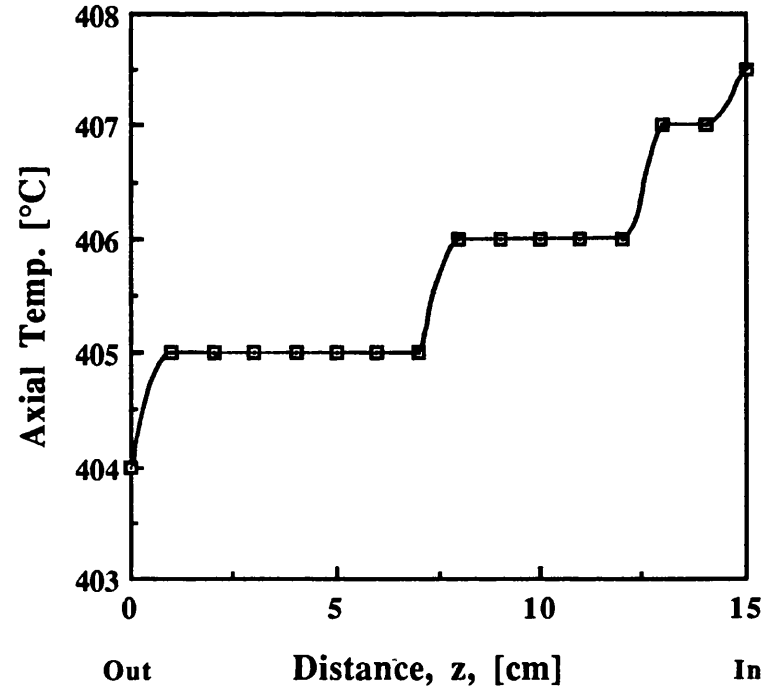

occurring whereas the axial thermocouple is measuring the exit temperature directly at the end of the monolith channel.

During reaction, once there is light-off, heat is generated at the catalytic surface. At steady state, this heat is transferred either to the bulk gases or lost to the surroundings. Thus the gases exiting the monolith under reacting conditions should be hotter than those entering. This can be seen in figure 3.8, for a reacting mixture consisting of 1% CO, 2% oxygen and 97 % nitrogen at a flowrate of 16.24 L/min (STP).The Re within each channel based on the inlet temperature of 400°C corresponds 91.2, and is therefore definitely in the laminar regime. The conversion under steady state conditions was found to be 95.8 %. The radial inlet temperature seems to be fairly uniform at 400°C ±5°C. The outlet radial temperature profile on the other hand, shows a maximum temperature rise of approximately 50°C, and seems to peak at around 5 mm from the bottom of the monolith. The gases, prior to entering the monolith are fully developed and in the laminar regime. Hence, the velocity of the gases entering the monolith reactor should be fastest in the centrally placed channels, (Howitt and Sekella, 1974). The extent of reaction is a function of the flow within each channel. One may expect that as the flowrate is increased the conversion should fall as a result of reduced residence time. Hence it may be expected that the extent of conversion should be lowest within the centrally placed channels compared to the peripheral, and therefore the corresponding temperature rise between the inlet and outlet gases, for an adiabatic reactor, to be greater in the peripheral channels. However, the exiting radial temperature profile of figure 3.8 shows that the temperature rise is greatest towards the centre of the monolith. In reality it is very rare for a reactor to be completely adiabatic, and heat losses to the surroundings are inevitable. Indeed, this was found to be the case during the experimental investigation. The fact that there is a greater temperature loss at the top of the pipe for the exiting temperature profile indicates that the radial thermocouple and its housing acts as a heat sink, conducting heat away along the housing shaft and then to the surroundings (ie. laboratory air) by convection. The expected adiabatic temperature rise of 88.8°C based on the exiting conversion (ie. 95.8 %) is indicated in figure 3.8, and corresponds to a heat production of 33.8 Watts. For an average outlet radial temperature of 437.8°C, the extent of heat losses can be calculated to be 19.85 Watts. This shows that up to 60 % of the heat is being lost, due mainly to the peripheral thermocouples. In real catalyst exhaust situations, there is indeed heat loss to the surroundings, with the result that the centrally placed channels within the monolith are hotter than those at the periphery (Albow and Wise,

Fig.3.8 Radial temperature profiles across the pipe before and after the monolith, for a reacting mixture for Tin=400°C

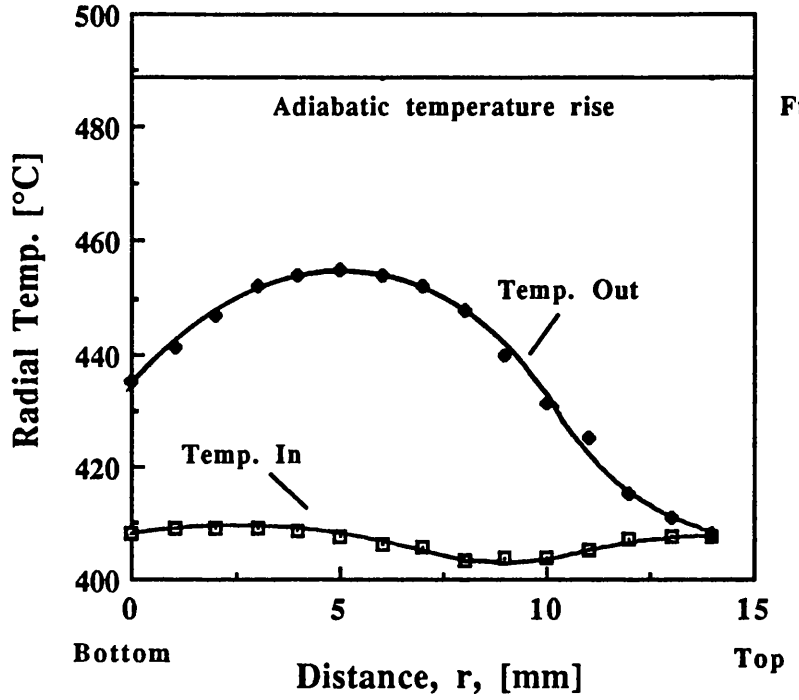

Fig. 3.9 Axial temperature profile along a channel during reaction for Tin=400°C, Ft=16.2 L/min (STP)

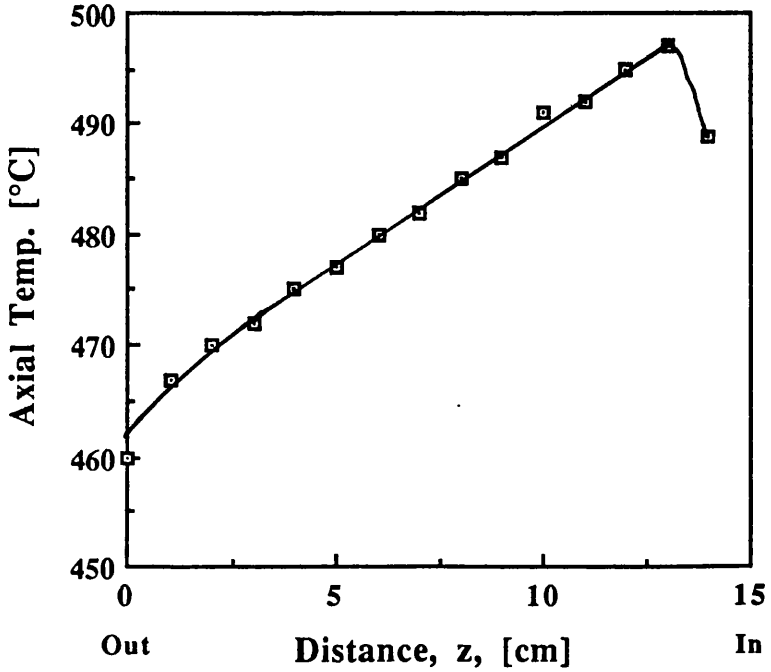

1979). Therefore, it is evident from this investigation that conditions within the channels are not identical, and therefore any detailed modelling should include this effect.

The axial temperature profile for the same inlet conditions is given in figure 3.9. It can be seen that there is a rapid rise in channel surface temperature at the monolith entrance, to reach a maximum at 1.5 cm, suggesting that much of the reaction and heat release occurs at the start of the monolith. The trend is then downwards suggesting that heat is being lost both to the gas phase and to the surroundings. Ignition is characterised by a rapid rise in the catalyst surface temperature. Figure 3.9 shows that light-off occurs at the entrance to the reactor. The temperature at the entrance is slightly below that of the maximum temperature probably due to heat losses at the front face of the monolith, resulting in a slight rise in gas inlet temperature (compare inlet gas temperatures of fig. 3.6 and 3.8 for r=7.5 mm) from 403°C to 408°C when reaction begins.

The pressure drop during reaction was measured to be 11.9 cm of water (1170.4 N/m^2).

Figures 3.10 and 3.11 are the radial and axial temperature profiles at an inlet temperature set point of 400°C and for the same gas composition as given previously except the total flowrate is 13.3 L/min which corresponds to a Re of 74.8 at 400°C. The conversion was found to be 98% and the pressure drop was 8.3 cm of water (815.1 N/m^2).

The gas outlet radial profile given in figure 3.10 shows a profile similar to that given in figure 3.8 (ie. F_t= 16.2 L/min) except that the maximum outlet temperature is 15°C lower. Adiabatic temperature rise is proportional to conversion for a fixed gas composition. Therefore, since conversion increases with decrease in flowrate, one would expect that in an ideal reactor the temperature rise to be greater at the lower flowrate. The fact that there is a lower temperature rise at lower flowrates, even though the conversion is greater than at higher flowrates is obviously due to heat losses to the surrounding. This effect is discussed further in section 6.4.1 of chapter 6. The axial profile given in figure 3.11 shows a similar trend to that of figure 3.9 with the maximum temperature occuring early on along the channel.

Figure 3.12 is a plot of the peak radial temperature rise measured experimentally compared to the adiabatic temperature rise expected (based on the overall conversion) for varying inlet flowrates. This figure shows that there is a large discrepency between the experimental and adiabatic temperature rise, which is obviously due to the heat losses to the surroundings. It is

Fig. 3.10 Radial temperature profiles across pipe before and after the monolith, for a reacting mixture at Tin=400°C

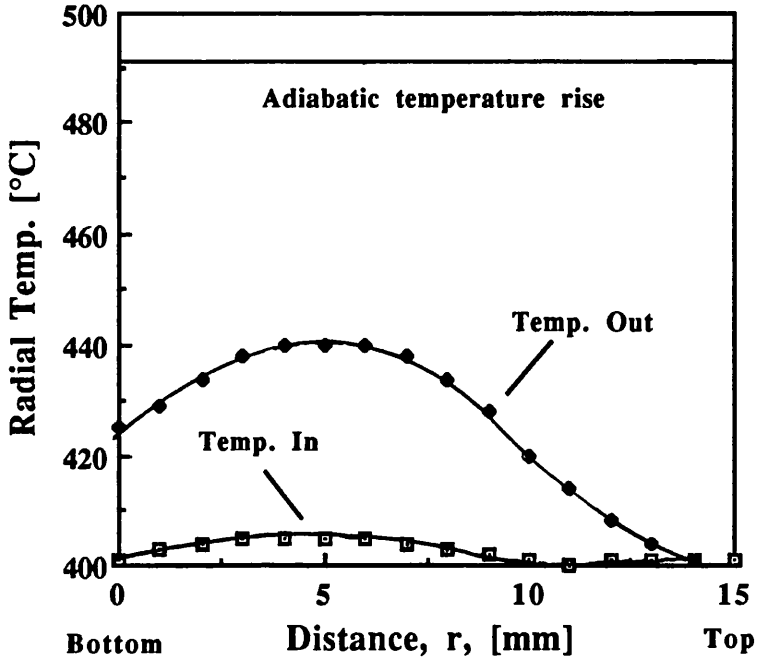

Fig. 3.11 Axial temperature profile within a channel during reaction for Tin=400°C, Ft=13.3 L/min

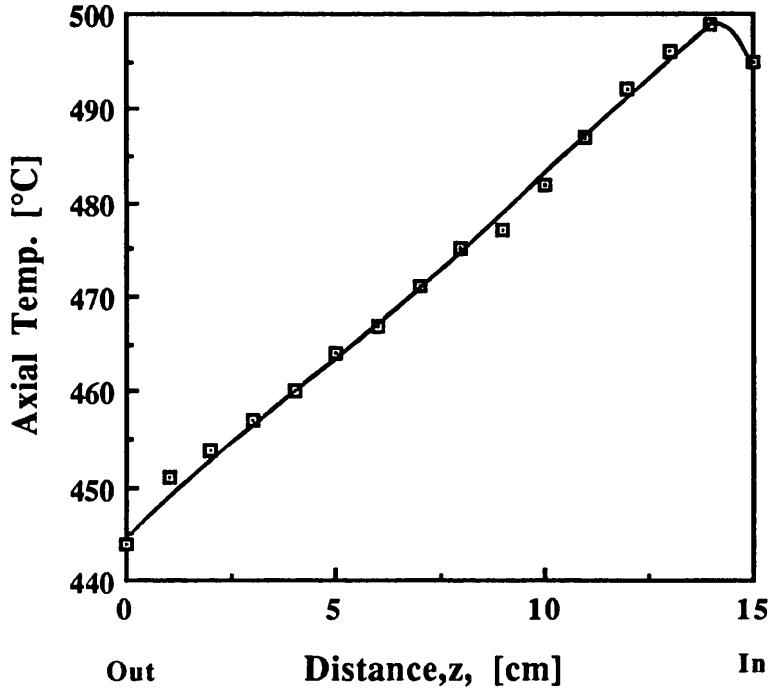

Fig 3.12 Experimental and adiabatic gas temp. rise across the length of the monolith, under reacting conditions

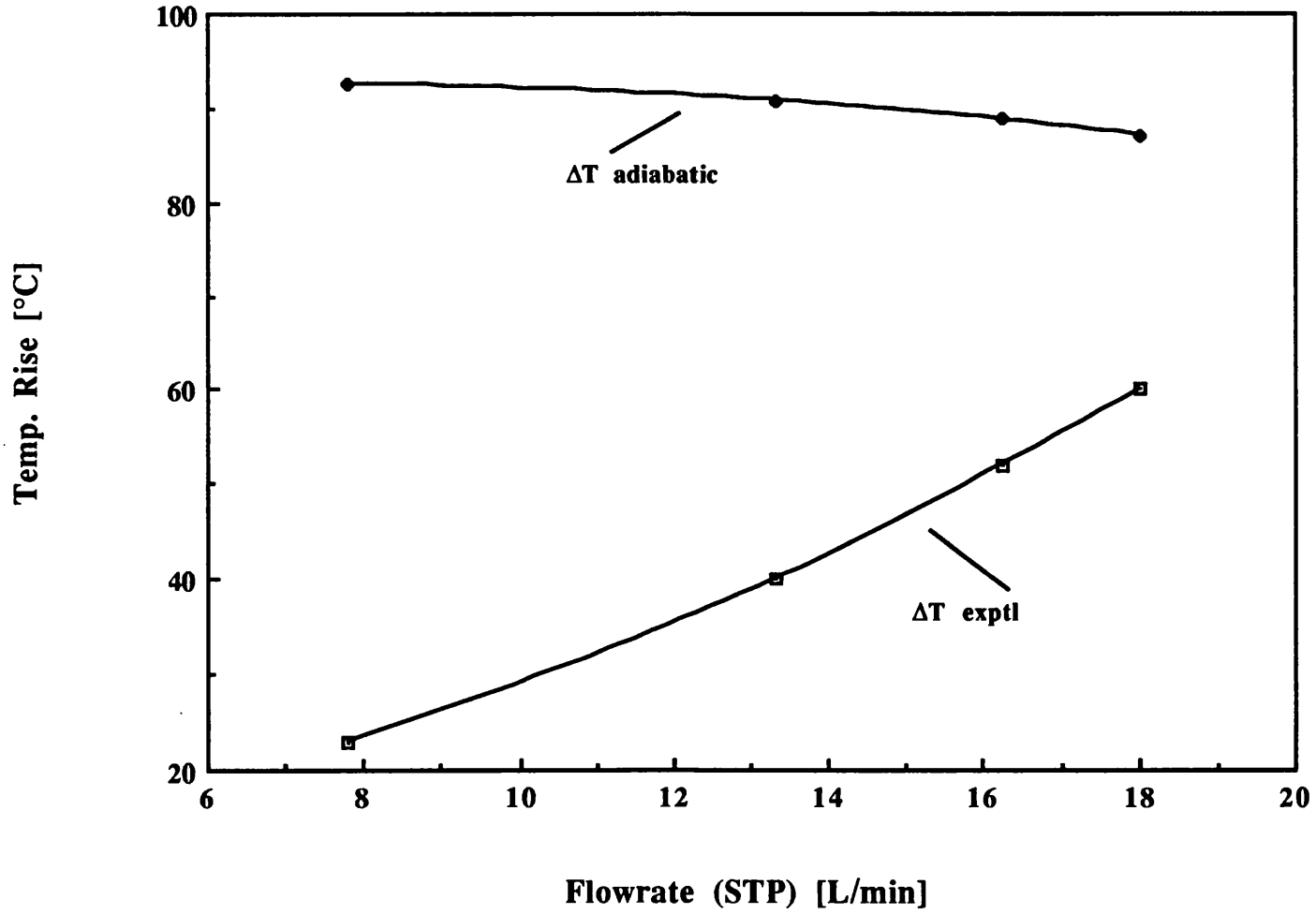

interesting to note that the experimental and adiabatic temperature rise trends are in opposite directions. The reasons for this are explained in section 6.4.1 in chapter 6.

3.6 Comments

The results although limited due to equipment restrictions give an indication as to the temperature profiles occuring within a monolith system and therefore aid in the understanding of the processes involved.

It was obvious from the results that there were large temperature profiles across the cross section of the monolith particularly for the gases entering, probably due to the velocity profile and heat losses to the surroundings, with the result that the extent of reaction varies within each channel.

Little progress was achieved with the set-up as it stood due to temperature control being limited and inflexible. The program "Chromatochart" for integration of the peaks from the gas chromatograph was found to be inadequate. Therefore only a limited number of measurements in conversion were undertaken in the final stages of work using the N.D.I.R. which is discussed in further detail in section 4.2.6 of chapter 4.

For a more detailed study of the monolith system as well as other systems a second apparatus was used. This is described in chapter 4, with the corresponding results given in chapters 5, 6, and 7.

CHAPTER 4

EXPERIMENTAL SET-UP FOR ALTERNATIVE REACTOR INVESTIGATIONS

4.1 Introduction

Experimental investigations were undertaken to examine the behaviour of the conventional auto-catalytic converter (i.e. the ceramic monolith coated with catalyst, supplied as core samples by Johnson Matthey) and the Active Transport Catalytic Reactor (ATCR, which consisted of a catalytically coated tubular reactor with static mixer inserts), for the oxidation of carbon monoxide over a platinum/rhodium (Pt/Rh) catalyst.

The experimental studies were carried out as follows:

(i) The kinetics of heterogeneous CO oxidation over a Pt/Rh coated monolith were studied, in the temperature range of 200-300°C for a CO concentration range of 0.05-2%. The findings from this study are used in the mathematical model presented in chapter 8.

(ii) The behaviour of the monolith reactor under varying conditions of operation (i.e. for an inlet gas temperature range of 250-400°C, and Re range of 73 to 440 at STP within the channels) was investigated. Monolith segmenting experiments to measure conversion, temperature rise and pressure drop were also carried out to investigate the effect of disrupting the boundary layer so as to enhance radial transport rates.

(iii) Under similar operating conditions to the monolith (which corresponded to a Re range of 160 to 2130 (STP) within the pipe), the experimental behaviour of the tubular reactor and ATCR were studied using three types of static mixer inserts including the Sulzer, Kenics and UCL designs.

The experimental work was performed using a synthetic gas made-up of carbon monoxide, oxygen and nitrogen. Typically the air to fuel ratio within the catalytic converter is kept close to stoichiometry. Therefore, for simplicity

the stoichiometric ratio of carbon monoxide to oxygen concentrations (ie. CO and oxygen inlet concentrations of 0.5 and 0.25 (vol. %) respectively) was chosen for the experiments of chapter 7 and 8.

Preliminary experimental work began with the investigations of axial and radial temperature profiles within a monolith reactor during reaction. This was performed using the initial experimental set-up described in chapter 3.

Due to the difficulty of installing a furnace for effective temperature control in conjunction with the use of traversing thermocouples, it was preferable to use an alternative apparatus described in this chapter.This apparatus was developed by a post-doctural research worker within the reaction engineering group and was funded through an SERC research grant. After it was designed and commissioned it became sensible to use it for the research discussed in this thesis since its performance was far superior to the equipment described in chapter 3.

The apparatus is based on the original equipment design of chapter 3, however, the thermocouples were fixed to allow for the installation of the furnaces. This enabled the temperature control to be more effective and flexible achieving precise temperature control at a wide range of temperature settings.

This chapter describes the apparatus and experimental as well as the safety procedures.

4.2 Experimental Set-up

A photograph of the experimental apparatus is given in figure 4.1 and a schematic diagram in figure 4.2. The system consisted essentially of a reactor, gas supply, gas analysis and sampling systems, heating systems as well as temperature and pressure instrumentation and a data acquisition system. Also a CO detector alarm was fitted in order to comply with safety regulations for toxic gases. A block diagram showing the temperature and pressure tappings and control is presented in figure 4.3. Table 4.1 summarizes the specifications of the equipment used. These are discussed in more detail below.

4.2.1 Gas supply and flow measurement

The experimental gases consisted of 99.99 vol% pure grade nitrogen, 99.97 vol% oxygen and 99.96 vol% carbon monoxide. These were fed into

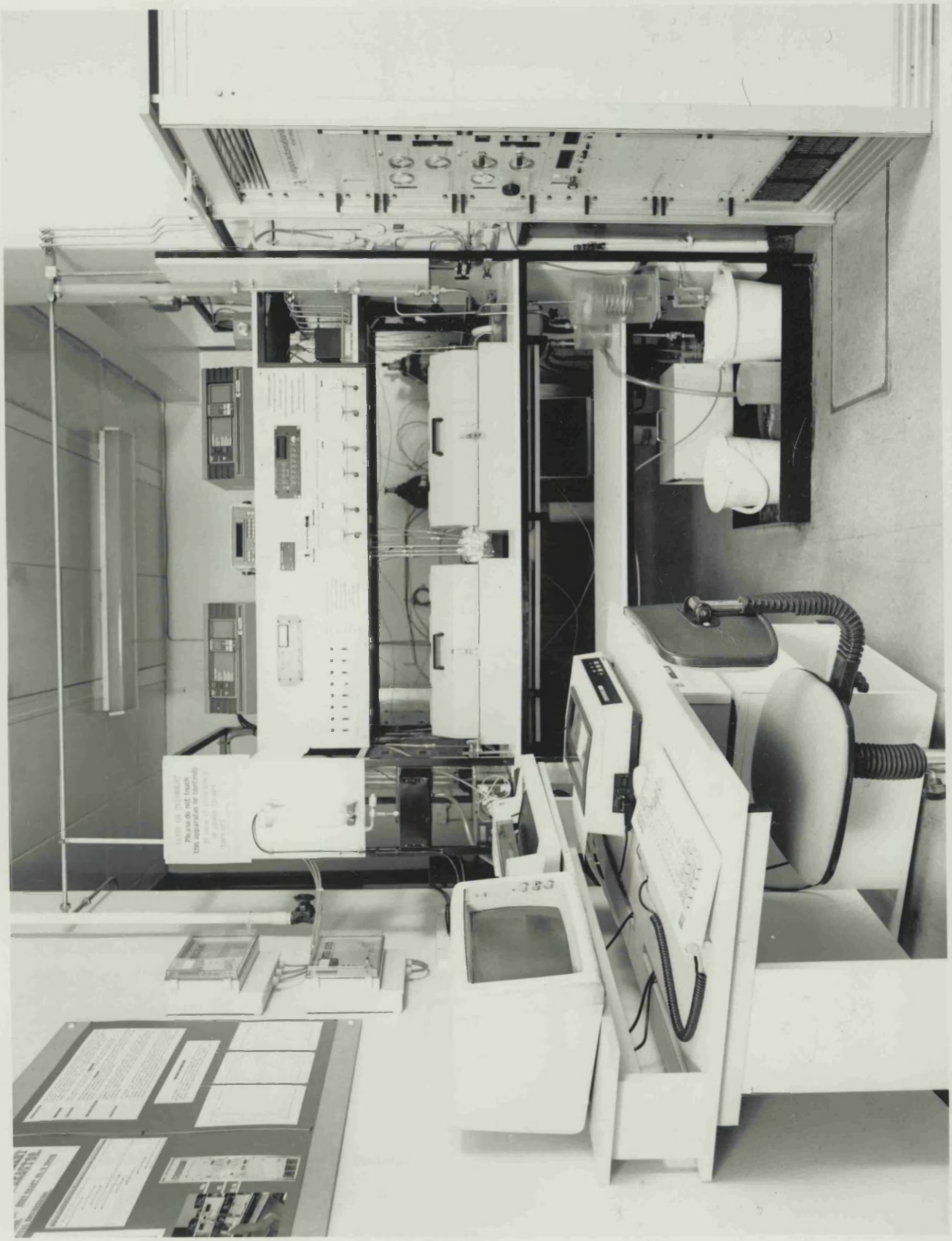

Fig. 4.1 Photograph of experimental set-up

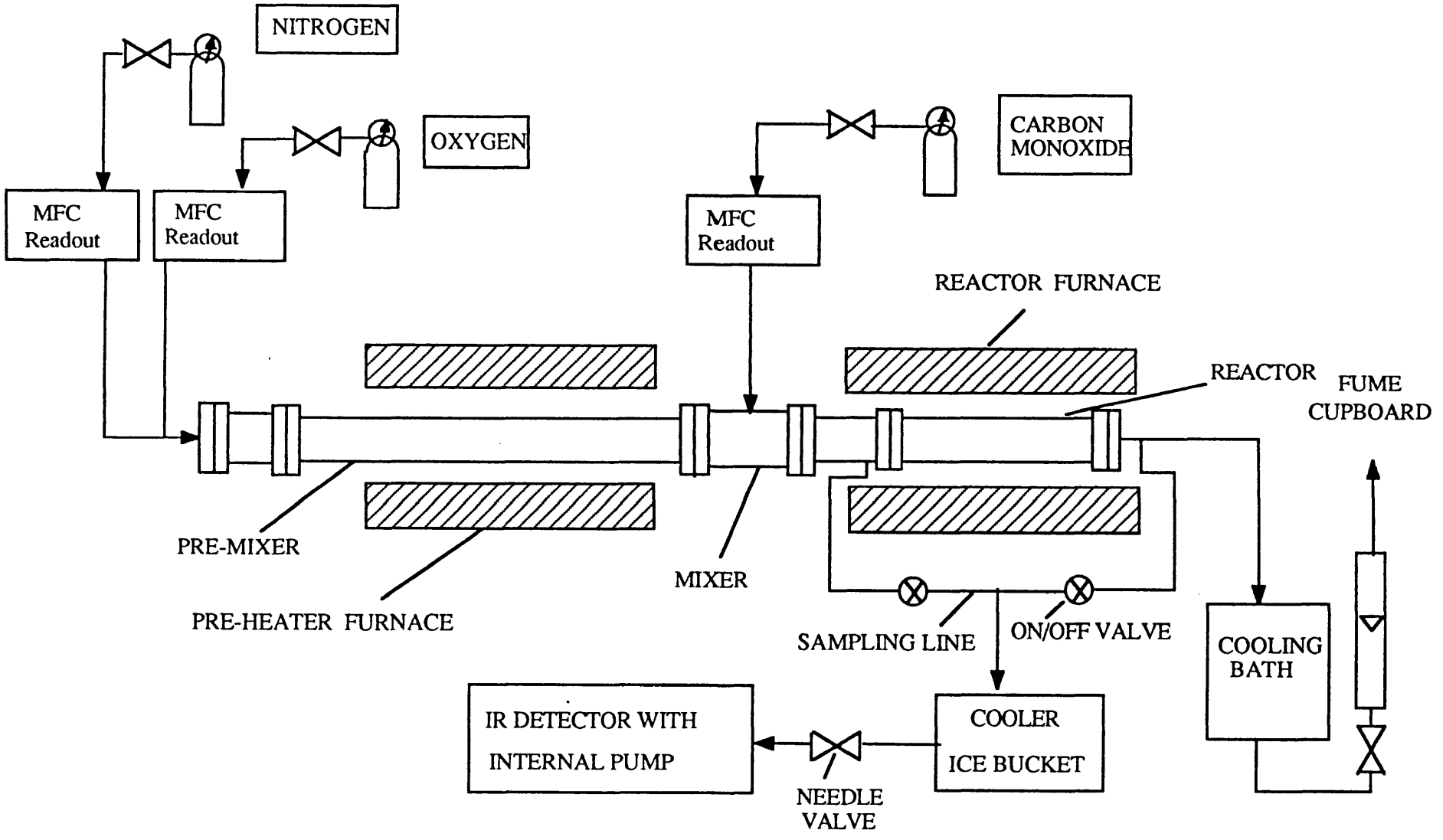

Fig. 4.2 schematic diagram of experimental setup

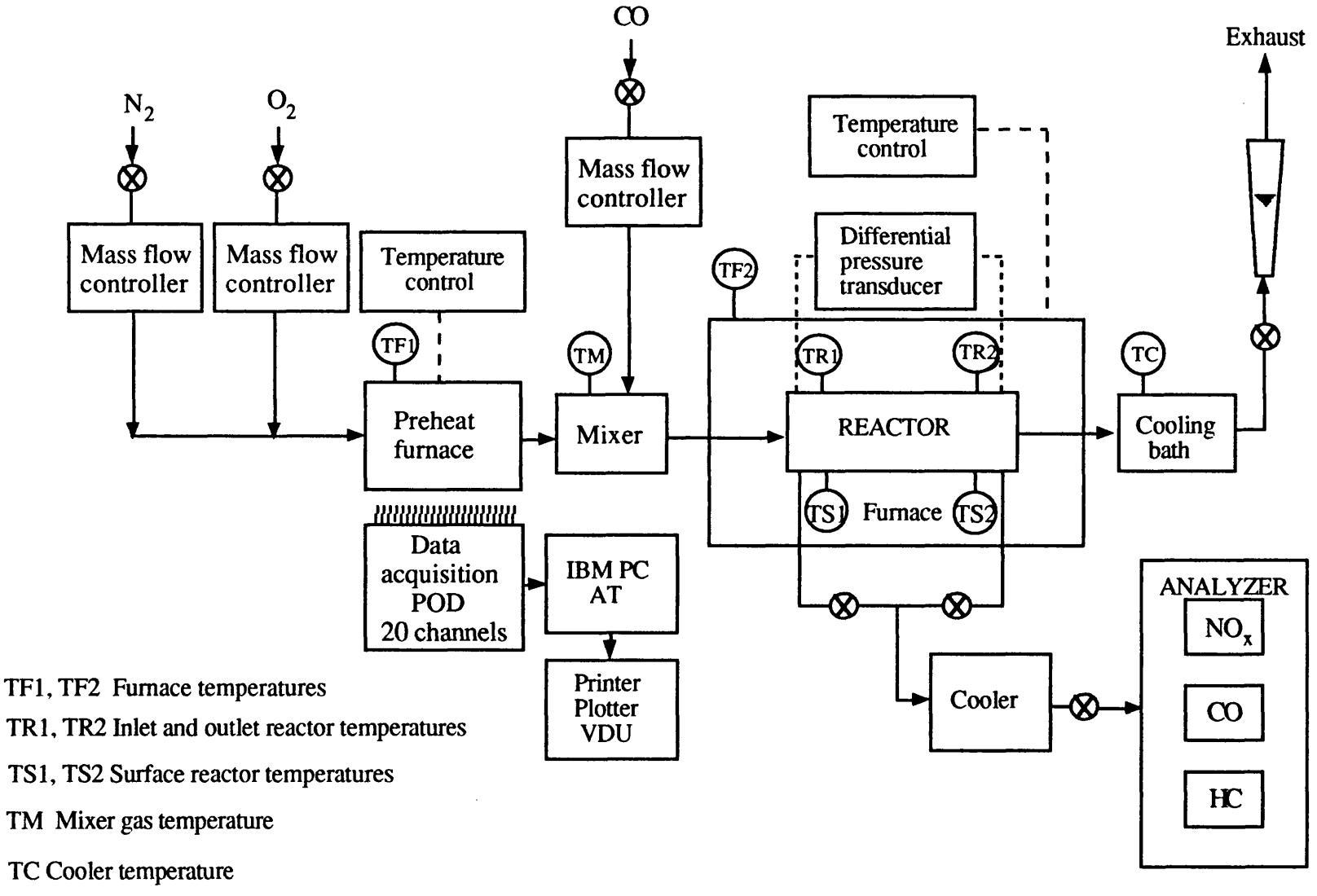

Fig. 4.3 Schematic diagram of experimental setup showing the temperature and pressure drop tappings

Table 4.1 Details of equipment specifications

Equipment	Supplier	Instrument type	Range	Inherent Error
Mass flow controllers and Flow meter	Chell Instruments Ltd.	MKS 259B and MKS 258B	0-20 cm^3/min 0-500 0-5,000 0-10,000 0-20,000 0-50,000	1.0 % of full scale
Furnaces	Carbolite furnaces Ltd.	CST 10/70	0-1000 °C	±5 °C across the central zone
Thermocouples	Labfacility Ltd.	Ni/Cr type K	0-1000 °C	±1 °C
Pressure transducer	Chell Instruments Ltd.	MKS Baratron 223B	0-100 Torr	0.1 Torr
Gas analysis system (N.D.I.R.)	Analysis Automation Ltd.	Model 401	0-2 % CO 0-2 % CO_2	1 % of full scale
CO detector and alarm	International Gas Detectors Ltd.	RMS 835 CO RMS 834 HC's	0-250 ppm CO 0-100% L.E.L.	——

MKS flow controllers, where their flow was controlled and monitored at the required value. The maximum range for each flow controller varied from 20 cm^3/min for the oxygen controller up to 50 L/min for the nitrogen controller depending on the total flowrate required. The flow controllers had digital flow readouts (Model 247C), and were calibrated in litres/min at standard operating conditions. In order to calculate the actual flowrate the inlet temperature and pressure conditions were required. Since the outlet of the reactor was open to the atmosphere, and the pressure drop across the reactor was negligible in comparison to this, it could be assumed that the reactor was at standard pressure.Thus the actual flowrate could be calculated from the ideal gas law at constant pressure:

$$F_{Act} = F_{STP} \times \frac{T_{Act}}{T_{STP}} \qquad (4.1)$$

where T_{Act} and T_{STP} correspond to the actual and standard temperatures respectively in K.

The gases nitrogen and oxygen were initially preheated and premixed and then passed to the mixer where CO was introduced and complete mixing was carried out, prior to the introduction of the reactant gases into the reactor.

4.2.2 The pre-mixer / pre-heater

This consisted of a 91 cm stainless steel tube of diameter 1.3 cm, filled with Sulzer mixers. These stainless steel static mixer inserts (supplied by Sulzer Ltd.) were introduced in order to promote mixing and aid heat transfer of the reactant gases prior to their introduction into the reactor. The pipe passed through a preheater furnace where heating of nitrogen gas as well as oxygen took place. Carbon monoxide was added in a mixer after the pre-heater stage in order to reduce any chance of homeogeneous reaction prior to its entry into the reactor. This mixer consisted of a 5 cm long by 3 cm internal diameter tube again filled with Sulzer mixers. The reactants then passed into the reactor. It was important that the gases were well mixed on entering the catalyst reactor to avoid "hot spots" caused by localized regions of high fuel concentration which may have led to temperatures exceeding the limit of the catalyst material and hence causing sintering and thermal degradation of the catalyst-washcoat-

support system. Since it was evident in chapter 3 that a laminar flow profile across the diameter of the pipe effects the overall conversion within each channel of the monolith, the decision was taken to fill the pipe section just before the reactor with Sulzer mixers, with the aim of disrupting this profile and so provide a uniform flow across the diameter of the pipe prior to its entry into the reactor.

4.2.3 The reactor

A photograph of the reactor section is given in figure 4.4. This consisted of a 15 cm long test section of tube attached to flanges welded at the ends enabling the reactor to be dismantled and reassembled easily. Depending upon the catalyst system to be investigated, the reactor was either a 1.3 cm stainless steel tube into which the monolith could be inserted or a 1.5 cm Fecralloy tube coated with catalyst into which mixer units could be inserted. The monolith section was slotted into the reactor section and this was kept in place by the use of gaskets made from Sindanyo of internal diameter 1.1 cm. Alternatively the Fecralloy tube coated with catalyst could be slotted into place. The reactor was bolted to the pre-mixing section so that it could be easily dismantled without disturbing the pre-mixing zone. The reactor section was enclosed within a furnace identical to that used in the pre-mixing zone.

Gases leaving the reactor frequently were at temperatures in excess of 400°C and therefore needed to be cooled prior to exiting as exhaust. These were cooled by passing them through a coil made from a 1 cm stainless steel tube immersed in a cooling bath. This consisted of a perspex container filled with ethylene glycol and water in the ratio of 1:2 vol%. The mixture was cooled using the cooling coil of a Dip cooler (Techne), down to temperatures of approximately -15°C. This was found to be effective in cooling the gases down to room temperature. The cooled exhaust gases then passed to a rotameter where the flow could be measured, and then to the fume cupboard.

4.2.4 Temperature measurement and control

Two 1 mm diameter thermocouples (Ni/Cr type K supplied by Labfacility Ltd.) were placed immediately prior to and after the reactor. These were fixed midway across the diameter of the pipe. Thermocouples of diameter

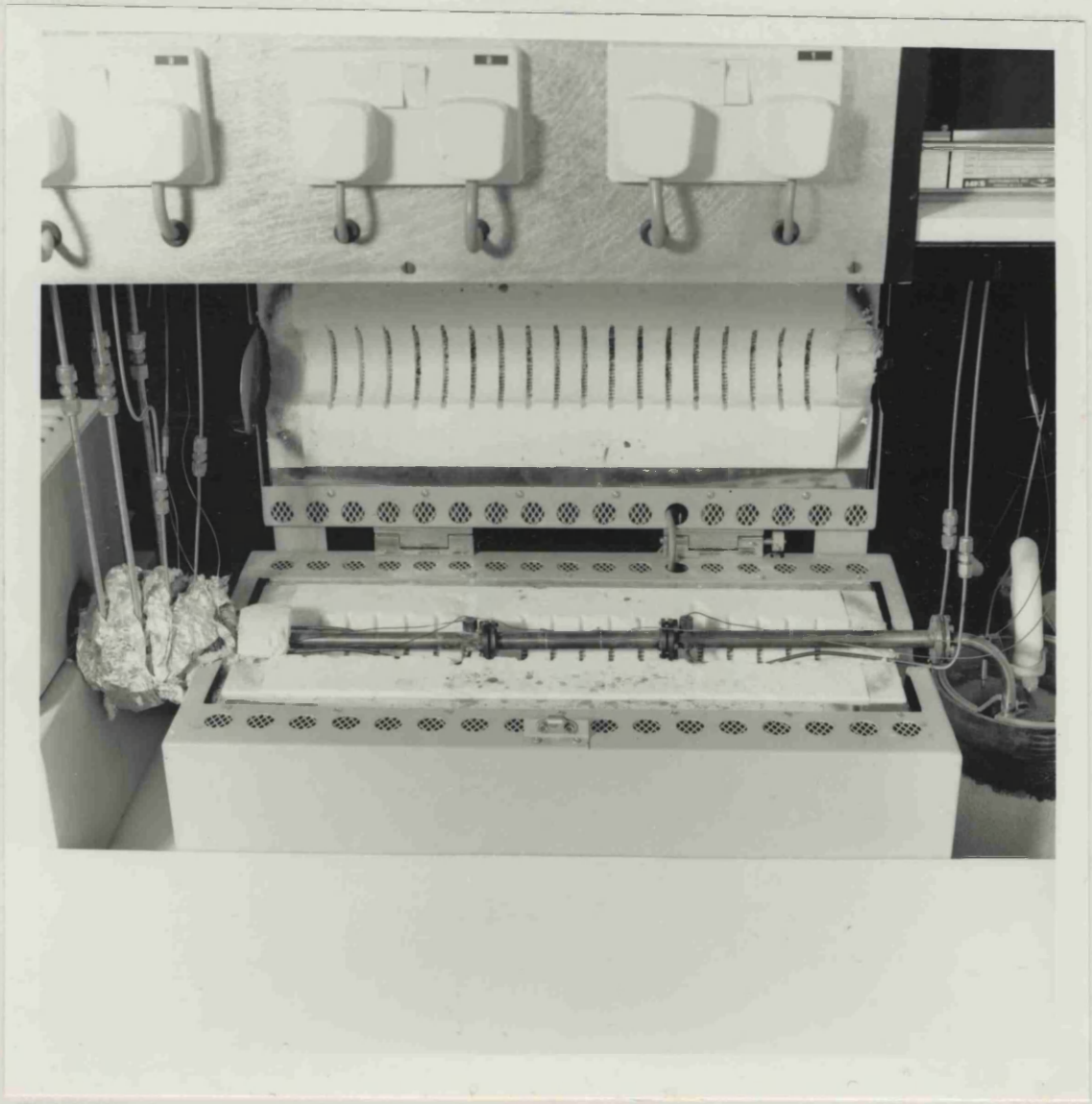

Fig. 4.4 Photograph of reactor test section

2 mm were also placed on the reactor external surface at the inlet and outlet of the reactor to measure reactor surface temperatures. The outputs from the thermocouples were recorded using a Comark recorder as well as a digital readout.

The furnaces, supplied by Carbolite Furnaces Ltd., were of the CST range type 10/70 using a NiCr/NiAl thermocouple sensor and with a maximum operating temperature of 1000°C. These consisted of split tube furnaces manufactured in two halves, hinged for easy loading and placing around tubes or test sections, enabling the reactor to be reached for ease of dismantling and reassembly. The resistance wire elements were embedded in lightweight ceramic fibre which also formed the heating chamber. Temperature control consisted of varying the power to the elements according to the "Set Point" in a proportional and derivative control manner. A positive break power isolation switch (ie. on opening the furnaces the power to them was switched off) and shuttered tube end covers were fitted as standard for total operational safety. The furnace bore tube diameters measured 7 cm and the total heated lengths measured 50 cm. However, the most uniform temperature control (to within ± 5°C) occurred in the central region of length 12 cm.

4.2.5 Pressure drop measurement

Pressure tappings were connected just upstream and downstream of the reactor. The pressure transducer, supplied by Chell instruments Ltd. (MKS Baraton type 223B), measured the pressure drop across the complete reactor length of 15 cm. This measured differential pressure according to its full scale range of 1-100 torr and provided a 0 to ±1 volts signal which was linear with pressure.

Pressure in the reactor could be controlled by pressure regulators on all three gas cylinders. Because the reactor was open to the atmosphere via the fume cupboard, the pressure in the reactor was considered to be close to atmospheric.

4.2.6 Gas sampling and analysis

Sampling probes consisting of 0.5 cm stainless steel tubing were connected to the inlet and outlet of the reactor section. The gas analysis system

consisted of an infrared detector N.D.I.R. Analyser (model 401), manufactured by Analysis Automation Ltd., detecting CO and CO_2 in the range 0-2%. The analyser measured concentrations based on the principle that each gas has a unique absorption pattern in the infra-red frequency spectrum.The system provided continuous gas analysis. A reciprocating pump built into the IR unit controlled the amount of sample entering the detector, this was generally fixed at 800 cm^3/min (N.T.P.). Prior to entry to the detector, the gases were required to be cooled. This was performed by passing them through a cooling coil made of 1 cm stainless steel tubing which was placed in a bucket regularly filled with ice.

4.2.7 Data acquisition

Signals from all the instruments, ie. flow controllers, thermocouples, pressure transducer and infra-red detector were fed to a 20 channel input POD and PC input card to give continuous monitoring using the Impulse software package on an IBM PC AT.

The POD, adapter card and Impulse package were all supplied by Solartron Instruments. The POD (Analog measurement IMP) was of the 35951A type and consisted of a 20 channel 3-pole solid state selector which was able to sample signals every second.

Interfacing of the IMP network and the IBM PC was achieved through a single adaptor card, 35954A, which plugged into an expansion slot within the PC.

The software package Impulse (RTM 3500) developed by Schlumberger Instruments, was menu driven and allowed the operator of the IBM compatible computer to receive, display and log data acquired in real time from the Schlumberger Isolated Measurement Pod (IMP). The data received could also be saved for later use.

The combined system was quite versatile and was found to be extremely useful. All the process variables were continuously monitored and it was possible to get an immediate impulse printout of all the variables.

4.3 Catalyst Pre-treatment

Prior to all experimental work it was necessary to pre-treat the catalyst to ensure that the activity remained constant during the testing. This was performed by first aging the catalyst by passing a reacting mixture over the catalyst for 20 hrs at around 400°C, then by calcining the catalyst by passing oxygen over the heated catalyst (at 300°C) for about 10 hr at a flowrate of 1 L/min (STP).This was found to be necessary from experimental experience since without pre-treatment the catalyst gave non-repeatable results. As discussed in the literature review, the catalyst is impregnated using chloroplatinic acid (H_2PtCl_6). When this is heated in oxygen, the platinum is deposited onto the washcoat and HCl is liberated. Thus heating in oxygen tends to stabilize the catalyst.

4.4 Experimental Technique

4.4.1 Procedures

During the course of all experimental work the safety procedures were strictly adhered to. These are described in detail in section 4.4.4 at the end of this chapter.

Prior to starting a run, nitrogen gas was passed at about 10 L/min and the reactor as well as the preheater furnaces were switched on. The temperature settings of the latter were raised gradually in order to heat the reactor slowly. After about an hour the nitrogen flowrate was adjusted to its required setting. This was performed in order to save gases during the pre-heat treatment. At the same time oxygen was introduced at the required flowrate. The furnaces were continuously adjusted until the required isothermal temperature was reached. This process took about 2 hrs. The temperature of the gases could be controlled to within ±1°C between the inlet and outlet of the reactor under non-reacting conditions.

Once a steady isothermal temperature along the reactor was reached CO gas was introduced at the required flowrate. The reaction was allowed to continue, and once all the process variables reached steady state (i.e. concentrations and temperatures) the inlet as well as the outlet concentrations, temperatures and pressure drops were measured and recorded on an Impulse printout.

4.4.2 Sampling

A continuous sample was taken from both the entrance and exit of the reactor and passed to the IR at a flowrate of 800 cm^3/min (NTP). The IR gave an online reading of the percentage composition of both CO and CO_2.

Precalibration of the IR was performed using calibration gases made to order. Initially, the IR was zeroed and then spanned to give the correct reading for sample inputs. The calibration was regularly checked to determine if there was any change. This was found to be fairly constant.

4.4.3 Experimental error bounds on outlet conversion

The error associated with a measured conversion is determined primarily by the composition of the reactants entering the reactor. These depend on the flowrate of each reactant determined by the accuracy of the flow controllers. However, the Infra-red detector served as a check on the composition of CO in the inlet and outlet streams from the reactor. The error associated with the IR is ± 2 % of full scale. Hence the combined error of both inlet and outlet CO concentration which make up the conversion is ± 4 % of full scale. Thus the total error for the outlet conversion is ± 4 %, assuming that the oxygen composition is accurate.

In an attempt to minimize the flow controller error, the smallest capacity controller was used for each flow rate, since the error associated with the flowcontroller is 1 % of the maximum operating flow. Thus the lower the flowrate the larger the percentage error. However, during the experimental investigation it was found that at the very highest flowrates there was some instability.

One controller was used for each gas constituent ie. nitrogen, carbon monoxide and oxygen. The actual composition of CO entering was checked using the IR detector. However, in the case of oxygen and nitrogen inlet compositions, accurate control was more important. Hence, in order to increase accuracy of inlet compositions the flow controllers were varied for each flowrate as shown in table 4.2, for an inlet compositions of 0.5 % CO, 0.25 % oxygen and 99.25 % nitrogen.

Table 4.2 Mass flow controllers used for each flow range during experimentation

Total flowrate L/min. (S.T.P)	Oxygen MFC cm^3/min.(S.T.P.)	CO MFC cm^3/min.(S.T.P.)	Nitrogen MFC L/min.(S.T.P.)
5.0	20.0	100.0	10.0
7.5	20.0	100.0	10.0
10.0	100.0	500.0	50.0
20.0	100.0	500.0	50.0
30.0	100.0	500.0	50.0

4.4.4 Safety procedures

The following safety measures were taken during and prior to all experimental work:

1) The fume cupboard and extraction fan were switched on, in order to prevent harmful CO from entering the room.
2) The CO detector alarm was switched on to detect any leaks.
3) The nitrogen flow was set and any leaks in the system were checked for using soap solution.
4) The cooling bath was checked to make sure it was topped up with coolant.
5) The cooler leading to the IR was filled with ice to ensure the sampled gases were at essentially room temperature.
6) The IR was switched on, checking that there was a constant flowrate of 800 cm^3/min passing through the IR pump.
7) The furnaces were switched on (never allowing these to go above the maximum limit of 1000°C) allowing for the gradual warm up of the system.
8) On completing experimentation, the O_2 and CO flows were terminated and isolated at the cylinder heads.
9) The furnace temperatures were lowered and nitrogen was allowed to flush the system to allow for gradual cooling to prevent support thermal shock fracture.
10) Once the system was cooled to 50°C the furnaces were switched off and the nitrogen flow was stopped and isolated at the cylinder head. All systems were switched off except for the mass flow controllers.

CHAPTER 5

THE KINETICS OF HETEROGENEOUS CO OXIDATION

5.1 Introduction

In general, in any gas/solid catalytic reaction, the processes involved are: (i) mass transfer of reactants to the catalyst surface (ie. interphase mass transfer), (ii) possible diffusion within the solid catalyst (ie. intraphase mass transfer), (iii) reaction at the surface at a rate determined by the intrinsic kinetics, and (iv) diffusion of the products away from the surface. In the case when one of these steps is very slow, it is this step that becomes rate limiting.

In a highly exothermic reaction, it is usually the mass transfer process which is limiting. However, depending on the conditions of reaction, this may alter and become intrinsically rate limiting, or indeed the two rates, ie. mass transfer and intrinsic kinetics, may both offer equal resistance. Therefore in order to determine the intrinsic kinetics it is necessary to eliminate the mass transfer limitation. This is possible and is presented in this chapter.

Much work has been performed on the kinetics of CO oxidation. This was reviewed in the Literature Survey in chapter 2.

This chapter is concerned with determining the experimental kinetics of CO oxidation on a $Pt/Rh/Al_2O_3$ catalyst supported on a monolith. A differential reactor approach was adopted.

Due to the highly exothermic nature of the reaction, much of the experimental work was concerned with the elimination of significant mass transfer effects ensuring an adequate approach to isothermal behaviour.

5.2 Differential Reactor Analysis

A differential reactor is one in which there are small changes in composition and temperature so that the rate of reaction can be considered to be constant at all points within the reactor (Levenspiel, 1976). Since rates are concentration dependent, this assumption is usually reasonable only for small conversions or short small reactors. This condition is achieved by considering only low conversions (of less than 15%) and temperature rise (less than 10°C). The justification for the choice of values is determined in section 5.7 of this

chapter. It is also necessary that the reaction is in the kinetically-controlled region ensuring that diffusional effects from the gas to the catalyst surface are negligible.The reaction rate can be measured directly and is found from the following equation (Levenspiel, 1976):

$$-(r_{CO})_{ave} = \frac{m_{CO,in}\,([CO]_{CO,in} - [CO]_{CO,out})}{S_A} \qquad (5.1)$$

where $[CO]_{CO,in}$ and $[CO]_{CO,out}$ are the concentrations (mol fract.) of CO entering and leaving the reactor respectively, $m_{CO,in}$ is the molar flowrate (kmol/s) of CO entering and S_A is the external catalyst surface area (m^2).

5.3 Kinetics of CO Oxidation on Pt/Rh Catalyst on γ-Al_2O_3

5.3.1 The model

The reaction proceeds according to the following stoichiometric relation:-

$$CO + \frac{1}{2}O_2 \rightarrow CO_2 \qquad (5.2)$$

The most widely accepted rate expression for the oxidation of carbon monoxide on monolithic platinum catalyst is that of Voltz et al.(1973) (discussed in chapter 2), and is of the form of a Langmuir-Hinshewood model:

$$-r_{CO} = \frac{k_r [CO]\,[O_2]}{(1 + k_a [CO])^2} \qquad (2.4)$$

where [CO] and $[O_2]$ are bulk concentrations of carbon monoxide and oxygen respectively, k_r is the rate constant, and k_a is the adsorption constant. These are given by:

$$k_r = A \exp\left(-\frac{E_r}{R T_S}\right) \qquad (2.5)$$

$$k_a = B \exp\left(-\frac{E_a}{R T_S}\right) \qquad (2.6)$$

This form of equation is adopted for the present analysis.

5.3.2 The observed kinetics

In general, the observed reaction kinetics may be affected by the intrinsic kinetics as well as the interphase and intraphase limitations.

If the reaction is affected by interphase (ie. external mass transfer) processes only, then the observed order of reaction should equal one, and the activation energy should be approximately zero (Carberry, 1976).

If the interphase or pore diffusion processes are limiting then the the effect may be amalgamated into the intrinsic rate expression to give an observed rate constant:

$$(k_r)_{obs} = \eta\, k_r \qquad (5.3)$$

where η is the effectiveness factor (Froment and Bischoff, 1979, Haynes, 1982), and k_r is the intrinsic rate constant. Equation 5.3 can be written in terms of the observed activation energy as:

$$(k_r)_{obs} = A_{obs}\, Exp\left(-\frac{E_{obs}}{R T_S}\right) \qquad (5.4)$$

where T_S is the wall temperature and E_{obs} is the observed energy of activation. In the case when the reaction has strong diffusion limitation the observed activation energy according to Froment and Bishoff (1979) is then:

$$E_{obs} = \frac{1}{2}(E_r + E_d) \qquad (5.5)$$

where E_r and E_d are the energies of reaction and diffusion limitation, respectively. Since diffusion is a physical process, the diffusion activation energy is characteristically small, relative to the activation energy for chemical reaction except in the diffusion of zeolites (Haynes, 1982). Thus in the general case for a reactor with mass transfer limitation:

$$E_{obs} \cong \frac{1}{2} E_r \qquad (5.6)$$

A generalized Arrhenius plot is given in figure 5.1 for a positive order reaction. This shows the transition between the various controlling regimes as the temperature is varied.

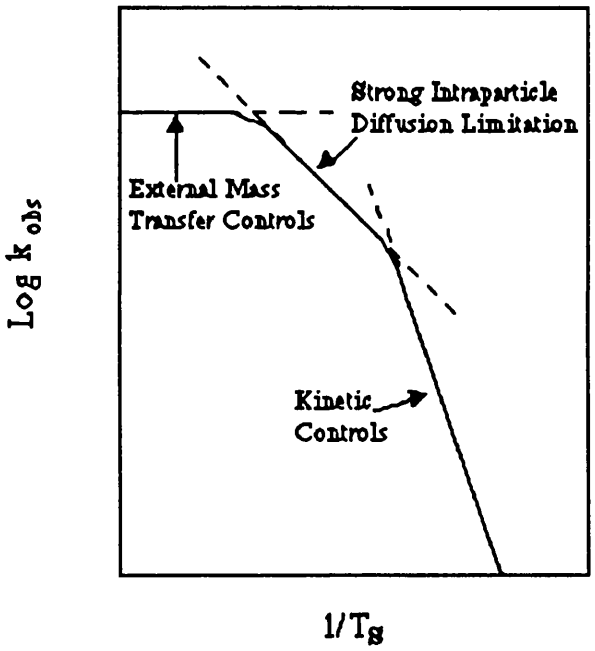

Fig. 5.1 Arrhenius plot under different mass transfer regimes (Haynes, 1982)

5.4 The Reactor

The complete experimental apparatus is described in chapter 4. The reactor test section is shown in a schematic diagram in figure 5.2. This consisted of a mixing section placed prior to the reactor sample. The mixer was essentially a 1.3 cm diameter by 4 cm long stainless steel tube containing

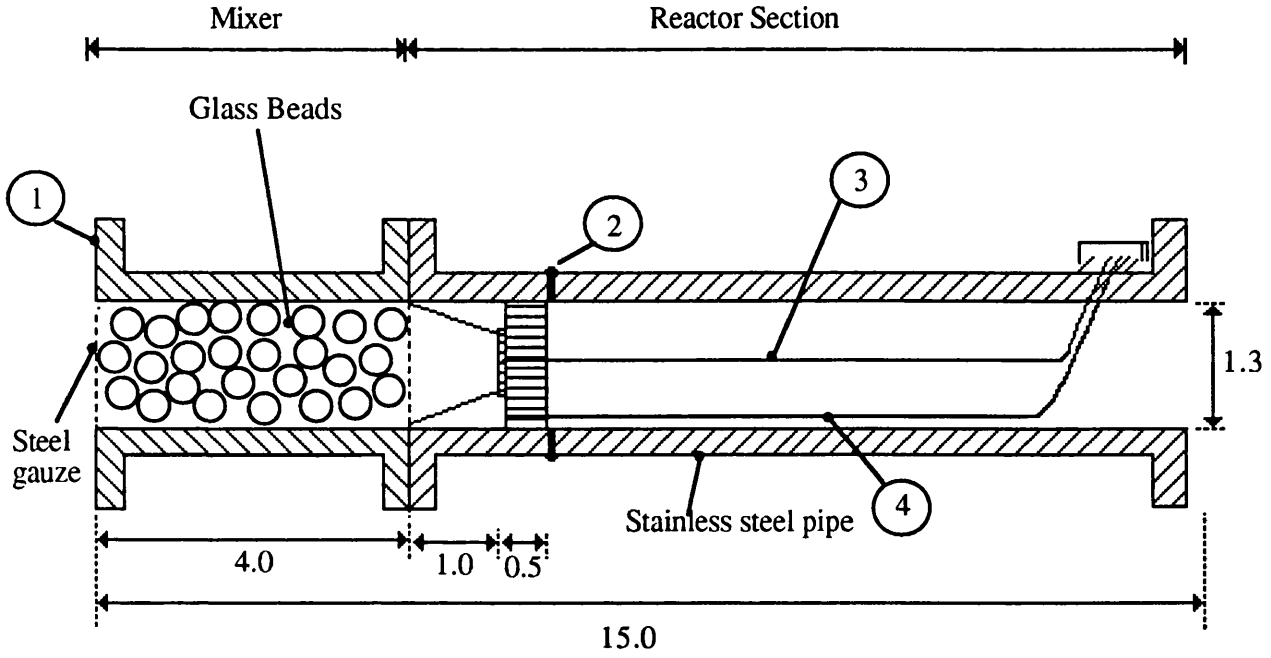

a) Section through the reactor and mixer

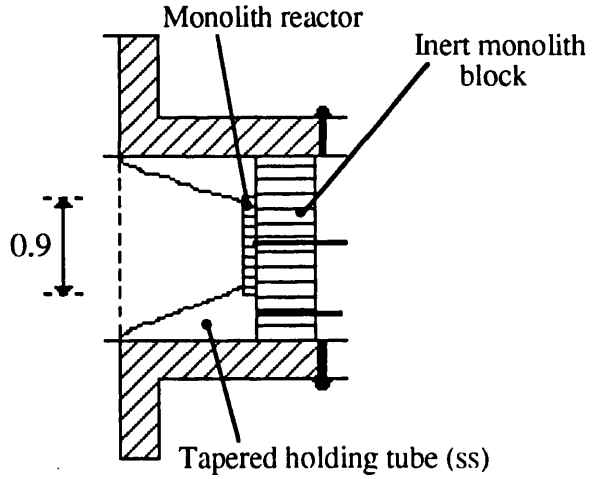

b) Detail of reactor test section

All dimensions in cm.

1. Flange, with 6 screw holes with equal radial spacing
2. Three stainless steel pins with equal radial spacing
3. Central thermocouple, 0.5 mm OD
4. Peripheral thermocouple, 0.5 mm OD

Fig. 5.2 The kinetic reactor (not to scale)

sodium and lead glass beads of diameter 2 to 4 mm. These were tested prior to experimentation to check for any reaction and were found to be inert. The catalyst sample was mounted in an 11 cm stainless steel pipe section of similar diameter to the mixing section. These were joined by means of a flange for easy access to the catalyst test sample. An inert monolith block of length 1 cm and diameter 1.25 cm was placed into the stainless steel pipe section and was prevented from moving using three pins welded equally spaced into the sides of the reactor. It was also secured in place using a high temperature cement. The inert block was used for two reasons, firstly to hold the reactor sample in place and prevent its movement and secondly to form a frame for the passing of two thermocouples. The two thermocouples of diameter 0.5 mm were placed within a central and a peripheral channel within the inert monolith. These were cemented into place so that the ends were just protruding from the end of the inert monolith block. The reactor slice could then be slid into place along side the inert monolith so that the thermocouples were just inside the reactor. These were placed in contact with the reactor wall and therefore they recorded reactor surface temperatures. The reactor test section was sandwiched between the inert block on one side and a stainless steel tube on the other. The latter, depending on the diameter of the test sample to be tested, consisted of either a thin walled tube of OD 1.25 cm, or a tapered holding tube of similar OD, but with an inside diameter at the wide end of 1.2 cm and at its smallest end of 8.5 mm (ie. at the tapered end).The reactor slice was held in place using a groove in the tube and cemented to the walls of the groove using a high temperature cement. These were slotted into the 1.3 cm diameter pipe along side the reactor sample to prevent its movement (refer to figure 5.2).

A variety of different sized reactor samples were chosen from monolith cores of random selection and used to test for catalyst activity at various positions along a core sample and from sample to sample. These are specified in table 5.1. The desired size of the reactor was achieved by filing the monolith using emery cloths and the reactor lengths were accurately measured using a micrometer. The catalyst surface area is based on the external surface area of the channels. Initially a 1.25 cm diameter monolith sample was used, but later runs were performed using a smaller diameter reactor.

Table 5.1 Dimensions of catalyst samples used in kinetic experiments

d=1.04mm

	Sample 1	Sample 2	Sample 3	Sample 4
Monolith diameter, (cm)	1.25	1.25	1.25	0.9
Length of monolith, (mm)	1.00	0.8	0.8	1.5
Catalyst external surface area, (m^2)	2.912×10^{-4}	2.3296×10^{-4}	2.3296×10^{-4}	2.7456×10^{-4}

5.5 Procedures

In order to establish a differential reactor and eliminate mass transfer, the following preliminary methods were followed:

i) The total flowrate was varied for a fixed inlet gas temperature and concentration,

ii) The inlet temperature was varied for a fixed inlet concentration and flowrate,

iii) The sample size was varied by altering the length and diameter of the monolith test sample.

In order to keep the temperature rise below 10°C during experimentation, it was necessary to operate at a low oxygen concentration. Obviously, the lower the temperature and the greater the velocity the less likely the reaction is in the mass transfer limited regime. Also for a particular temperature the greater the velocity the less likely the reaction is mass transfer limited.

A small sample of catalyst was placed into the reactor. The catalyst samples used were the cut samples from experiments used in the monolith experiments given in chapter 6, thus they were aged, ensuring constant activity of the catalyst throughout the experimentation.

In order to achieve good gas flow distribution, layers of glass beads were placed prior to the catalyst. The system was initially flushed with nitrogen and the reactor temperature raised. The catalyst was calcined for approximately 10 hours at 400°C with oxygen (1 L/min) to ensure the constant activity of the monolith catalyst during a run (pre-treatment). Oxygen flow was then terminated and the system was again flushed with nitrogen.

The procedures in chapter 4 were followed for the prelimary experiments of parts i)-iii). Once an optimum reactor size and total flowrate were established for differential analysis, the following procedures were followed for the kinetic experiments.

When starting a run the procedures followed were similar to those outlined in chapter 4. Nitrogen was first introduced into the reactor at the required flowrate, and the temperature set and allowed to reach steady state. Oxygen was then introduced into the reactor at an inlet concentration of 0.25% followed by CO. The reaction was then allowed to proceed and once steady state was reached (ie. constant outlet concentration and temperature), usually after approximately 30 mins, inlet and outlet samples from the reactor were taken to the IR. This was performed for different concentrations of CO at constant oxygen concentration. Similarly for a constant CO inlet concentration of 0.5% the oxygen concentration was varied and the conversions noted. Between consecutive runs, approximately an hour was needed for the system to settle to a new steady state.

During the course of all experimentation, experiments were frequently repeated in order to check the reproducibility.

Since the necessary requirement of a differential reactor is low conversion (ie. less than 15 %), it follows that the change in concentrations between the inlet and outlet are small, and therefore it is reasonable to calculate reaction rates (equation 5.1) on an inlet CO and oxygen concentration basis, with this assumption producing little error. Indeed for the experimental analysis using equation 2.4 for a total conversion of 15% this represents a maximum experimental error of 3%. Hence, this assumption is taken for all the experiments in this chapter.

5.6 Results and Discussion

5.6.1 Preliminary investigation

The preliminary investigations were performed in order to eliminate mass transfer limitations, and therefore record actual kinetic rates rather than those affected by mass transfer.

There are various options, as described in section 5.5 above, which can be taken to eliminate this factor. Due to the highly exothermic nature of this process, this task was not particularly easy since there is a compromise to be made between elimination of mass transfer resistance and accurate recordible conversion measurements. This was due to the fact that as flowrate increases, conversion falls as the residence time drops, however if the conversion is too low it cannot be measured very accurately.

(i) Effect of flowrate

The range of inlet conditions are:

Total inlet flowrate: 5-40L/min (STP)
Inlet temperature: 371°C
Inlet CO concentration: 0.5 vol%
Inlet oxygen concentration: 0.25 vol%

The experimental data for the preliminary runs are supplied in appendix C in table C.1.

The effect of flowrate on CO conversion for catalyst sample 1 is given in figure 5.3. The conversion falls as expected and as the velocity within the monolith channels increase the entry length effects rise causing the average mass transfer rate to increase (refer to table 2.2, p.50). If the velocity can be increased to such an extent that the mass transfer rate is very large and therefore is not limiting, the reaction rate recorded represents the intrinsic kinetics. In figure 5.3 it can be seen that conversion falls below the 15% necessary for differential analysis to be valid for flowrates of 15 L/min and above. Figure 5.4 shows the temperatures at the central and peripheral channels. The central channel surface temperature is higher than the peripheral surface channel temperature by approximately 5°C for all flowrates. Hence, it

Fig. 5.3 Conversion versus flowrate, for Tin=371°C and [CO]=0.5% [O_2]=0.25%

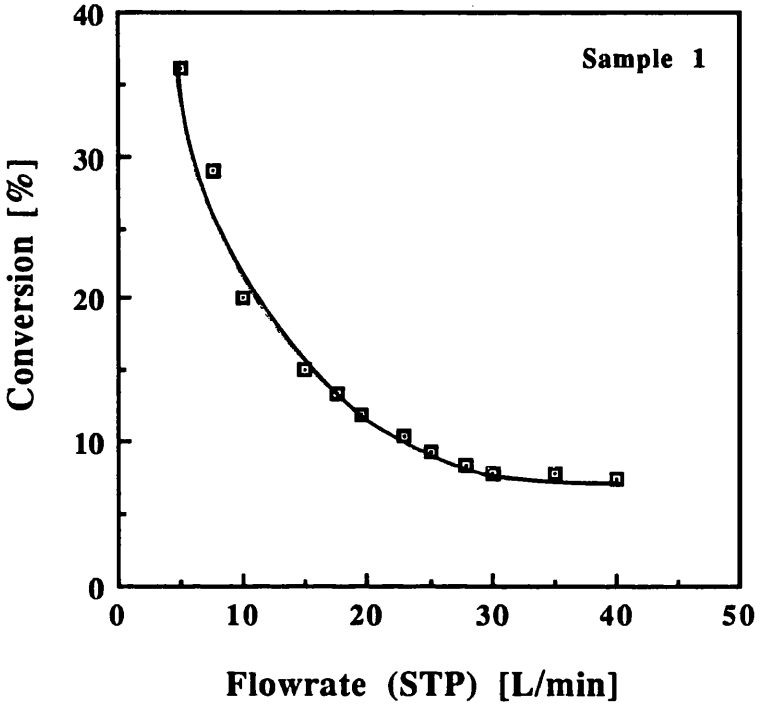

Fig. 5.4 Surface temperatures of reactor slice versus flowrate, Tin=371°C

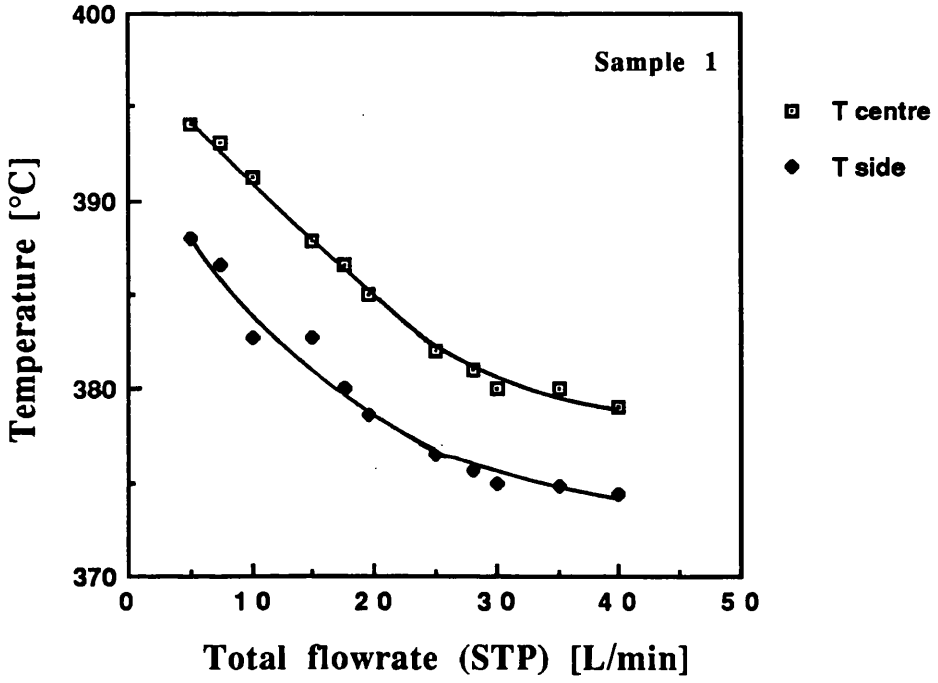

is reasonable to assume that the temperature across the monolith reactor cross-section is constant during differential operation. Using equation 2.4 and using Voltz's parameters given in table 5.2 (p.125), a 5°C temperature rise corresponds to a difference in rate of 15% across the diameter of the monolith sample. If the average temperature is taken this error is reduced to 7.5% as a result of the temperature variation across the reactor. Thus the average cross-sectional surface temperature is taken for the rest of this chapter. In figure 5.4 the difference between the temperature of gases entering (ie. 371°C) and the average surface temperature falls below the 10°C required for differential analysis for a flowrate of 25 L/min and higher. In general therefore from figures 5.3 and 5.4 the reactor is behaving differentially at flowrates of 25 L/min and above. However even if the reactor is behaving differentialy it is still not certain whether the reactor is in the intrinsic kinetic regime.

Figure 5.5 is a plot of reaction rate versus total flowrate. The experiments were repeated 3 to 4 times. The maximum and minimum experimental scatter of the data are also shown in the figure. It can be seen that as the flowrate is raised the average scatter of the data increases. Thus at 40 L/min (STP) the average scatter is 30% whereas at 5 L/min it is only 6.5%. This was probably due to the fact that at the highest flowrate oscillations in the flow stream were observed in the case of the nitrogen flow. High flow operation was also disadvantageous because the cooling system was not very effective, therefore the maximum tolerable flowrate was 30 L/min. In figure 5.5 a best fit curve is drawn through the points and in general it can be seen that the rate continues to rise as flowrate is increased. This is due to a reduction in the mass transfer limiting effects. For the reaction to be behaving intrinsically the reaction should be independant of flowrate. Thus at an inlet temperature of 371°C for test sample one, it seems that the reactor is still in the mass transfer limited region for all flowrates.

(ii) Effect of Temperature

Inlet conditions:
T_{Gin}= 325-425°C
F_t= 30 L/min (STP)
$[O_2]$= 0.25%

Fig. 5.5 Average rate versus total flowrate, [CO]=0.5%, [O_2]=0.25%, at an inlet gas temperature of 371°C

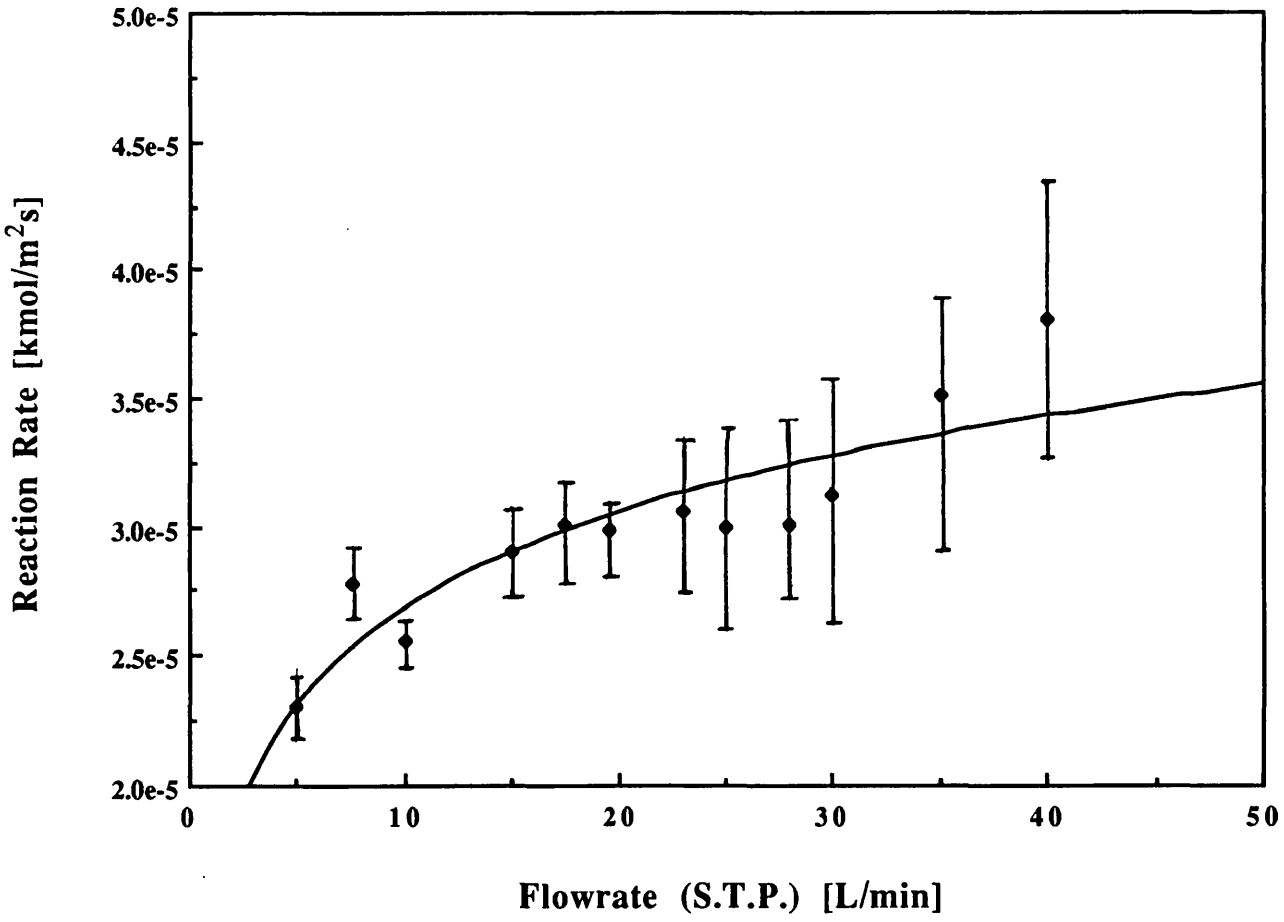

The experimental data are presented in appendix C in table C.3.

A plot of conversion versus inlet temperature for varying inlet CO concentrations is given in figure 5.6 for sample 2. As inlet temperature rises the conversion also increases as would be expected. However, there seems to be a plateau at around 350°C suggesting that the reaction becomes mass transfer limited for CO concentrations of less than 0.5% at these operating conditions.

The fact that the data are mass transfer limited for certain inlet conditions can be seen more clearly in figure 5.7 for sample 2 at a total flowrate of 30 L/min. These data are presented for a differential reactor, hence the temperatures quoted are given to within ±10°C. The behaviour is similar to a Langmuir-Hinshelwood type curve with an initial rise in rate to reach a maximum and then a fall in rate as CO concentration continues to rise. At high CO concentrations (greater than or equal to 0.6 %) the data show a fall in rate as CO concentration is increased, which is an expected trend (refer to equation 2.4). As the temperature increases, the reaction rate should rise because of the Arrhenius relationship. However, at CO concentrations below 0.5%, it can be seen that there is considerable overlap in the rates and therefore there is no significant rise in reaction rate with temperature increase in the inlet gases. Thus the data is mass transfer limited at these concentrations and temperatures. It follows that temperatures well below those investigated should be adopted to be sure of eliminating mass transfer limitation. However, to be certain of eliminating mass transfer the velocity within the channels was also increased (refer to figure 5.5). This was achieved by reducing the total number of channels in a smaller diameter monolith reactor sample as in the case of sample 4. The reactor was placed in a tapered tube, as indicated in figure 5.2.

(iii) Effect of sample size

As discussed above the methods for reducing mass transfer limitations include reducing temperature, and increasing velocity within each channel. The data were found to be free from mass transfer limitation by the following approach.

Fig. 5.6 Conversion versus temperature at varying inlet CO concentrations

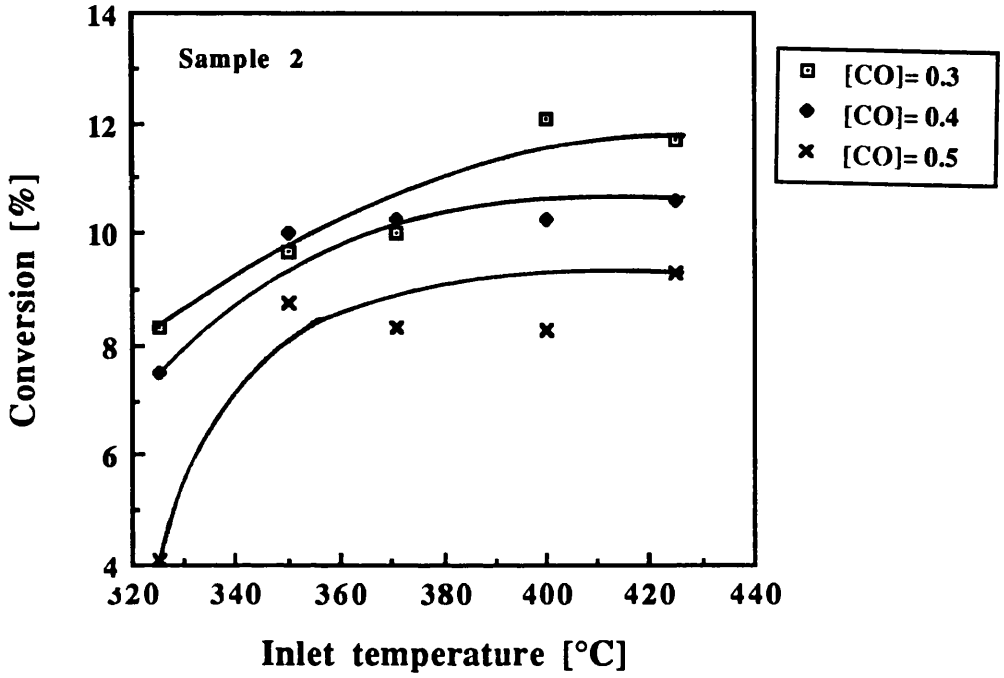

Fig. 5.7 Rate versus CO concentration at varying inlet gas temperatures

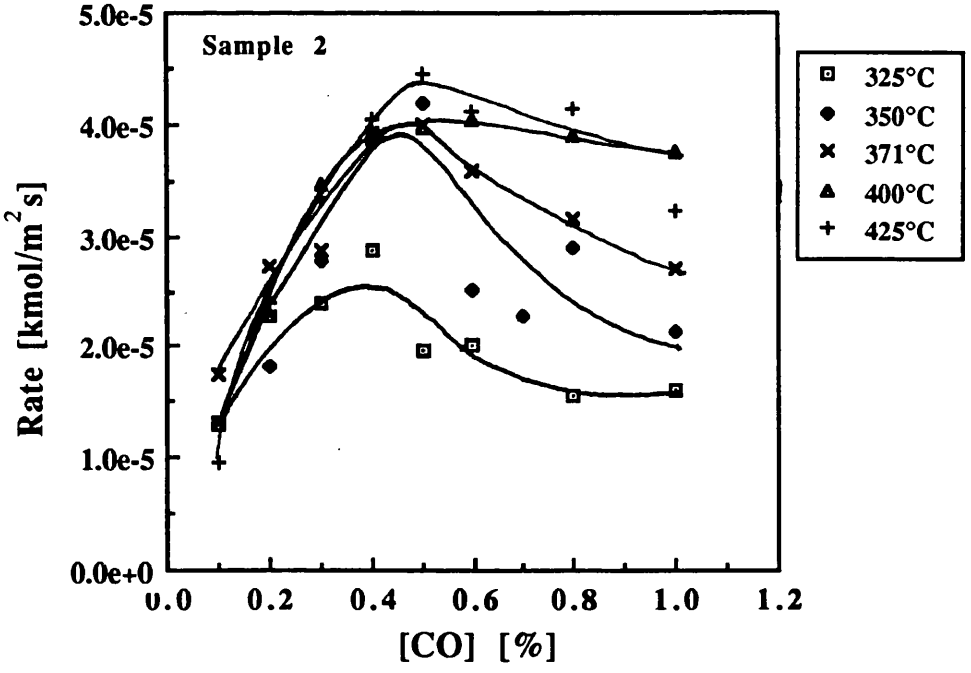

The curves in figure 5.7 show that at low CO concentration, the rate is positive with respect to CO concentration. Thus the rate equation at low CO concentration can be written as:

$$(r_{CO})_{obs} = (k_r)_{obs} [CO]^a [O_2]^b \qquad (5.7)$$

where a and b are unknown constants representing the order of reaction with respect to CO and oxygen respectively.

If equation 5.4 is substituted in to equation 5.7 above then for constant CO and oxygen concentrations, a plot of ln r_{obs} versus $1/T_S$ gives a slope equal to the $-E_{robs}/R$.

In order to eliminate mass transfer limitation, the reactor size as well as the flowrate within each channel was varied. Figure 5.8 is a plot of ln observed rate versus $1/T_S$ for constant CO concentration of 0.2%, drawn for various samples. Compare this plot to the generalized diagram in figure 5.1. As the temperature is reduced the intrinsic kinetics fall below the mass transfer limited kinetics and therefore the observed kinetics are intrinsic. At low temperature, the intrinsic reaction rate is slow relative to the rate of diffusion, and the observed activation energy is the same as the true activation energy, E_r. As the temperature is increased the reaction becomes mass transfer limited.

Figure 5.8 shows, the shift from mass transfer limited situation at high temperatures (above 300°C) to the kinetically-controlled regime (from 225 to 300°C). According to equation 5.6, for strong diffusional limitations the observed activation energy should equal half the actual activation energy. However for complete external mass transfer limitations the activation energy should be almost zero. In figure 5.8 the activation energy is found from the slope. Hence in the intrinsic kinetic regime the slope corresponds to -8643.0 K. The slope corresponding to the mass transfer limited regime is -1245 K. The mass transfer value is rather lower than half the intrinsic value (ie. -8643 K), it follows therefore that the diffusional limitations are relatively unimportant and much of the limitation is due to external mass transfer. Thus it is reasonable to assume that most of the reaction occurs on the external surface of the catalyst with very little occurring within the porous region. Hence an effectiveness factor of one at the surface may be assumed.

Figure 5.8 also shows that the activity of different samples seems to be fairly constant.

Fig. 5.8 Ln observed rate versus $1/T_S$ for varying samples at [CO]=0.2%, [O_2]=0.25 %

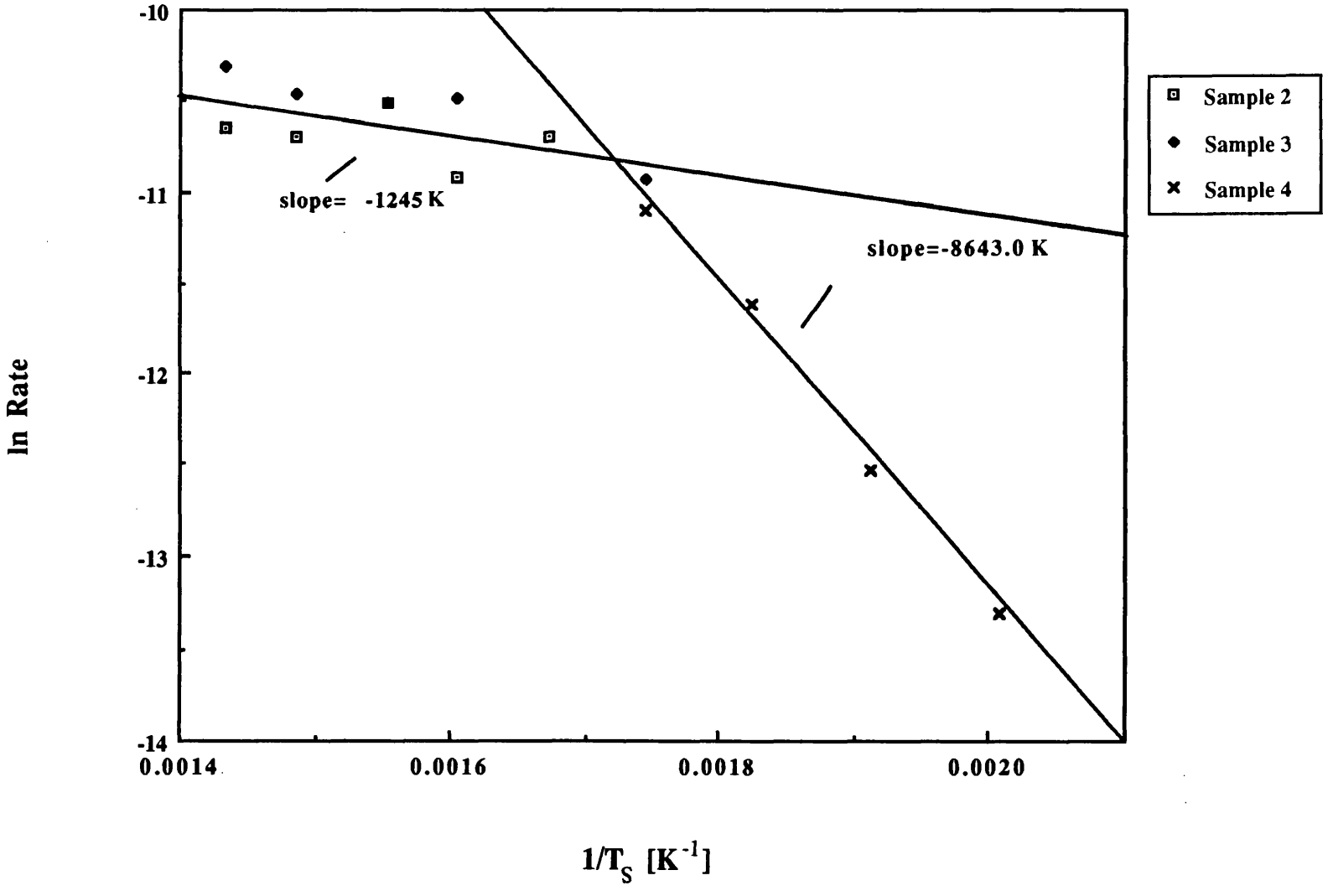

5.6.2 Reaction order with respect to each reactant

The reaction order with respect to each reactant was determined by varying the initial concentration of the reactant, and keeping the initial concentration of the other reactant constant under a fixed total flowrate. It should be noted that in order to measure small changes in conversion at low temperature it was necessary to vary the total flowrate for each particular temperature investigated. Refer to appendix C for the experimental data.

5.6.2.1 Check on reaction order with respect to oxygen

The experimental results are summarized in table C.6 in appendix C. The density change during reaction is assumed to be negligible since there is a large excess of dilutents (refer to appendix D). The experimental data was first tested by the methods described above to test for any mass transfer limitation. Sample 4 data was found to be completely free from mass transfer limitation (T_{Gin}=225-300°C), and is therefore used in the rest of this analysis.

The following inlet conditions are used:

[CO]= 0.5% (vol),
F_t =5-30 L/min (STP), this corresponds to a velocity of 5.8-35 m/s (371°C) within the channels
T_{Gin}= 225-300°C

The order with respect to oxygen can be found for a fixed CO concentration and temperature, from the slope of a plot of rate versus oxygen concentration on logarithmic axes.

The data used in the analysis are given in table C.6 of appendix C. Those data in which excessive temperature rise was found, are underlined and are not used.

A plot of experimental rate versus oxygen concentration drawn on logarithmic axes is given in figure 5.9. The slopes are found by drawing least squares fit lines through the data points and on average these can be seen to be close to one, therefore a first order reaction with respect to oxygen is justified.

Fig. 5.9 Ln rate versus ln oxygen concentration at various temperatures, [CO]=0.5 %

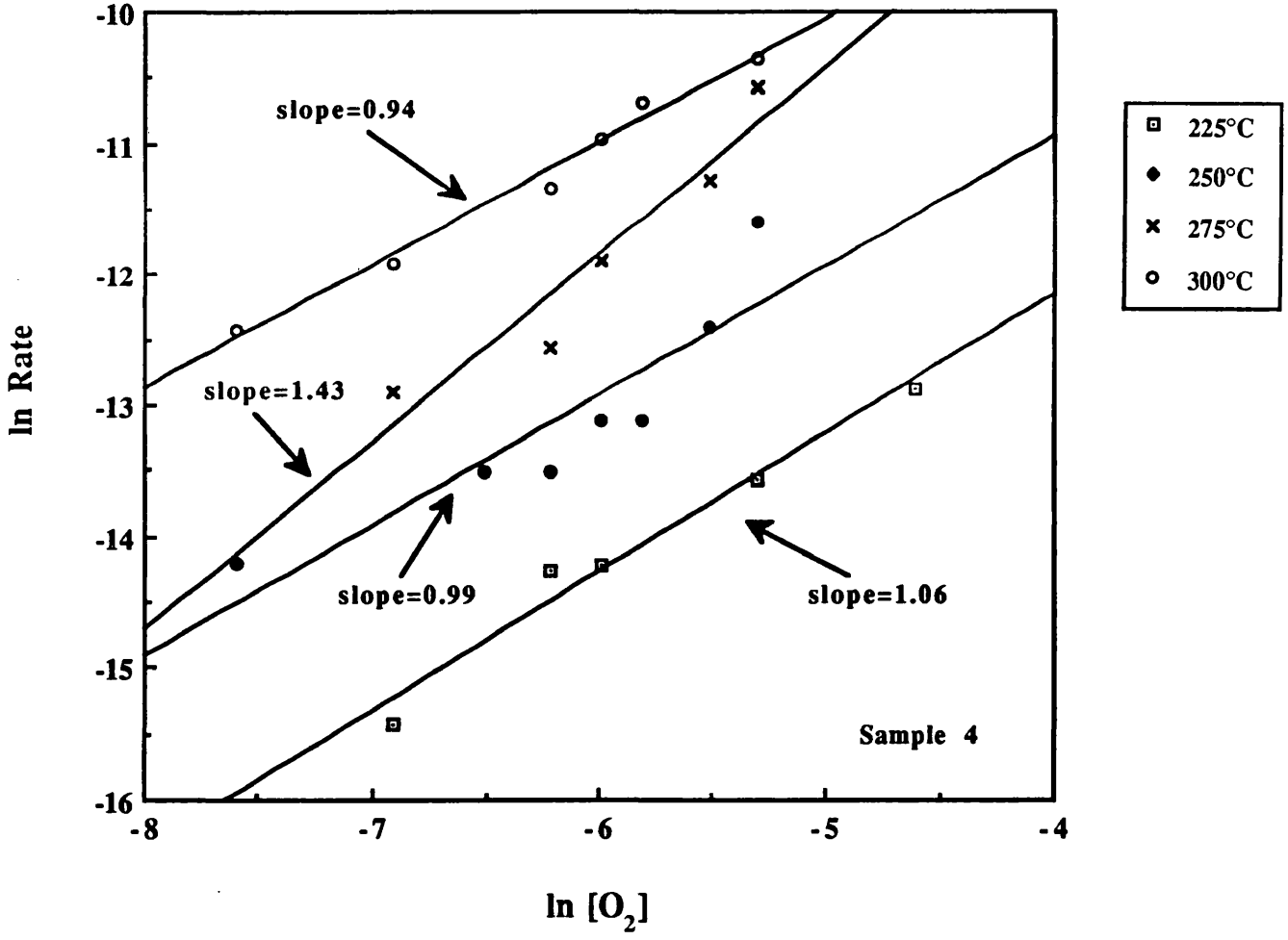

5.6.2.2 Order with respect to carbon monoxide

The order with respect to CO is more complex since at certain inlet conditions it is self inhibiting. For a detailed picture as to the order with respect to carbon monoxide and oxygen the rate data should be curve fitted to a general formula:

$$r_{CO} = \frac{k_r [CO]^a [O_2]^b}{(1 + k_a [CO]^c)^d} \qquad (5.8)$$

with the unknowns a, b, c, d, k_r, and k_a found by minimizing the residual, described by eqn. 5.9 below. However, many data points would be required. It should be stressed that the present work should be regarded as an empirical rate model only and therefore as such it is not attempting to discover or attempt to explain the mechanisms of the reaction. Since much experimental evidence (Literature survey, chapter 2) suggest that a Voltz type Langmuir-Hinshelwood type equation (eqn. 2.4) is acceptable, this will be adopted. Within this equation however, the k_r and k_a values (given by equations 2.5 and 2.6 respectively) are required and are dependent on the type of catalyst used and its corresponding surface area. There are therefore four unknowns ie A, B, E_r and E_a. The rate is non-linear with respect to each of these except for A. Thus a non-linear regression technique is required to solve for these. The non-linear parameter estimation approach is an optimization problem, in which the kinetic parameters are solved by varying them until their combination minimizes the residual, R*, where:

$$R^* = \sum_{1}^{n} (r_i - r_i^*)^2 \qquad (5.9)$$

n is the number of data points, r_i are the experimentally measured reaction rate values, for the ith data point, and r^*_i is the predicted rate value as computed by equation 2.4.

5.6.2.3 Solution method

The rate constants were determined from the quasi-Newton algorithm for finding the minimum of a function fn(A, B, E_r, E_a), subject to fixed upper and lower bounds on the independent variables A, B etc. (Grill and Murray,1976). This was performed with a computer program using the NAG routine (E04JAF) in the Chemical and Biochemical Engineering Department at UCL, in order to minimize the function (5.9) above by fitting experimental data to the model equation 2.4. The data ie. carbon monoxide and oxygen concentrations, surface temperature and rates for each experimental point were fed in to equation 5.9 and using initial estimates of A,B, E_r and E_a, optimum values of A,B, E_r and E_a were generated through minimizing the residual R*, as discussed above.

Initial estimates were taken from the data of Voltz (1973) for platinum on pellet supports based on surface area. The initial guesses are given in table 5.2.

Table: 5.2 Voltz kinetic data constants, used as initial estimates

Kinetic parameter	Value
A	4.14×10^8 kmol/m^2 s
E_r/R	12,600 K
B	65.5
E_a/R	-961 K

The experimental data used in the analysis are given in table C.6 in appendix C. The resulting parameter values are shown in table 5.3 below.

Table 5.3 Calculated kinetic parameters for optimum residual

Kinetic parameter	Calculated Value
A	5.1×10^9 kmol/m^2 s
E_r/R	11,230 K
B	469.3
E_a/R	-100.8 K

The overall average squared error is calculated using:

$$(\text{error})^2 = \frac{\sum_{1}^{n} \left(\frac{r_i - r_i^*}{r_i}\right)^2}{n} \qquad (5.10)$$

This is found to be 0.0833, which corresponds to an overall average error between experimental result and theoretical function of 28.86 %. This error may seem high, however if the difficulty experienced in measuring conversions at low inlet CO and oxygen concentrations is considered this result is quite good. Obviously there is a difference between the calculated kinetic parameters (table 5.3) and those of Voltz (table 5.2) which is attributed to the different catalysts used.

Figure 5.10 is a plot of the experimental and calculated rate data for the temperature range of 225-300°C. The theoretical curves shown are for constant inlet temperatures whereas the experimental data taken at actual conditions are presented in the figure and correspond on average to ±5°C from those specified. This may produce a slight error however it is not significant compared to the errors of the overall fit. This figure gives a qualitative comparison of experiment and theory. Although not used in the calculations the data of sample 3 at 300°C are also shown for comparison purposes. The data seem to compare well considering these were from two different samples. Thus the final overall rate equation found from this study is given by:

$$r_{CO} = \frac{5.1 \times 10^9 \exp\left(-\frac{11,230}{T_s}\right) [CO]\,[O_2]}{\left(1 + 469.3 \exp\left(\frac{100.8}{T_s}\right) [CO]\right)^2} \qquad (5.11)$$

5.7 Differential Reactor Conditions

In the present analysis the reactor is considered to be differential if the conversion is less than or equal to 15%, and the temperature rise along the

Fig. 5.10 Rate versus CO concn. (theory and expt) at constant oxygen concn. for varying inlet temperatures

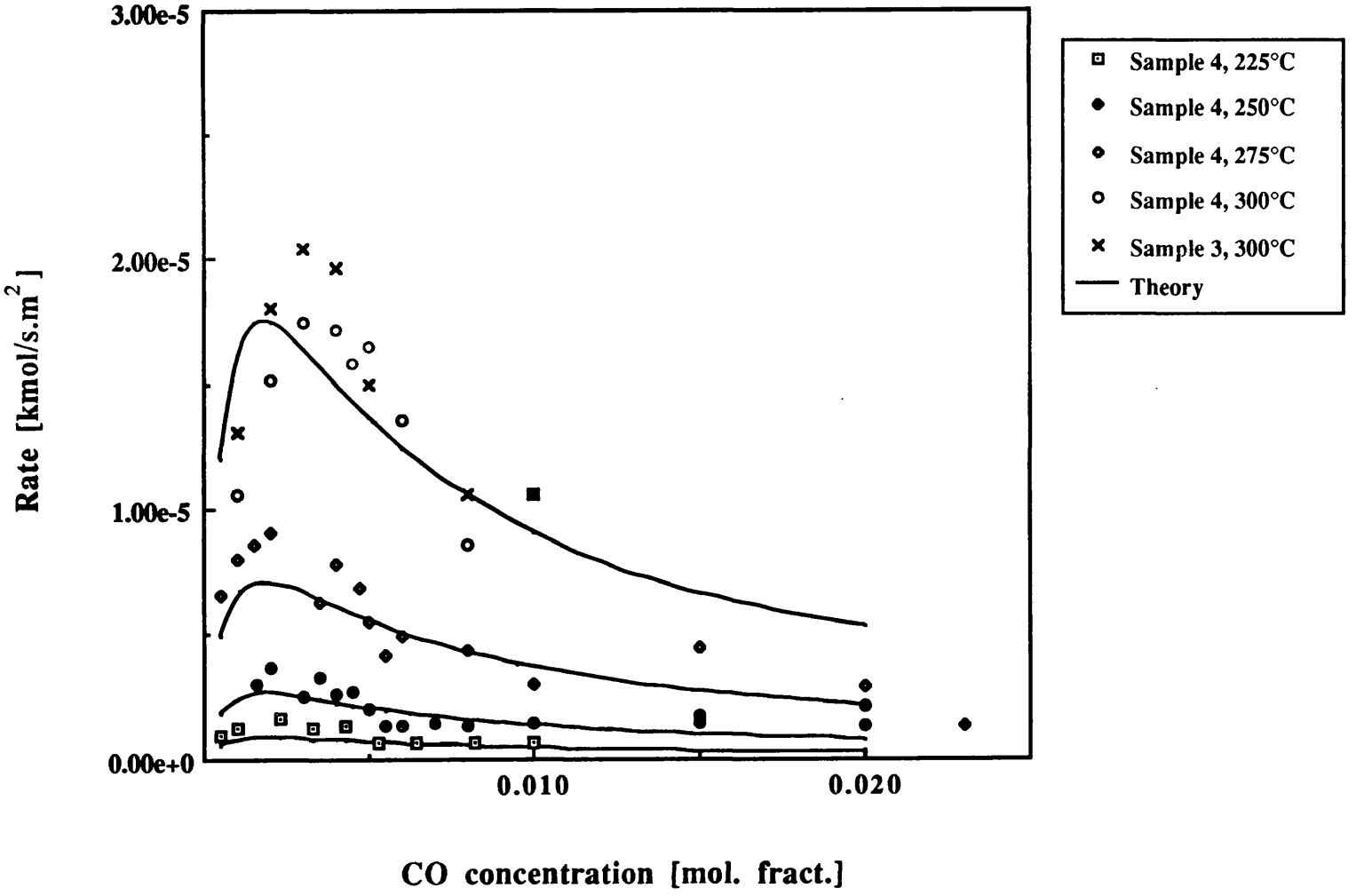

reactor is less than or equal to 10°C. For example, from equation 5.11, this represents an average error of 3.4% for a 15% difference in the CO concentration at 371°C, for [CO]=0.5%, and $[O_2]$=0.25%. A 10°C rise in temperature represents an average error of 27.0% at 371°C and [CO]=0.5%, $[O_2]$=0.25%. However, experimentally the temperature rise on average was no more than 5°C which represents an average error of 14%. These errors are acceptable in any kinetic analysis. Similar errors were also found using Voltz's equation (2.4), and with the parameters in table 5.2.

Note: During experimentation multiplicities and oscillations were not observed. It is possible however, that the instrumentation was not sensitive enough to detect small fluctuations in exit CO concentrations.

CHAPTER 6

EXPERIMENTAL INVESTIGATION OF MONOLITH SYSTEMS

6.1 Introduction

Monoliths have proved to be very effective in catalysts for the auto-industry. However, as discussed in the literature survey, under certain operating conditions their performance has been found to be limited by the rate of mass transfer to the catalyst surface as opposed to reaction rate limited. One method of mitigating this limitation would be to enhance the convective transport processes by axially segmenting the monolith, and therefore causing the flow to continuously re-develop at each successive monolith channel boundary.

In this chapter, the performance of the monolith is studied. The first part describes the experimental reactor and catalyst followed by the procedures. The experimental data are then presented for various core samples, as well as the results of segmenting the monolith.

6.2 The Reactor

The complete experimental apparatus is described in chapter 4. This section describes the monolith reactor.

Monolith cores were supplied by Johnson Matthey as 2.54 cm diameter by 15 cm long samples. These were hand shaped to produce a close fit inside a 1.3 cm internal diameter by 15 cm long stainless steel pipe section. The monolithic catalyst remained in place during experimentation by virtue of friction against the pipe wall. The monolith properties are given in table B.1 of appendix B.

In order to determine the velocity within each channel the total open cross sectional area is required. This can be found from the voidage (given in table B.1 of appendix B) multiplied by the area across the diameter of the pipe.

Due to the cylindrical nature of the pipe, some part channels were removed in order to obtain a tight fit inside the 1.3 cm diameter tube. Therefore for the purposes of surface area the actual number of channels were counted and found to be 70.

Experiments were performed using various sample cores of different lengths. In particular, monolith segmenting work was performed using two sample cores of initial length 15 cm and 8 cm. These are designated set I and set II respectively.

In order to disrupt the flow, the monolith cores were sliced into various sections of equal length. Each of these was rotated at 45° from one another and separated by 2 mm. This was possible by slotting 2 mm spacers on to a stainless steel rod of diameter 0.5 mm which passed axially through the peripheral channel of each consecutive segment. On segmenting, approximately 1-2 mm of sample was lost in the cutting procedure as indicated in table 6.1, which gives the actual segment lengths and the total overall combined length of the segments for sets I and II.

Table 6.1 Overall and segment lengths of monolith core samples tested

Number of segments N	Set I		Set II	
	Length of each segment (cm) L_s	Overall length of catalyst (cm) L_T	Length of each segment (cm) L_s	Overall length of catalyst (cm) L_T
1	15.00	15.00	8.0	8.0
2	7.40	14.80	—	—
4	3.61	14.44	1.91	7.65
8	1.62	12.92	0.90	7.20
16	0.66	10.60	—	—

6.3 Experimental Method

The experimental method followed is described in detail in chapter 4.

Prior to any experimental testing the catalyst is pre-treated to ensure that the catalyst activity remains constant throughout the investigation. This was carried out by passing a reacting mixture of 0.5% CO and 0.25 % (volume basis) oxygen in nitrogen at 400°C for about 20 hrs. This aging process is important, since initial experimental evidence showed unreliable catalyst activity using fresh samples. Also prior to investigation, the catalyst was calcined by passing oxygen at a flowrate of 1 L/min at 400°C for approximately 10 hrs. Regular checks on catalyst activity were performed by arbitrarily repeating experiments from day to day. Once the initial aging

process was followed, repeatability was found to be good, with errors of up to 5 % occurring.

The investigation was carried out to determine the effects on the performance of the reactor, of disrupting the flow, by causing the boundary layer to redevelop. The three measurable effects detected were conversion, temperature rise and pressure drop across the catalyst. During the segmenting experiments, for any changes to be detected in the overall conversion across the reactor an initial conversion for the integral core length should be less than 100 %. Thus an initial core length was experimentally determined, to give an initial conversion of around 50-80 % for a total inlet flowrate of 12.5 L/min which was the average flowrate used in the study. This was performed at relatively high temperatures of around 371°C. Hence for set II the initial core length of 15 cm was reduced to 8 cm for this condition to be met. The remaining 7 cm core was sliced to give 1 cm and 1 mm sample lengths to test the effect of core length on overall conversion (refer to section 6.4.2).

6.4 Results and Discussion

The study was carried out in order to investigate the effect of flowrate, temperature and number of segments on the behaviour of monolith conversion and pressure drop. All the data given were for inlet concentrations of 0.5% and 0.25% (volume basis) for CO and oxygen respectively. The results used in this chapter are given in appendix E.

6.4.1 Effect of total inlet flowrate, F_t

Inlet flowrate has the following effects on reactor performance:

(i) as flowrate is increased the residence time is reduced thus allowing less time for the reaction to take place,

(ii) as the flowrate is increased there is a corresponding rise in mass and heat transfer rates due to the reduction in the thickness of the boundary layer as a result of increased influence of entry length effects.

The two effects are in opposition, with the resulting performance depending on the dominant effect for any particular experimental condition.

Figures 6.1, 6.2 and 6.3 show the conversion, temperature rise (in the gas phase), and pressure drop versus total flowrate for set I (N=1, ie. a core of length 15 cm), at an inlet gas temperature of 371°C. In all the figures presented smooth curves are drawn through the data points unless otherwise stated. An unusual trend is observed for conversion as shown in figure 6.1 where conversion initially decreases with increase in flowrate but then at around 10 L/min begins to rise.

Figures 6.4, 6.5 and 6.6 are the corresponding plots for set II (N=1, ie. core length of 8 cm) at an the inlet temperature of 371°C. These plots show similar behaviours of conversion, temperature rise and pressure drop to those of set I, except that they are extended up to a total flowrate of 30 L/min. In particular, the conversion of figure 6.4 shows the unusual trend of figure 6.1, where conversion tends to decrease with flow then rises to a local maximum. However, with increased flow the conversion then drops off. This can be seen more clearly in figure 6.7 where the conversions of the two samples are plotted on the same graph. The corresponding velocity and Reynolds numbers within the channel as well as the Reynolds number at STP are also indicated in this figure. The fact that set I data lie below set II data even though set I has 87.5 % more effective surface area as compared to set II data, is clear from experimental observations. It was observed that after an experimental run in which reaction took place the catalyst tended to darken in colour. This blackening of the catalyst was observed for set II data, however set I data showed a blackening of only 3/4 of the catalyst along the complete length of the core. This would suggest that the catalyst for set I data was not fully utilized. This could be due to the following reasons:

a) the catalyst was not distributed uniformly across the monolith cross-section,
b) the catalyst sites were unreactive in approximately 1/4 of the monolith.

Both figures 6.2 and 6.5 show a rise in the gas temperature from the inlet to the outlet of the reactor as the reaction proceeds and this tends to become larger as the flowrate is increased. A possible explanation is outlined below.

As mentioned in chapter 3, for an adiabatic reactor with fixed gas inlet compositions, the temperature rise is proportional to the overall conversion,

Fig. 6.1 Conversion against flowrate for set I data, N=1 at 371°C

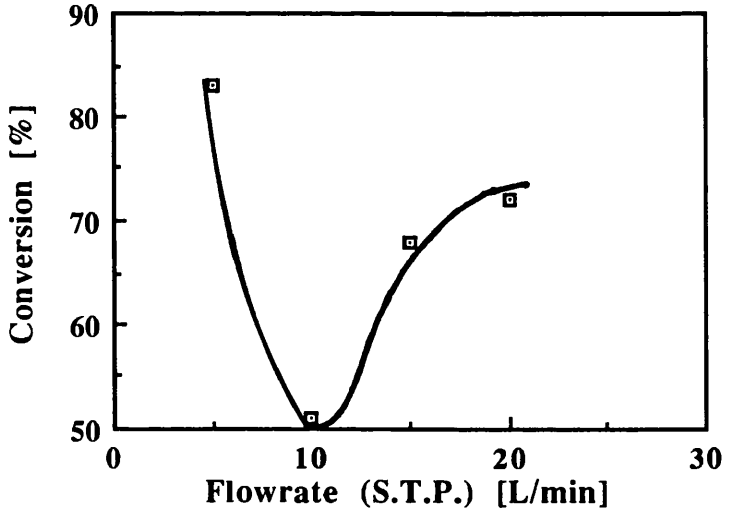

Fig. 6.2 Temperature rise vs flowrate for set I data, N=1 at 371°C

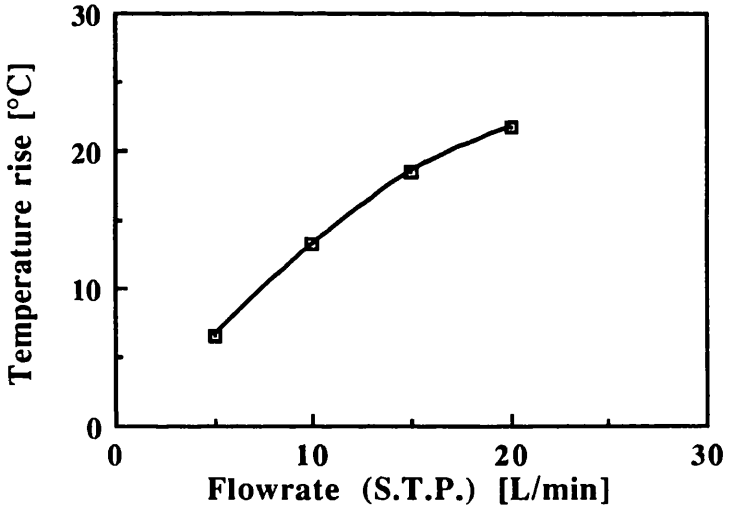

Fig. 6.3 Pressure drop vs flowrate for set I data, N=1 at 371°C

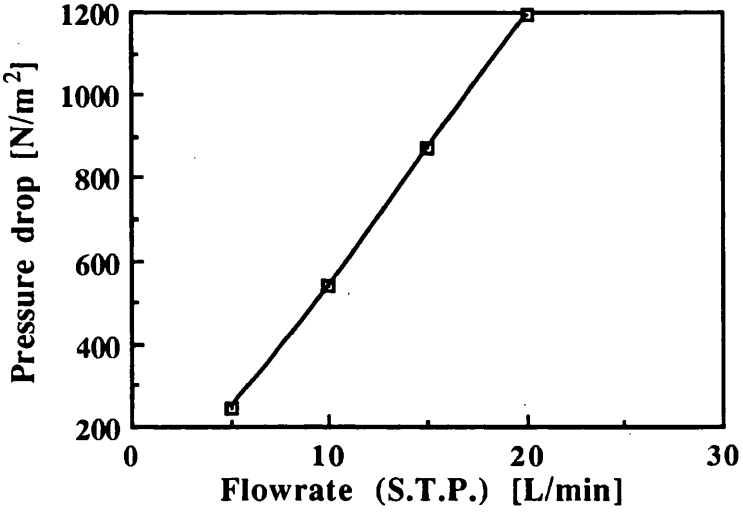

Fig. 6.4 Conversion vs flowrate for data set II, N=1 at 371°C

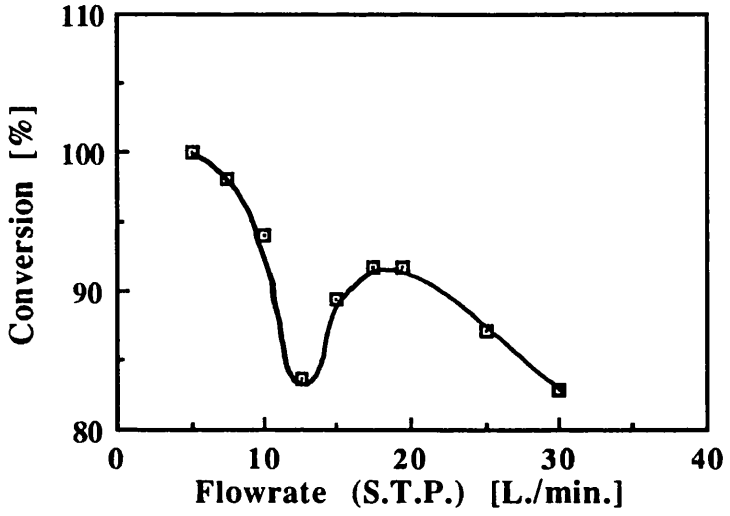

Fig. 6.5 Temperature rise vs flowrate for set II data, N=1 at T=371°C

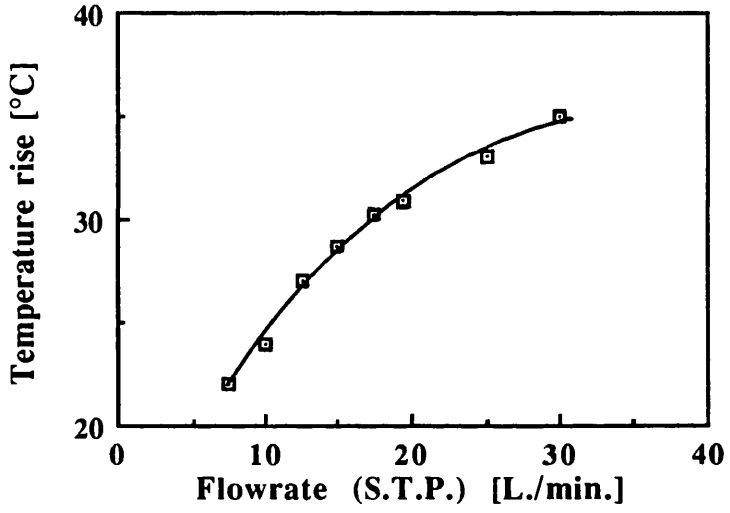

Fig. 6.6 Pressure drop vs flowrate for data set II, N=1 at 371°C

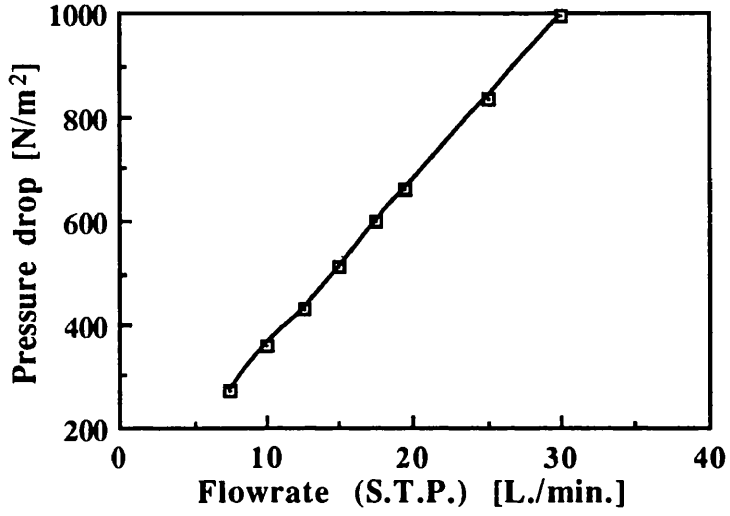

Fig. 6.7 Conversion against flowrate for data sets I and II at 371°C

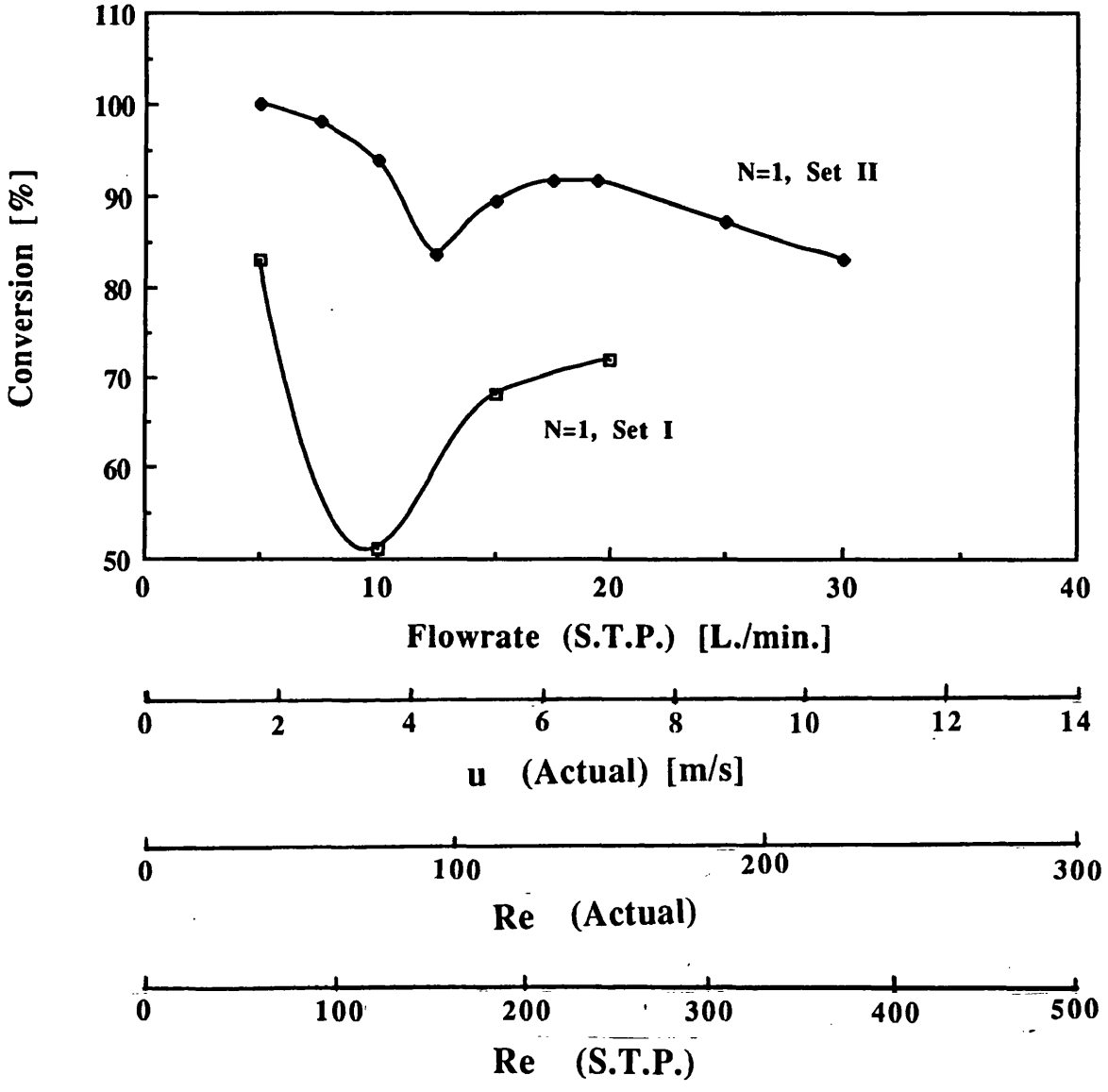

with the result that the adiabatic temperature rise should follow a similar trend to that of conversion. In practice however, this is not the case as seen in figures 6.2 and 6.5 when compared to figures 6.1 and 6.4 respectively. The difference is due to heat losses to the surroundings (ie. by conduction along the pipe wall and then by convection and radiation to the surrounding air), which appear to be independant of flowrate. The latter effect is discussed in more detail later in this section. Figure 6.8 is a plot of overall rate of reaction versus flowrate, taken from data set II, for example. This shows that as the flowrate increases the total number of moles converted also rises even though the fractional conversion in general falls. This is a result of more reactant molecules reaching the catalyst active sites because of an increase in mass transfer. If more moles per unit time are reacting then there should be an increase in the heat released per unit time at the catalyst surface. Therefore, as the flowrate is increased there is an increase in the heat produced, and although this energy is required to heat more moles of gas, the heat losses to the surroundings are less significant as a proportion of the total energy produced. This results in a greater rise in the bulk gas temperature at higher flowrates when compared to lower flowrates.

Prior to reaction, under steady state, in an effort to try to keep the reactor under adiabatic conditions the reactor was placed within a furnace which was run at a higher temperature to that of the reactor. This was in order to balance the heat losses to the surroundings. During reaction, however, it is very rare for the reactor to be completely adiabatic, and therefore it may be expected that there may be heat losses from the reactor surface to the surroundings, by conduction along the pipe and then by convection and radiation to the surroundings.

The difference between the adiabatic and experimental heat production corresponds to the heat lost to the surroundings. Thus:

$$Q_{loss} = Q_{ad} - Q_{expt} \qquad (6.1)$$

where

$$Q_{expt} = m_T \, c_p \, \Delta T_{expt} \qquad (6.2)$$

and

$$Q_{ad} = \Delta H_r \, m_{CO} \, X \qquad (6.3)$$

Fig. 6.8 Total amount of CO converted vs flowrate for data set II at 371°C

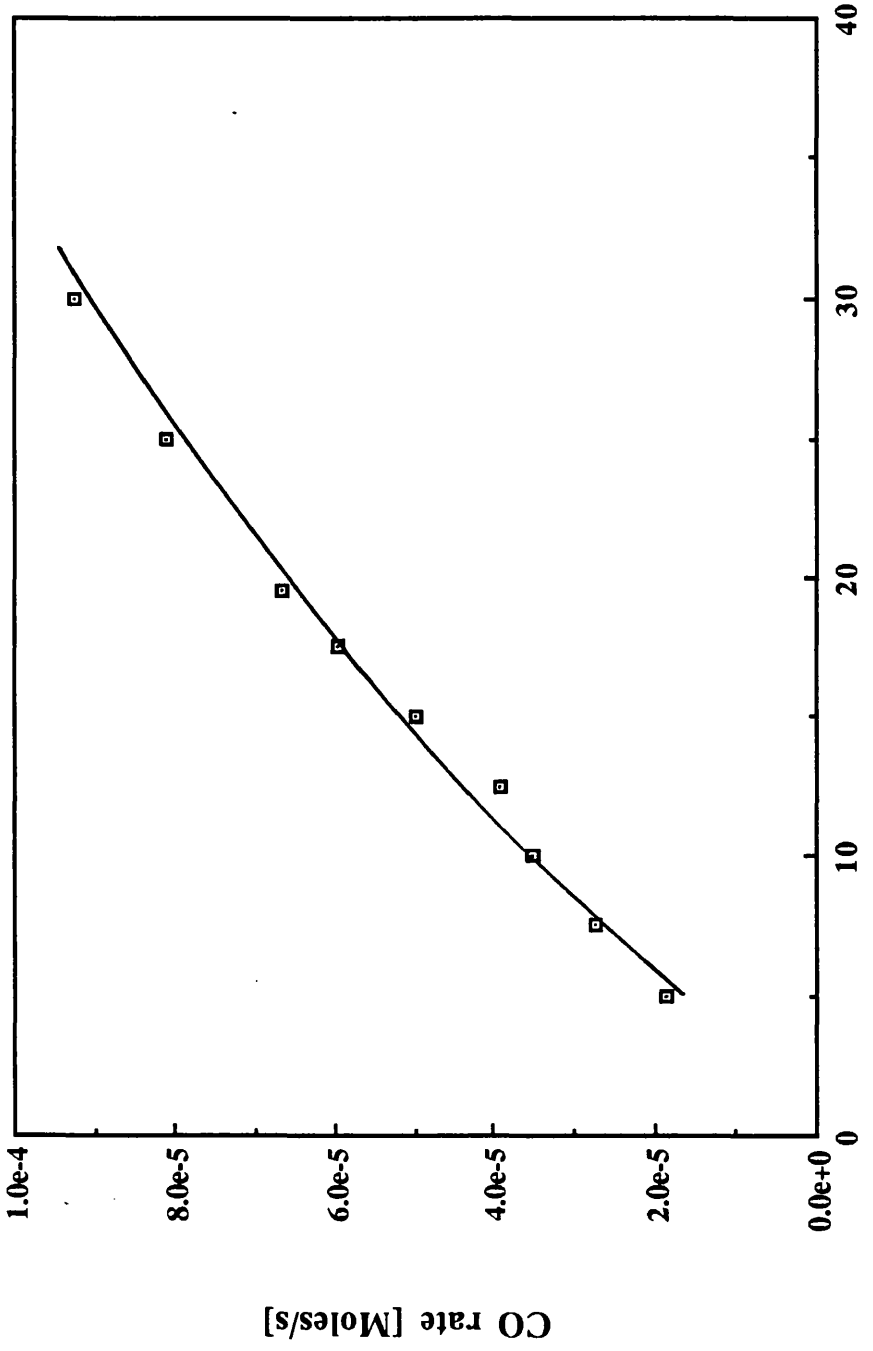

where Q_{loss} is the heat lost to the surroundings, Q_{ad} is the predicted adiabatic heat production, and Q_{expt} is the experimentally detected heat production (ie. from the bulk gas temperature rise).

Figure 6.9 shows the experimental and adiabatic heat production, as well as the heat loss for data set II (N=1) at an inlet gas temperature of 371°C. The heat production tends to increase with flowrate corresponding to the increase in overall amount of reactant being consumed. The experimental heat production runs parallel to the adiabatic heat production curve, with the difference between the two being the heat lost to the surroundings. As mentioned above, heat loss to the surroundings occurs by conduction along the pipe wall and then by convection to the laboratory air. The extent of heat loss is therefore determined by the temperature driving force between the catalyst surface and the laboratory air. In general, at low flowrates, the conversion is higher than at higher flowrates (eg. compare conversion at 5 and 30 L/min in figure 6.3) and therefore it may be expected that the catalyst surface temperature (since the reaction occurs at the wall) is slightly higher than for the lower flowrates, with the result that more heat loss occurs. However, the difference in the surface temperatures is not large with the result that heat losses remain relatively constant for all the flowrates investigated, as seen in figure 6.9.

Figures 6.3 and 6.6 for pressure drop as a function of flowrate give straight lines as would be expected for laminar flow in a tube with fully developed flow (note equation 2.17). The effect of entry lengths for channels with d/L ratios of 0.007-0.013 can be seen in figure 2.9 (Literature Survey) to be up to 10 % of the total channel length for a Reynolds number of 200. It follows therefore that fully developed flow is reasonable through the 8 and 15 cm long channels. The pressure drop data are compared to theory in chapter 8.

6.4.2 Effect of core length

A clearer understanding of the processes occurring during reaction within a monolith can be obtained from axial profiles of concentration and temperature of CO in the gas phase along the channel length. With the experimental set-up, these cannot be measured directly within each channel, however the average channel outlet gas concentration and temperature may be measured using samples of varying core length.

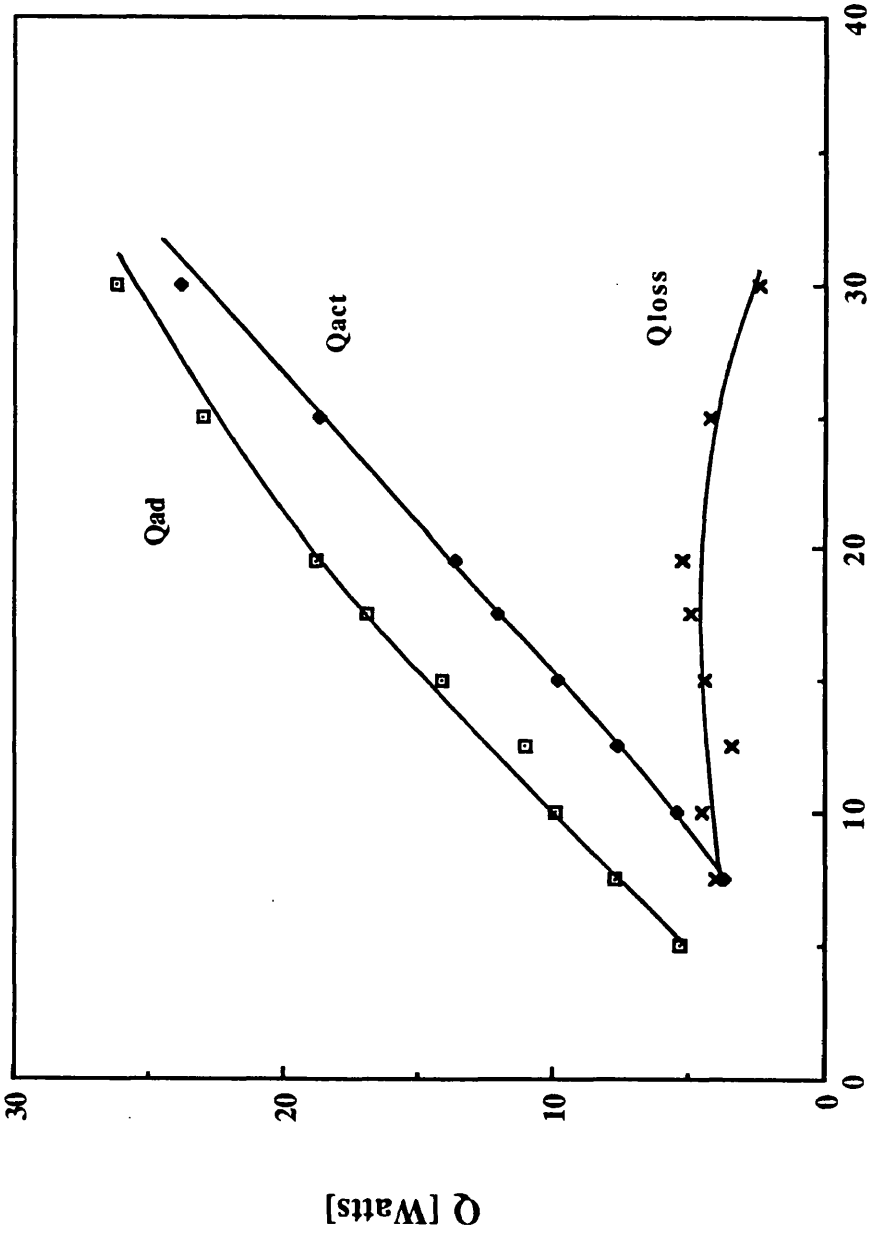

Fig. 6.9 Experimental and adiabatic production of heat, and heat losses for set II, N=1 at 371°C

The effect of core length was examined using the core samples of set II cut at varying lengths. Figure 6.10 is a plot of conversion versus flowrate for various core lengths at an inlet temperature of 371°C. The unusual trend observed for L=8 cm at 12.5 L/min (ie. local minimum/maximum) is not seen for the shorter length monolith reactors. The trend, for L=8 cm core length, however is very real and was found to be repeatable from day to day as well as for various samples (sets I and II refer to figure 6.7). Indeed all the experimental results were found to be very repeatable to within ±5 %. At first glance, one may postulate a possible explanation in terms of multiplicity, particularly in the case of CO oxidation, ie. at 12.5 L/min (STP) the reaction jumps from the lower steady state to the higher steady state as flowrate is increased. However, as mentioned in chapter 5, at 371°C the reactor is completely mass transfer limited, and therefore, multiple steady states are not plausible.

Figure 6.10 can be re-drawn to give figure 6.11 of conversion against core length. It can be seen that at the lower flowrates ie. 10 L/min (STP) and less, much of the conversion occurs in the first few centimetres along the length of the monolith, but with increase in total flowrate the conversion is spread along the length of the monolith. This shows that an increase in inlet velocity causes the ignition point to move along the channel length towards the exit of the reactor. This is due to the fact that as the velocity within the channel increases the Sherwood and Nusselt numbers increase. Increased Sherwood number leads to improved conversion after light-off, however, for light-off to occur a minimum wall temperature is required for the heterogeneous reaction to take place. The effect of high Nusselt number is to increase heat loss from the catalyst to the gas stream with the result that the surface temperature rises less rapidly leading to later ignition along the channel length. Once the reaction is self-sustaining it may be regarded as ignited. In all cases however, light-off occurs very close to the channel entrance, since in figure 6.11 there is conversion for all flowrates, even at 0.1 cm along the channel monolith length. Hence, the assumption that light-off occurs at the catalyst entrance (in chapter 8) is reasonable.

Increasing the reactor length has a similar effect to reducing the inlet velocity by increasing the residence time. Hence, higher exit CO conversion is expected for longer reactor lengths. Indeed for the study, it would seem that most of the conversion occurs within the first 8 cm of the reactor for all flowrates.

Fig. 6. 10 Conversion vs flowrate for various core lengths at 371°C

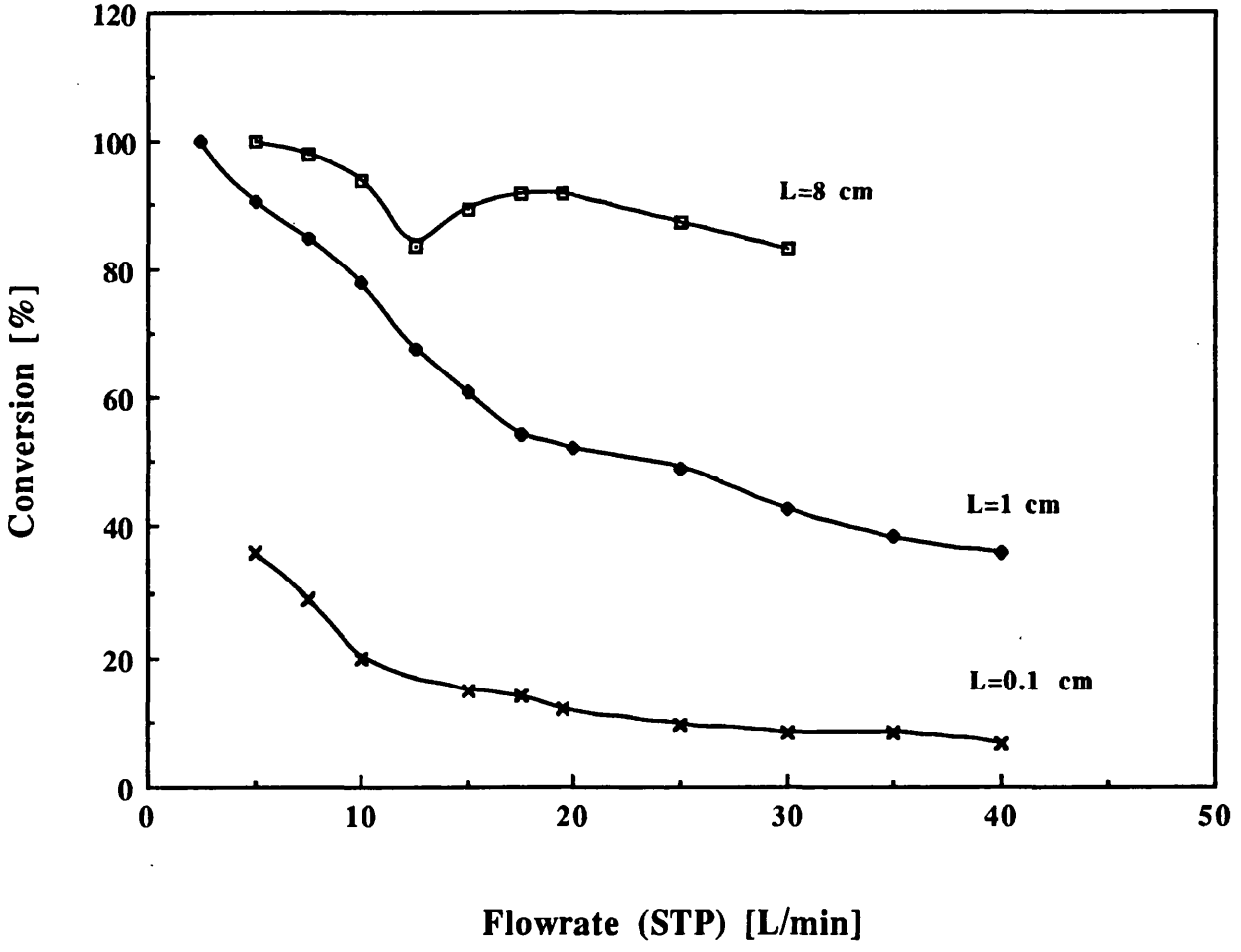

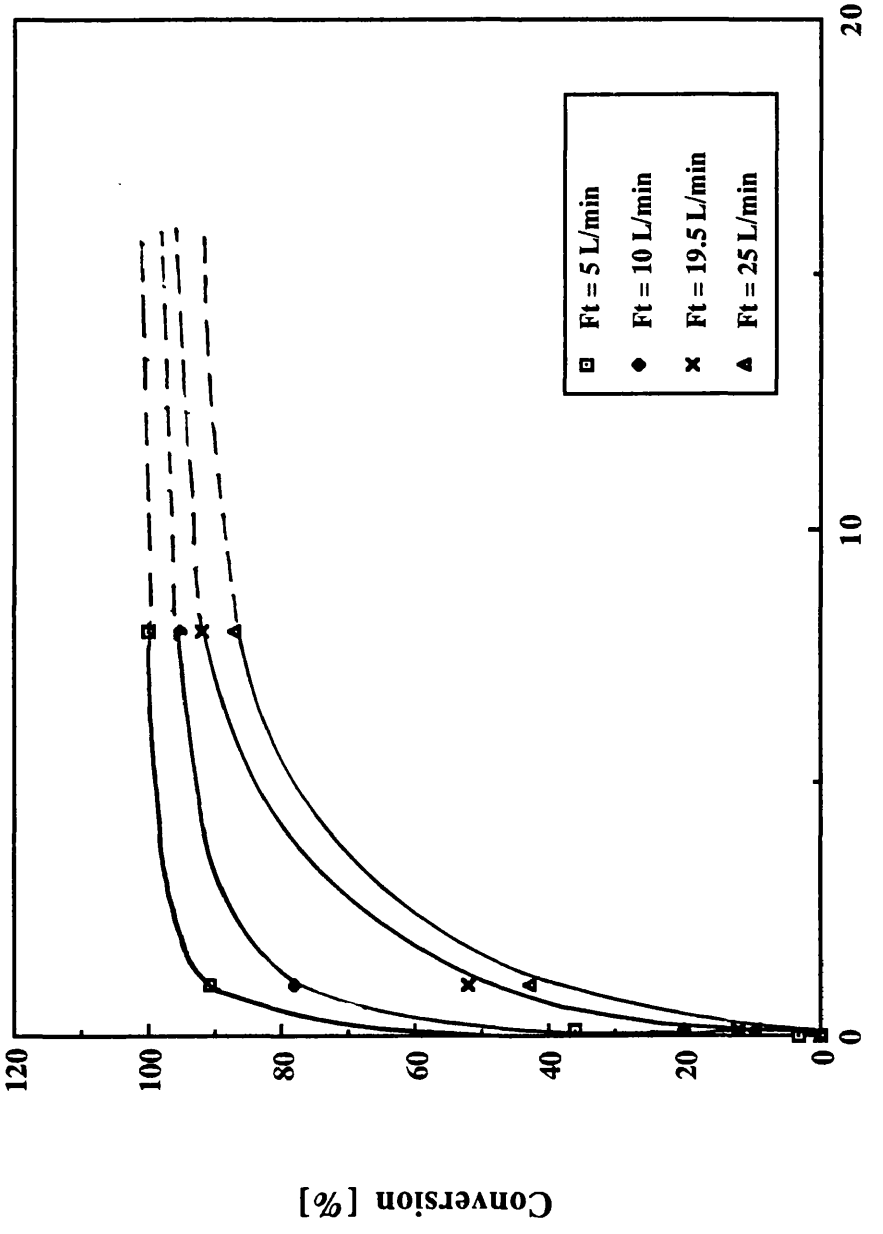

Fig. 6.11 Conversion vs core length at 371°C

Note that a more accurate shape for each curve could have been drawn if more data was available ie. for different monolith core lengths. However, in figure 6.11 there are only three data points per curve, therefore these can be extrapolated for large reactor core lengths to approach 100 % conversion.

6.4.3 Effect of number of segments

On segmenting the monolith, approximately 1-2 mm of sample was lost at each segment slice due to the cutting procedure. In general, since some catalyst is lost when segmenting, direct comparisons are not strictly correct between the integral and segmented monolith conversions. However, in figure 6.11 it can be seen that at the far end of the catalyst, ie. 7.5 cm and longer, the overall conversion does not change by very much and therefore can be assumed to be constant. Thus direct comparisons of conversion between integral and segmented monoliths can be made for both sets I and II.

Figures 6.12, 6.13 and 6.14 show the effects of segmenting the monolith core for data set I (at 371°C), on conversion, temperature rise and pressure drop. Figures 6.15, 6.16 and 6.17 are the corresponding results at 371°C for set II data. It is clear from figures 6.12 and 6.15 that there is an enhancement effect on conversion as the number of segments is increased even though there is some small loss of catalyst when segmenting occurs. Hence at a total flowrate of 10 L/min (STP) for set I the conversion increases from 53 % to 68 % as the number of segments increases from one to 16. This represents an enhancement in conversion of 28.3 %. This is a substantial increase in overall conversion and is primarily due to the increased entry length effects as a result of segmentation.

Similarly, for data set II at a flowrate of 10 L/min (STP) the overall conversion increases from 94 % up to 100 % as the number of segments is increased from one to 8 representing an enhancement of 6.4 % in conversion as a result of segmentation.

The unusual trend (ie. upturn in conversion at around 12.5 L/min) observed for N=1 for sets I and II is seen to occur for all N in the case of set I data, shown in figure 6.12. This is not so for set II data. However, since the experimental conversions for N=4 and 8 at flowrates close to 12.5 L/min are very nearly 100 %, it is possible that the upturn is not discernible.

Temperature rise in the gas phase versus flowrate for varying number of segments is given in figures 6.13 and 6.16 for data sets I and II respectively.

Fig. 6.12 Conversion vs flowrate for data set I for various N at 371°C

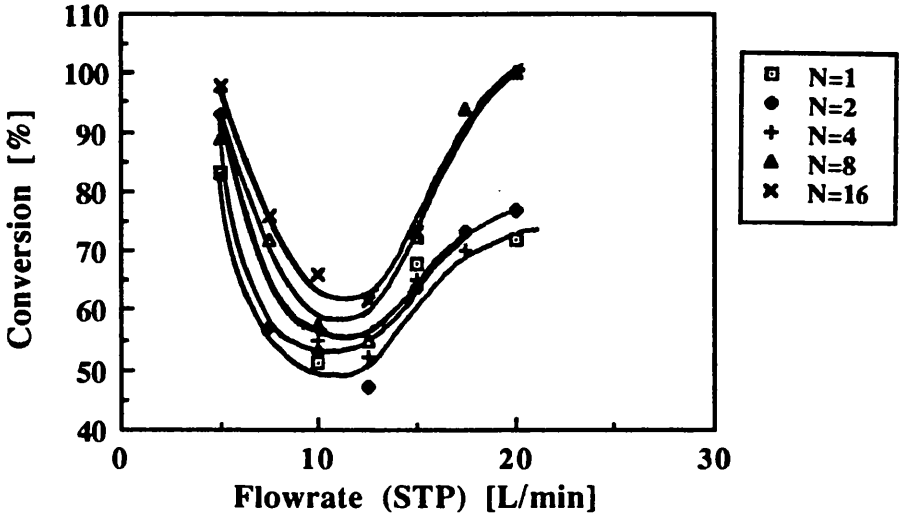

Fig. 6.13 Temperature rise vs flowrate for various N for set I data at 371°C

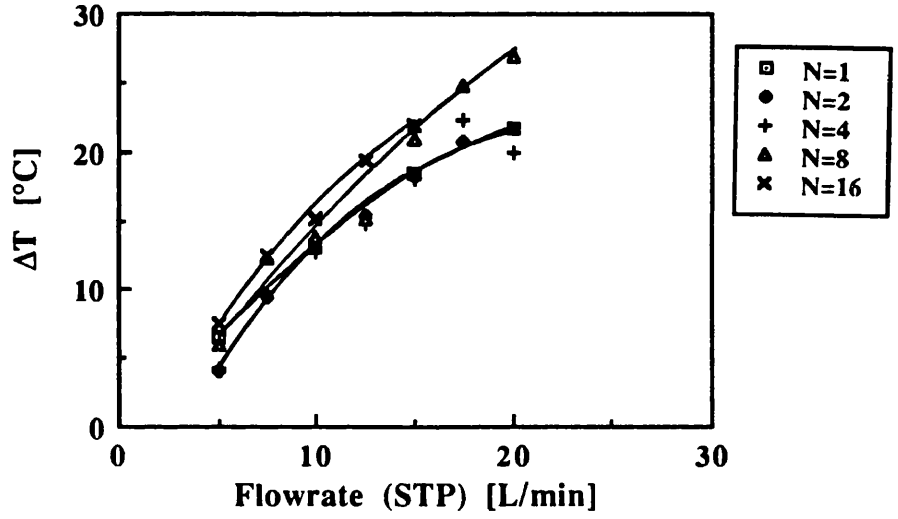

Fig. 6.14 Pressure drop vs flowrate for various N for data set I at 371°C

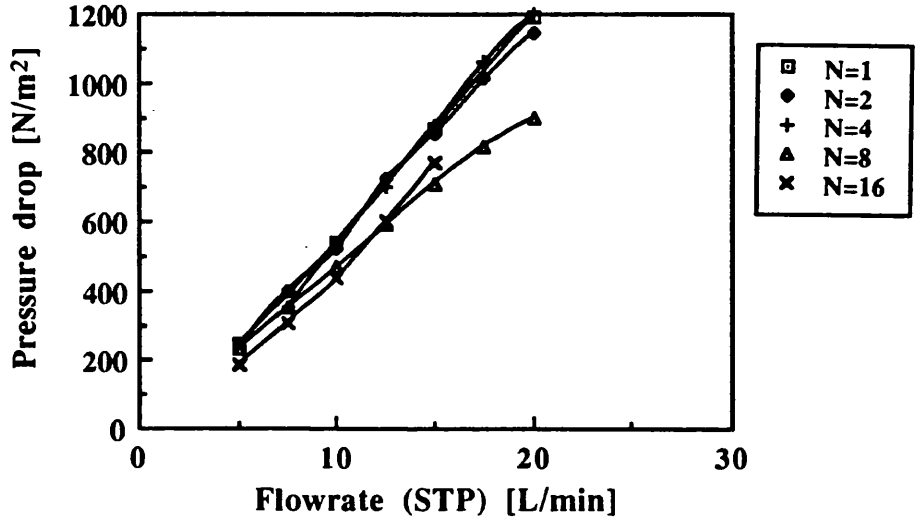

Fig. 6.15 Conversion vs flowrate for different N (set II) at 371°C

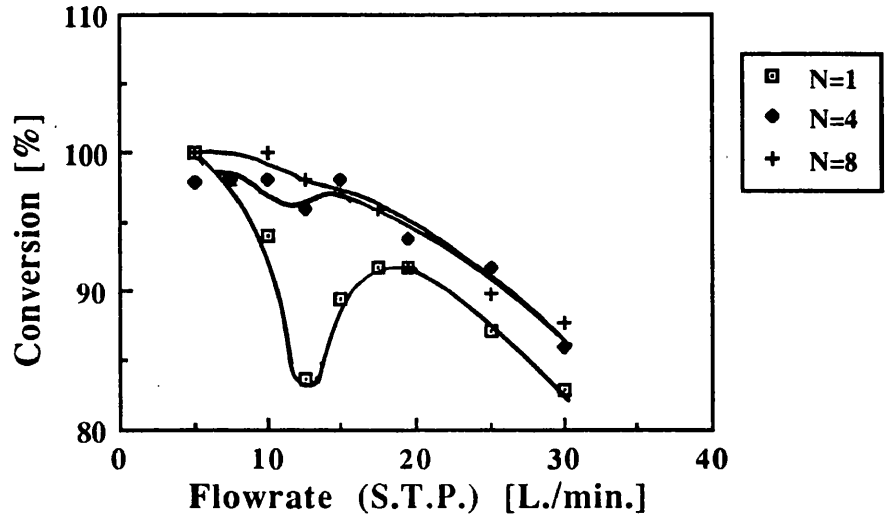

Fig. 6.16 Temperature rise vs flowrate for various N (data set II) at 371°C

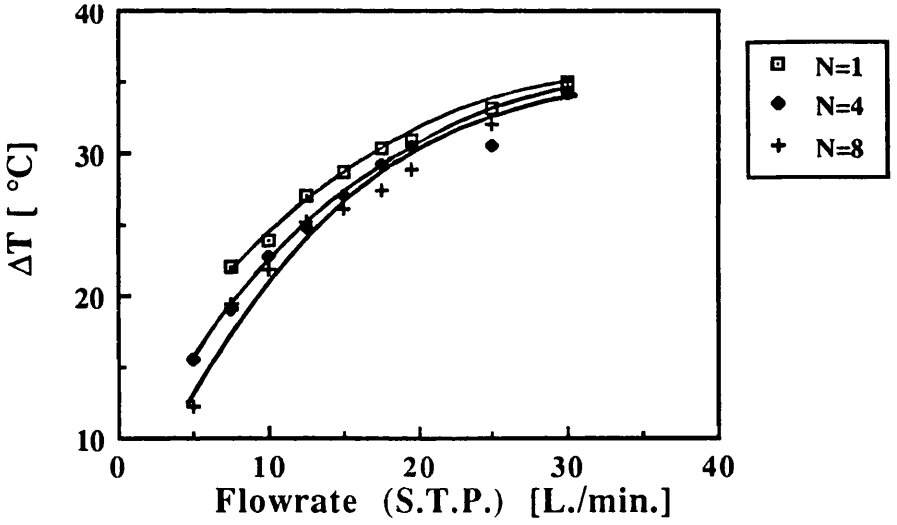

Fig. 6.17 Pressure drop vs flowrate for different N (set II) at 371°C

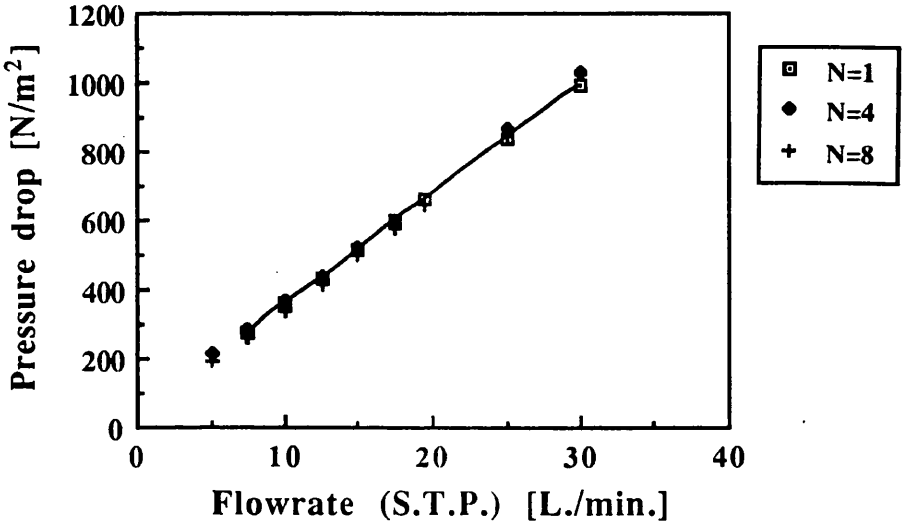

Although there is some experimental scatter it can be seen that the data lie essentially on one or more curves. It is difficult however, to separate these in any particular order but in general the greater the rate of reaction, the greater is the heat produced as a result of reaction at the catalyst wall. The extent of reaction increases with the number of segments as a result of increased overall average Sherwood number. However, although the bulk gases are heated within the segment sections they tend to lose heat within the inter-segment spacing. As the number of segments is increased the overall average Nusselt number as well as the effective surface area for heat loss increase. Both these effects lead to increased heat losses (ie. to the surroundings first by convection from the bulk gases to the pipe wall, then by conduction and then convection to the laboratory air) within the inter-segment spacing. Therefore, the resulting temperature rise in the gas phase is a function of two opposing factors ie. increased heat release from reaction as Sherwood number increases as opposed to increased heat losses to the surroundings as Nusselt number and effective surface area for heat loss are increased.

Figures 6.14 and 6.17 are the pressure drops measured across the varying total number of segments for sets I and II respectively. As the flowrate is raised the pressure drop increases, however unexpectedly it can be seen that as the number of segments increases the pressure drop decreases rather than increases as might be expected for increased friction resistances experienced when disrupting the flow. This can be explained since when sliced approximately 1-2 mm length of the catalyst core was lost at each section. Therefore although the overall average friction factor increases, the total channel length decreases which counteracts the increase in pressure drop.

6.4.4 Effect of inlet temperature, T_{Gin}

Figures 6.18 ,6.19 and 6.20 show the effect of temperature on conversion, temperature rise and pressure drop for set II data (N=1).

In figure 6.18, for flowrates below 7.5 L/min, inlet temperature does not seem to effect the overall conversion to any significant extent between 250 and 400°C a rise of 150 °C. As the inlet temperature is increased the heterogeneous reaction kinetics would be expected to rise exponentially, resulting in an increase in outlet conversion. This suggests therefore that the reaction is predominantly mass transfer limited at flowrates of 7.5 L/min and

Fig. 6.18 Conversion vs flowrate at varying inlet temperatures for data set II

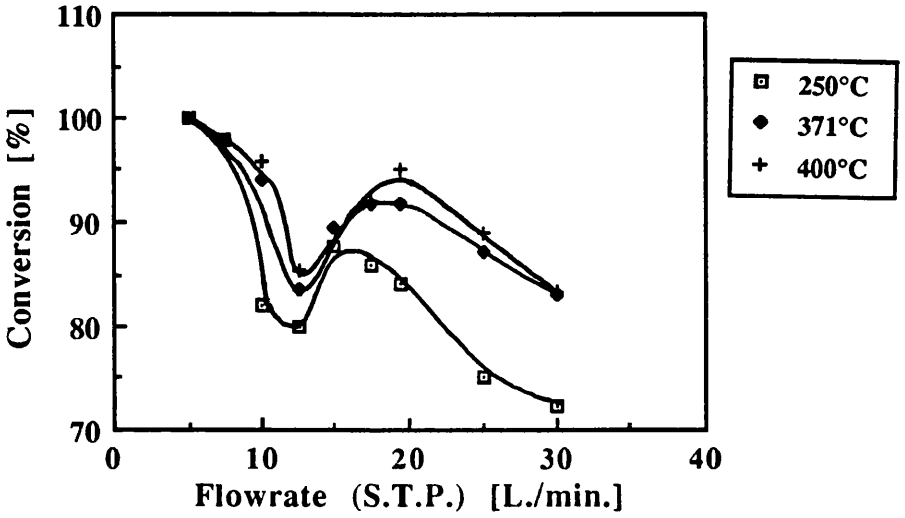

Fig. 6.19 Temperature rise versus flowrate at different inlet temperatures for data set II

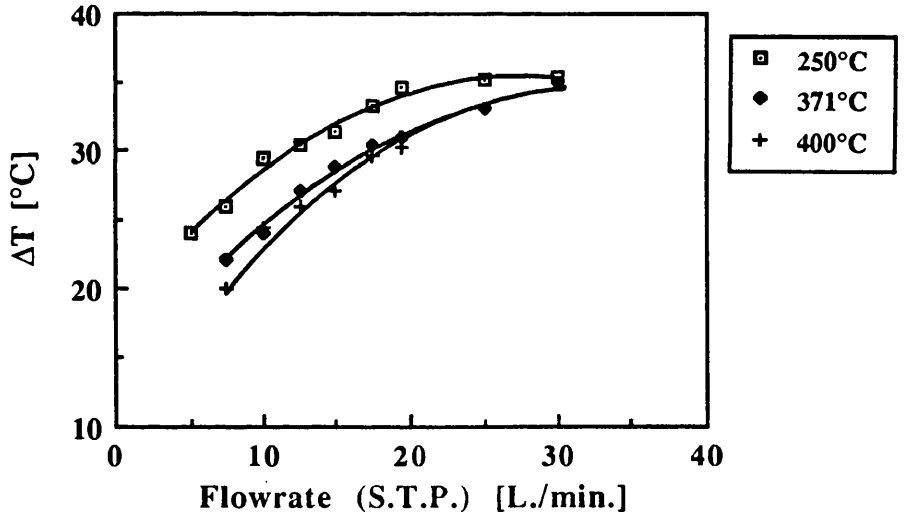

Fig. 6.20 Pressure drop versus flowrate at varying inlet temperature for data set II

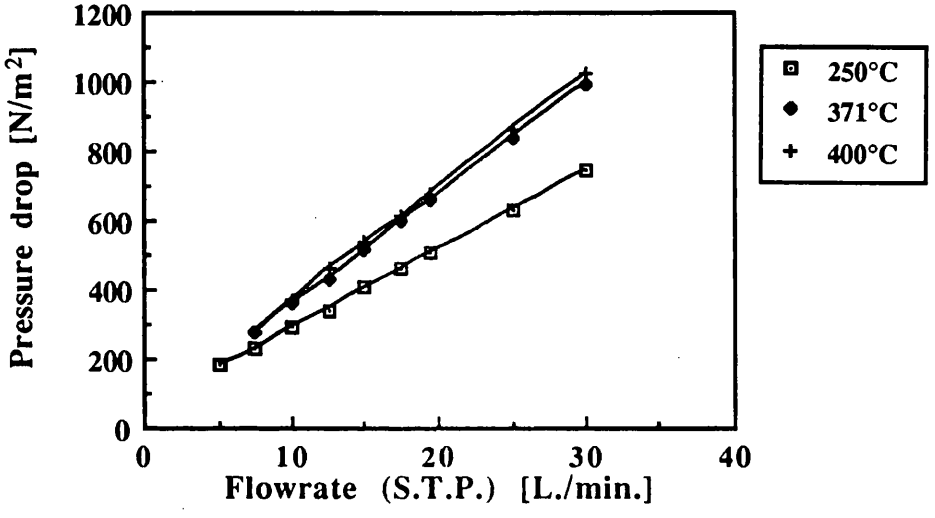

less. As the temperature increases from 250 to 371°C at higher flowrates however, there is a significant difference in the extent of conversion (ie. at 30 L/min the conversion rises from 72 % at 250°C up to 83 % at 371°C a difference of 11 % in conversion). Hence temperature is indeed influencing the reaction, and therefore the reaction is kinetically limited for at least some of the monolith length, but not necessarily all, at 250°C. In chapter 5, a 1 mm long sample experienced complete mass transfer limitation at temperatures above 300°C. It follows therefore that at the temperatures 371 and 400°C the reaction is completely mass transfer limited for all the flowrates in figure 6.18. The only effects at higher temperature are therefore mass transfer and residence time. The shape of the curve is therefore determined by these two competing effects.

Figure 6.19 is the corresponding temperature rise at varying inlet temperatures. This shows that the higher the temperature, the lower is the temperature rise. As discussed in section 6.4.1 heat losses occur as a result of conduction along the pipe wall and then by convection to the laboratory air. At higher temperatures there is a greater temperature driving potential between the reactor and the laboratory air and therefore it is expected that there should be greater heat losses. However, as the temperature is increased from 250 to 371°C there is also greater conversion with more heat being generated. The final outlet gas bulk temperature of the gases is a result of these competing effects. For a flowrate 10 L/min (STP) the amount of heat generated from the reaction is 9.92 Watts and 8.66 Watts at 371°C and 250°C respectively. However, the heat lost to the surroundings is 4.5 Watts and 2.14 Watts at 371°C and 250°C respectively. Thus at higher temperatures the overwhelming effect is the greater heat lost to the surroundings.

Pressure drop as a function of inlet temperature is illustrated in figure 6.20. This shows that the lower the temperature then the lower is the pressure drop. Pressure drop may be evaluated using eqn. 2.17:

$$\Delta P = f \frac{L}{2d} (\rho u^2) \qquad (2.17)$$

where f is the Moody friction factor which for fully developed laminar flow is inversely proportional to Reynolds number. The effect of increase in temperature is to increase the velocity, increase viscosity, reduce the density, reduce the Re and therefore increase the friction factor. Therefore, from equation 2.17, it is expected that pressure drop should increase with increase in

temperature. For the case when the flow is not fully developed, the friction factor is given by equation 2.18, but the overall effect is still similar to that for fully developed flow.

Experiments were also performed for varying number of segments at 250°C and 400°C for set II data. These are shown in figures 6.21, 6.22 and 6.23 for an inlet temperature of 250°C, and figures 6.24 , 6.25 and 6.26 at an inlet temperature of 400°C.

Figure 6.18 seemed to suggest that at 250°C the reaction was kinetically limited above 7.5 L/min. However, in figure 6.21 at flowrates below 17.5 L/min there is enhancement in conversion as the number of segments is increased showing that the reactor is mass transfer limited. There seems at first glance to be an apparant contradiction. However, this can be resolved by the following explanation. The reaction can be both kinetically and mass transfer limited, with the mass and kinetic rates being of the same order of magnitude, (refer to section 8.8 in chapter 8). Along the channel the reaction can start off being kinetically limited, however, as the temperature increases with reaction, the kinetic rate is enhanced sufficiently for the mass transfer to become the rate limiting step. Hence, it is possible for there to be improvements in conversion as a result of enhancing the mass transfer, in this case by segmentation. Also, as the flowrate is increased the mass transfer increases sufficiently for the reaction to become kinetically rather than mass transfer limited with the result that above 20 L/min the curves in figure 6.21 tend to approach one another. The fact that the conversion for N=8 falls below that for N=1 could be a result of increased heat losses as a result of segmentation (refer to section 6.4.3) causing the kinetics of the reaction to be reduced.

At 400°C there is a clear indication of enhancement in conversion for all flowrates as the number of elements is increased as shown in figure 6.24.

Figures 6.22 and 6.25 for temperature rise versus flowrate behave similarly to that of figure 6.16 at 371°C for similar reasons. Also figures 6.23 and 6.26 for pressure drop may be compared to figure 6.17 at 371°C, again for the same reasons.

6.5 Enhancement Factors for Conversion

The figures 6.12 and 6.15 for sets I and II respectively at 371°C show

Fig. 6.21 Conversion versus flowrate for varying N at 250°C for data set II

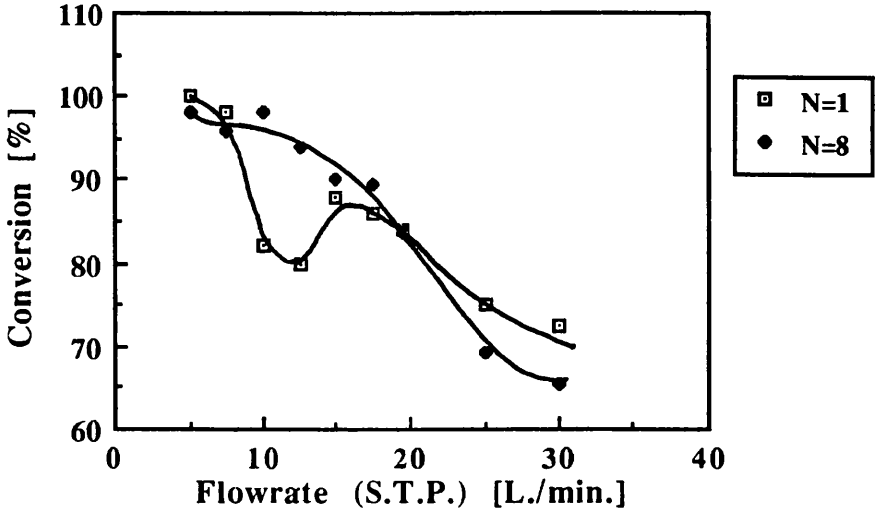

Fig 6.22 Temperature rise versus flowrate for varying N for data set II at 250°C

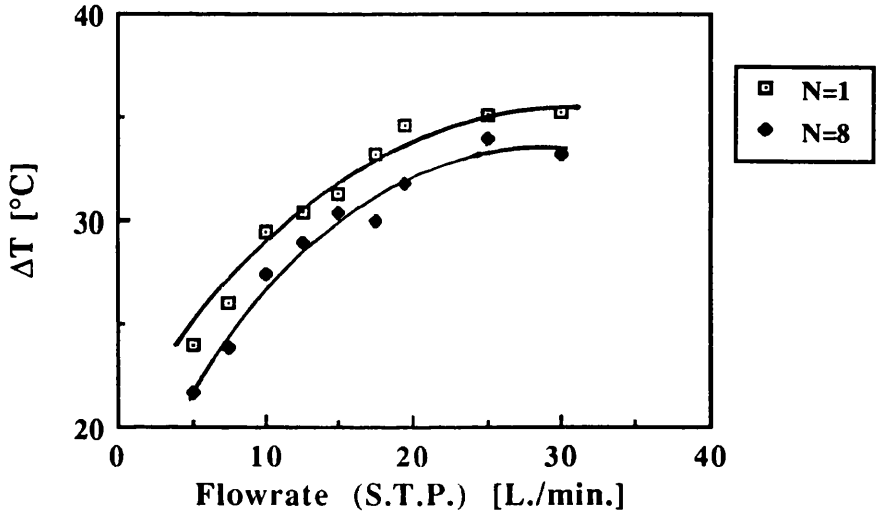

Fig. 6.23 Pressure drop versus flowrate for varying N for data set II at 250°C

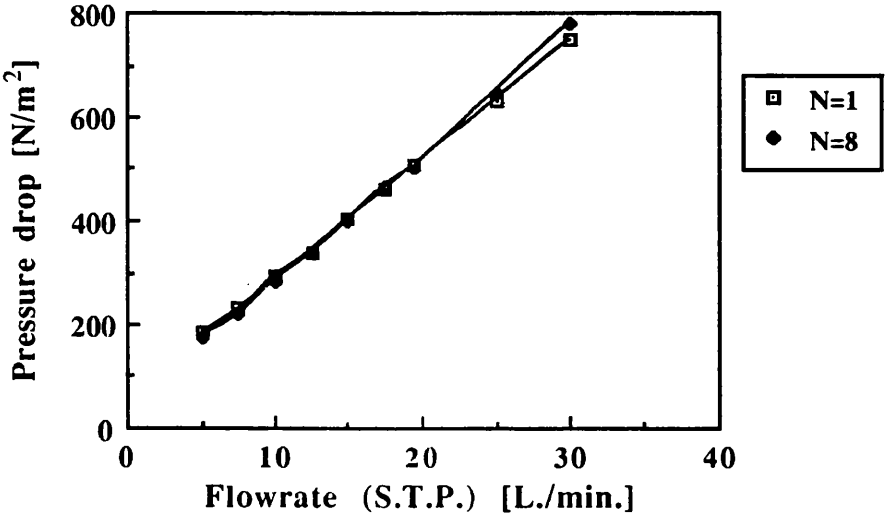

Fig. 6.24 Conversion versus flowrate for varying N for data set II at 400°C

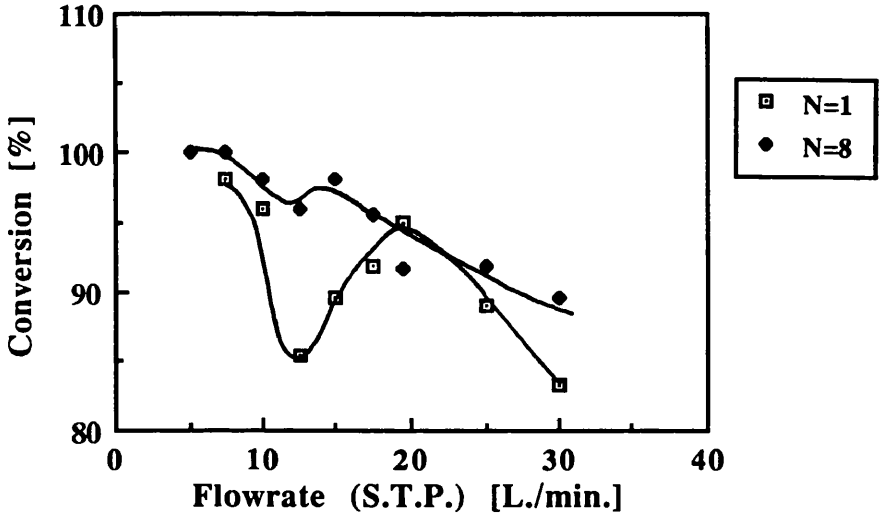

Fig. 6.25 Temperature rise versus flowrate for varying N for data set II at 400°C

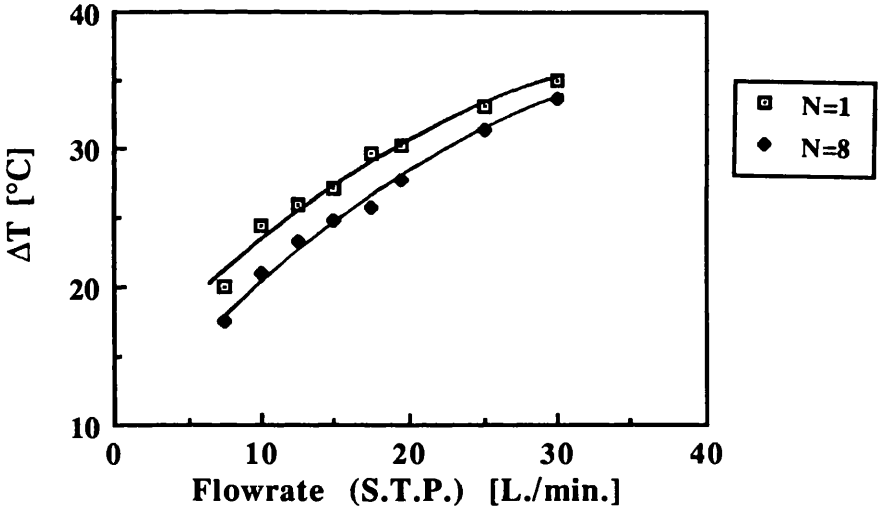

Fig. 6.26 Pressure drop versus flowrate for varying N for data set II at 400°C

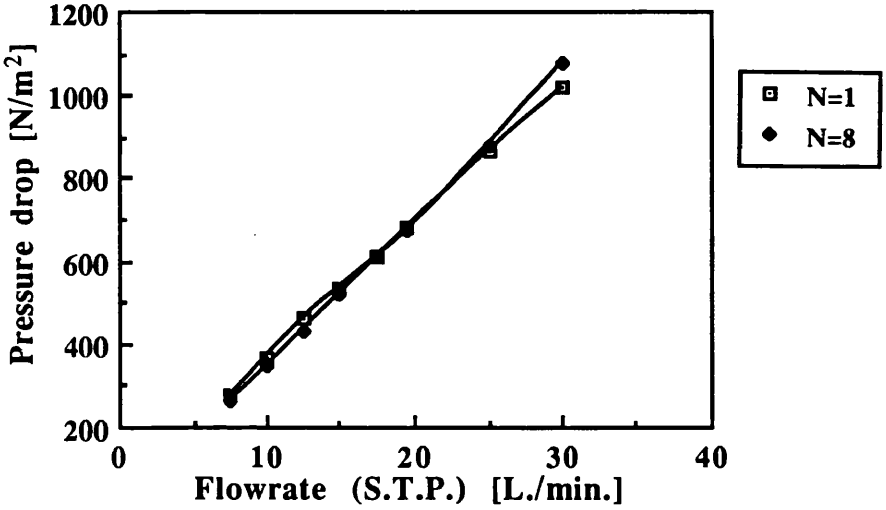

how conversion is improved by segmenting, indicating that there are mass transfer limitations within monolith reactor systems. Enhancement factors are calculated as the overall conversion for N segments divided by the conversion for the integral core (ie. N=1) under identical conditions of operation:

$$\lambda_{Mon} = \frac{X_{N=N}}{X_{N=1}} \qquad (6.4)$$

In the case when the reaction is totally mass transfer limited, this factor (λ) is a direct consequence of the enhancement in Sherwood numbers between the segmented and integral monoliths.

The conversion for the integral core was determined from the curves of figures 6.1 and 6.4 for set I and set II data respectively, drawn as smooth fits through the data points. The resulting enhancements are found for varying flowrates and are given in figures 6.27 and 6.28 for data set I and II respectively at an inlet temperature of 371°C. The data with conversions close to 100 % were neglected for the purpose of these figures since improvements in conversion on segmenting could not be determined at this high conversion. In both figures 6.27 and 6.28 it can be seen that as d/L_s increases (ie. the number of segments rises), the enhancement in conversion also increases, as might be expected, as a result of improvement in the average overall mass transfer coefficient due to increased entry length effects. Hence, for data set I at 10 L/min (STP) for example, using Langhaar's equation (2.7) for entry length, the total entry length increases from 4.65 mm up to 74.4 mm for N=1 and 16 respectively. This represents a percentage increase in developing flow (ie. Le/L_T) of 3 % to over 50 % for N=1 and 16 respectively. Experimentally, this in manifested in a 30% improvement in conversion as the number of segments goes up from 1 to 16 (d/L_s of 0.0069 to 0.216) at 10 L/min, (refer to figure 6.27). This result is in spite of the fact that approximately 5 cm of catalyst was lost as a result of slicing (refer to table 6.1). Thus the total amount of catalyst can be reduced (in terms of catalyst length) by about 30% , and still produce enhanced overall conversion, by segmentation. These results highlight the obvious advantages of segmentation.

Also in figures 6.27 and 6.28 it can be seen that at high d/L_s ratio's, λ tends to plateau off. This is of interest because it shows that there is a limit to the extent to which segmentation can improve matters. In both figures the point at which the plateau occurs is a function of flowrate, however it is interesting to

Fig. 6.27 Experimental enhancements in conversion experienced by segmentation for set I data at 371°C

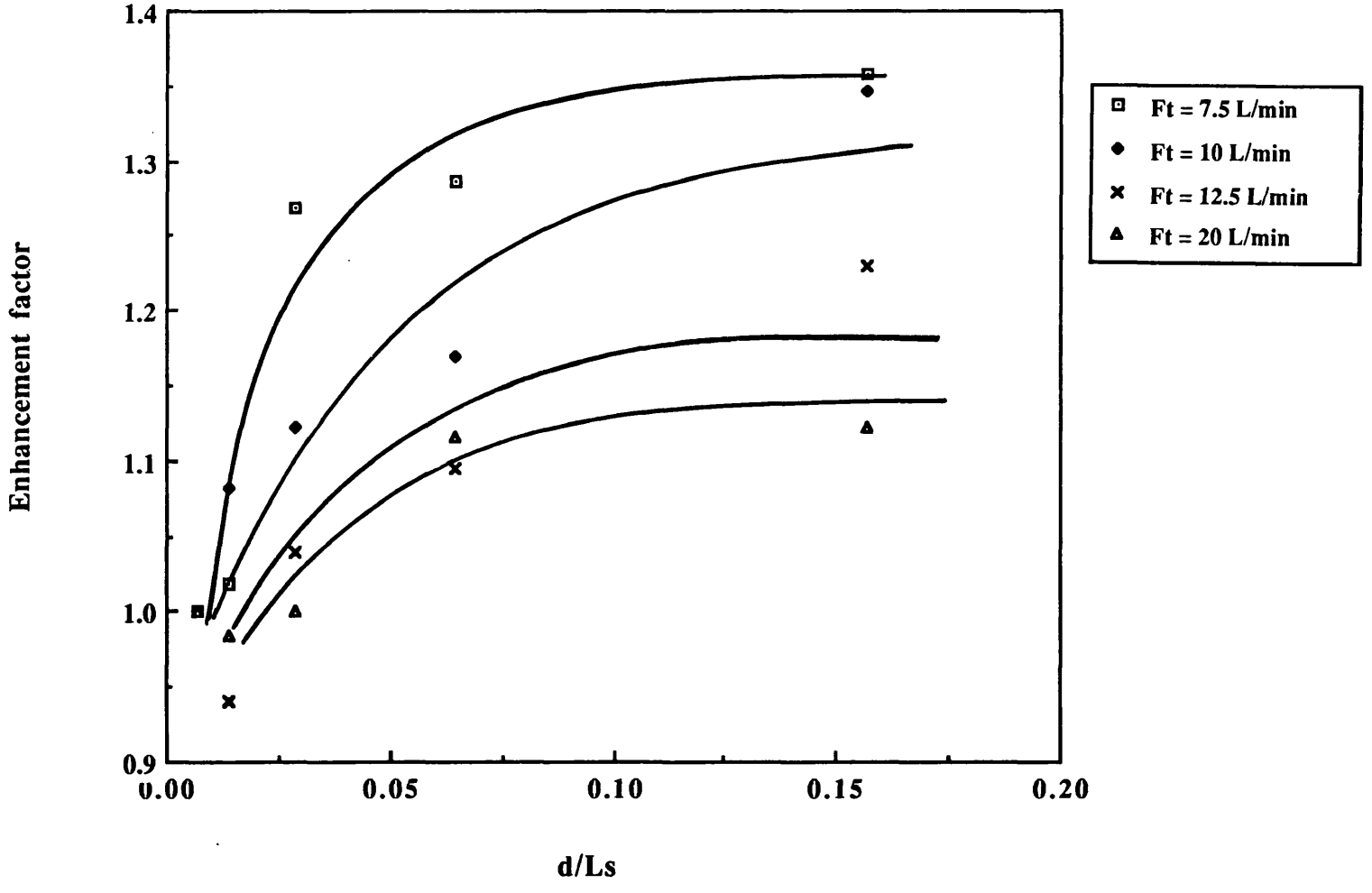

Fig. 6.28 Experimental enhancements experienced by segmentation for data set II at 371°C

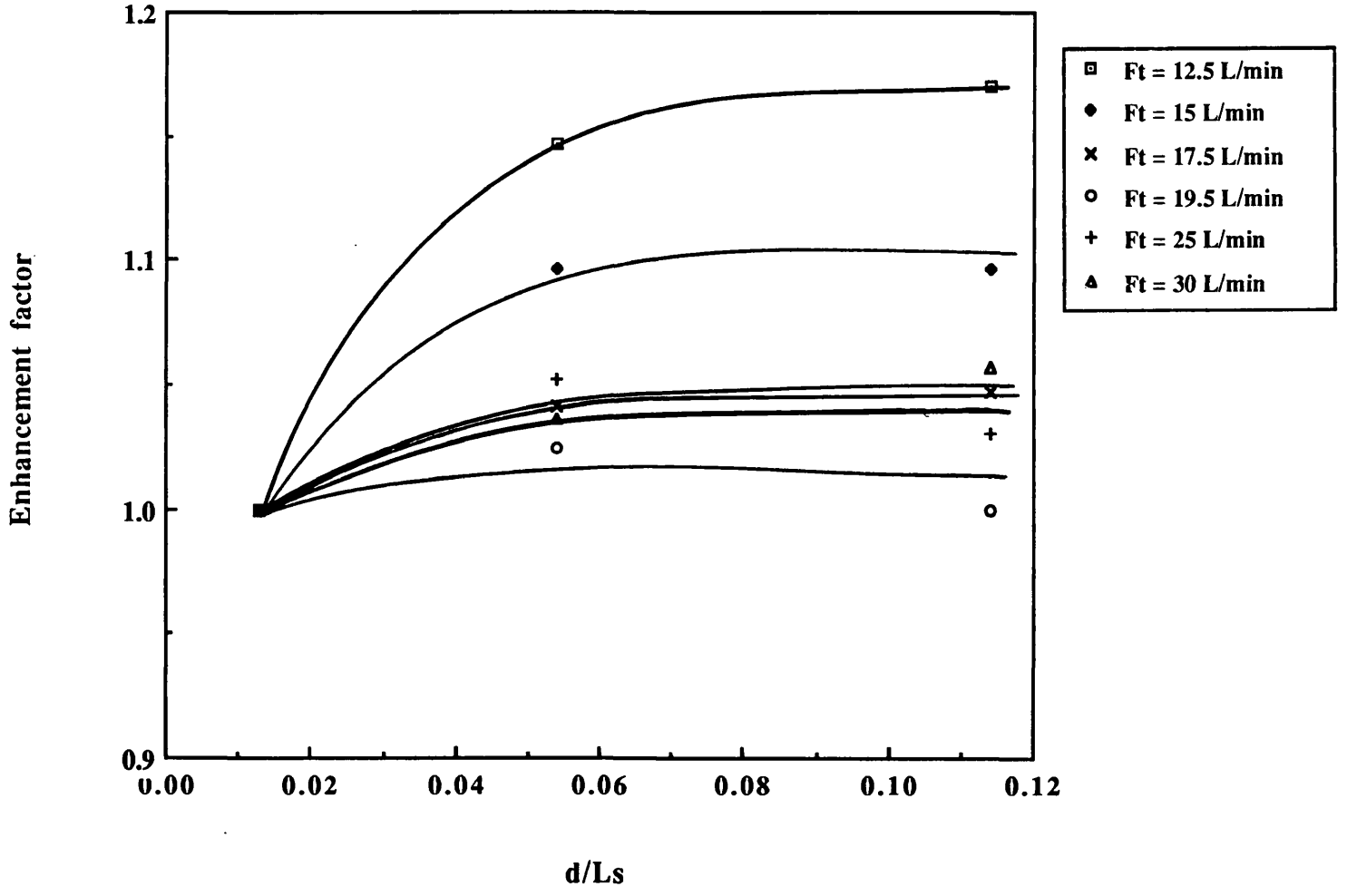

note that on average in both figures the plateau occurs at around $d/L_s=0.1$ which corresponds to a segment length of 1 cm (for d=1.04 mm). This may be explained if it is envisaged that the entry lengths for each segments may overlap. That is to say, if the flow is already disturbed, any further disturbance has no effect. Thus for example at an inlet flowrate of 15 L/min (STP), using Langhaar's equation, the entry length is 7 mm. Therefore disrupting the flow by segmenting, at shorter intervals than 7 mm would lead to premature disturbances with the result that little further improvement in conversion is achieved.

In figures 6.27 and 6.28 in general as flowrate is increased at fixed d/Ls the enhancement in conversion is reduced. The explanation is similar to that of premature segmentation, since entry length increases as flowrate goes up, and therefore any subsequent disturbance has less impact at higher flowrates, with the result that as flowrate goes to infinity λ should approach one. This is indeed the result found from experiment, see figure 6.28. Alternatively this may be thought of as a result of the rate of change of Sh with respect to Re for the integral core being greater than the rate of change of Sh for the segmented monolith, ie. the effect of developing flow on the segmented core is less pronounced than for the integral core as the Re is increased.

The data of set I and II cannot be compared directly on such graphs of enhancement in conversion since the integrated core lengths in both cases are not the same (ie. 15 cm for set I and 8 cm for set I). Both sets of data do however show good improvements in overall conversion on segmenting the monolith core.

Note: An alternative method of expressing enhancement is to base it on the unachieved conversion rather than achieved conversion ie.:

$$\lambda_{Mon} = \left(\frac{X_{N=N} - X_{N=1}}{100 - X_{N=1}} \right) \qquad (6.5)$$

At high conversions for the unsegmented core there is less scope for improvements in conversion by segmentation. Equation 6.5 is a means of reflecting this.

6.6 Conclusions

The experimental investigations of this chapter on monolith systems lead to the following general conclusions:

1) The overall conversion falls as the flowrate is increased due to reduced residence time. However, in some instances (ie. for an 8 cm and 15 cm long monolith core) an unusual trend was observed in which at a particular flowrate the conversion increased to reach a maximum, then proceeded to fall. There is no obvious explanation for this trend.

2) Heat losses to the surroundings are significant at lower flowrates (for example at 7.5 L/min (STP) up to 50 % of the heat produced from the reaction is lost to the surroundings). Therefore, in any detailed model, the effects of heat loss may be important.

3) At temperatures of 371°C and above the reaction ignited at the channel entrance for all flowrates.

4) The studies conducted on segmented monolith systems (for inlet temperatures of 371°C and above, and inlet CO and oxygen concentrations of 0.5 and 0.25 % respectively) showed clear enhancements in the overall conversion of up to 30 % as d/Ls increased from 0.0069 to 0.216 at an inlet flowrate of 10 L/min (STP). Also pressure drops were found to be insignificantly affected due mainly to the loss of catalyst length during the segmentation process.

5) The enhancement factors were found to increase as the d/L_s ratio increased to reach a plateau at high d/L_s. Thus there is a minimum segment length depending on the flowrate below which there is no further increase in enhancement. This is because entry lengths correspond to a significant part of the reactor, and any subsequent reduction in segment length has little effect.This may be explained if it is envisaged that the entry lengths for each segment may overlap.

6) As flowrate is increased the enhancement factor between the segmented and integral cores is reduced for similar reasoning to point 5 above.

CHAPTER 7

EXPERIMENTAL STUDY OF THE TUBULAR AND ACTIVE TRANSPORT REACTORS

7.1 Introduction

Current methods for removing pollutants from automobile exhausts involve the preferential use of monoliths. The process is carried out by reactants diffusing to the catalytic wall where they react. In the tubular reactor where the flow is laminar and the reaction is relatively fast, the reaction is usually mass transfer limited, with the result that a high surface area is required.

The present work was designed to investigate alternative reactor geometries with the view to enhancing the mass transfer of reactants from the bulk stream to the active catalyst sites.

In this chapter the effects of the ATCR (Active Transport Catalytic Reactor) are investigated. This consists of a tube coated with active catalyst which contains static mixing devices. These devices encourage mixing, in some cases producing eddies in the form of induced turbulent flow.

The reactor and the various mixer types are described in the next section. Each mixer type was tested experimentally for its effects on conversion and pressure drop when inserted into the tubular reactor. Comparisons were then made in order to discuss the relative merits of each mixer type. The effects of varying the number of equally spaced mixers was also investigated.

7.2 The Reactor

The reactor consisted of a Fecralloy pipe of dimensions 15 cm long by 1.5 cm inside diameter coated with a γ-alumina washcoat.This was impregnated with platinum /rhodium catalyst similar to that used in the monolith (by Johnson Matthey). Mixers of various configurations were inserted into this tubular reactor to form the Active Transport Catalytic Reactor (ATCR).

The three types of mixer tested were the Sulzer, Kenics and a "Star and Orifice" design. The Sulzer mixers were of the SMX variety supplied by Sulzer Ltd. and were made of 316 Ti stainless steel. These consisted of a framework of baffles inclined relative to one another. The elements were rotated at 90° between each successive element.

The Kenics mixers were made from stainless steel and supplied by Chemineer Ltd. These consisted of alternating left- and right-handed helices with an angle of twist of 180°. Each successive element was rotated 90° from the previous element. Figure 7.1 is a photograph of the Sulzer and Kenics mixers arranged end to end. A schematic diagram of the Kenics mixer is given in figure 7.2 illustrating the alternating elements, as well as the corresponding length and diameter of the element.
Table 7.1 shows the element dimension and aspect ratios of the Sulzer and Kenics mixers.

Table 7.1 Dimensions of Sulzer and Kenics mixers used in the study

Mixer Type	Element length, L_E (cm)	Diameter of element, d_E (cm)	Aspect Ratio (L_E/d_E)
Sulzer	2.00	1.22	1.64
Kenics	2.15	1.27	1.69

The mixer designed in the department consisted of a star and orifice. The dimensions of the star and orifice are given in the sketch shown in figure 7.3. This type of mixer is termed a flow inverter since its intended design is to invert the flow between the centre and the edge of the pipe. In this case the flow is forced to the walls at the star and then through the hooded orifice.The combination of a star and orifice plate forms a single mixing element. As indicated in figure 7.3 the star and orifice plates are separated from one another using three rods equispaced radially and passing through each element in succession. Each rod in turn is covered with a spacer, consisting of a small 2 mm long hollow tube covering the rod, in order to prevent the movement of each of the plates. A photograph of the Star and Orifice element arrangement is given in figure 7.4.

During experimentation the number of elements was varied. These were arranged in such a way as to keep the mixers equally spaced, as shown in figure 7.5 for the Sulzer and Kenics mixers (for example, N_E=5).

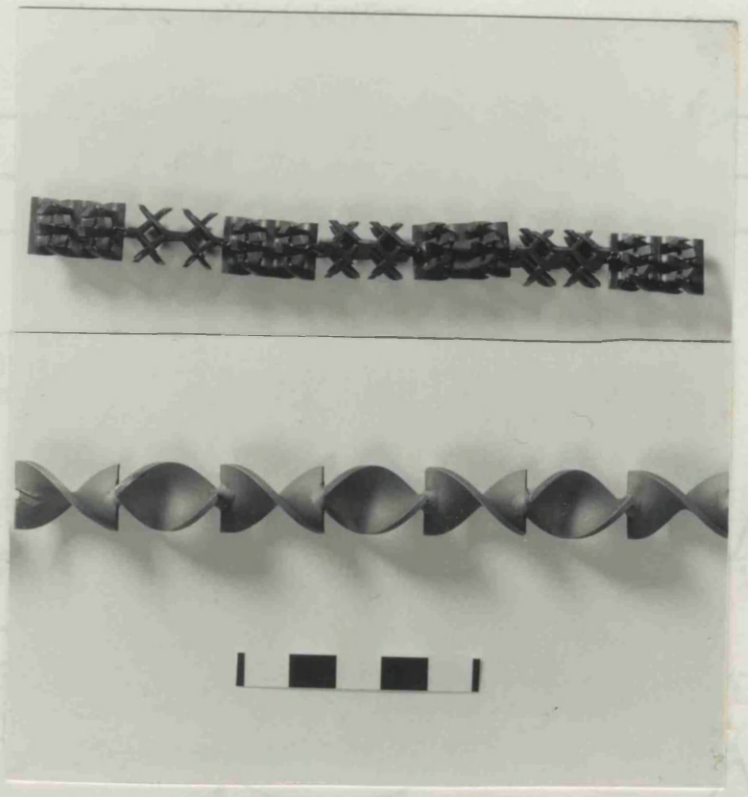

Fig. 7.1 Photograph of the Sulzer and Kenics mixer elements arranged end to end

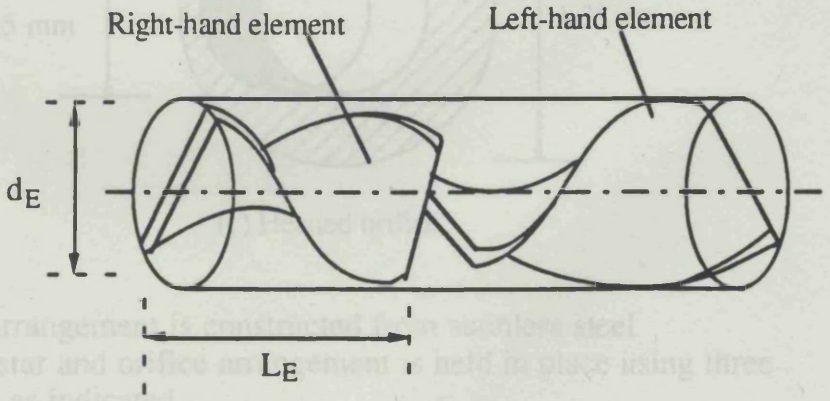

Fig. 7.2 Schematic diagram of the Kenics mixers placed end to end

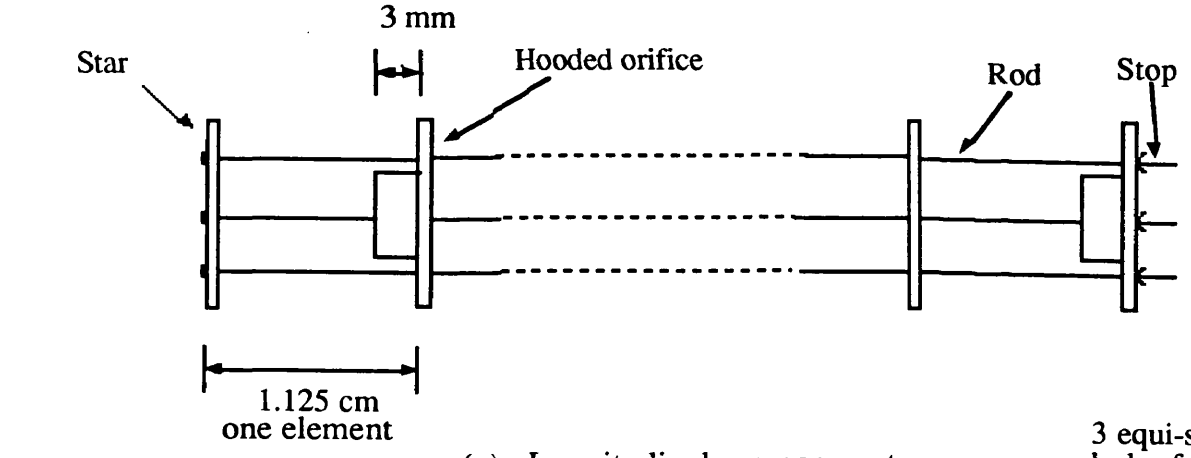

(a) Longitudinal arrangement

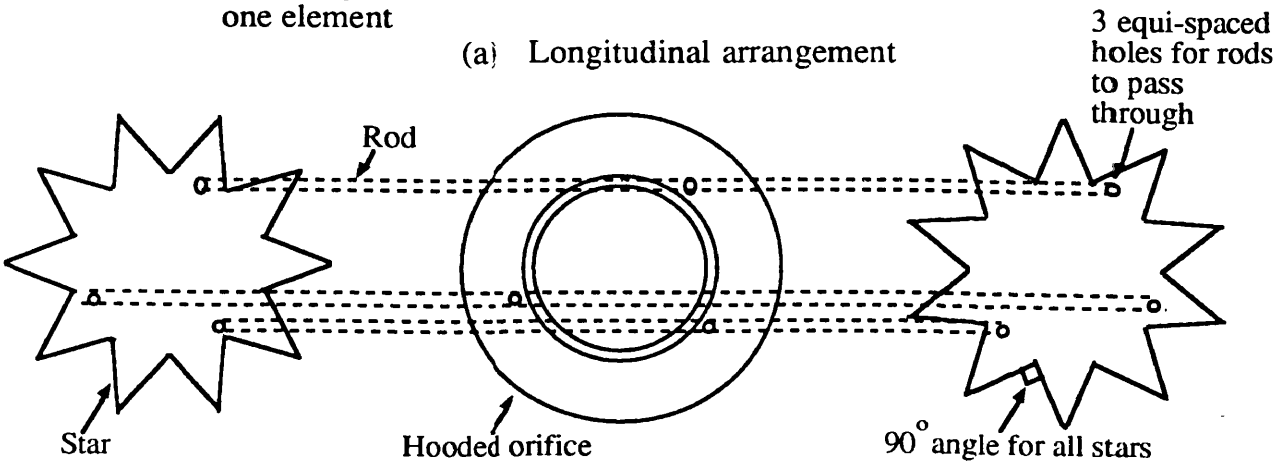

(b) Cross-section of star and orifice in sequence

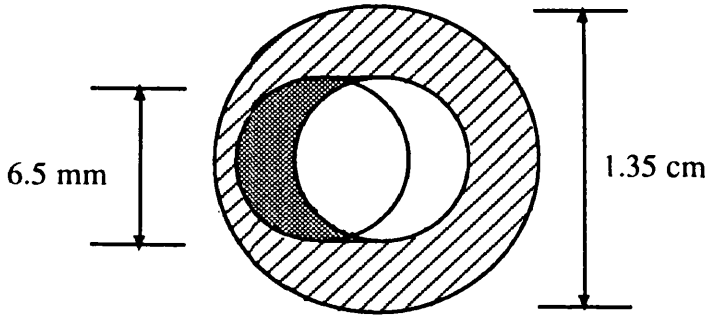

(c) Headed orifice

Note:

1) The arrangement is constructed from stainless steel
2) The star and orifice arrangement is held in place using three rods as indicated
3) The star and orifices are equally spaced using spacers

Fig.7.3 Schematic diagram of Star and Orifice arrangement

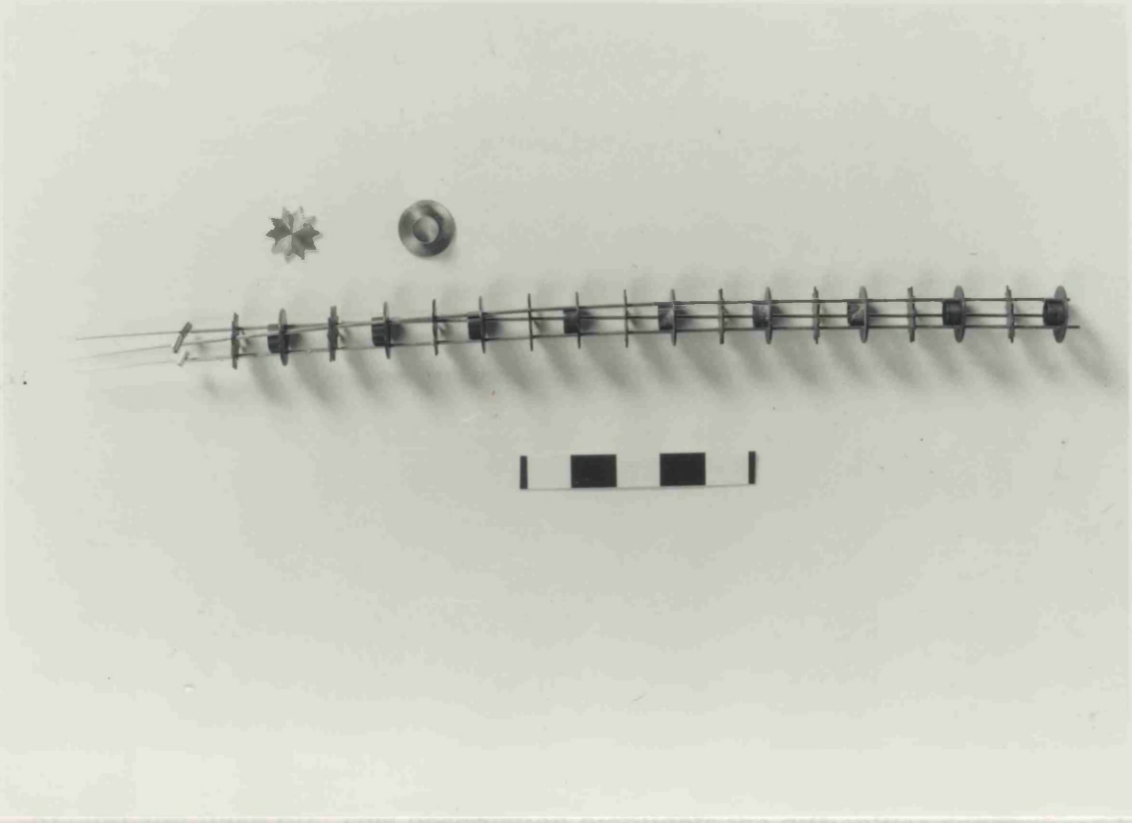

Fig. 7.4 Photograph of the Star and Orifice arrangement

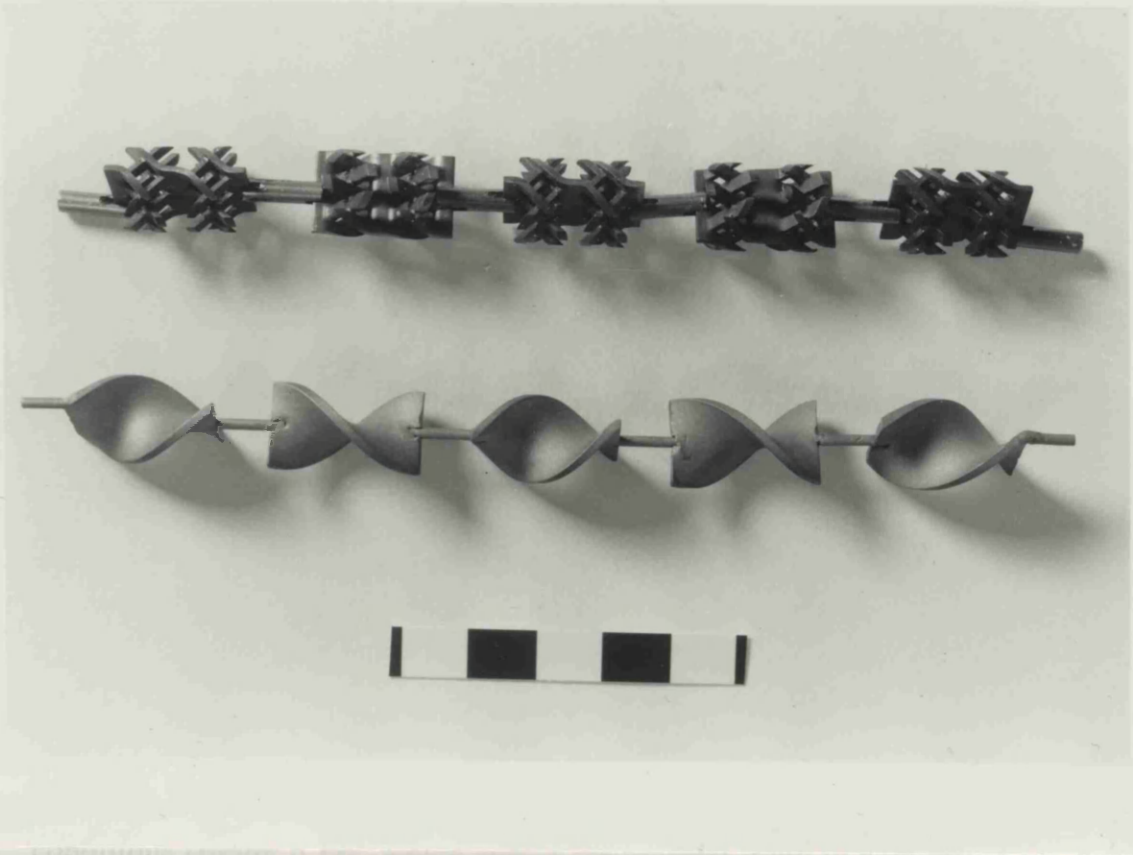

Fig. 7.5 Photograph of the Sulzer and Kenics mixers for N_E=5

7.3 Experimental Methods

The detailed procedures were described in chapter 4. The reactor (as for the monolith) requires catalyst pre-treatment by passing oxygen over the catalyst at a flow rate of 1 L/min for about ten hours.This allows for the calcination of the catalyst. Also as part of the aging procedure a reacting mixture at 400°C of the same composition as that for the monolith was passed for approximately 10 hours.

Each experimental run consisted of setting several total inlet flow rates and then measuring pressure drops and exit concentrations for varying numbers of elements at a constant inlet temperature of 371°C.

An experiment was also performed with the empty tube reactor for comparison purposes. All runs were performed for inlet CO and oxygen concentrations of 0.5 and 0.25 vol% respectively. The experimental results are given in appendix F.

It should be noted that during experimentation the catalyst coating tended to chip and flake off. This observation highlights the difficulties experienced by manufacturers in dealing with catalyst adhesion to metallic surfaces. The effect was minimized however, by careful insertion of the mixing elements being mindful not to scrape the sides of the catalyst coated wall. On repeating the experiments from day to day, it was found that there was no change in the overall conversion as a result of slight catalyst flaking.

7.4 Results and Discussion

7.4.1 The empty tubular reactor

7.4.1.1 Effect of flowrate

Figure 7.6 shows the influence of flowrate on the overall conversion at 371°C. The corresponding Re at actual conditions, as well as at STP, are also presented. The conversion drops continuously with increase in flowrate. As discussed in chapter 6, the parameters effecting the overall conversion for a mass transfer limited reactor, are the transfer coefficients and residence time. As flowrate is increased mass transfer goes up whereas the residence time is reduced, and therefore in figure 7.6 the overpowering effect is the residence time. Contrast this result with that for the monolith reactor under similar inlet conditions (figure 6.18), which shows the unusual trend in conversion (ie. local

Fig. 7.6 Conversion vs flowrate for the tubular reactor at an inlet temperature of 371°C

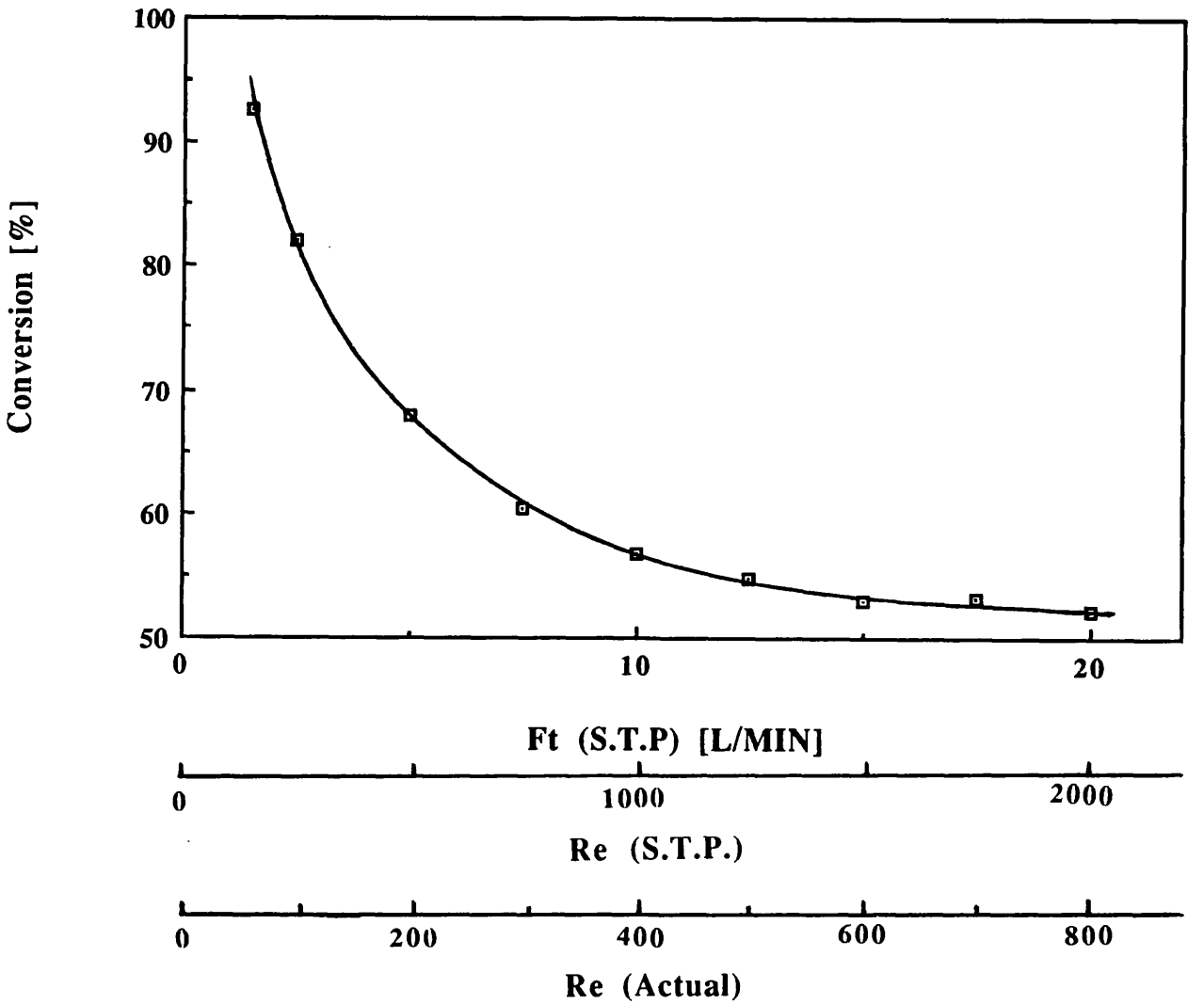

minimum and maximum in conversion as flowrate increases).This effect, is not detected in this case.

Temperature rise across the reactor is not significant as can be seen in figure 7.7, which suggests that much of the heat of reaction is being lost to the surroundings (ie. via conduction along the reactor wall and then by convection and radiation to the surroundings), with the result that the reactor behaves essentially isothermally. Although this result does not affect the present work it may be important in real situations, particularly in cold start up operation. Thus in such cases when the heat losses exceed the heat produced from the reaction, the reaction does not light-off. Therefore in any determined effort in testing ATCR systems, this effect should be investigated.

Pressure drop is seen to rise with flowrate as in figure 7.8. This is expected for the reasons mentioned in section 6.4.1 of chapter 6 (p.131).

7.4.1.2 Effect of temperature

The effect of temperature on the overall conversion for the tubular reactor is illustrated for T_{Gin}=250, 371 and 400°C in figure 7.9. This shows that over the range 250-400°C the conversions show little sensitivity to temperature, (eg. at a total flowrate of 10 L/min the conversion corresponding to 250°C is 54%, whilst at 400°C it has risen to only 58%). This suggests that the reaction is mostly mass transfer limited at these conditions.

7.4.2 The ATCR

7.4.2.1 Effect of mixer configuration

Mixers are essentially designed to disrupt flow. The commercial mixers, ie. the Kenics and Sulzer, fulfill their mixing functions in slightly different ways. The Kenics divides the flow into two at the first element or helix, and on meeting the second element the flow is divided again to give four divisions. This process continues for each successive element to give 2^{N_E} divisions or striations, (where N_E is the number of elements), and therefore mixing is progressively improved as N_E is increased.

The mixing element bars of the Sulzer mixer, positioned at an angle to the pipe axis, repeatedly divide the flow into layers across the pipe cross-section. The mixing action is a result of strong secondary cross flow that

Fig. 7.7 Temperature rise for the tubular reactor at an inlet temperature of 371°C

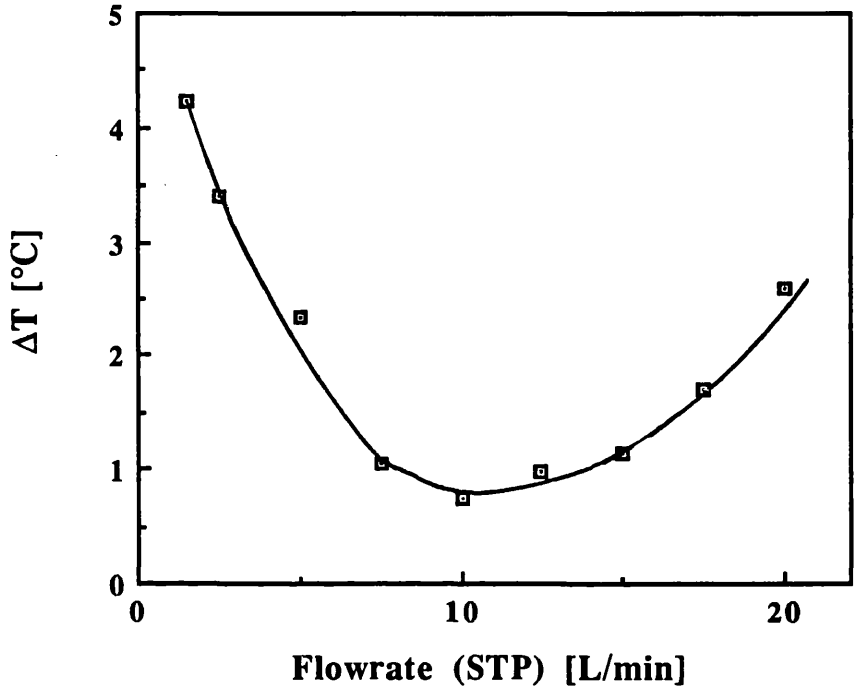

Fig. 7.8 Pressure drop vs flowrate for the tubular reactor at an inlet temperature of 371°C

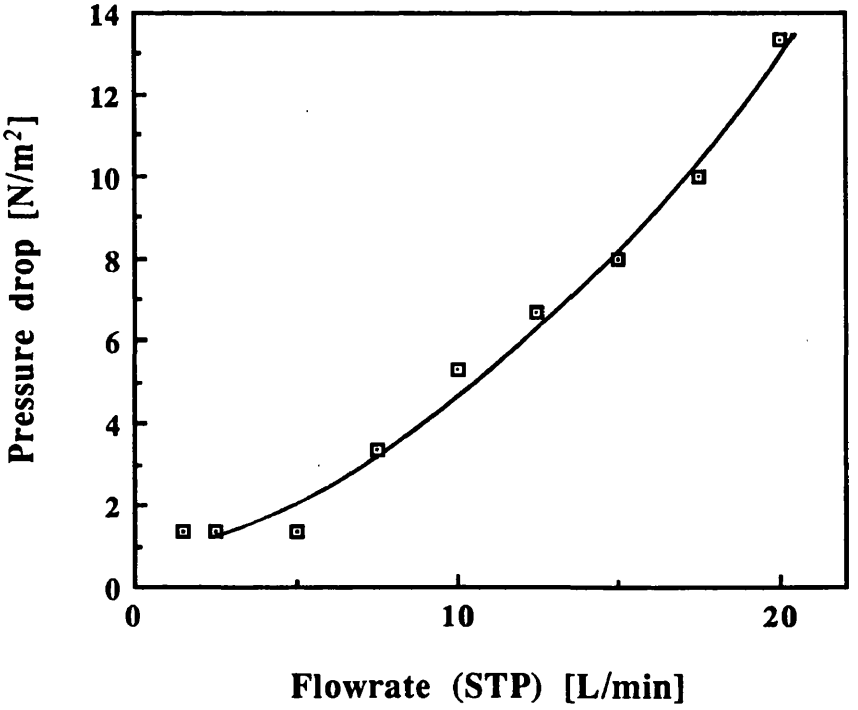

Fig. 7.9 Conversion vs flowrate for the empty pipe reactor at different inlet temperatures

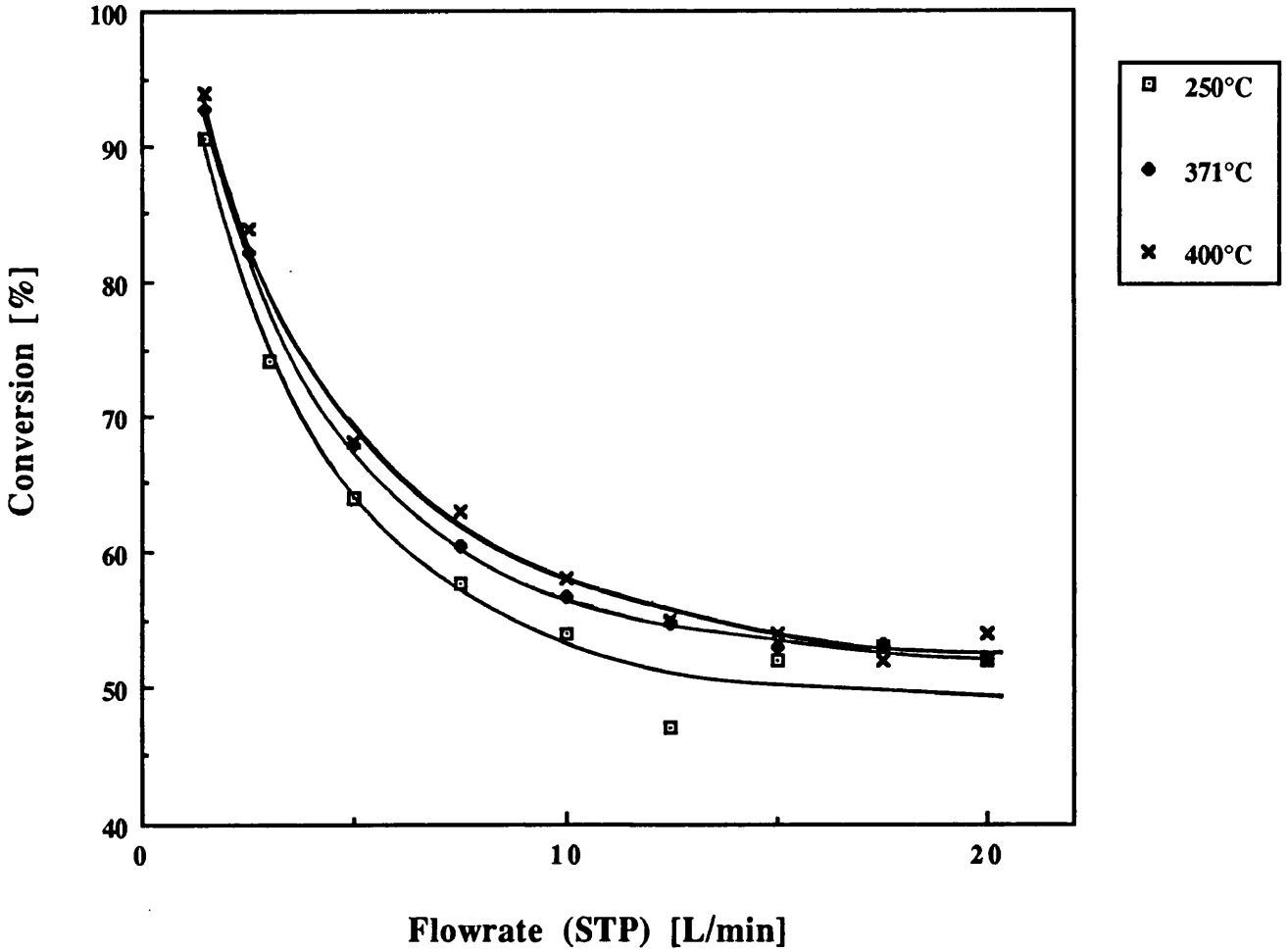

develop behind the inclined bars, and cause the fluid to be stretched laterally. In a similar manner to the Kenics mixer, as the number of elements increases, the number of layers formed also rises while their thickness diminishes.

The star and orifice design behaves as a flow inverter ie. causing the flow to alternate between the sides and the centre of the tube, between each successive star and orifice element to produce maximum mass transfer.

In general however, an increase in mass and heat transfer is associated with a corresponding penalty of increased pressure drop.

Each type of mixer was tested separately by placing a single element in the centre of the tube. Runs were performed at 371°C for flowrates of 1.5 to 20 L/min (at STP). Figure 7.10 compares the conversions with a single unit of each type of mixer to that in the empty tubular reactor. Also in a desire to reduce pressure drop a star element alone ie. without an associated orifice, was tested. It is clear that for all flowrates the Sulzer mixer type reactor behaves in such a way as to enhance the conversion as compared to the empty tubular reactor. The Kenics, Star and Orifice and Star element mixer reactors also improve enhancement for flowrates below 10 L/min, however above this flow there is no improvement, if anything there is a drop in conversion compared to the empty tubular reactor. This is an unexpected result, and a possible explanation may be due to their method of mixing. The configuration of the Sulzer mixer is such that it diverts the gas flow to the wall of the tube for all flowrates. The Kenics mixer provides a swirling effect, which causes the flow to be rotated. At low flowrates, this effect encourages mass transfer of reactants to the wall of the reactor. However, as the flowrate is increased, there is less time for the reaction to take place, particularly in the vicinity of the mixer unit. Hence, for the case of the single Kenics element, the effect of reduced local reactant residence time close to the catalyst surface outweighs the effect of increased mass transfer. However, when two or more Kenics mixers are in place, their arrangement (ie. at right angles from one another) offers more resistance to flow and therefore possibly offsets the effect of reduced residence time close to the mixer units. Similarly, in the case of the Star and Orifice arrangement, although the flow is diverted towards the catalyst surface (in the case of the Star), there is also an increase in flowrate at the wall. Hence for the single element of the Star and Orifice the overwhelming effect is the reduced residence time.

Obviously for each system a detailed picture of the flow behaviour is required to determine how mass and heat transfer are influenced by flow for each type of mixer.

Fig. 7.10 Comparison of a single mixer unit ATCR and empty tube reactor conversions at an inlet temp. of 371°C

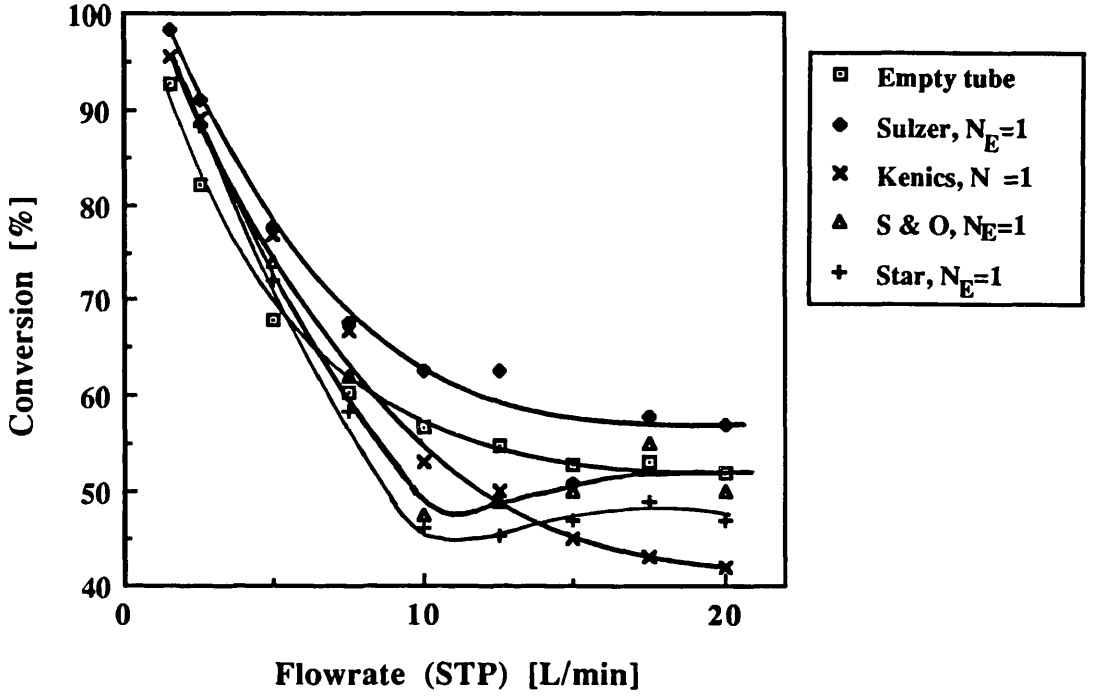

Fig. 7.11 Pressure drop vs flowrate for each type of mixer and the empty tube, for N_E=1 at 371°C

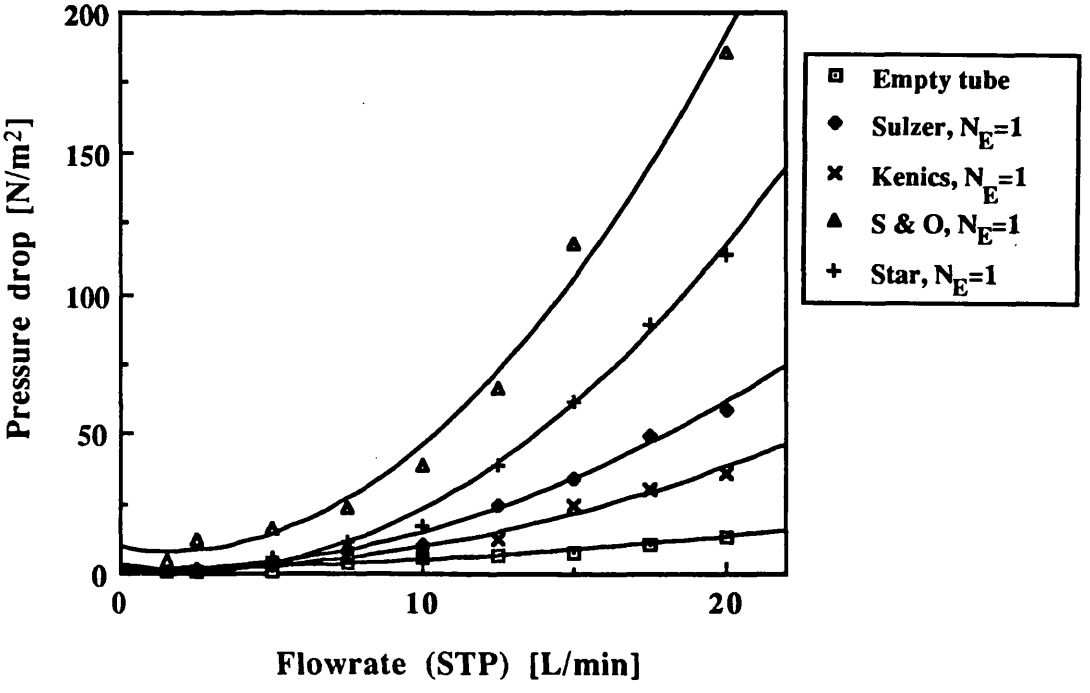

A plot of pressure drop for the various mixer configurations is presented in figure 7.11. The curves drawn through the experimental data correspond to simple second order polynomial best fits. It can be seen that the pressure drop for the star and orifice mixer is the highest for all flowrates, followed by the Sulzer, and with the Kenics giving the lowest pressure drop out of these mixers. The pressure drop for the star and orifice is on average approximately 1.8 times that of the Sulzer mixer which in turn is on average about 1.5 times that of the Kenics mixer .

The various mixers were then tested by placing them end to end to fill the tube. This corresponds to N_E=7 for the Kenics and Sulzer mixers and N_E=6 for the star and orifice mixers. The resulting conversions are depicted in figure 7.12 where for all flowrates all three types of mixer give improved conversions compared to the empty tube reactor. It can be seen that the overall conversion is comparable for all three types of mixers, with perhaps the Sulzer being marginally better. Hence for example, at an inlet flowrate of 10 L/min, the conversion for the star and orifice is 78 %, the Kenics 80 % and the Sulzer 82 %, an overall difference in conversion of 4 %. Comparing this to the errors associated with the experimental data, chapter 4 section 4.4.3 of 5%, shows that the difference in conversion between the three mixers is indistinguishable within the limits of the experimental accuracy. At 10 L/min (STP) the conversion rises from 56 % for the empty tube reactor up to 80 % for the ATCR for N_E=7 (Sulzer mixer). This is a further confirmation that the performance of the tubular reactor is mass transfer limited at these conditions, due to the marked increase in conversion brought about as a result of disruption of developing boundary layers in the tubular reactor.

Alternatively if the pressure drops across the various mixers are compared in figure 7.13 it can be seen that the highest pressure drop occurs for the star and orifice arrangement, followed by the Sulzer mixer with the Kenics giving the least pressure drop. Although the star and orifice is comparable in performance in terms of enhanced mass transfer to the other types of mixers, the pressure drop is by far the highest, giving on average a pressure drop of 46 times that of the empty tube. Therefore, since the main aim of the investigation is to create the maximum mass transfer rate with the least additional pressure drop, the star and orifice arrangement can be eliminated from the investigation.

Therefore the rest of the investigation proceeded using the Kenics and Sulzer mixers only.

Fig. 7.12 Conversion vs flowrate for the Sulzer, Kenics and Star and orifice reactors at an inlet temp. of 371°C

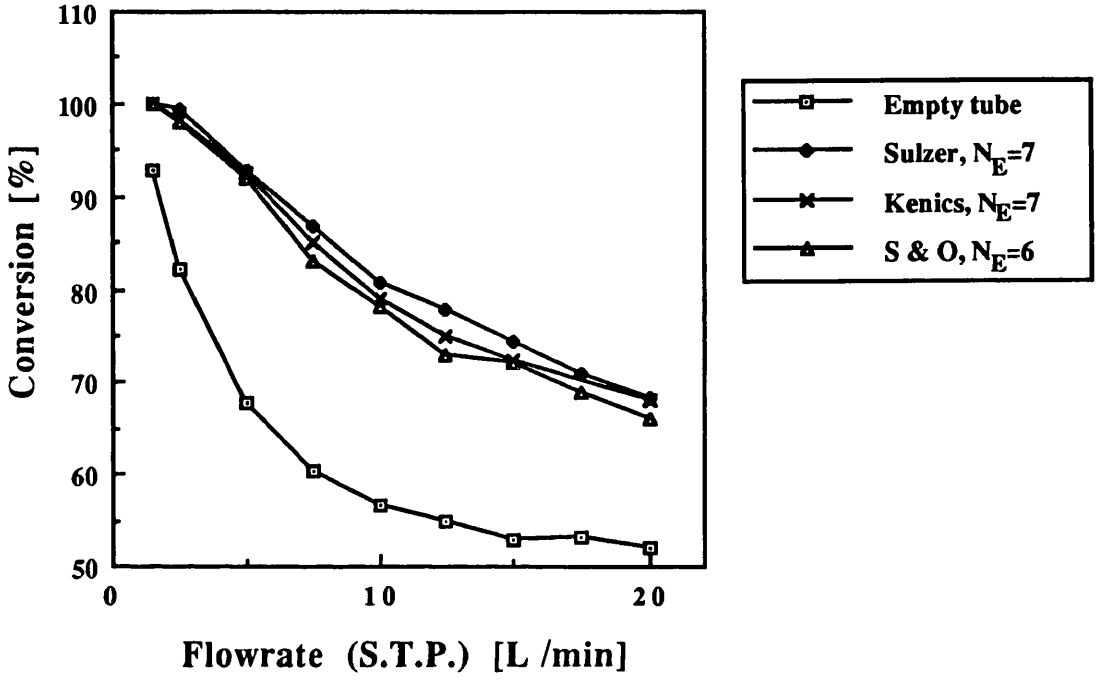

Fig. 7.13 Pressure drop vs flowrate for various mixer configurations at an inlet temp. of 371°C

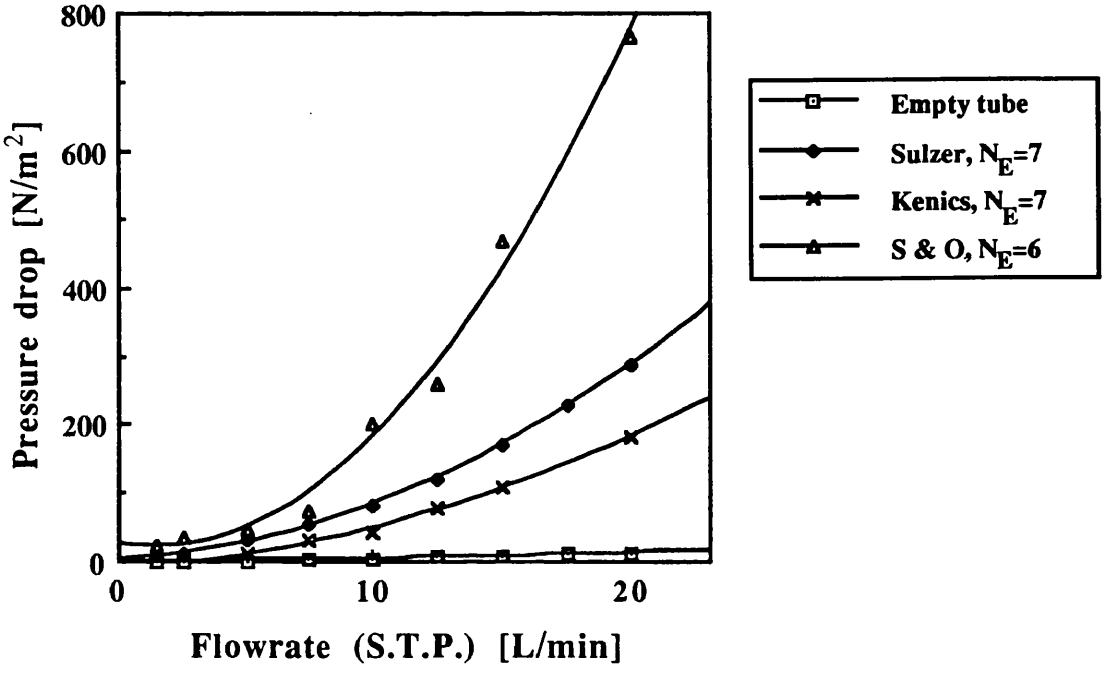

7.4.2.2 Effect of number of mixers

Figures 7.14 and 7.16 are plots of conversion versus flowrate for the Kenics and Sulzer mixers respectively. In both cases as the number of mixers is increased there is a clear improvement in conversion. Indeed the performance of these are very nearly the same with perhaps the Sulzer mixer having a slight edge especially for N_E=1. As for pressure drop, shown in figures 7.15 and 7.17 for the Kenics and Sulzer mixers respectively, it can be seen that the Kenics has the lower pressure drop and therefore in this respect is more advantageous. As the number of elements increases, the overall pressure drop rises as would be expected through increased friction losses. The pressure drop, therefore seems to be directly proportional to the number of mixer elements (N_E). This result may not necessarily follow, since one may envisage that the flow pattern should change as the spacing between the mixers is varied. This in turn should effect the friction factor and hence presumably the pressure drop, leading to the pressure drop not being directly proportional to the number of elements. However, plots of pressure drop versus number of elements are given in figures 7.18 and 7.19 for the Kenics and Sulzer mixers respectively for varying flowrate. The straight lines drawn in the figures correspond to simple best fit lines. It is clear in both cases that pressure drop is directly proportional to the number of elements. It follows therefore that the friction caused by the changing flow profile (ie. as a result of spacing of the elements) is insignificant compared to the friction as a result of the presence of the inserts. This is also confirmed by Sulzer results in the manufactures booklet (Sulzer, 1987) .

In general therefore it would seem that, for the types of mixers investigated, the mass transfer enhancements and their effect on conversion are effectively the same irrespective of the mixer configuration. However, mixer configuration does affect pressure drop and therefore is important in the choice of mixer.

7.5 Enhancement Factors for Conversion

The enhancement factor is defined for the ATCR as the conversion for the tubular reactor with N_E inserts divided by the empty tube reactor conversion under similar operating conditions:

Fig. 7.14 Conversion vs flowrate for ATCR with Kenics inserts, for varying N_E at an inlet temp. of 371°C

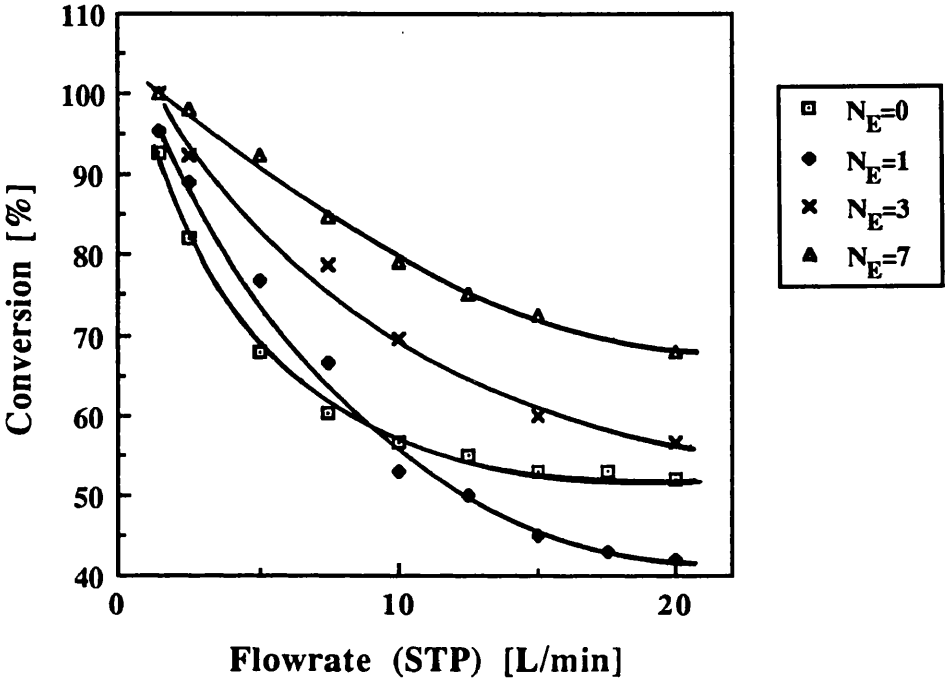

Fig. 7.15 Pressure drop vs flowrate for the Kenics mixer for varying N_E at an inlet temp. of 371°C

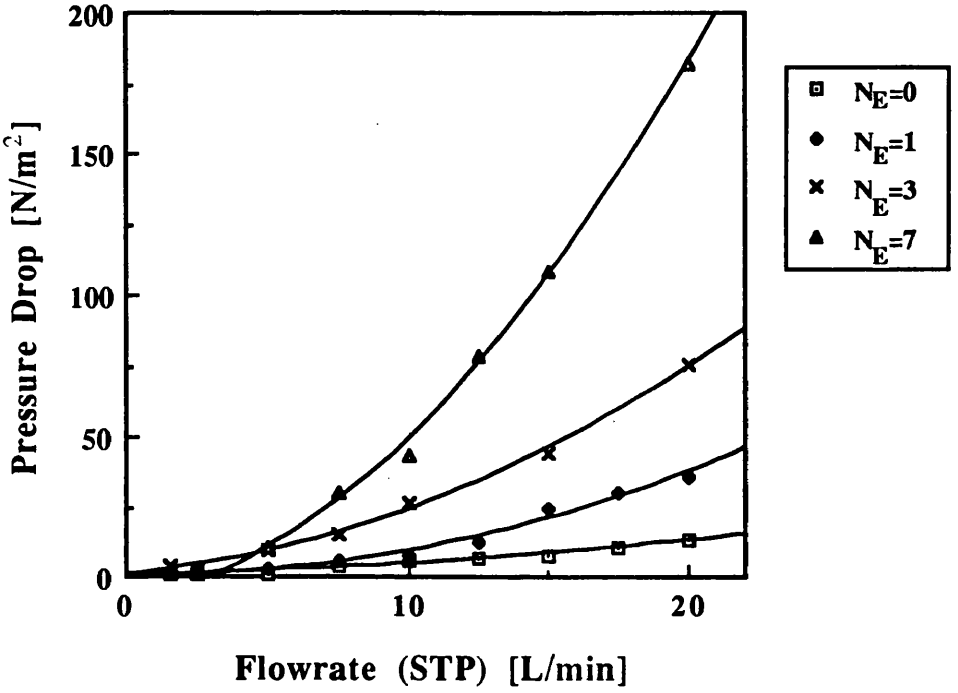

Fig. 7.16 Conversion vs flowrate for the ATCR with Sulzer inserts, for varying N_E at an inlet temp. of 371°C

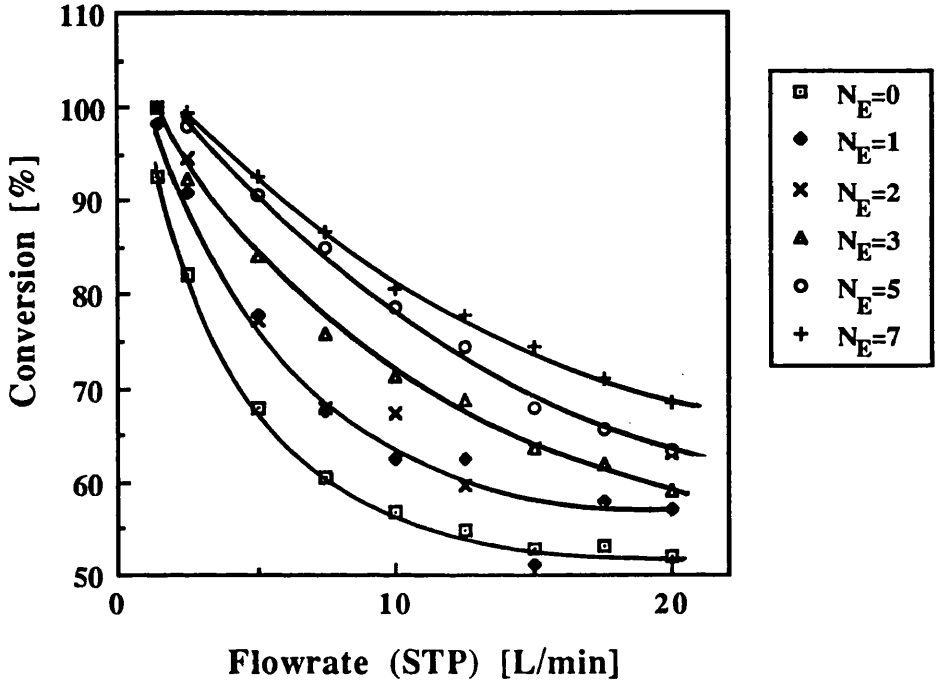

Fig. 7.17 Pressure drop vs flowrate for the Sulzer mixer for varying N_E at an inlet temp. of 371°C

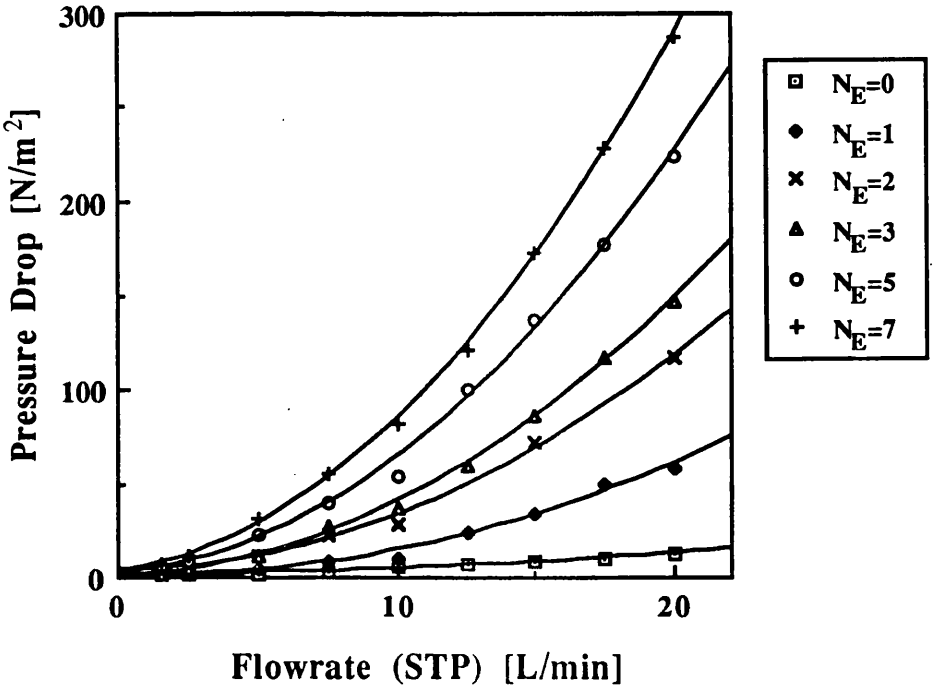

Fig. 7.18 Pressure drop vs number of elements for the Sulzer mixer for varying flowrates

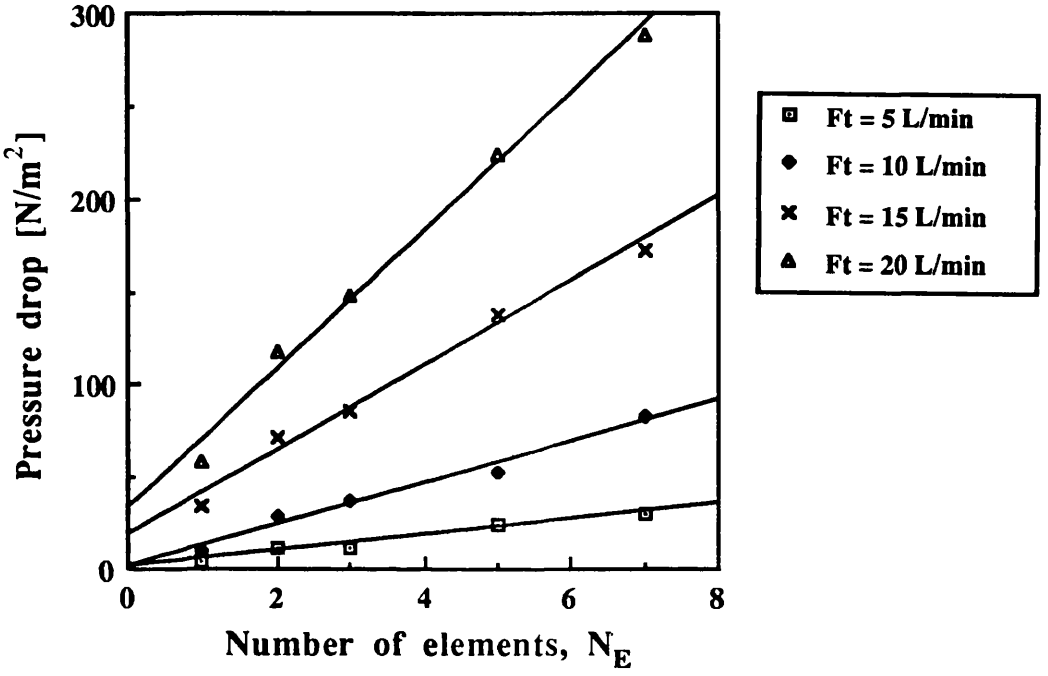

Fig. 7.19 Pressure drop vs number of elements for the Kenics mixer for varying flowrate

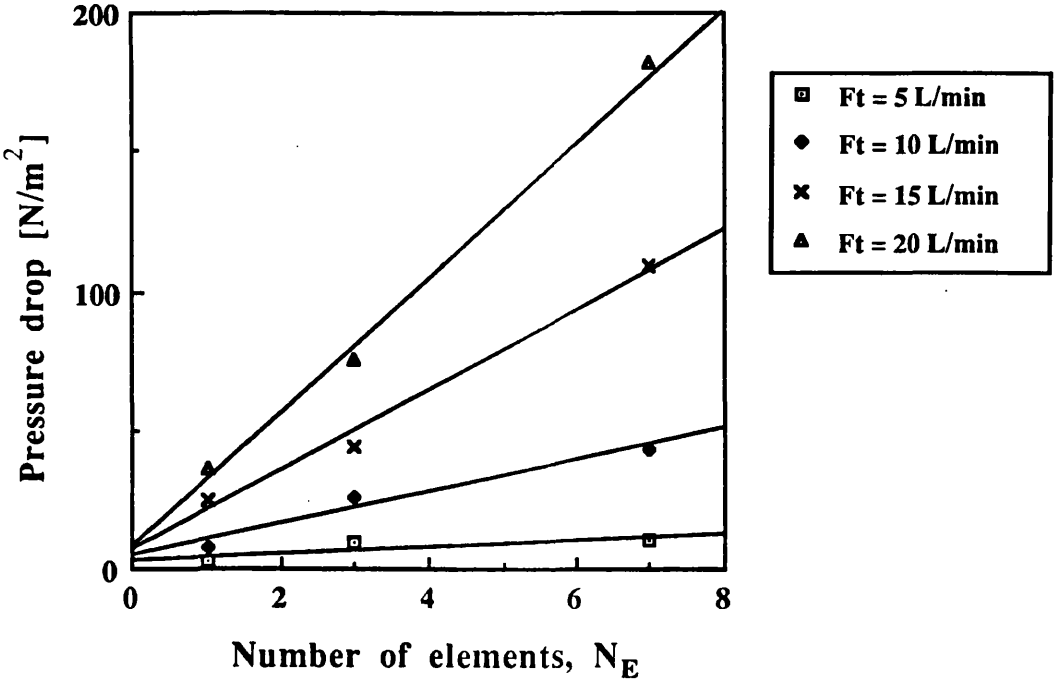

$$\lambda_{ATCR} = \frac{X_{N_E}}{X_{ET}} \qquad (7.7)$$

Enhancements for the Sulzer mixer are given in figure 7.20, but could have been drawn for any of the mixer configurations since the conversion for all three types of mixers were very close except at N_E equal to 1. The d/L_D corresponds to the diameter of the tube divided by the re-development or re-disturbance length, where the re-development length is defined as the length over which the velocity profile is developing between two disturbances (refer to figure 8.10 in chapter 8). This is equal to $L/(1 + N_E)$.

The experimental data presented in figure 7.20 is given for inlet flowrates of 5 to 20 L/min (STP). It can be seen that for all flowrates as d/L_D increases the enhancement in conversion rises as expected, due to increased entry length effects, ie. the flow is encouraged to redevelop with the result that the average Sh is increased. These curves seem to plateau off at high d/L_D ratios. This result is similar to that experienced by monolith segmenting (refer to figures 6.27 and 6.28). It may be explained if it is remembered (as discussed in the Literature Survey section 2.10.4) from the work of Dudukovic et al. (1979), when two objects are placed in the path of a flowing fluid, the extent to which the Sherwood number is enhanced depends on the spacing of the two objects. Therefore, as the objects approach one another, the enhancement in mass transfer becomes less significant, since the wake of the first object interferes with the disturbance of the second with the result that the two disturbances merge and eventually seem to become one. From the experimental results it can be seen that as the number of mixers increases (and therefore the space between each element is reduced) the amount of increase in conversion (and therefore mass transfer) is reduced. This effect is portrayed in a sketch in figure 7.21 where the rate of change of Sherwood number decreases as the number of elements is increased in a given length of pipe.

Fig. 7.20 Enhancement in X for the ATCR compared to the empty tubular reactor as N_E is increased

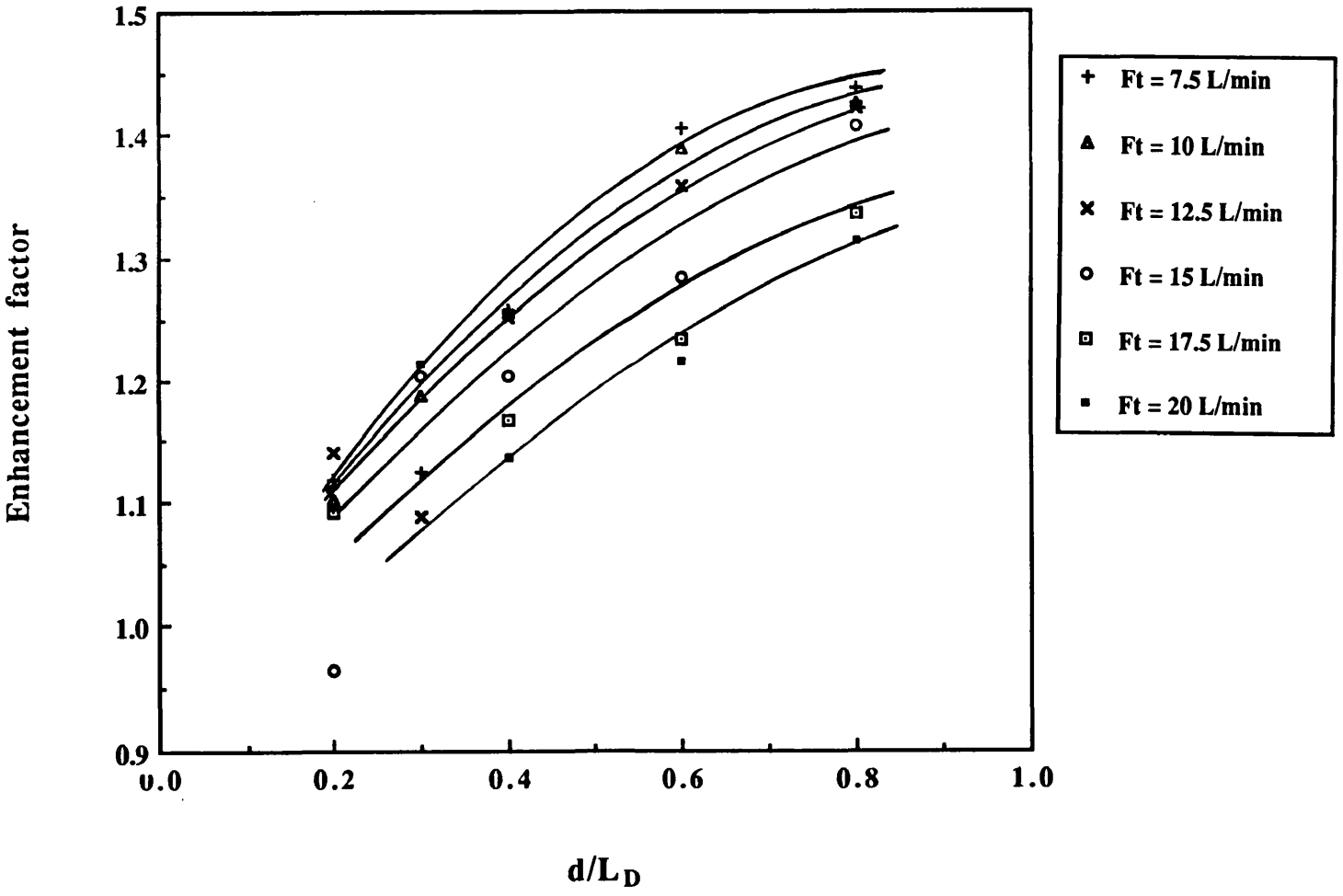

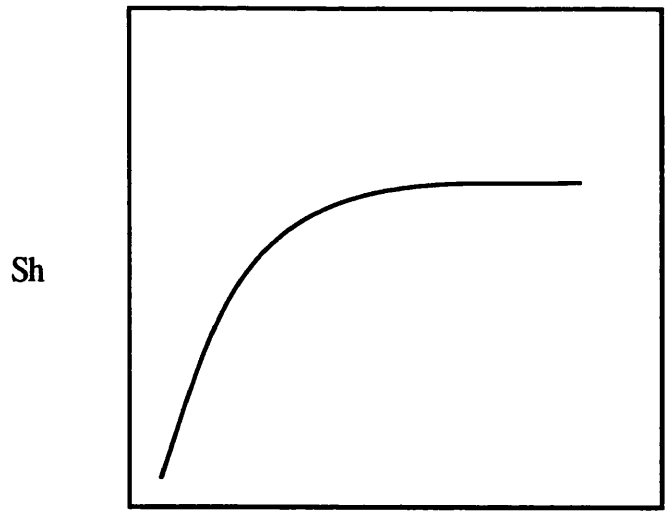

Fig. 7.21 Schematic sketch of Sh versus number of elements for a fixed length tube

The effect of increased flowrate results in increased entry length. Thus as the flowrate is increased from 5 to 20 L/min (STP), ie. Re is increased from 282 to 1130 (371°C), using Langhaar's equation (2.7) the entry length increases from 24 cm to 97 cm respectively. The reactor length is only 15 cm and therefore any disturbance created by the insertion of mixer elements occurs early on in the entry region of the pipe for all the flowrates tested. The effect therefore is similar to that described above, ie. of two disturbances occurring close together, and therefore it may be expected that any enhancement as a result of improvement of mixing should be more pronounced at lower flowrates. This matches exactly with what was observed during experiment, ie. as the flowrate is increased the enhancement factor is reduced (figure 2.20). Indeed, it is envisaged that as the Re goes to infinity the enhancement in conversion for the ATCR compared to the empty tubular reactor should approach one.

7.6 Conclusions

Various catalytic reactor arrangements were investigated in this chapter. The following results were found from experiment:

1) Clear improvements in the overall conversion were observed when static mixers were inserted into catalytically coated tubular reactors, for the conditions tested in this study. Hence for example at a flowrate of 10 L/min (STP) (ie. Re=565 at 371°C) a conversion of 80 % was observed for the ATCR (using Sulzer elements N_E=7) compared to 56 % for the empty tube reactor at similar operating conditions (371°C). This represents an enhancement in conversion of 42.9 %, as a result of disturbing the flow. This shows that the tubular reactor is mass transfer limited and therefore there is a potential for improving reactor performance in the form of enhanced conversion.

2) Three types of mixer configuration were tested ie. Sulzer, Kenics and the Star and Orifice designs. The performance in terms of conversion was found to be independant of mixer configuration to within ± 3 % at 371°C and for all the flowrates tested ie. 1.5 - 20 L/min (STP) and for all N_E except at N_E=1, where the Sulzer mixer gave the best performance.

3) Mixer configuration effects the overall pressure drop. The pressure drop was found to be directly proportional to the number of elements present. Of the mixers tested the Kenics type gave the lowest pressure drop, giving pressure drops of between 5 and 13 times those for the empty tube at flowrates of 5 and 20L/min (ie. a Re of 283 and 1130 at 371°C) respectively for N_E=7.

4) The enhancement in conversion at 371°C for the ATCR compared to the empty tubular reactor increases as the number of inserts is increased for all the flowrates tested (ie. F_t between 1.5 to 20 L/min at STP, or Re between 85-1130 at 371°C). This is a result of increased average Sh. However, for a high number of closely packed elements the rate of increase in conversion with respect to increased N_E becomes very small and approaches zero. Also, as the flowrate is increased and the spacing between the elements is reduced the increase in enhancement becomes less pronounced, and eventually as the Re goes to infinity the enhancement factor should approach one.

CHAPTER 8

COMPARISON OF EXPERIMENT WITH THEORY FOR THE MONOLITH AND ATCR SYSTEMS

8.1 Introduction

There are many models describing monolith behaviour, the complexities of which depend on the reactor and the conditions at which it operates as discussed in the Literature Survey.

The present work is concerned not only with the monolith but also with the Active Transport Catalytic Reactor (ATCR). Hence, a general model is required to describe both situations.

The flow distribution is fairly complex for static mixer devices. The experimental data given in chapter 7 is not sufficiently detailed to be able to describe the concentration and temperature profiles occurring within the ATCR, therefore some degree of approximation is required even for a two dimensional approach. Hence, it has been considered that a one dimensional model is most appropriate at the initial stages.

In this chapter therefore a simple steady state, plug flow model is described under adiabatic and stoichiometric reactant conditions.

This model is compared to the experimental data for the monolith as well as the ATCR, described in chapters 6 and 7 respectively. In both cases the flow is laminar, ie. the Re is less than 2000, however in the case of the ATCR and segmented monolith systems this profile is disrupted. Hence the effects of flow development are also investigated in the model.

The present chapter is concerned with comparing experimental and theoretical predictions of conversions and pressure drops for both the monolith reactor and the ATCR. The resulting ATCR model will serve as a basis for the simplified optimization procedures adopted to minimize the catalytic surface area for conversions and pressure drops similar to those of the monolith.

8.2 Model Assumptions

Experimental results of chapter 3 and evidence of Howitt and Sebella (1974), showed that the flowrate in each channel of the monolith is not the

same. Also the nonuniform flow distribution between the cells tended to decrease the effectiveness of the converter under a given set of conditions. For this reason, as discussed in chapter 4, static mixer elements were placed prior to the reactor test section, as discussed in chapter 4, to minimize the effect of the laminar parabolic profile and to create a uniform gas flow on entry into the reactor. Therefore, the assumption that there is a uniform gas flowrate and temperature distribution within each channel of the monolith seems reasonable in this case.

For the conditions investigated in this study there are no significant homogeneous gas phase reactions. Indeed, this was found from experiment in chapter 4, where no homogeneous reaction was observed for the oxidation of CO for temperatures up to 500°C.

The experimental results for the monolith are given in chapter 6 and for the ATCR in chapter 7. All the recorded observations are for steady state at inlet gas temperatures ranging from 250-400°C.

There are a number of simplifications that may be assumed for the present work, as discussed in section 2.9.2.4 of chapter 2 (Lit. Survey).

These are adopted in the present model and are given below:

1) the reactor operates in the steady state ,
2) in the case of the monolith, the reaction within each channel is assumed to be the same, therefore one channel will be taken to typify conditions through the whole monolith,
3) gas phase conditions (flow, temperature and concentration) follow the plug flow model, ie. their profiles are uniform across the channel cross-section except at the boundary conditions where the film theory is applied,
4) the reaction is adiabatic,
5) there is no axial conduction within the gas or solid,
6) the gases entering the reactor are assumed to react heterogeneously with no homogeneous reaction taking place,
7) the physical properties, including , ρ , μ , D_i , c_p , k_g and ΔH_r are assumed to be constant along the length of the reactor (refer to appendix D),
8) the inlet fuel concentration is sufficiently low so that the properties of nitrogen can be used as the properties of the inlet gas (refer to appendix D),

9) the pressure drop across the channel length or the ATCR reactor is sufficiently low so that the system is essentially isobaric (refer to section 8.10.2),
10) radiation effects are neglected,
11) the fluid axial diffusion of heat and mass are negligible in comparison to the convective heat and mass transport. This is valid for systems with Peclet numbers (Pr × Re) greater than 30-50 (Michelson and Villadsen,1974),
12) the intrinsic reaction kinetics are so fast that reaction may be assumed to occur on the exterior surface alone.

Axial conduction in the metallic tubular reactor may in reality be significant, however this was neglected for ease of computation.

8.3 The One Dimensional Model

The equations consist of mass and energy balances across the fluid and solid phases. These are derived in appendix G.

The mass balance in the gas phase gives:

$$-u\frac{dC_G}{dz} = k_m S\,(C_G - C_S) \qquad (8.1)$$

Similarly an energy balance on the gas phase gives:

$$c_P \rho u \frac{dT_G}{dz} = h S\,(T_S - T_G) \qquad (8.2)$$

A mass balance on the solid phase gives:

$$r_{CO} = k_m\,(C_G - C_S) \qquad (8.3)$$

A heat balance on the solid phase gives:

$$r_{CO} \Delta H_r = - h \ (T_G - T_S) \qquad (8.4)$$

The rate equation was found in chapter 5, and is of the Voltz (1973) form:

$$- r_{CO} = \frac{k_r [CO] [O_2]}{(1 + k_a [CO])^2} \qquad (2.4)$$

where [CO] and [O_2] are the mole fractions of carbon monoxide and oxygen respectively.

For a stoichiometric mixture the concentrations of oxygen can be related to the concentration of carbon monoxide by the following:

$$[O_2] = \frac{1}{2} [CO] \qquad (8.5)$$

The difficulty in using a one dimensional model lies in the effect of the reactions on the mass and heat transfer coefficients particularly at light-off (refer to figure 2.10). However, for situations when light-off occurs at the start of the reactor length, the use of mass and heat transfer correlations determined under non reacting conditions may become feasible.

8.4 Solution Method

The experimental work of chapters 6 and 7 was carried out using the stoichiometric ratio of carbon monoxide and oxygen of 2:1. The concentration terms in equation 2.4 represent bulk gas concentrations in a kinetically limited situation. However, for mass transfer limited conditions, the equation should be written in terms of the surface concentration of CO. Also equation 2.4 is written in terms of mole fraction, but can be re-written in terms of concentration (kmol/m^3). Hence using equation 8.5 the rate equation can be simplified to give:

$$-r_{CO} = \frac{k_r C_S^2}{2 (C_T + k_a C_S)^2} \qquad (8.6)$$

where C_S is the surface CO concentration and C_T is the total surface concentration. Also combining equations 8.3 and 8.4 gives:

$$T_S = T_G + \frac{k_m (C_G - C_S) \Delta H_r}{h} \qquad (8.7)$$

where T_S is the surface temperature.

If equation 8.7 is substituted into the rate in equation 8.3 then T_S may be eliminated and the resulting equation is in terms of C_S. For given inlet values of $C°_G$, $T°_G$ and the rate parameters, the inlet value of $C°_S$ can be calculated by the Newton Raphson technique (Press et al., 1989). Hence the inlet value of $T°_S$ can also be calculated from equation 8.7. The equations 8.1 and 8.2 can therefore be solved simultaneously using the Runge-Kutta technique (Press et al., 1989) in which the boundary conditions are supplied at the start of the axial length. The values of C_G, T_G, C_S, T_S can then be solved stepwise along the length of the tube.

Programming was carried out on the SUN computers in the Department of Chemical and Biochemical Engineering (UCL) using the NAG library for the Runge-Kutta technique (D02BBF). The incremental step was very small and was determined by the automatic NAG increments.

The computer flowchart is given in appendix H. The inlet constant parameters depend on the inlet operating temperatures and are given in appendix B.

8.5 Choice of Sherwood and Nusselt Numbers for Use in the Model

The major factors determining the accuracy of the one dimensional model predictions are the mass and heat transfer coefficients as well as the intrinsic kinetics (established for the present catalyst in chapter 5).

Correlations for determining mass and heat transfer coefficients under non-reacting conditions for laminar flow in empty tubes have been put forward

by several workers (Hawthorn, 1973; Votruba, 1975; Bennett et al., 1990), as discussed in the Literature Survey, table 2.2. Those of Hawthorn (1973) and Votruba (1975b) are the most well known, representing average values determined across the length of the reactor.

Figure 8.1 compares the correlations of Hawthorn (cylindrical channels), Votruba and Bennett at various Re d/L ratios (for Sc=0.78). It can be seen that Hawthorn's correlation is the least sensitive to the ratio Re d/L, whereas Votruba and Bennett's equations are more sensitive but generally give lower Sherwood numbers at lower Re d/L ratios. The most obvious method of testing each correlation would be to experimentally determine Sherwood and Nusselt numbers under reacting conditions. In chapters 5, 6 and 7 for temperatures greater than or equal to 371 °C the reactors investigated were found to be completely mass transfer limited. It follows that the rate at which the reaction takes place is determined by the rate at which reactants are transferred to the catalytic wall rather than the intrinsic rate of reaction. In such cases some simplifications to the one dimensional model may be made, as performed by Hegedus (1973).

For a completely mass transfer limited reaction it can be assumed that :

$$C_S = 0$$

ie. the reaction occurs instantaneously at the surface and therefore the rate equation becomes redundant. Therefore equation 8.1 becomes:

$$-u\frac{dC_G}{dz} = S\,k_m\,C_G \qquad (8.8)$$

or

$$\int_{C_{Gin}}^{C_{Gout}} \frac{dC_G}{C_G} = -\frac{S\,k_m}{u}\int_0^z dz \qquad (8.9)$$

to give

$$\ln\frac{C_{Gout}}{C_{Gin}} = -\frac{S\,k_m\,z}{u} \qquad (8.10)$$

Knowing the inlet and outlet concentrations of CO as well as the reactor length and velocity in the tubular reactor the mass transfer coefficient may be calculated. Hence the Sherwood number may be found from:

Fig. 8.1 Proposed Sh correlations in honeycomb converters or pipes, Sc=0.78

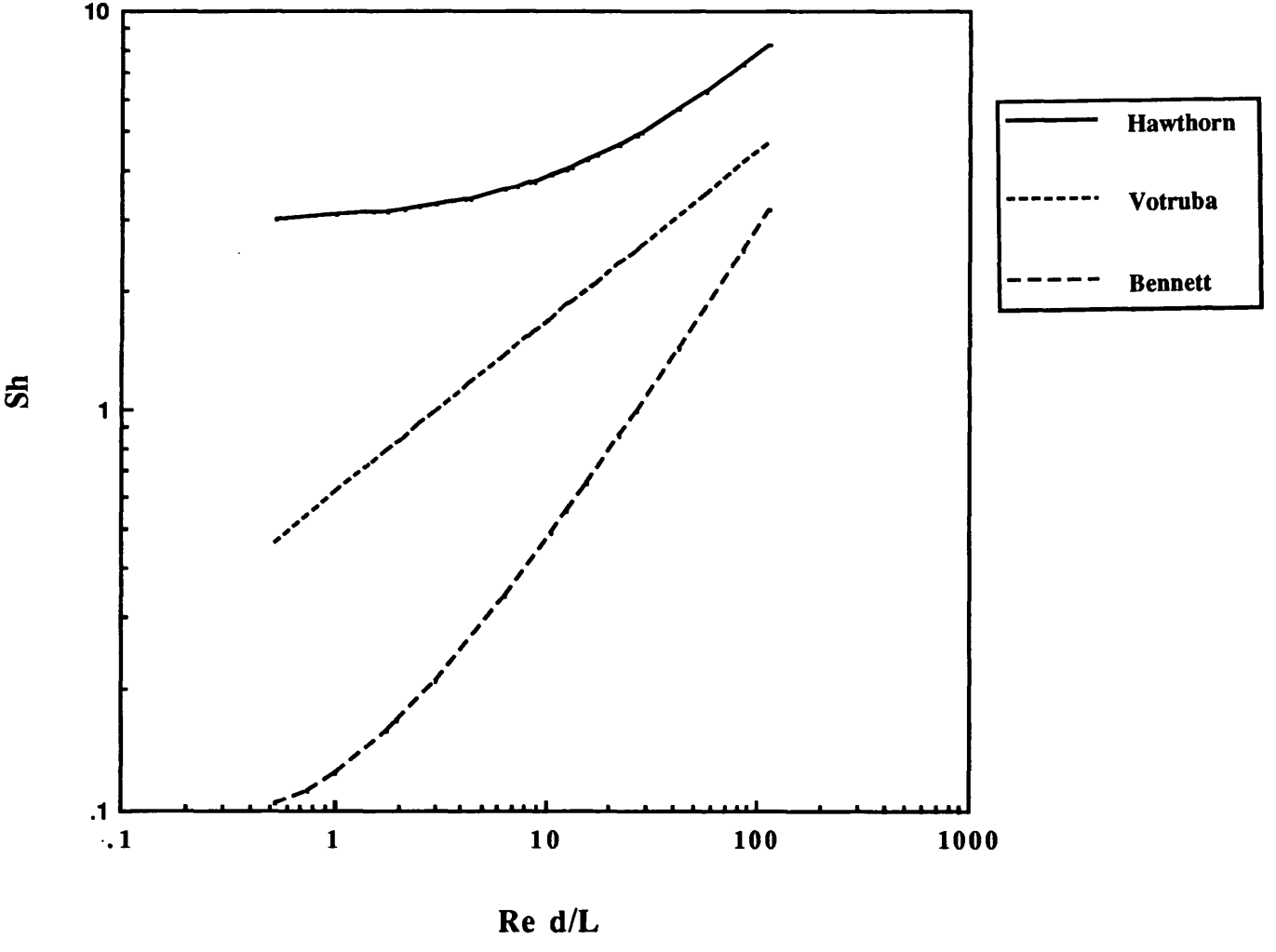

$$Sh = \frac{k_m\, d}{D_i} \qquad (8.11)$$

Also, by analogy the correlation for heat transfer may be found.

8.6 Sherwood and Nusselt Numbers for the Monolith

The above procedure was carried out for the completely mass transfer limited data of the monolith (data set II, chapter 6) at 371 °C for varying core lengths. Figure 8.2 is a plot of Sh versus Re d/L for the monolith using the following inlet conditions:

T_{Gin}= 371 °C	,	L=0.1, 1.0, 8.0 cm
$[CO]_{in}$=0.5 % (vol)	,	Re= 39 - 311
Sc=0.78	,	u= 2.2 - 17.7 m/s
S=3846.15 m^{-1}		

Included in figure 8.2 are data derived from 8, 1, and 0.1 cm monolith core samples. These data are compared to Hawthorn's (for square channels) and Votruba's correlations. It can be seen that the experimental Sherwood numbers for the monolith seem to follow the Votruba type correlation more closely, with an average scatter of 40.6%.

It should be stressed that the experimental Sherwood numbers found are not measured directly but are inferred from the experimental conversions measured at completely mass transfer limited conditions. Subsequent work in the reaction engineering group at UCL has confirmed the validity of these statements (Ullah et al., 1992).

8.7 Effect of Segmentation on Sherwood and Nusselt Numbers

Segmentation disrupts the flow causing it to redevelop at the entrance to each monolith segment. A possible qualitative description of the effects on the local Sherwood number is shown in figure 8.3. It may be envisaged that at every segment the flow is induced to redevelop. Physically this means that the boundary layer becomes thinner. Therefore the effect of segmentation is to increase the d/L ratio and so enhance the average Sherwood number over the whole reactor. The re-development or re-disturbance length is defined

Fig. 8.2 Experimental and theoretical comparisons of Sh for the monolith at 371 °C

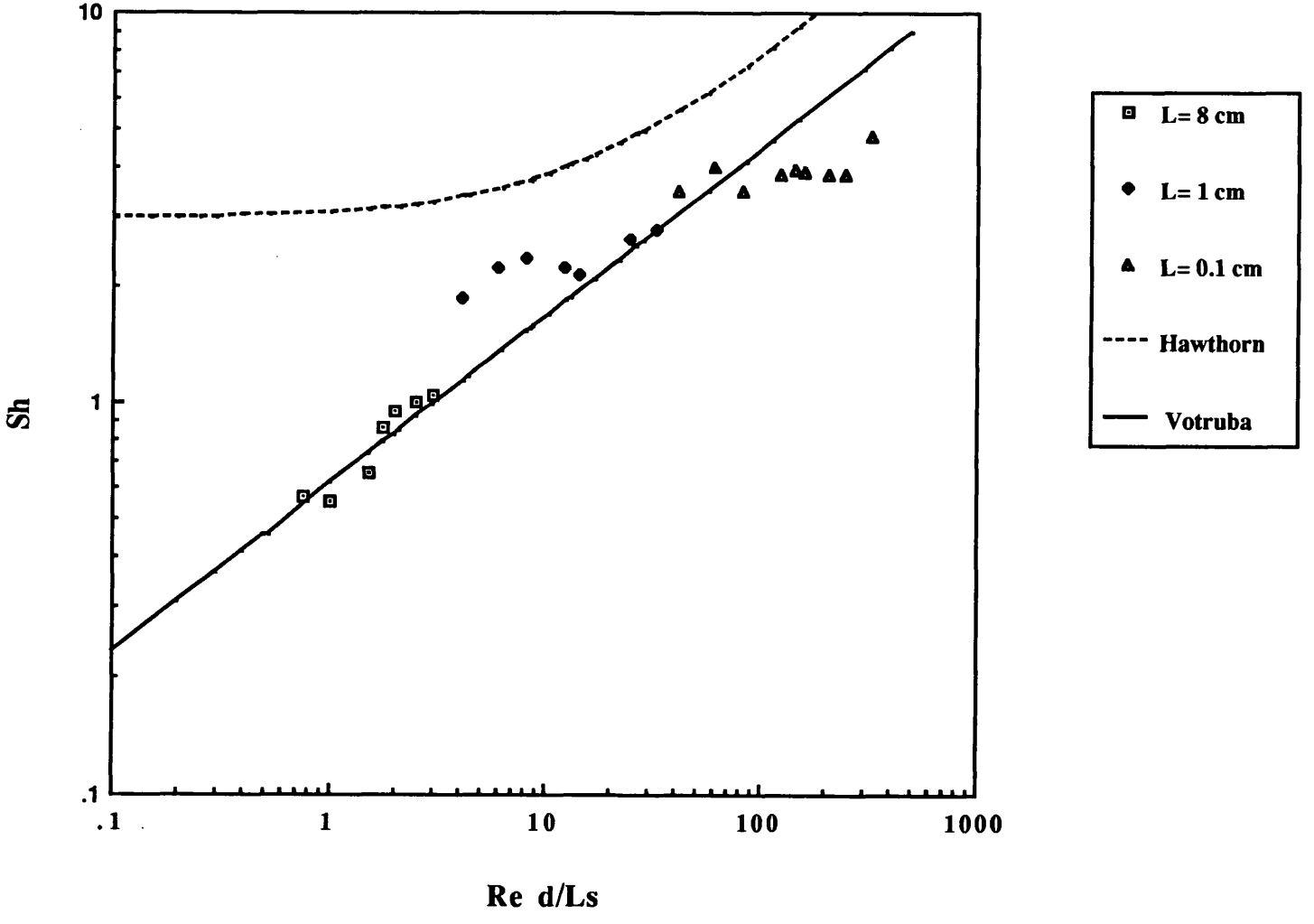

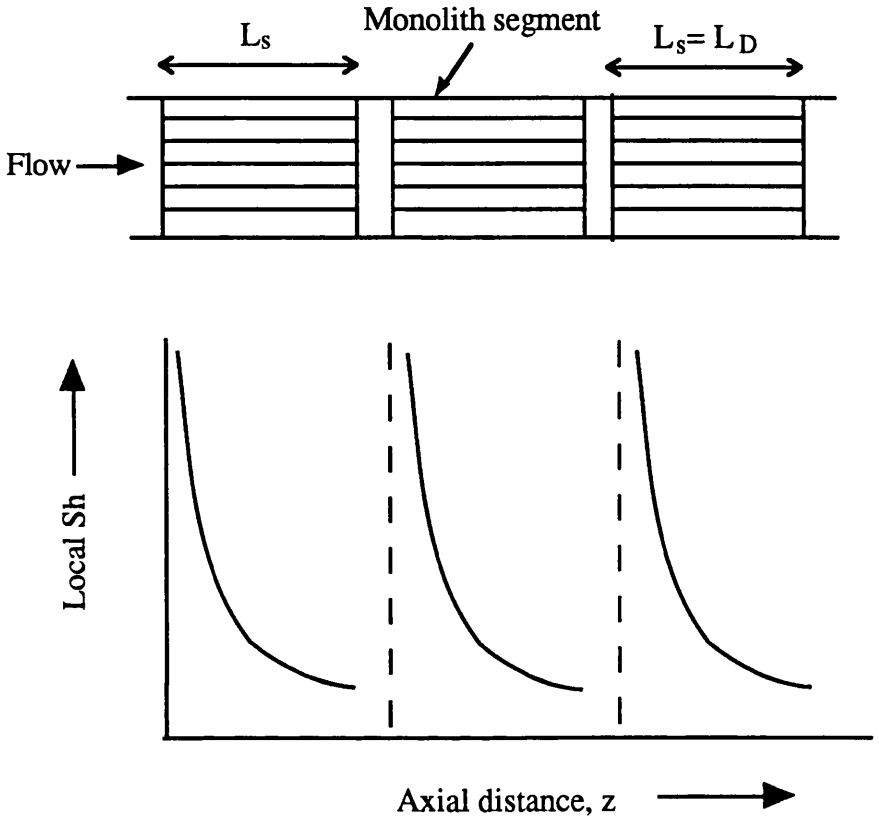

Fig. 8.3 Schematic diagram of local Sh vs axial distance along a segmented monolith reactor

as the length between each disturbance. The re-developement length (L_D) is indicated in figure 8.3 and is equal to the segment length (L_s).

The experimental Sherwood numbers across the monolith segment cores were calculated as above using equations 8.10 and 8.11. The ratio of d/L_D is taken to be equal to the channel diameter to the segment or re-development length (L_s). The resulting Sherwood numbers are shown in figure 8.4, for N=4 and 8, and compared to both Hawthorn's (for square channels) and Votruba's predictions for the same Schmidt number of 0.78. Previous data from figure 8.2 are also shown to give an idea of the scatter.

Since Sherwood numbers are determined from the conversions, at around 100% no improvements in performance by segmentation can be detected. Therefore, data at high conversions (ie. for flowrate below 12.5 L/min, for N=4 and 8) are neglected. It should be noted that the d/L_D ratios were found using the actual segment lengths given in table 6.1. The data for N=4 and 8 lie slightly below Votruba's correlation, indicating that the enhancements are not as effective as those predicted by Votruba. This result shows that perhaps the flow at each intersegment spacing is not fully disrupted, and therefore the average Sherwood number is lower than expected. However, the data lie close enough to Votruba's prediction for the difference to be due to experimental scatter. Hence Votruba's correlation would seem to be adequate in describing the experimental data for segmented monoliths, as predicted at 371°C.

8.8 Comparison of Experimental Conversion and Temperature Rise for the Monolith using the One-Dimensional Model for Varying Inlet Temperature

In general when the reaction is not completely mass transfer limited, the kinetic equation may become important, and as such the reaction may be controlled by either or both of these regimes. For temperatures below 371°C, the reaction may not be completely mass transfer limited (refer to chapter 5) and therefore the full one dimensional model should be solved.

Figure 8.5 shows the experimental and predicted (using 1-D model) conversions at 250 and 371 and 400°C for a monolith (set II, L_s=8 cm, of chapter 6). The one dimensional model uses the kinetics determined in chapter 5 (eqn. 5.11), and Votruba's correlation. It can be seen that theoretical curves at 371 and 400°C lie close enough to the experimental data for the difference to

Fig. 8.4 Experimental and theoretical comparisons of Sh for integral and segmented monolith cores at 371°C (set II)

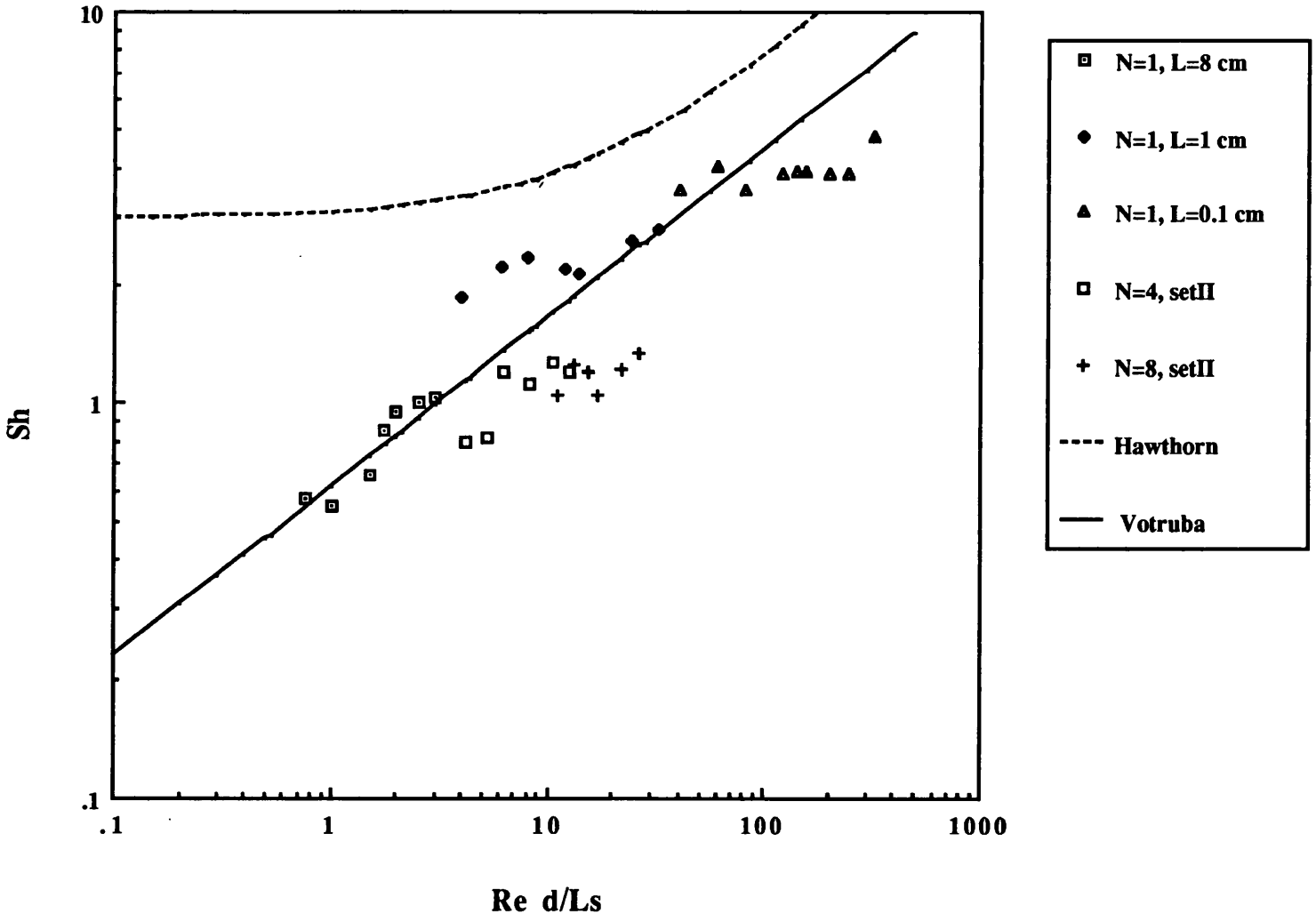

Fig. 8.5 Comparison of experimental and theoretical data for the monolith for various temp.'s, using Votruba's corr. for data set II, Ls=8 cm

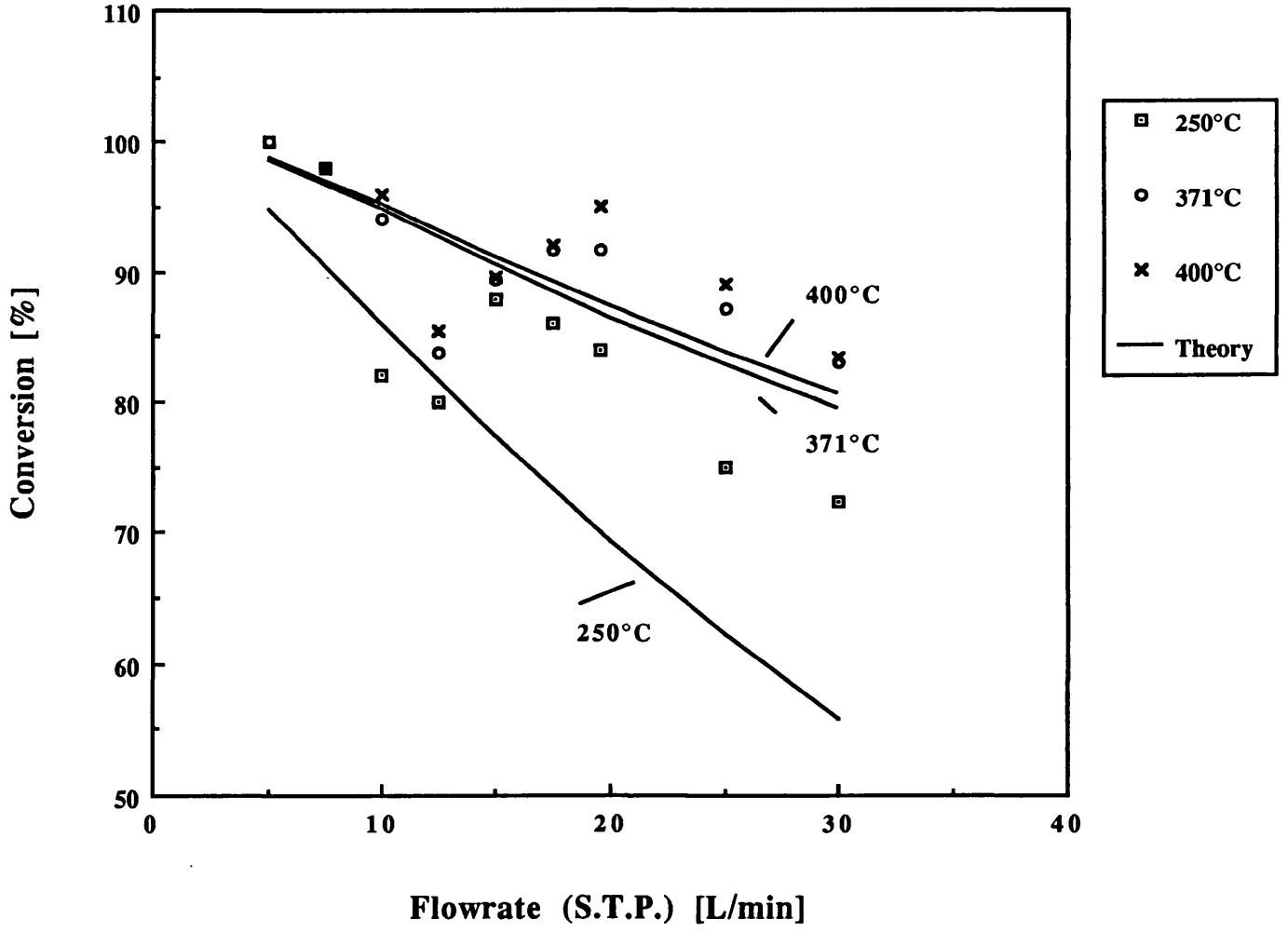

be due to experimental error. However, at 250°C there seems to be a large error (of up to 27 % in predicted conversion) at high flowrates (ie. 30 L/min). Estimates of mass transfer and kinetic rates can be determined at inlet conditions. Thus for example, using the kinetic equation 2.4 the reaction rate at 371°C is 1.215×10^{-4} kmol/m^{2}s when there is no mass transfer limitation. The maximum mass transfer rate at the entrance to the reactor occurs if $C_S=0$, giving a rate of 4.27×10^{-6} kmol/m^{2}s at an inlet total flowrate of 10 L/min (STP). Thus the mass transfer rate is much lower than the kinetic rate. It therefore follows that at 371°C the reaction is mass transfer limited. At an inlet temperature of 250°C on the other hand the kinetic rate is 2.04×10^{-6} kmol/m^{2}s and the mass transfer rate is 3.89×10^{-6} kmol/m^{2}s for an inlet flowrate of 10 L/min (STP). Thus at 250°C the reactor is kinetically limited at the entrance. However, these two rates are very nearly equal, and as the surface temperature rises, as a result of reaction, there should be a switch along the channel length when the reaction moves from being kinetically to being mass transfer limited. It follows therefore that there are both kinetic and mass transfer limited regimes occurring along the 8 cm core length at 250°C. This is indeed the case, since if an arbitrarily higher mass transfer rate is introduced into the 1-D model at 250°C there is an increase in the total oulet conversion, suggesting that the reaction is mass transfer limited at some point along the channel length. Therefore, the discrepancies between the experimental data and theoretical predictions at 250°C in figure 8.5 could be attributed to the errors associated with the kinetic equation 5.11 (ie. up to 29 % error) and the correlations of Votruba eqn. 2.10 and 2.11 (ie. up to 41 % error, refer to section 8.6). In comparison with these errors it would seem that the maximum error experienced between the experimental data and the model at an inlet temperature of 250°C and flowrate of 30 L/min (STP), in figure 8.5, is rather small and therefore there is fairly good agreement between theory and experiment. However, for a more accurate comparison, a two dimensional model should be adopted as discussed in section 2.9.2.4 in chapter 2.

The unusual trend at 12.5 L/min (STP) (refer to figure 6.4) is not predicted theoretically by the one dimensional model. Extended ranges of inlet parameters including flowrate, temperature, and mass transfer coefficients were fed into the 1-D model to attempt to predict this trend theoretically. However, the one dimensional model was unable to reproduce this trend.

The experimental and predicted outlet temperatures at 250°C and 371°C are given in figures 8.6 and 8.7 respectively. It can be seen that the

Fig. 8.6 Experimental and theoretical outlet gas temperature at T in=250°C, using Votruba's correlation

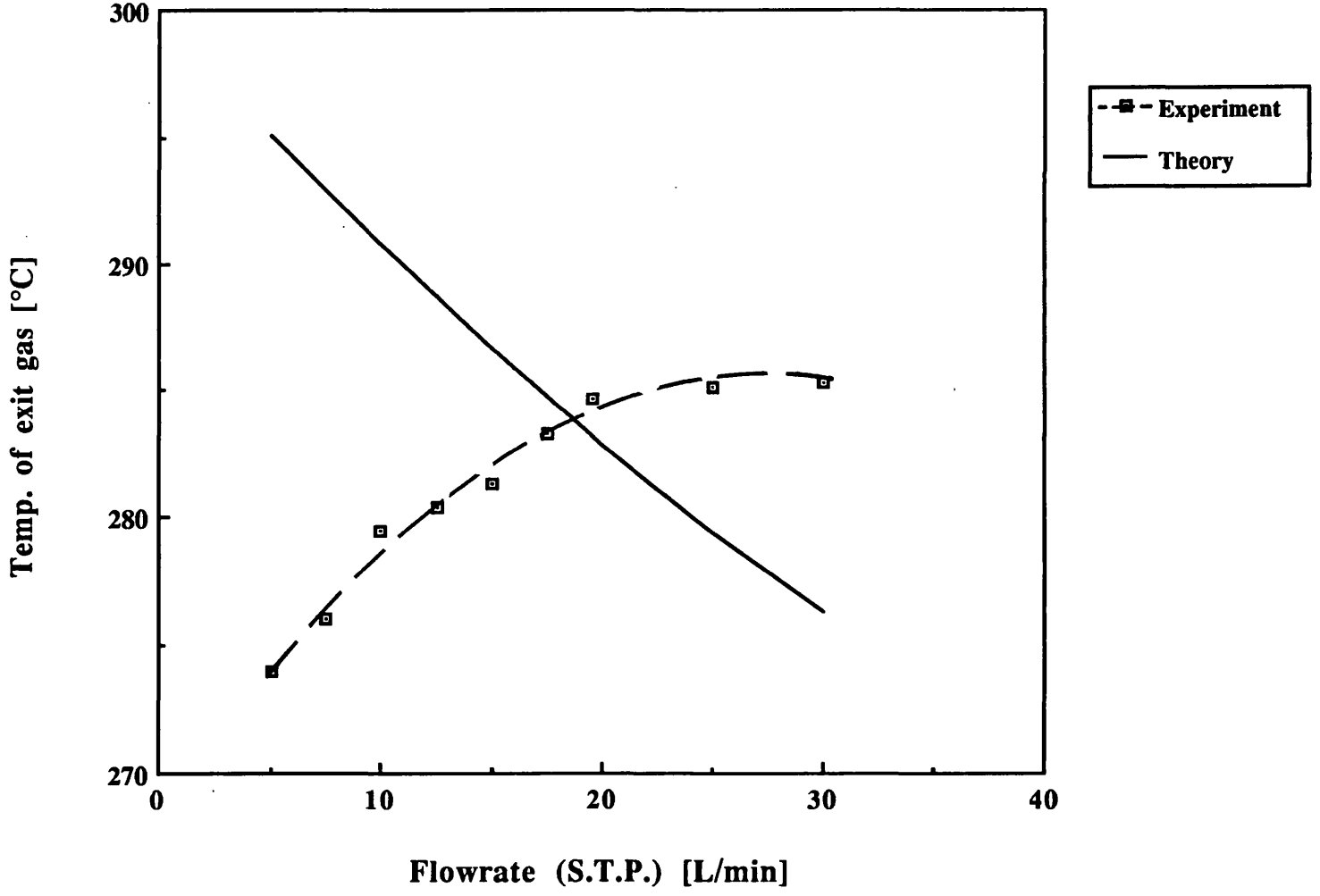

Fig. 8.7 Experimental and theoretical T out vs flowrate for the monolith at T in= 371°C, using Votruba's corr.

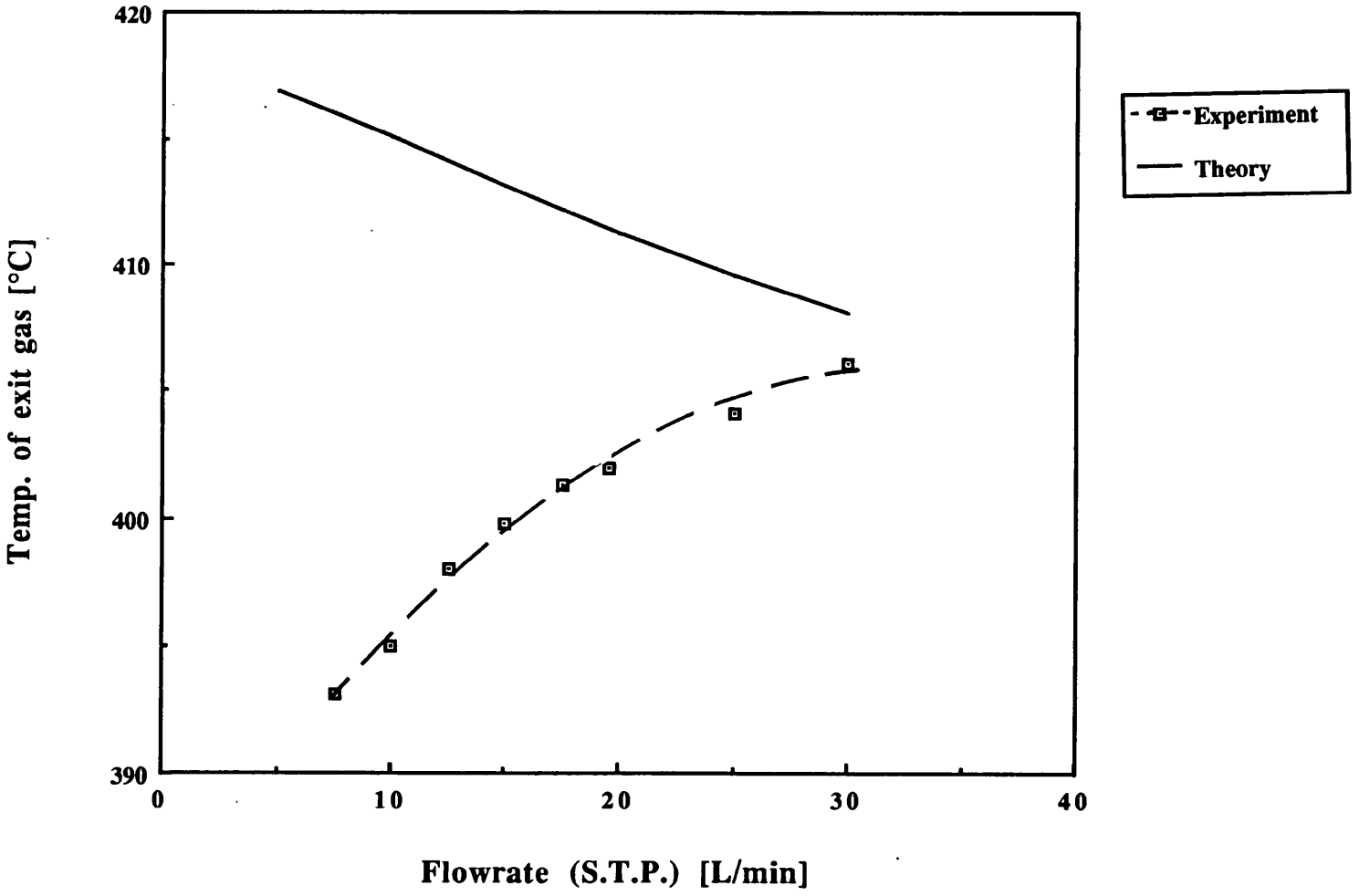

experimental gas outlet temperature rises as flowrate increases, however theoretically the trend is the opposite. Obviously the difference is due to heat losses which occur in reality as discussed in chapter 6, whereas the theoretical predictions are found for an adiabatic reactor. The adiabatic heat production, for example, at 10L/min for an inlet temperature of 250°C, is 8.7 Watts. This corresponds to a temperature rise in the gas phase of 39°C, as indicated in figure 8.6. According to chapter 6, heat losses correspond to 2.14 Watts, which is responsible for the discrepancy between the experimental and thereoretical temperature rise of approximately 10°C. In any case the differences are quite small and represent in the worst case less than 4 % deviation in terms of outlet gas temperature. Similarly, figure 8.7 at 371°C can be explained with the same rational. Compare these figures (ie. 8.6 and 8.7) to figure 3.12 of chapter 3, where the adiabatic and experimental temperature rise was also found to be in opposite directions.

8.9 Sherwood and Nusselt Numbers in the Active Transport and Tubular Reactors

As discussed in the Literature Survey, there are Nusselt and Sherwood number correlations available for both the Kenics and Sulzer mixers (given in table 2.5). The general form of the equations in table 2.5 may well be applicable for the purposes of modelling. However, the constants of proportionality are restricted to the aspect ratios given as well as the number of elements per unit length of the tube and therefore are given for a fixed N_E/L. The correlations indicate that the increase in Sherwood number for the static mixer device compared to the empty tube is a constant factor, although the correlation of Morris and Misson (1974) gives the Sherwood number in terms of number of elements. These correlations however, are for static mixing devices placed end to end. In the present experiments the mixers are spaced equally within a fixed reactor length.

The experiments performed for the tubular and ATCR were found to be completely mass transfer limited (chapter 7, refer to fig. 7.9) at 371°C, as in the case of the monolith reactor. Hence a similar procedure to that for the monolith was adopted to establish experimental Sherwood numbers for the tubular reactor and ATCR.

Sherwood numbers were found as shown in figure 8.8 using the following inlet conditions:

T_{Gin}= 371 °C	,	L= 15 cm
$[CO]_{in}$= 0.5% (vol)	,	u=0.33-4.45 m/s
Sc=0.78	,	Re= 85-1130 at 371 °C
S=266.7 m^{-1}		

The effect of inserting a mixer into the empty tube is to disrupt the flow. In reality however, when two flow disturbances occur close to each other the wake of the first may interfere with the presence of the second and therefore the overall Sherwood number increase may not be as high as expected.

Figure 8.8 is a plot of determined Sherwood numbers versus Reynolds numbers drawn on a logorithic axis for the Sulzer mixer for an inlet gas temperature of 371°C. It can be seen that the difference between the empty tube Sherwood number and that of the ATCR Sherwood number (ie. reactor including mixers) reduces as the Re increases. This shows that by increasing the Re there is more impact on the creation of turbulence in the empty tube than in the tube with mixers, since the mixers have already created some turbulence. Hence it would seem that at the conditions investigated the Sherwood number for the ATCR is not a constant factor multiplied by the Sherwood number for the empty tube. This can be seen more clearly in figure 8.9 of Sherwood number for the mixer divided by the Sherwood number for the empty tube. Thus as the Reynolds number increases the ratio is reduced, and the curves converge at higher Reynolds numbers. This result is expected as discussed in section 7.5 in chapter 7, in the case of enhancement factors, and indeed the ratio should approach one as the Re increases to infinity.

The curves in figure 8.8 seem to follow a Hawthorn type trend (discussed later), and therefore a general equation for the Sherwood number for the ATCR could take the form:

$$Sh = 3.66\left(1+\omega\left(Re\,\frac{d}{L_D}\right)^{\psi} Sc\right)^{0.45} \qquad (8.12)$$

Given the differences in shapes of the curves in figure 8.8, it can be seen that the power ψ is a function of the number of elements present per unit length of reactor. In reality, there may be interference between the disturbances of each mixer. However, as a first approximation it may be assumed that at each

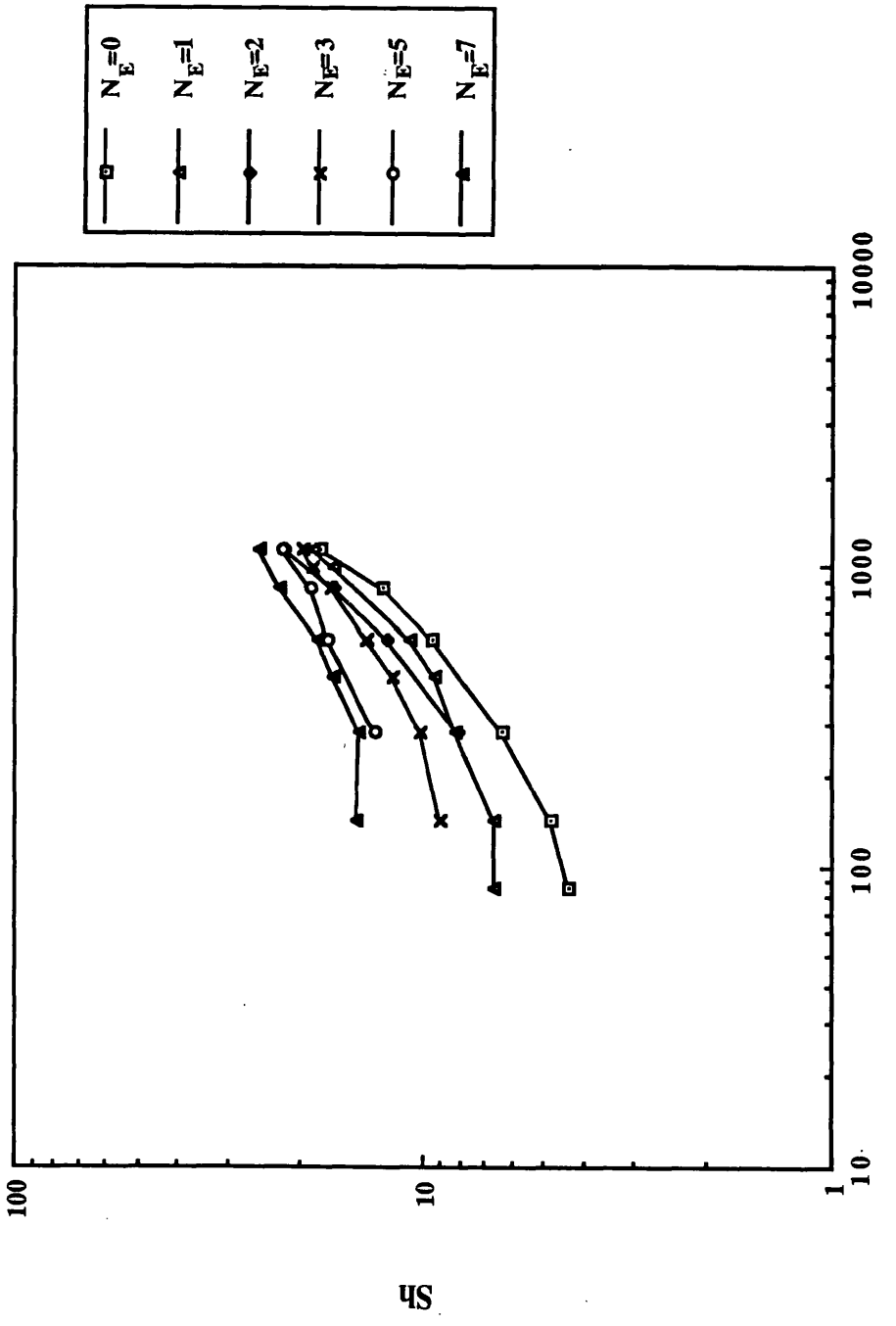

Fig. 8.8 Experimentally inferred Sherwood numbers for the Sulzer and empty tube reactors

Fig. 8.9 Enhancements in Sherwood numbers for the ATCR containing Sulzer mixer compared to the empty tube for varying N_E

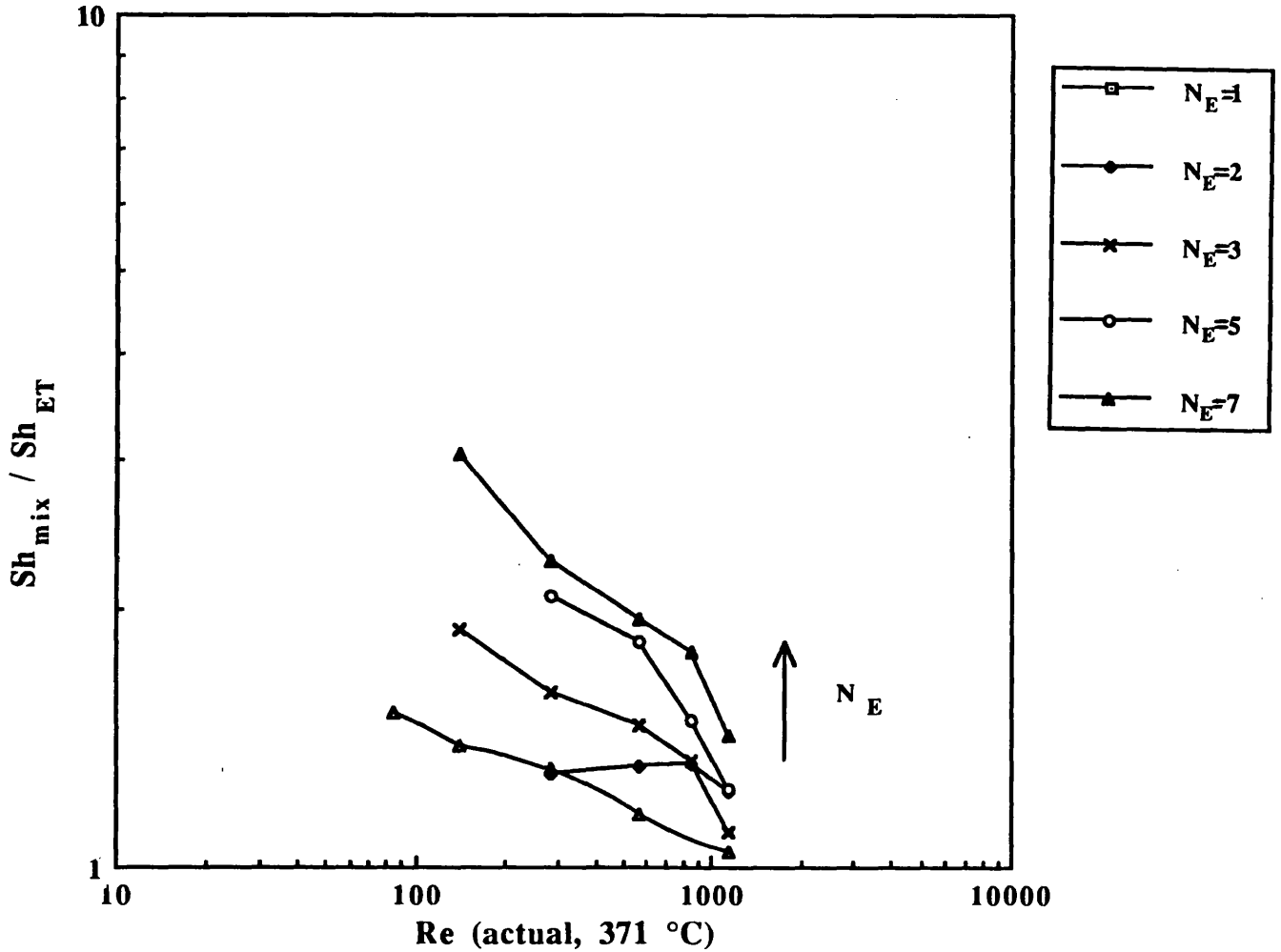

mixer unit there is complete mixing with little or no interference from the previous or the following mixer disturbance.

An interesting conclusion of chapter 7 showed that the enhancement in conversion is independent of the mixer configuration (except for N_E=1). This suggests that all three types of mixer, tested in chapter 7, disrupt the flow to produce similar Sherwood and Nusselt numbers. It follows that the flow is disrupted to the same extent, and it may be envisaged that the effect at each mixer is similar to the effect of segmentation within the monolith, ie. at each mixer the flow is disrupted and then starts to re-develop.

Figure 8.10 is a sketch of mixers within a tube with the corresponding re-development or re-disturbance length (L_D) value indicated. Hence in a similar fashion to that for the monolith, Sherwood numbers can be calculated from the outlet CO concentrations found from experiment. The conversions for the ATCR using all three mixer types (Kenics, Sulzer and Star and Orifice) were found to be the same except for N_E=1. Since the Sulzer mixer gave enhancements for all the N_E tested, the data for this mixer (appendix F) was chosen for the calculations of Sherwood numbers, however, the corresponding Sherwood numbers found apply equally well to all three static mixer devices except for N_E=1.

The Sherwood numbers are plotted in figure 8.11 and compared to the correlations of Votruba and Hawthorn (cylindrical pipes). The ATCR data seem to correlate well with Hawthorns correlation, with an average scatter of ±40.6% excluding the empty tube Sherwood numbers. This suggests therefore that the approximation that the disturbances act independently, without interference from the previous disturbance, is a reasonable one. The errors associated with the empty tube Sherwood numbers are large with an average error of up to ±67% compared to experiment occurring at the highest Re.

In figure 8.12 the one dimensional model using Hawthorn's correlation and the kinetics found in chapter 5 (refer to equation 5.11) is compared to the experimental conversions at an inlet temperature of 371°C for the empty tube and Kenics mixer for varying N_E. It can be seen that the largest error when compared to the theoretical predictions occurs for the empty tube reactor, due to the large errors associated with the Sherwood and Nusselt numbers determined above. However, when mixers are inserted there is good agreement between experiment and theory with the largest error of 6.4% occurring for N_E=1 at a flowrate of 15 L/min.

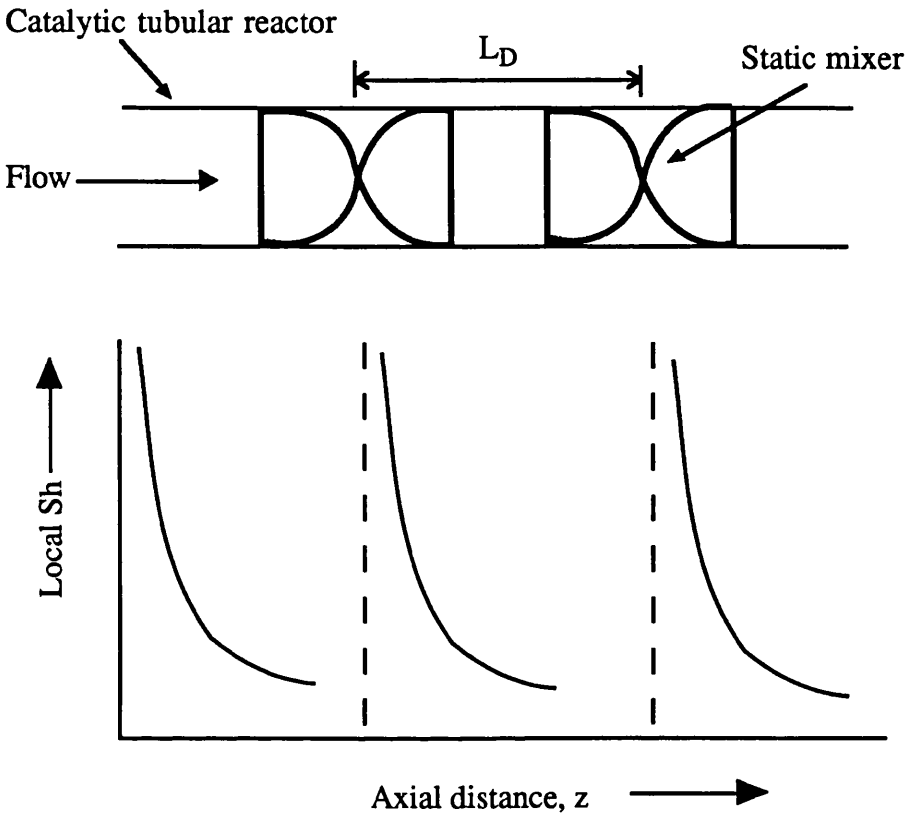

Fig. 8.10 Schematic diagram of local Sh vs axial distance along a tubular reactor with static mixer inserts (ATCR), for $N_E = 2$

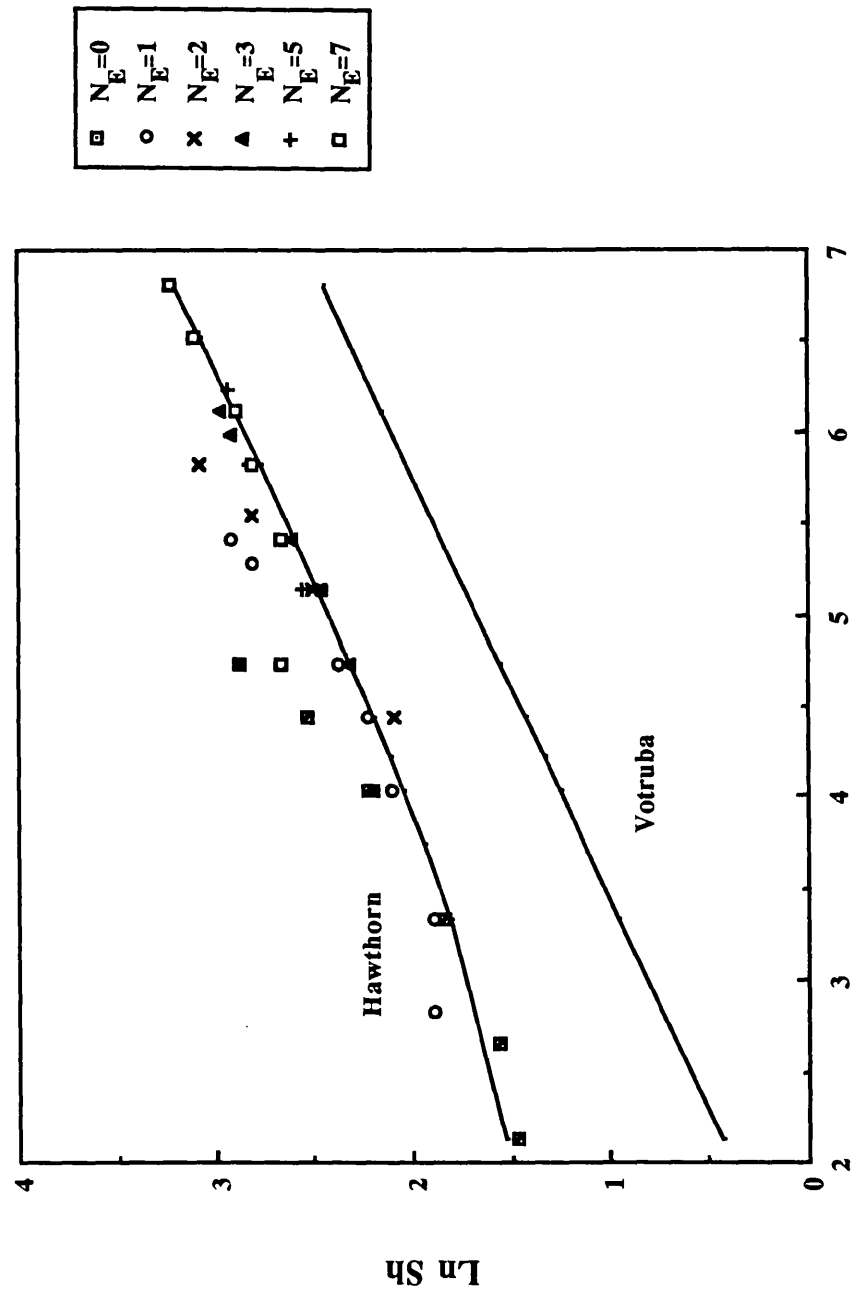

Fig. 8.11 Predicted Sh's for the ATCR containing Sulzer mixers at a gas inlet temperature of 371°C

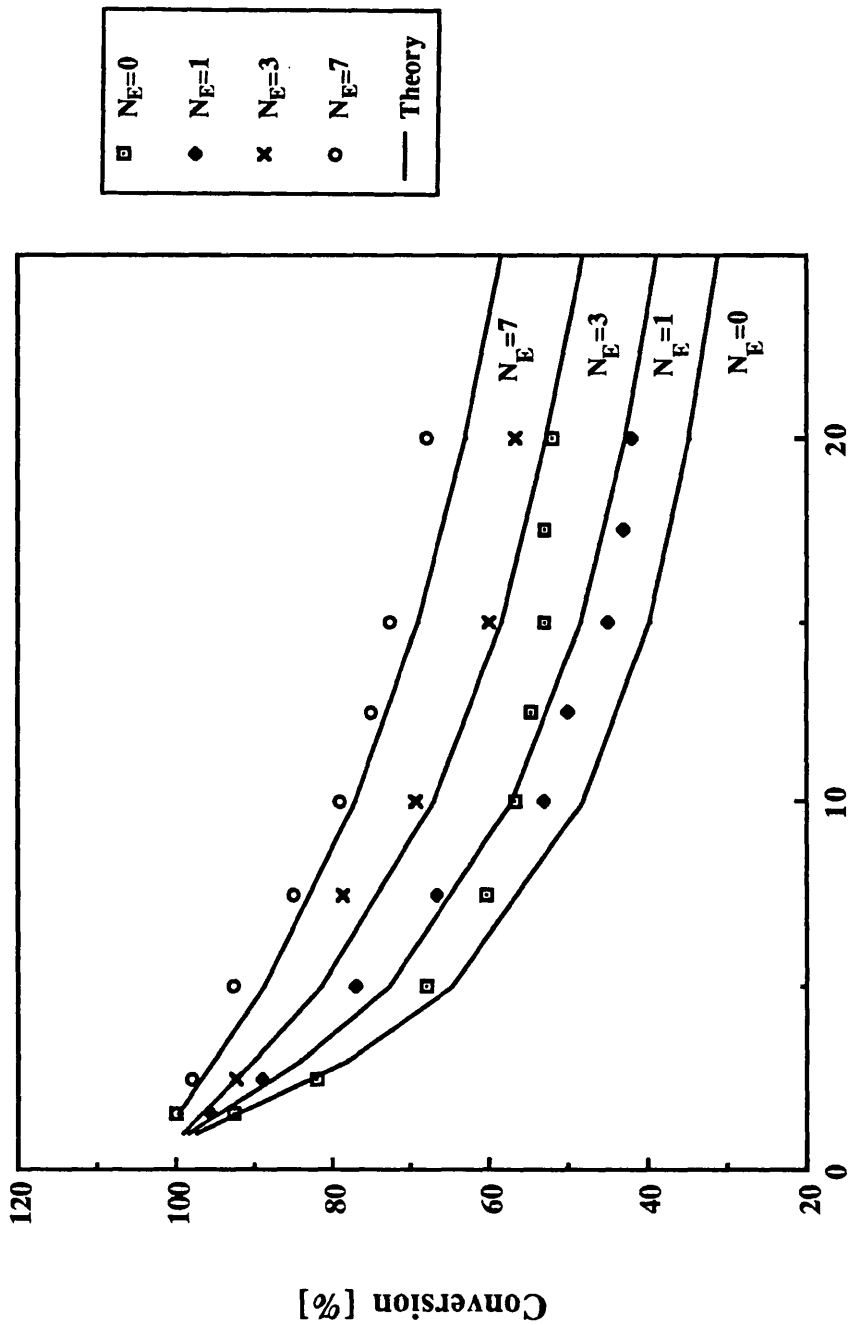

Fig. 8.12 Experimental and theoretical conversions for the ATCR with Kenics mixers for varying N_E at 371°C

Figure 8.13 shows the corresponding experimental and theoretical curves for the Sulzer mixer for varying N_E. Again it would seem that the experimental and theoretical curves tie up closely except for the empty tube reactor and for the single element insert ie. N_E equals to one.

In general therefore Hawthorn's correlation, for cylindrical pipes, can be used to predict conversions within the ATCR, and the re-development at each mixer element seems reasonable in predicting Sherwood, and hence Nusselt numbers, for use in the ATCR.

It is interesting to note that whereas the experimental Sherwood numbers for the monolith seem to be adequately described by Votruba's correlation, those for the ATCR are comparable to Hawthorn's. The literature indicates clearly that Votruba's data were found for monoliths of diameters ranging from 0.1-1 cm and therefore may not be applicable to pipes of larger diameters. Hawthorn extends the work of Shah and Kay (1971) for heat transfer data and by analogy describes the Sh. However, it is not clear which tube sizes were used, but Hawthorn predicts the correlation to apply to monoliths. However, Shah and Kay's (1971) work was performed mainly with pipes for the purpose of heat exchanger work.

8.10 Pressure Drop Predictions

In general, the total pressure drop consists of the pressure drop for the device being tested (ie. monolith or static mixer inserts) as well as the pressure drop for the empty tube in which the device is being held ie:

$$\Delta P_T = \Delta P_{Device} + \Delta P_{ET} \qquad (8.13)$$

As mentioned in chapter 2, the pressure drop within an empty pipe is given by :

$$\Delta P = f \frac{L}{2d} \rho u^2 \qquad (2.17)$$

where f is the Moody (Moody, 1944) friction factor which in laminar flow is a function of the Reynolds number. Also, in the general case, for developing flow Hawthorn (1973) predicted that :

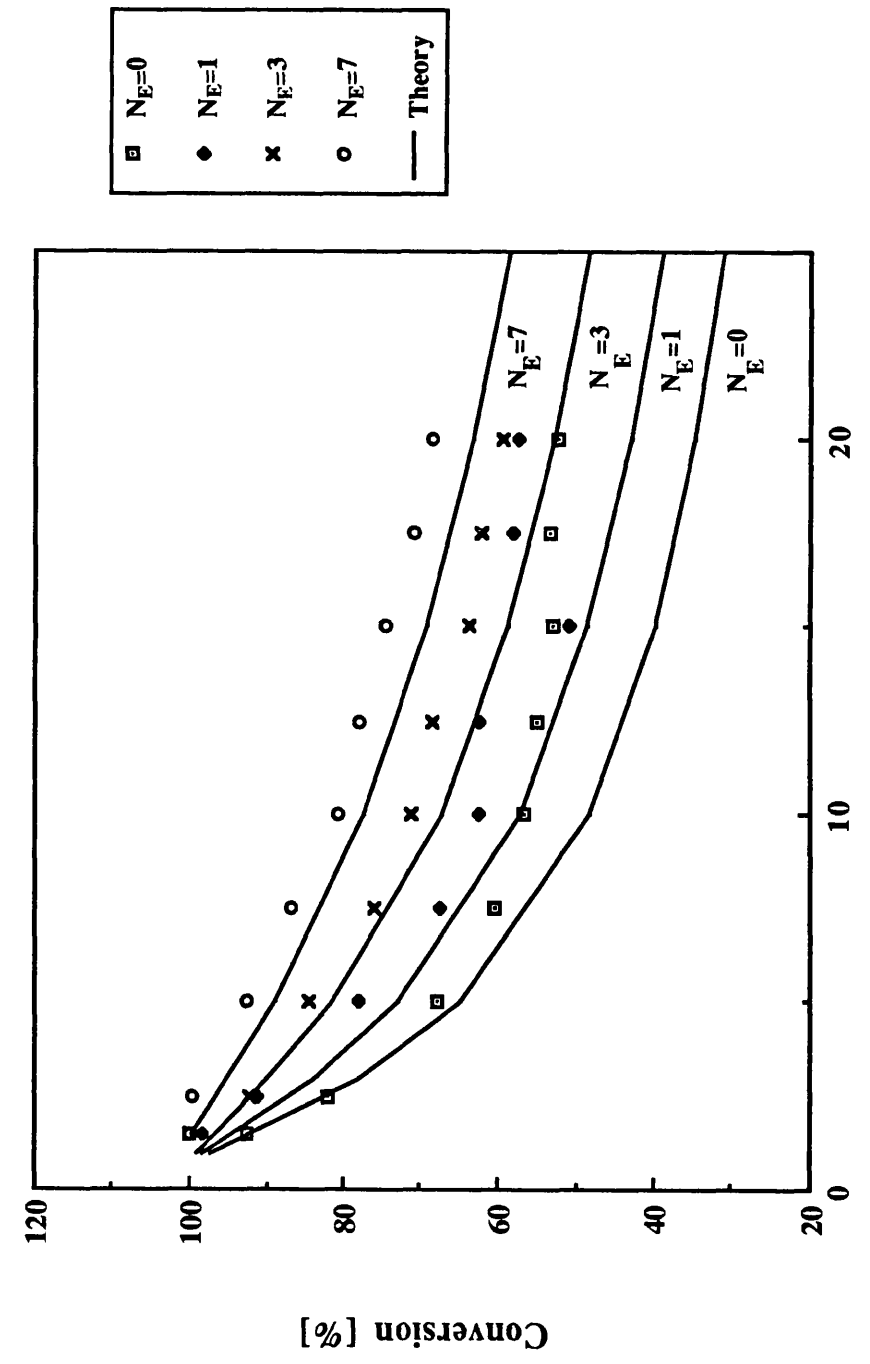

Fig. 8.13 Experimental and theoretical conversions for the ATCR with Sulzer mixers for varying N_E at 371°C

$$f = \frac{\beta}{Re} \left(1 + 0.045\ Re\ \frac{d}{L} \right)^{0.5} \qquad (2.18)$$

where the constant β equals 64 for a cylindrical pipe and 56.92 for a square tube.

8.10.1 Pressure drop for the monolith

In general, the pressure drop for the monolith should include expansion and contraction effects. However, when these effects were included ie. using the friction factor of Votruba et al. (eqn. 2.19), the predicted pressure drop was found to be high. Therefore the pressure drop within the monolith was found using the general friction factor of Hawthorn for developing flow (equation 2.18) for a square channel, in conjunction with equation 2.17.

It should be noted that in reality the total pressure drop measured included the effects of gaskets etc. as well as a small length of 1.3 cm diameter pipe section, in which the monolith is held. However, these effects were negligible compared to the pressure drop of the monolith.

Figures 8.14-8.16 compare the experimental results for data set II at an inlet temperature of 371°C for varying inlet flowrate, and varying N. A maximum error of 14.5 % occurs at 30 L/min for N=8. The data lie close enough to the theoretical predictions for the difference to be due to experimental error. Hence a developing flow friction factor as in equation 2.18 is accurate enough to describe the pressure drop for segmented monoliths

8.10.2 Pressure drop for the ATCR

The total pressure drop within the ATCR consists of the pressure drop caused by the presence of mixers as well as the pressure drop caused by the developing flow within the empty pipe between each mixer. Hence :

$$\Delta P_{ATCR} = \Delta P_{mix} + \Delta P_{ET} \qquad (8.14)$$

For a 15 cm tube the effect of the empty tube pressure drop may be negligible, however in order to generalize for any tube length this effect is included within the pressure drop calculation.

Fig. 8.14 Experimental and theoretical pressure drop for the monolith at 371°C and N=1 (set II)

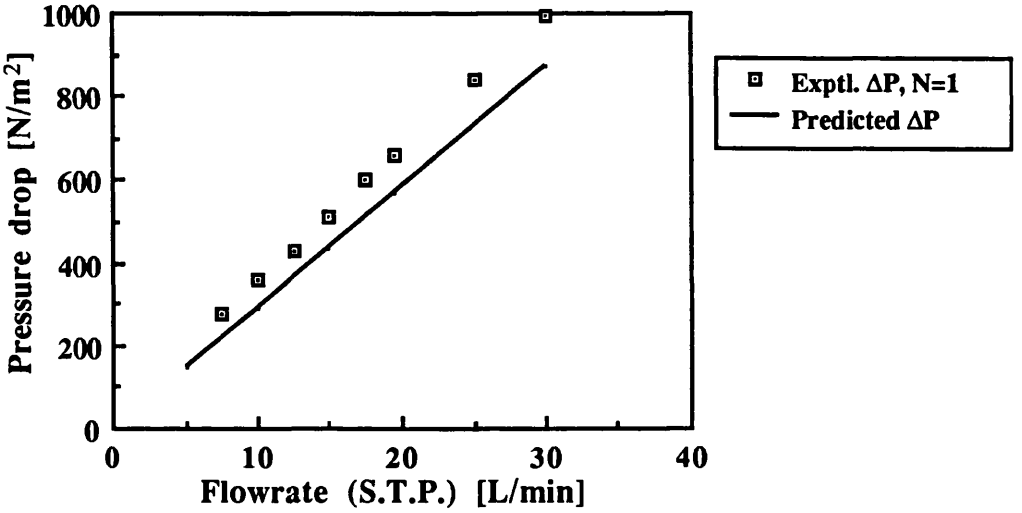

Fig. 8.15 Experimental and theoretical pressure drop for the monolith N=4 at 371°C (set II)

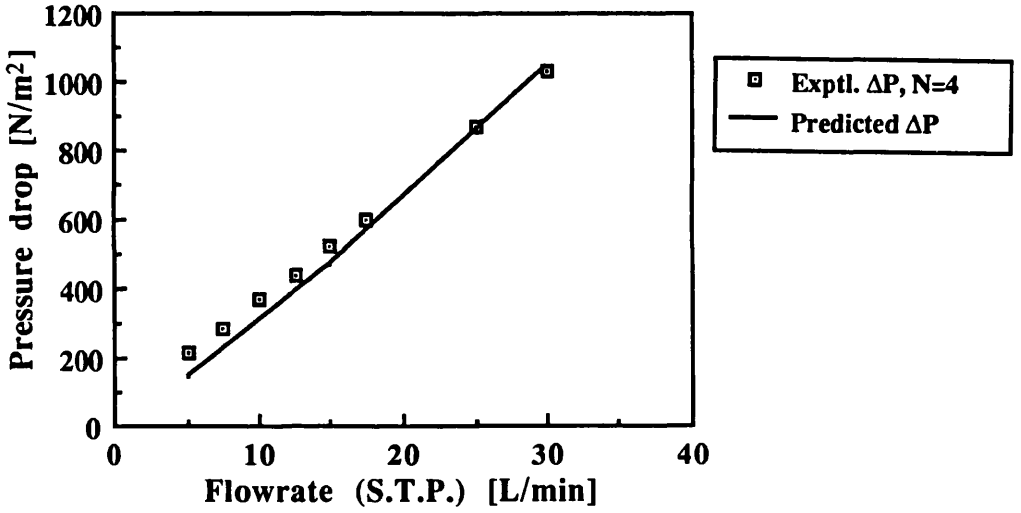

Fig. 8.16 Experimental and theoretical pressure drop for the monolith for N=8 at 371°C (set II)

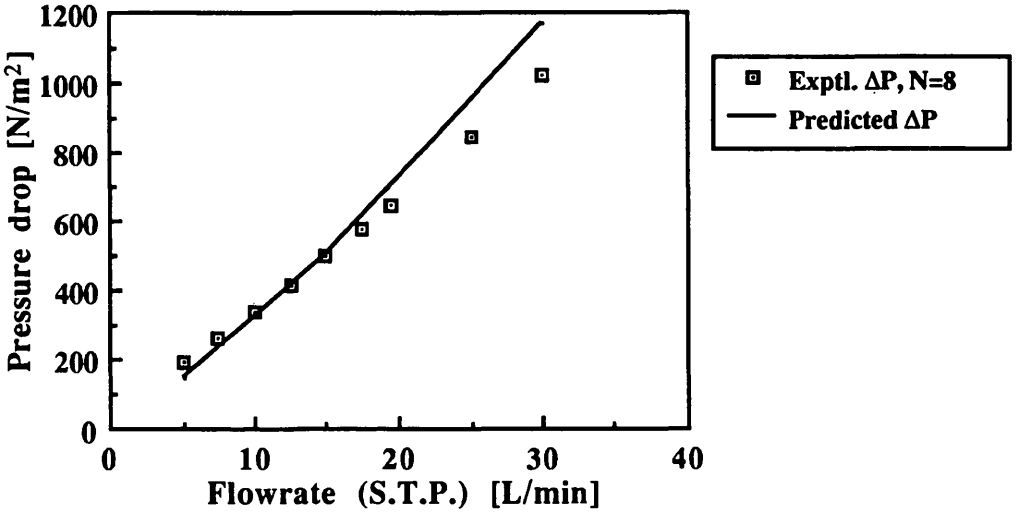

Pressure drops for developing flow in an empty tube can be found using equations 2.17 and 2.18 above.

As mentioned in chapter 2, the pressure drops across the mixers may be calculated using:

$$\Delta P_{Mix} = f_{SM} \frac{\rho u^2}{2} N_E \frac{L_E}{d} \qquad (2.26)$$

with the friction factors being dependent on the type of mixer used. Table 2.6 in chapter 2 gives a summary of the friction factors for the Kenics and Sulzer mixers for a variety of aspect ratios and are generally of the form:

$$f_{SM} = A' + \frac{B'}{Re} \qquad (2.27)$$

The friction factor specified by the Sulzer manual (1987) was found to best describe the pressure drop results found in the experiment. The equation is given for Re<2000 as:

$$f = 5.1 + \frac{1100}{Re} \qquad (8.15)$$

The experimental pressure drops measured for the Sulzer mixers at a gas inlet temperature of 371°C are compared to those predicted using the friction factor described by equation 8.15, for varying number of elements in figure 8.17. It can be seen that there is good agreement, with a maximum error of 16.1% occurring at 20 L/min for N_E=1, and with the most accurate fit being for N_E=7. This is reasonable since the difference between the predicted and experimental pressure drops for smaller N_E values is due to the pressure drop attributed to the empty tube section between the mixers, and therefore there are two friction factor correlations (ie. equation 2.18 and 8.15) to consider and consequently the result is bound to be more erroneous.

The aspect ratio of the Kenics mixer is 1.69 which is not given in table 2.7. Hence a curve fitting software package (RS/1) within the Department was used to find the friction factor for the experimental data for N_E=7. N_E=7 was chosen because there are no spaces between the mixers and hence the empty tube pressure drop equals zero (ie. DP_{ET}=0). This package uses an iterative technique known as the Marquardt's compromise method, in which a set of

Fig. 8.17 Experimental and theoretical pressure drop for the Sulzer mixer for varying N_E at 371°C

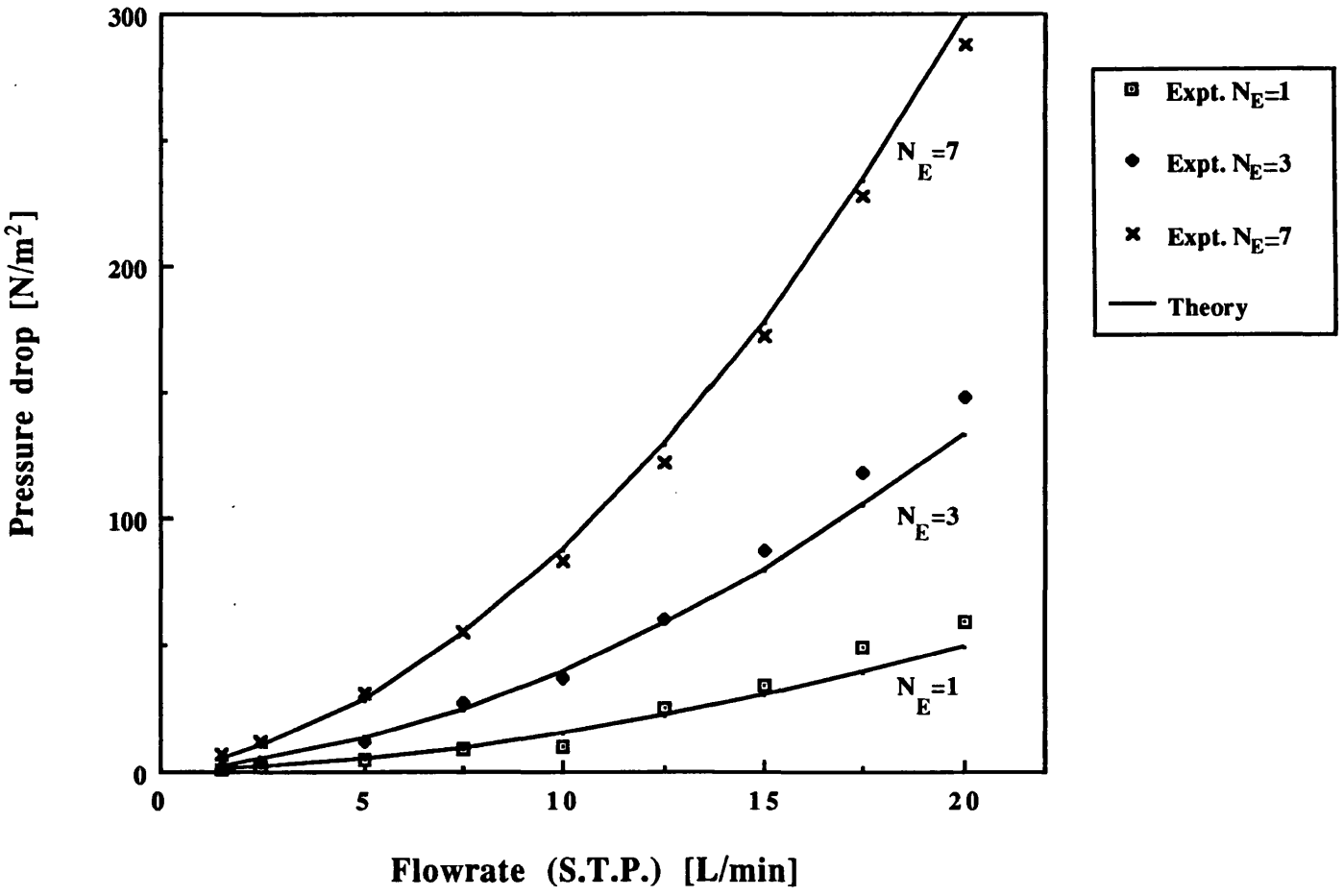

initial guesses for the parameter values (A' and B' in eqn. 2.27) are supplied and the program minimizes the residual (refer to eqn. 5.9 in chapter 5, ie. the sum of the squares of the differences between the experimental and theoretical predictions using equation 2.26 and 2.27, where the constants A' and B' are the unknowns to be found) with respect to the experimental data supplied. The friction factor was therefore found for 85 ≤Re≤1130 (371°C) to be:

$$f = 3.32 + \frac{225.7}{Re} \qquad (8.16)$$

Figure 8.18 compares experimental and calculated pressure drops for the Kenics mixer for varying number of mixers at 371°C. It can be seen that the fiction factor in equation 8.16 adequately describes the experimental pressure drops, with a maximum error of 12.5 % occurring at 20 L/min for N_E=3, again for the reasons mentioned above, however in general the error is much lower than this.

The maximum range of pressure drops found experimentally was from 200 to 1000 N/m^2 for the monolith, 0.1 to 300 N/m^2 for the Sulzer mixer and 0.1 to 180 N/m^2 for the Kenics mixer. This represents a maximum deviation of up to 1 % from atmospheric pressure. Hence the assumption that each reactor system reacts under isobaric conditions at atmospheric pressure is reasonable.

8.11 Simplified Optimization of ATCR

The optimization process described in this section is specific, and is only applicable to the ATCR reactor under completely mass transfer limited conditions. Hence a simplified one dimensional model (Hegedus, 1973) is used for the purposes of optimization. An ATCR in its optimal form would be attractive if it could combine the following features:

1) the performance in terms of overall conversion is similar to that of the monolith for the same inlet conditions,
2) the pressure drop is similar or lower than that of the monolith,
3) the catalytic surface area is minimized and lower than or equal to that of the monolith for the same catalyst loadings.

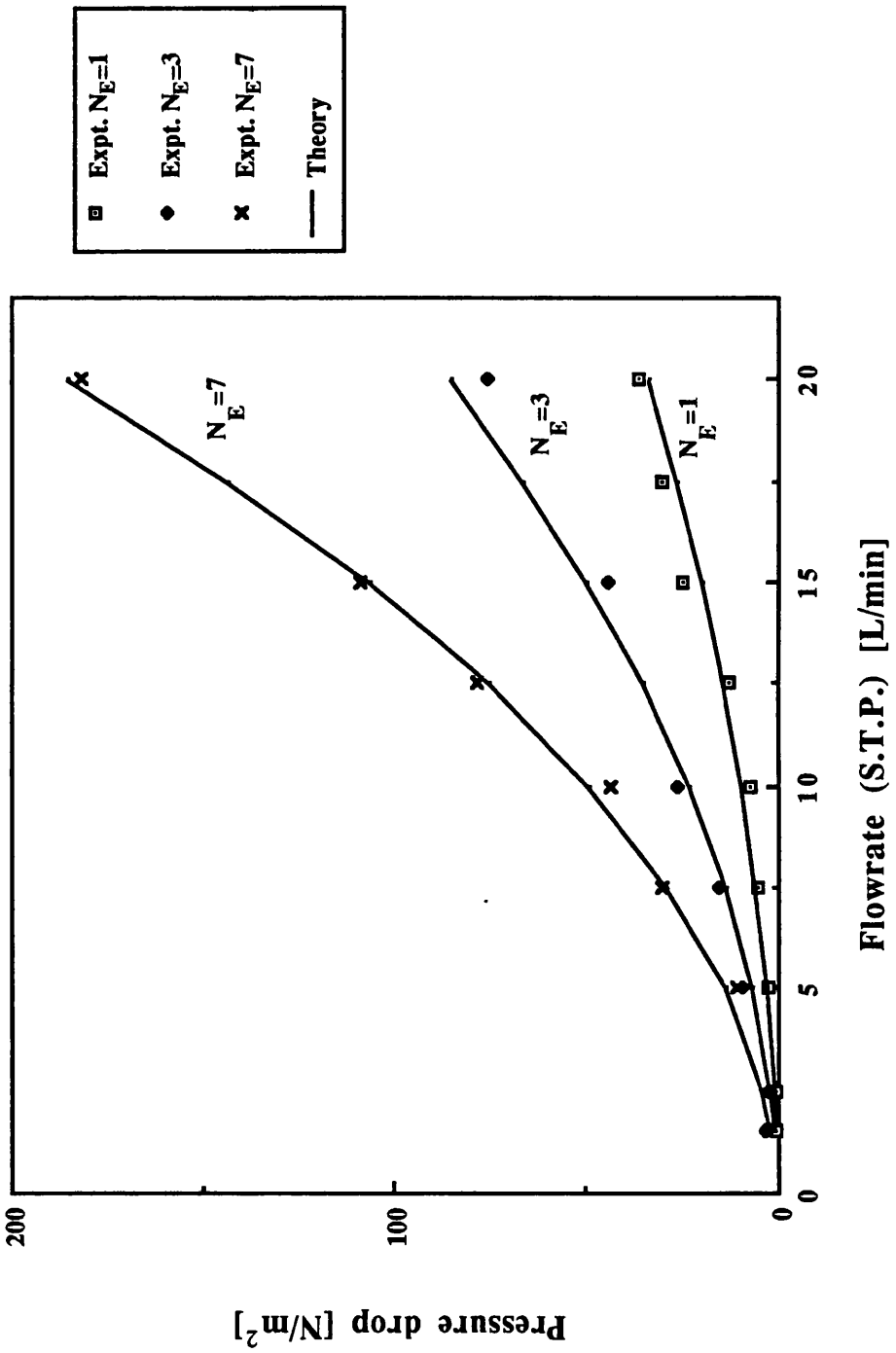

Fig. 8.18 Experimental and theoretical pressure drop for the Kenics mixer for varying N_E at 371°C

In general the space velocity within a monolith is up to 100,000 hr^{-1} (NTP). This corresponds to a flowrate of around 10 L/min (STP) within the 8 cm monolith of data set II from chapter 6.

i) Optimization of ATCR for fixed diameter

As a first approximation, a comparison of experimental data from the monolith (data set II at 371°C) and the theoretical data of the ATCR (using Kenics inserts placed end to end) for a fixed diameter pipe of 1.5 cm is made in figure 8.19, at 10 L/min. For the purposes of optimization the static mixer with the lowest additional pressure drop at any particular flowrate is chosen, ie. the Kenics mixer.

The data are presented as conversion and pressure drop versus the external catalyst surface area. Thus for a total conversion of 94%, for example, the total monolith surface area is 2.33×10^{-2} m^2 whereas for a similar conversion the ATCR with 13 elements has an external catalyst surface area of 1.32×10^{-2} m^2. Also, the pressure drop for the ATCR is lower than that for the monolith at the corresponding conditions (ie. 95 N/m^2 for the ATCR compared to 361.3 N/m^2 for the monolith). Hence, for a fixed diameter ATCR of 1.5 cm, it is possible to save up to 43.3 % of catalyst for similar performance to that of the monolith at 371°C and 10 L/min flowrate.

ii) Optimization of ATCR for varing diameter

Figure 8.20 is a plot of predicted conversion using Hawthorn's correlation for cylindrical pipes versus overall length of ATCR for varying numbers of mixers at 10 L/min (STP).

It should be noted that from equation 8.10, for a fixed velocity and length of reactor, the outlet CO concentration is constant for any diameter. Thus if k_m in equation 8.11 is substituted into equation 8.10, and S and u are written in terms of d and F_t, then the diameter cancels out and therefore the conversion is independent of diameter, ie:

$$\ln \frac{C_{Gout}}{C_{Gin}} = -\frac{4}{\cancel{d}} \frac{D_i\, Sh}{\cancel{d}} z \frac{\pi \cancel{d}^2}{4\, F_t} \qquad (8.17)$$

Fig. 8.19 Conversion and pressure drop vs catalyst external surface area for a flowrate of 10 L/min at 371°C

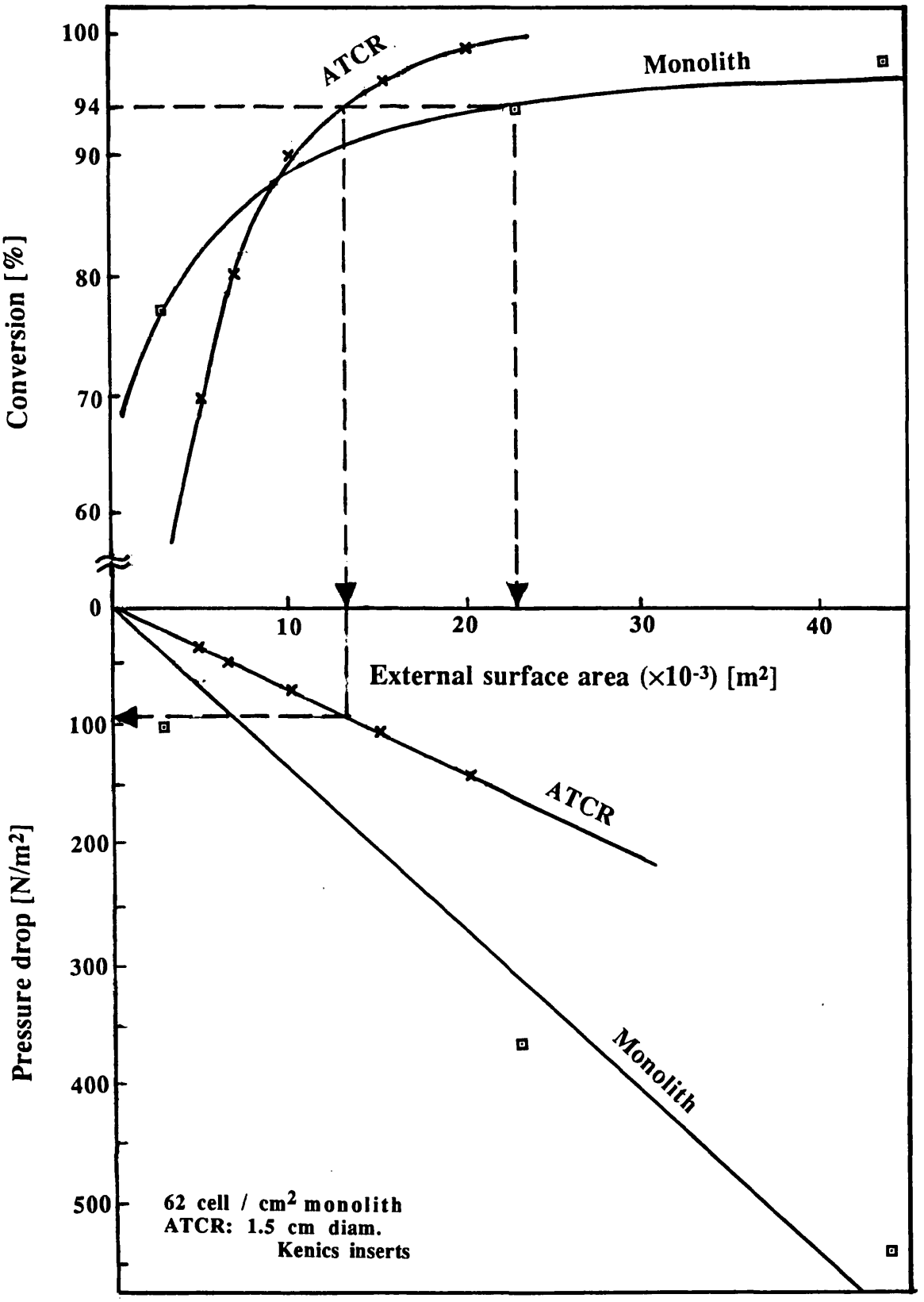

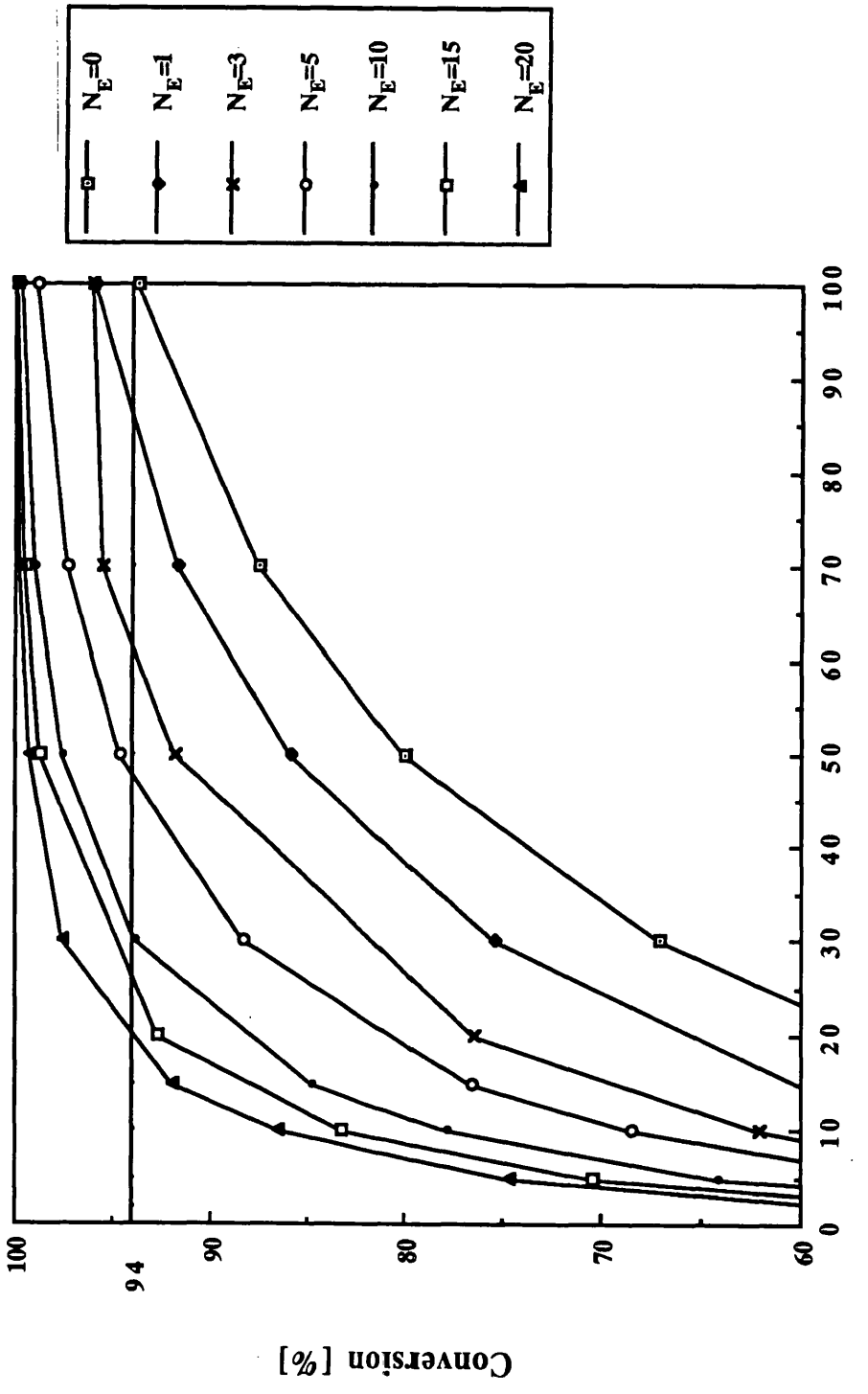

Fig. 8.20 Predicted conversion for varying numbers of inserts within the ATCR at 371°C, 10 L/min (STP)

where F_t is the total flowrate in m^3/s. Hence figure 8.20 is a generalized plot for any diameter reactor, for a fixed mixer aspect ratio of 1.69 as for the Kenics mixer.

At 10 L/min the monolith gives a 94 % conversion for an overall pressure drop of 361.3 N/m^2. The external catalyst surface area of the monolith is 2.33×10^{-2} m^2.

Hence there are three requirements to be met by the ATCR, for conditions analagous to that of the monolith:

1) The conversion should be at least 94 % at 10 L/min.
2) The pressure drop should be less than or equal to 361.3 N/m2
3) The external catalyst surface area should be less than or equal to 2.33×10^{-2} m^2.

Figure 8.20 can be re-drawn to give length of reactor required for 94% conversion versus the number of inserts as in figure 8.21. It can be seen that as the number of elements is increased, the total reactor length requirement is reduced, as expected, since the effect of the mixers is to enhance conversion.

As above the Kenics mixer is chosen for the purposes of optimization due to its lower pressure drop when compared to the Sulzer or the Star and Orifice mixers. The Kenics mixer used in this study has an aspect ratio of 1.69.

For a fixed overall conversion of 94% and also length specified from figure 8.21, the diameter of the reactor at each particular number of elements is varied to produce a constant pressure drop of 361.3 N/m^2. This is shown in figure 8.22, where it can be seen that as the number of elements is increased the diameter required for constant pressure drop is also increased. However, for a fixed length of reactor required to achieve 94% conversion, and a constant aspect ratio of 1.69, for a high number of elements there are some physical impossibilities which prevent the achievement of the required pressure drop. For example, for N_E=20, the total reactor length required to give 94% conversion is 18 cm. The maximum diameter of the reactor, for a fixed aspect ratio of 1.69, is 0.53 cm. This gives a pressure drop of 10643 N/m^2 and therefore the requirement of a pressure drop of 361.3 N/m^2 cannot be achieved.

The optimal reactor is therefore one which gives the same performance as the monolith with the lowest surface area. Hence figures 8.21 and 8.22 can be combined to give a vertical axis which is proportional to the surface area, as

Fig. 8.21 Required reactor length as a function of number of elements for a constant conversion of 94 %

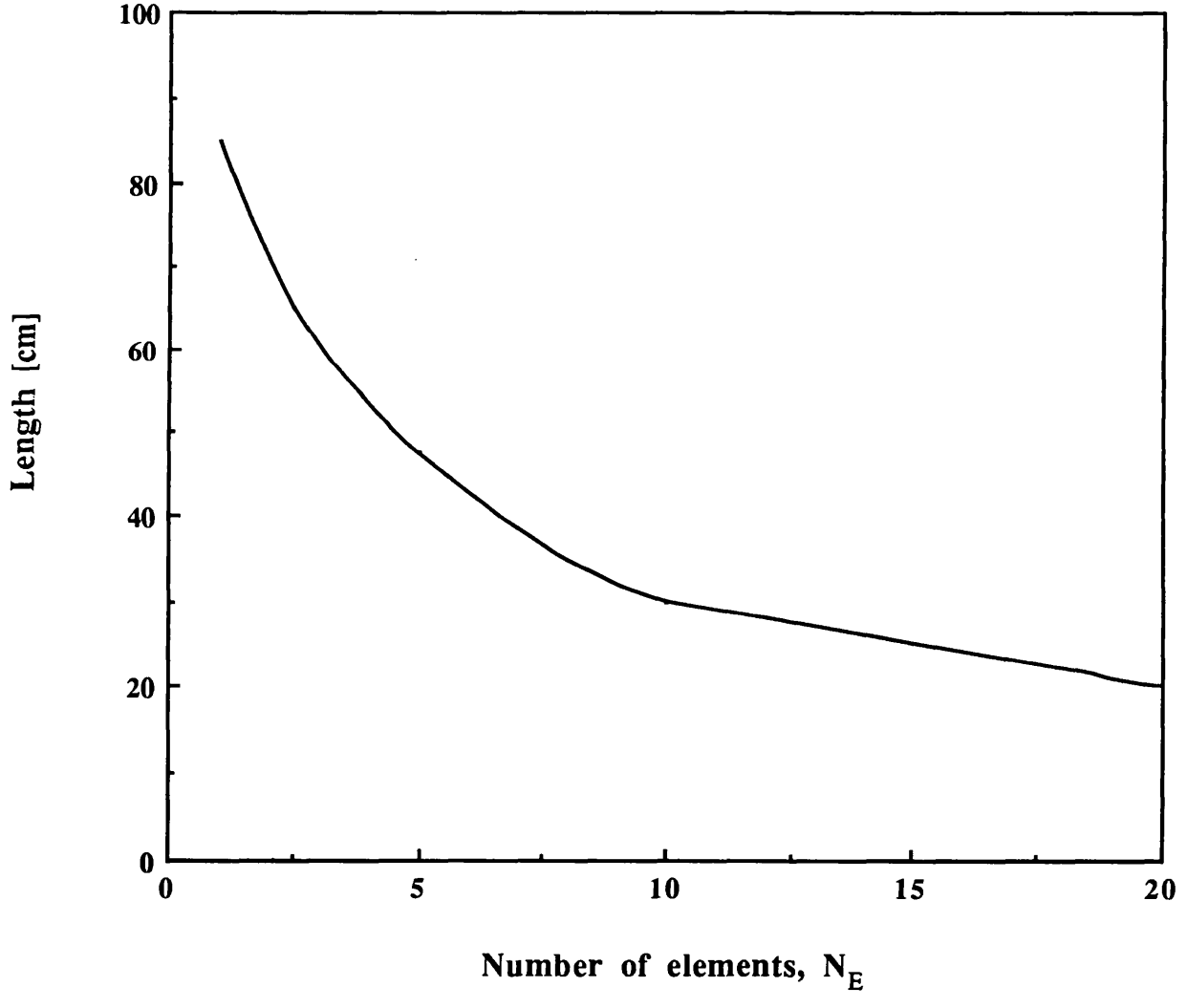

Fig. 8.22 Diameter versus number of Kenics elements for constant pressure drop of 361.3 N/m^2 and conversion of 94 %

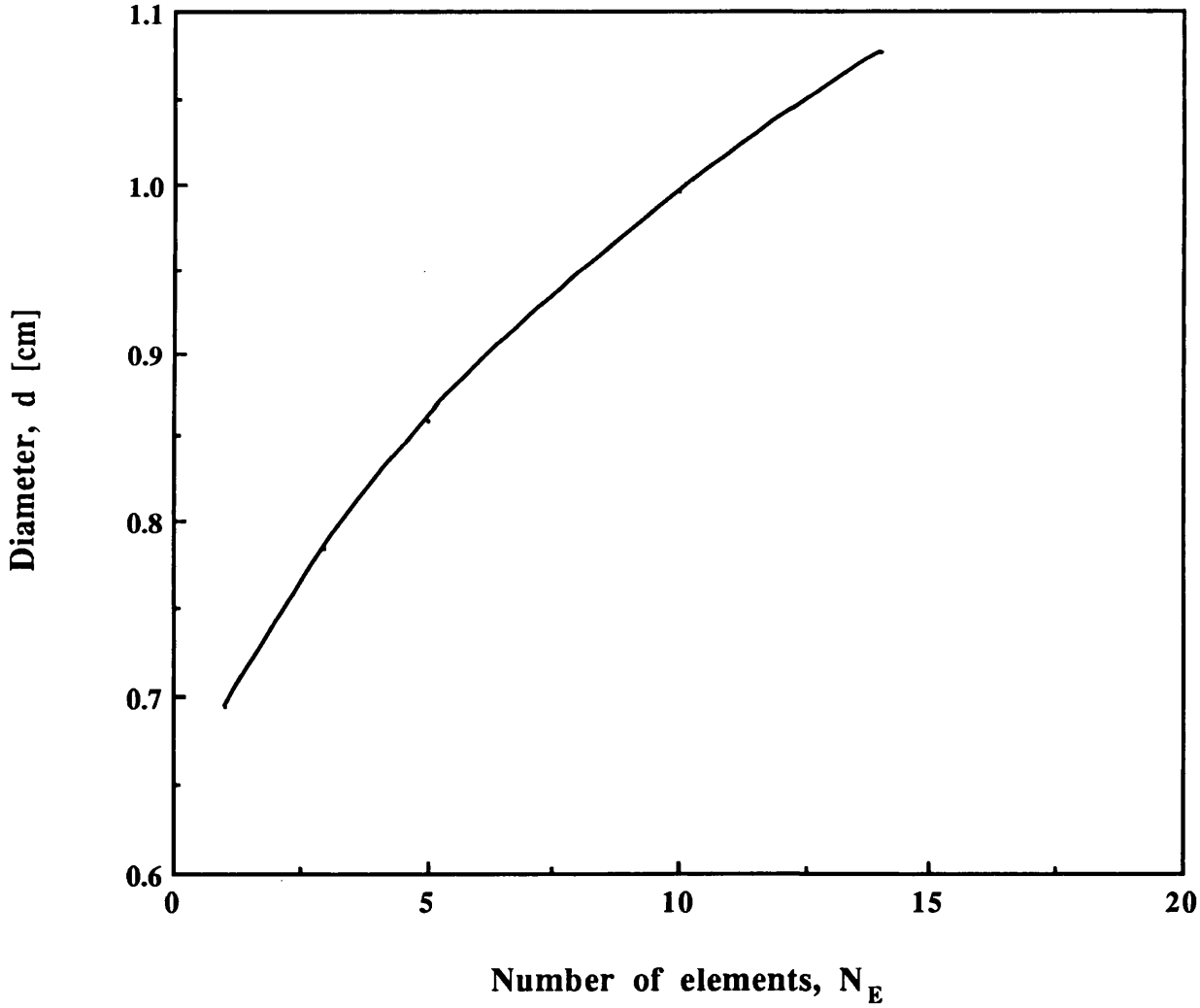

shown in figure 8.23. It can be seen that as the number of mixers is increased the product L×d decreases. Due to the constraint of mixer configuration however, the number of elements is limited to the main pressure drop requirement, and therefore N>14 elements is not in reality possible and therefore is not shown in the plot.

From figure 8.23 the minimum L×d which gives the same conversion and pressure drop as the monolith is 26 cm^2. This corresponds to an ATCR with 14 mixer elements. Thus from figures 6.21 and 6.22, for N_E=14, the ATRC total length equals 24 cm and the diameter equals 1.08 cm. Therefore the minimum surface area which gives the same performance as the monolith equals 8.12×10^{-3} m^2.

Obviously many other configurations are possible depending on the criteria to which one wants to operate.

Comparing the external surface area requirement of the ATCR to that of the monolith gives a 65.14 % saving in catalyst for the same catalyst loadings.

8.12 Cost Estimates

The prices of typical mixers used in industry may be substantial. However, these do not necessarily correspond to the cost of their manufacture. Indeed this was the major reasoning for developing the Star and Orifice mixer. This mixer was designed essentially for ease of production. Indeed in the case of the Star and Orifice its cost of manufacture is insignificant compared to the cost of the catalyst. If it is assumed therefore that a mixer can be designed to give the performances described in this chapter for a total cost which is similar to the cost of manufacture of the honeycomb ceramic support, then the total cost saving corresponds to a total saving in precious metal costs. Hence from the analysis above a total catalyst and therefore cost saving of up to 65 %, is possible for an ATCR compared to the monolith reactor.

8.13 Conclusions

A simplified one dimensional model was used in the calculations. Sherwood numbers were predicted from the experimental data and for the monolith reactor the Votruba correlation (1975) seemed to fit the data more successfully whereas the Hawthorn correlation (1973) was found as a first

Fig. 8.23 L×d versus number of elements for constant pressure drop of 361 N/m^2 and 94 % conversion

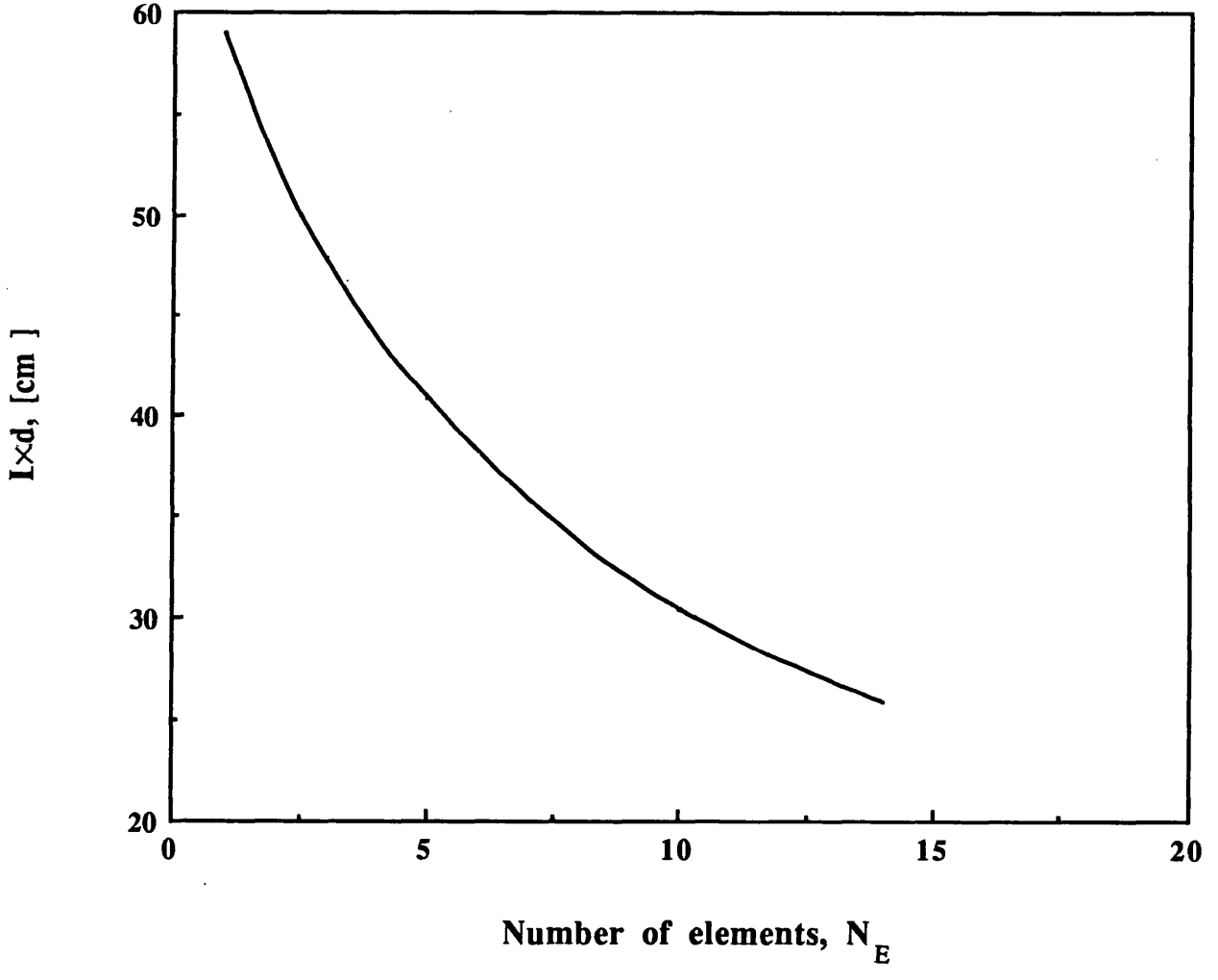

approximation to best represent the ATCR data. This is an interesting result, since it shows that both correlations may be applicable however for different tube size ranges ie. the Votruba correlation being applicable to small diameter channels of 1 mm and Hawthorn's correlation being more applicable to larger diameter tubes of 1.5 cm. Also, a single correlation was found to be successful in predicting conversions for a reactor such as the ATCR, which by any other method would prove to be very taxing especially if the flow distribution description is required.

In the case of the monolith, the one dimensional model was found to be adequate as a first approximation, however it was unable to predict the unusual trend of a local minimum/maximum in conversion found from experiment at an inlet flowrate of 10 L/min (refer to figure 6.4) at inlet temperatures of 250, 371 and 400°C.

Pressure drop within the segmented and integral monolith systems was found to be adequately described using the developing friction factor of Hawthorn (1973), with a maximum error of 14.5 %.

Pressure drop predictions for the Sulzer mixer were found using the friction factor described by Sulzer Ltd. for laminar flow in pipes (Sulzer, 1987). However, in the case of the Kenics mixer for an aspect ratio of 1.69, a best fit technique for the experimental data was used to find the friction factor. Pressure drop predictions were found to be good when compared to experimental data for both mixers for N_E ranging from 1 to 7 for $85<Re<1130$, giving a maximum error of 12.5 %.

A simplified optimization procedure was then followed in order to minimize the catalyst surface area of the ATCR compared to the monolith for similar performances. Thus in the monolith, for a space velocity of 100,000 hr^{-1} (NTP) and an inlet temperature of 371°C, the conversion was 94 % and the pressure drop 361 N/m^2 for a total catalyst surface area of 2.33×10^{-2} m . A two thirds reduction in overall surface area in the ATCR was found to be possible at similar operating conditions. This is achievable for an ATCR containing 14 Kenics mixers inserted into a 24 cm long pipe of diameter 1.08 cm. The result shows that there is indeed much scope for the use of re-development of flow to encourage mass transfer and therefore reduce this limiting factor and make better use of the effective catalyst surface area. Depending on the performance requirement, alternative ATCR configurations are possible which may be more economical and commercially viable.

The monolith model can be used as a means of assessing the implications for monolith design caused by a changing emission standard. Hence, in the

future, emission controls will become more stringent as discussed in the Literature Survey, and therefore the monolith model is a useful tool for predicting the relationship between conversion and catalyst surface area, and may be used for comparison purposes with the ATCR.

CHAPTER 9

CONCLUSIONS AND RECOMENDATIONS FOR FUTURE WORK

9.1 Conclusions

The catalytic oxidation of CO within a monolith system is effective in the sense that there is good conversion at low pressure drops, and it is therefore adequate for use in the automobile industry. However, the performance may be enhanced if the limiting factor ie. mass transfer is promoted. This was performed in the present study by first segmenting the monolith core axially in order to force the flow to re-develop at the entrance region of each monolith segment. The second method was performed using a tubular reactor with inserts (ATCR) where the flow was disrupted at each mixing element.

The following conclusions were found in this study:

1) Segmentation of the monolith showed marked improvements in the overall conversion for inlet CO and oxygen concentrations of 0.5 % and 0.25 % respectively at an inlet temperature of 371°C. As much as 28 % improvement in overall conversion was found for a space velocity of 100,000 hr^{-1} (NTP) between an integral and 16 segment monolith. Also pressure drop was not raised significantly due to the loss of axial length caused by the segmentation procedures.

2) During the experimental testing of the ATCR the effect of increase in the number of inserts produced a corresponding increase in the overall observed conversion at an inlet temperature of 371°C. This is obviously a result of improved mass transfer due to increased radial mixing. Mixer configuration showed little effect on the performance in terms of outlet conversion except for N_E=1 where the Sulzer element performed the best. However, configuration does effect the overall pressure drop, and it was found that for the mixers tested in this study the Kenics mixer gave the lowest pressure drop followed by the Sulzer followed by the Star and Orifice mixers.

3) The effect of inserting mixers into the tubular reactor is similar to segmenting the monolith in that in both systems the flow profile is

disrupted and then re-develops until it reaches a new mixer or monolith element.

4) At temperatures around 371-400°C light-off occurs at the entrance to the channel length for the conditions investigated in the present study, and therefore the assumption of constant average Nusselt and Sherwood numbers along the axial length of the monolith is reasonable.

5) It is possible to use a simple one dimensional model to describe the ATCR system. Good predictions in conversion were possible for a temperature of 371°C. The Hawthorn correlation was found to be the most effective and predicted the outlet conversions to within ±40 %.

6) A simplified one dimensional model was found to be adequate for describing the monolith system in which light-off occurs at the beginning of the monolith channel length. Hence for an inlet composition of 0.5 and 0.25 % (vol.) CO and oxygen respectively at temperatures of 371°C and above the reactor was mass transfer limited along the whole length of the monolith core for all the flowrates tested. In order to describe the monolith more accurately the two dimensional model should be adopted. In the case of the one dimensional model, the Votruba correlation was found to be the most effective in describing the experimental results of the monolith at temperatures of 371°C and above.

7) Experimental results for the monolith showed that there is an average of 38.8 % loss of heat compared to the expected adiabatic heat production, and this therefore corresponds to a significant loss of heat to the surroundings. However, in the model presented this corresponded to only 4 % difference in exit gas temperature for experiment and theory. Hence, it follows that for a more accurate model the effect of heat losses should be incorporated.

8) Hawthorn's correlation for friction factor for developing flow within square channels was found to be adequate for describing the pressure drops experienced in monolith systems including segmented cores for Reynold numbers ranging from 39 to 233 within the channel at 371°C.

9) Good agreement between experimental and theoretical pressure drops for the ATCR were found using the friction factor described by Sulzer Ltd. (1987) for the Sulzer mixer and a friction factor described by equation 8.19 for the Kenics for a Re range between 85 and 1130 (at 371°C).

10) The simplified optimization process showed that the ATCR using Kenics inserts can perform as effectively as the monolith with a 65 % saving in catalyst surface area. This corresponds to an ATCR external catalyst surface area of 8.12×10^{-3} m^2 compared to the monolith surface area of 2.33×10^{-3} m^2 for an overall conversion of 94 % and pressure drop of 361 N/m^2. It follows therefore that the ATCR system has much potential and may be important for processes which are mass transfer limited and where the catalyst cost is a significant component of the overall cost.

9.2 Recommendations for future work

The following areas of study are recommended:

1) Independent testing of mass and heat transfer correlations for varying sized channels and tube, in particular in the range of 0.1-5.0 cm diameter tubes, under both reacting and non-reacting conditions, in order to verify the validity ranges for the correlations of Votruba and Hawthorn.

2) Extension of the experimental range of parameter variables ie. inlet gas temperature, flowrate, concentrations, types of reactants (hydrocarbons, nitrogen oxides, and water) for both the monolith and ATCR testing. In particular cold start reactor testing should be performed since much of the pollution from auto-exhaust converters occurs in this region of operation.

3) Experimental testing of alternative mixer configurations to find the most efficient mixing device with the least pressure drop. The effect of coating the mixing elements with catalyst should also be investigated.

4) An unusual but completely repeatable trend was observed during the experimental testing of the monolith (ie. local minimum/maximum in plot of conversion vs inlet flowrate at an inlet flowrate of around 10 L/min) which could not be predicted by any combination of parameter values in the one dimensional model. Hence a more detailed two dimensional model may be required. This could incorporate terms to describe:

   a) axial conduction in the substrate,
   b) radiation exchanges between the gas, solid and the surroundings,
   c) heat losses to the surroundings,
   d) non-uniform temperature and flow distributions across the monolith diameter,

   Also the effects of multiplicity within the reactor should be investigated for negative order kinetics such as CO oxidation in the non-mass-transfer limited regime.

5) Optimization of segmented monolith systems to include the number and size of segments, as well as tensile strength, as well as crushing and brittleness study measurements for robust operation.

6) Improving the method of attachment of the catalyst to the metallic surface, as this was found to be a problem due to catalyst chipping and flaking during experimental testing.

REFERENCES

Ablow, C.M. and Wise H., "Theoretical Analysis of Catalytic Combustion in a Monolith Reactor", Combustion Science and Technology, vol.21, pp.35-42, 1979.

Ahn, T. W. S., "Catalytic Combustion of Gas Turbines: Process Modelling and Kinetic Study of Iso-Octane Oxidation", Ph.D. Thesis, University of New South Wales, 1983.

Bagley, R.D., Doman, R.C., Duke, D.A. and McNally, R. N., Paper no. 720274 presented at the January meeting of The Society of Automotive Engineers, 1973.

Bennett, C.J., "Monolith reactors for automobile catalysts", Ph.D. Thesis, University of Bath, 1990.

Bensalem, O., and Ernst W,R., "Mathematical Modeling of Homogeneous-Heterogeneous Reactions in Monolithic Catalysts", Com. Sci. and Tech., vol. 29, pp.1-13, 1982.

Beuch, H., Fieguth, P., and Wicke, E., Chem. -Ing.-Tech., vol.44, p.445, 1972.

Bird, R. B., Stewart, W. E., and Lightfoot, E. N., "Transport Phenomena", Wiley and Sons, Inc., 1960.

Bonzel, H. P., and Ku, R., "Carbon Monoxide Oxidation on a Pt(110) Single Crystal Surface", The J. of Vacuum Sci. and Technology, vol. 9, no. 2, pp. 663-667, 1972.

Bor T., " The Static Mixer as a Chemical Reactor", British Chemical Eng., vol.16, pp. 610-612, 1971.

Brokaw, R. S. and Bittker,D. A. NASA Technical Note D-7024, 1970.

Campbell, C. T., and White, J. M., "The Adsorption, Desorption, and Reactions of CO and O_2 on Rh", J. of Catalysis, vol. 54, pp.289-302, 1978.

Carberry, J.J., "Chemical and Catalytic Reaction Engineering", McGraw-Hill, Inc., 1976.

Carey, C.F. and Finlayson, B.A., Chem. Eng. Sci., vol. 30, p.587, 1975.

Carol, L. A., Newman, N. E., and Mann, G. S., "High Temperature Deactivation of Three-Way Catalyst", S.A.E., paper no. 892040, pp. 731-744, 1989.

Cerkanowicz, A.E., Cole, R.B., and Stevens, J.G., J. Eng. for Power, p.593, 1977.

Chen, S. J., "Static Mixing of Polymers", Chem. Engng. Progr., Vol. 71, pp. 80-83, 1975.

Cho, B. K., and Stock, C. J., " Dissociation and Oxidation of Carbon Monoxide over Rh / Al_2O_3 Catalysts", J. of Catalysis, vol. 117, pp. 202-217, 1989.

Church, M.L., Cooper, B. J., and Willson, P.J., "Catalysts in Automobiles: a History", Automotive Engineering (SAE), vol.97, no. 6, pp. 456-463, June 1989.

Cooper, B.J., Evans, W.D.J., and Harrison, B., "Aspests of Automotive Catalyst Preparation, Performance and Durability", Catalysis and Automotive Pollution Control, Elservier Science Pub., Amsterdam, 1987.

Cooper, B.J., and Keck, L., "NiO Incorporation in Three Way Catalyst Systems", SAE, paper no. 800461, 1980.

Crumpton, P. I., "Modelling of a Non-Adiabatic honeycomb reactor", Ph.D. Thesis, University of Bath, 1988.

Davy, H., "The Collected Works of Sir Humphrey Davy" (J. Davy, ed.), vol. 6, Smith, Elder and Co., Cornhill, London, 1840.

Day, J. P., and Socha, L. S., "Impact of Catalyst Support Design Parameters on Automotive Emissions", S.A.E. paper No. 881590, 1988.

DeCorso, S.M. and Carl, D.E., 3rd Workshop on Catalytic Combustion, Asheville, North Carolina, p.139, October 1978.

Dennis, S. C. R., Mercer, A. McD., and Poots, G., "Forced Heat Convection in Laminar Flow Through Rectangular Ducts", Q. appl. Math., Vol. 17, pp. 285-297, 1959.

Doory, L. K., Said, B. E., Ullah, S. P., and Waldram, S. P., "The Design and Development of an Active Transport Catalytic Reactor", I. Chem. E. Symposium Series, no. 121, pp. 425-433, 1990.

Doory, L. K., Said, B. E., Ullah, S. P., and Waldram, S. P., "Automobile Exhaust Gas Treatment in an Active Transport Catalytic Reactor", Trans. IChem. E., vol.69, Part A., May 1991.

Dudukovic, A.P. and Koncar-Djurdjevic, S.K., "The Effect of the Array of Disks on Mass Transfer Rates to the Tube Walls", AIChE Journal, vol. 25, no. 5, pp. 895-899, 1979.

Edelbock, W. and Lintz, H.G., "Oscillatory Instabilities in the CO-Oxidation on Polycrystalline Pt", Chem. Eng. Sci., vol.37, no.,9,p1435, 1982.

Elnashaie, S. S. E., and Cresswell, D. L., "Dynamic Behaviour and Stability of Non-Porous Catalyst Particles", Chem. Eng. Sci., vol. 28, pp. 1387-1399, 1973.

Engel, T. and Ertl, G.,"Elementary Steps in the Catalytic Oxidation of Carbon Monoxide on Platinum Metals", Advances in Catalysis, vol 28, p. 1-78 ,1980.

England, W.A., Gilmore A., Greenhalgh D. A., Thomas W.J., Ullah U., and Whittley, S.T., "Applications of Lasar Diagnostic Techniques to the Catalytic Oxidation of Carbon Monoxide in a Tubular Wall Reactor", Applied Catalysis, Elsevier Science Publishers, Amsterdam,1987.

Erdmann, E. R., " Statisch Arbeitender Rohrmischer", Chemie Anlagen Verfahren, pp. 93-98, 1977.

Froment, G. F., and Bischoff, K. B., "Chemical Reactor Analysis and Design", Wiley, New York, 1979.

DeCorso, S. M., Mumford, S., Carrubba, R. V., and Heck, R., "Catalysts for Gas Turbine Combustors- Experimental Test Results", J. Eng. for Power, 99A, p.159.

Gambill, W., Chem. Eng. Progr. Symp. Ser.,vol.57 (9), p.127, 1961.

Gaugin, R., Graulier, M. and Pappee, D., "Thermally Stable Carriers, Catalysts for Control of Automotive Pollutants", Adv. Chem. Ser. 143, Ed. J. E. McEvoy, American Chemical Society, Washington D.C., pp. 147-160, 1975.

Genetti, W. E., " Laminar Flow Heat Transfer with Inline Mixers Inserts", Chem. Eng. Commun., vol. 14, pp.47-57, 1982.

Gill, P. E., and Murray, W., "Minimization Subject to Bounds on the Variables", National Physical Laboratory report NAC 72, 1976.

Grace, C. D., Chem. Process Eng., vol. 52, p. 57, 1971.

Grigull, V. and Tratz, H., J.R., AIChE Journal, vol. 22(3), p.477, 1976.

Groenendaal, W., "The Market for Car Exhaust Catalysts in Western Europe- A Review of Trends and Development", Catalysis and Automotive Pollution Control, Elsevier Science Pub., Netherlands, p. 81-95,1987.

Gulati, S. T., Summers, J. C., Linden, D. G., and White, J. J., "Improvements in Converter Durability and Activity via Catalyst Formulation", S.A.E., paper 890796, pp.388-395, 1989.

Harned, J. L., Paper No. 720520, SAE National Automotive Engineering Meeting, Detroit, Mich., May 1972.

Harrison, B., Diwell, A.F., and Hallet, C., " Promoting Platinum Meytals by Ceria ; Metal-Support Interactions in Autocatalysis ", Platinum Metals Rev., vol. 32, (2), pp.73-83, 1988.

Hawker, P.N., Jaffray, C., Wilkins, A. J. J., and Alker, J., "Metal Supported Auto- Catalysts in Europe", S.A.E., paper 880317, 1988.

Hawthorn, R. D., "Afterburner Catalysts- Effects of Heat and Mass Transfer Between Gas and Catalyst Surface", AIChE Symposium Series- Recent Advances in Air Pollution Control, vol.70 , no.137, p. 428-438, 1973.

Haynes, H. W. Jr., "Diffusion and Reaction in Porous Media-II", AIChE Modular Instructions Series E, Module E3.2, Kinetics, vol 3, Heterogeneous Catalysis, pp. 9-15, 1982.

Heck, R. H., Wei, J. and Katzer, J. R., "The Transient Response of a Monolithic Catalytic Support", I.S.C.R.E., pp. 34-45, May, 1974.

Heck, R., Wei, J. and Katzer, J., "Mathematical Modeling of Monolithic Catalysts", AIChE J., vol. 22, p. 477, 1976.

Hegedus, L.L.,"Effects of Channel Geometry on the Performance of Catalytic Monoliths", Prepr. Div., Petr. Chem. (ACS, 18, 487502), vol. 18, p.487-502,1973.

Hegedus, L.L., Oh, SE. H., and Baron, K., "Multiple Steady States in an Isothermal, Integral Reactor: The Catalytic Oxidation of CO over Pt-Alumina", AIChE J., vol. 23, No. %., p. 632-642, 1977.

Hlavacek, V., Nguen-Khue, Sinkule, J., Skrivanek J., and Votruba, J., "Experimental Study and Mathematical Modeling of Monolithic Converters", ISCRE 4, 4th International / 6th European Symposium, Heidelberg, 6.-8.4., pp. vi-240-249, 1976.

Houzelet, J. L., and Villermaux, J., "A New Method for the Study and Characterization of Mass-Transfer Resistance in Open Reactors with Catalytic Walls", ISCRE 4, 4th International / 6th European Symposium Heidelburg, 6.-8.4., pp.iv 143-151, 1976.

Houzelet, J. L., and Villermaux, J., "Mass Transfer in Annular Cylindrical Reactors in Laminar Flow", Chem. Eng. Sci., vol. 32, pp. 1465-1470,1977.

Howitt J. S., "Advances in Automotive Catalysis Supports", Catalysis and Automotive Pollution Control, Elsevier Science Publishers, 1987.

Howitt, J. S. and Sekella, T. C., "Flow Effects in Monolithic Honeycomb Automotive Catalytic Converters", SAE, Paper No. 740244, Automotive Engineering Congress, Detroit, MI, 1974.

→ Hegedus, L. L., "Temperature Excursions in Catalytic Monoliths", A.I.Ch.E.J., 21, 849, 1975.

Hugo, P., and Jakubith, M., Chem. -Ing. -Tech., vol. 44, pp. 383-387, 1972.

Jagadeesh, V. and Satyanarayana, M., "Studies on Tubular Flow Reactor with Motionless Mixing Elements", Ind. Eng. Chem. Process Des. Develop., vol.11, no. 4, pp.520-525, 1972.

Johnson, W.C. and Chang, J. C., Paper 740196, presented at the February meeting of the Society of Automotive Engineerings ,1974.

Kabatek, J., Ditl, P., and Novak, V., "Helax- a New Type of Static Mixer-Operation Characteristics and Comparison with Other Types ", Chem. Eng. Progress, vol. 25, pp. 59-64, 1989.

Kays, W. M., and London, A. L., "Compact Heat Exchangers", 2nd Ed., McGraw-Hill, New York, 1964.

Kelly, J. T., Kendall, R. M., Chu, E., and Kesselring, J. P., Paper 77 - 33, Presented at the Fall Meeting, Western States Section / The Combustion Institute, Stanforrd, California, 1977.

Kemblowski, Z., and Pustelnik, P., "Mieszadla Statyczne", Inzynieria i Aparatura Chemiczna , vol. 1, pp. 16-21, 1974.

Kemblowski, Z., and Pustelnik, P., "Residence Time Distribution of a Power-Law Fluid in Kenics Static Mixers", Chem. Eng. Sci., vol.43, no. 3, pp.473-478, 1988.

Kenics Static Mixers Prospectus, KTEK Series, Chemineer, May 1988.

Kesselring, J.P., Krill, W.V., Angwin, M.J. and Atkins H.L., "Development of Improved Catalyst Systems", 4th Workshop on Catalytic Combustion, Cincinnati, Ohio, p.236-265, 1980.

Kim, G., "Ceria Promoted Three Way Catalysts for Auto Exhaust Emission Control", Ing. Eng. Chem. Prod. Res. Dev., vol. 21, pp. 267-274, 1982.

Koch, Ch, "A Honeycomb Structure - A New Chemical Engineering Element", Ph D. Thesis ,Univ. of Nurnberg-Erlagen , 1973, (in German).

Koncar-Djurdjevic, S.K., "Adsorption under fixed hyrodynamic conditions", Bull. Soc. chim. Beograd, vol. 14, p. 233, 1949.

Koncar-Djurdjevic, S.K., and Dudukovic, A.P., "The Effect of Single Stationary Objects Placed in the Fluid Stream on Mass Transfer Rates to the Tube Walls", AIChE J., vol. 23, p. 125, 1977.

Krill, W.V., Kesselring, J.P., and Anderson, S. J., 4th Workshop on Catalytic Combustion, Cincinnati, Ohio, p.314, May 1980.

Kummer, J.T. "Catalysts For Automotive Emission Control", Progress Energy Combustion Science, vol. 6, p.177, 1980.

Kuo, J. C. W., Morgan, C. R. and Lassen, "Mathematical Modelling of the CO and HC Catalytic Converter ssystems", SAE , Paper no. 710289, pp. 1098-1119, 1971.

Lamb, T., Scott, R. P., Watts, P., Holland, B., Gentry, S. J., and Jones, A., J. Chem. Soc., Chem. Commun., pp. 882-883, 1977.

Langhaar, H. L., Transactions of ASME, J. of Applied Mechanics, vol. A64, p.55, 1942.

Langmuir, I., Trans. Faraday Soc., vol. 17, p. 672, 1922.

Leak, R.J., Brandenburg, J.T., and Behrens, M.D., Env.Sci. Tech.,vol. 2,p.10 (October 1968).

Lee, S.T. and Aris, R., Chem. Eng. Sci., vol. 32, p.827, 1977.

Lemme, C. D., and Givens, W. R., "Flow through Catalytic Converters- An Analytical and Experimental Treatment", SAE, Paper no. 740243, Automotive Engineering Congress, Detroit, MI, 1974.

Levenspiel, O., "Chemical Reaction Engineering", Wiley , 2nd ed., New York, 1976.

Lindstrom, T.H. and Tsotsis, T.T., "Reaction Rate Oscillations During CO Oxidation Over Pt/gamma-AlO; Experimental Observations and Mechanistic Causes", Surface Science, vol. 146, pp.487-502, 1984.

McCarthy, E., Zahradnik, J., Kuczynski, G. C., and Carberry, J. J., "Some Unique Aspects of CO Oxidation on Supported Pt", J. of Catalysis, vol. 39, pp. 29-35, 1975.

Michelson, M. L., and Villadson, J., International J. of Heat and Mass Transfer, Vol. 17, p.1391, 1974.

Miyoshi, N., "Poisoning Deactivations of Automotive Catalysts by Lead and Phosphorous", SAE Trans., paper no. 852219, p.169., 1985.

Moody, L. F., "Friction factors for pipe flow", Trans. Am. Soc. Mech. Engrs., vol. 66, p.671, 1944.

Morris W. D. and Benyon, J., "Turbulent Mass Transfer in the Kenics Static Mixer",Ind. Eng. Chem., Process Des. Dev., vol.15, no.2, pp.338-342, 1976.

Morris, W. D. and Misson, P., "An Experimental Investigation of Mass Transfer and Flow Resistance in the Kenics Static Mixer", Ind. Eng. Chem., Process Des. Develop., vol.13, no. 3, pp.270-275, 1974.

Muhle, J., Chem. Ing. Tech., vol. 44, p. 72, 1972.

Musco, S. P.,"Reclaiming of Precious Metals from Automotive Catalytic Converters", SAE, paper no. 820189, 1982.

Nauman E.B., "Enhancement of Heat Transfer and Thermal Homogenity with Motionless Mixers", AIChE J. , vol. 25, no. 2, pp.246-258, March 1979.

Nauman E.B.,"Reactions and Residence Time Distribution in Motionless Mixers", The Canadian Journal of Chemical Engineering, vol. 60, pp.136-140, February 1982.

Nigam, K. D. P., and Nauman, E. B., " Residence time Distributions of Power Law Fluids in Motionless Mixers ", Can. J. Chem. Eng., vol. 63, pp.519-521, 1985.

Nigam, K. D. P., and Vasudeva, K., "Residence Time Distribution In Static Mixer", Can. J. Chem. Eng., vol. 58, pp.534-544, 1980.

Nonnenmann, M; Kuchlerfabrik, S; Fr-Behr Gmbtt and KG,C , "Metal Supports for Exhaust Gas Catalysts", SAE Transactions, vol. 94, no.1, paper no. 850131, 1985.

Nonnenmann, M., "New High-Performance Gas Flow Equalizing Metal Supports for Exhaust Gas Catalysts", ATZ Automobiltechnische Zeitschrift 91, 1989, (in German).

Oh, S. H., Fisher, G. B., Carpenter, J. E., and Goodman, D. W., "Comparative Kinetic Studies od $CO-O_2$ and CO-NO Reactions over Single Crystal and Supported Rhodium Catalysts", J. of Catalysis, vol. 100, pp. 360-376, 1986.

Otto, N. C. and LeGray, W. J., "Mathematical Models for Catalytic Converter Performance", Society of Automotive Engineers , Paper no. 800841, 1980.

Pacia, N., Cassuto, A., Pentenero, A., and Weber, B., "Molecular Beam Study of the Mechanism of Carbon Monoxide Oxidation on Platinum and Isolation of Elementary Steps", J. of Catalysis, vol. 41, pp. 455-465, 1976.

Pahl, M.H. and Muschelknautz, E.,"Static Mixers and their Applications", Int. Chem. Eng., vol. 22, no.2, pp.197-205, 1982.

Pereira, C. J., Kim, G., Hegedus, L. L., and Grace, W. R., and Co., "A Novel Catalyst Geometry for Automobile Emission Control", Chemical Industries / 21, Catalysis and Surface Science ed., by Heinemann, H., and Somerjai, G. A., pp. 201-221, 1984.

Pfefferle, L. D. and Pfefferle, W.C., "Catalysis in Combustion", Cata. Rev. Sci. Eng., vol. 29 (2 and 3), pp. 219-267, 1987.

Phang, B. H., " Adiabatic Catalytic Combustion in a Monolith Reactor", Ph.D. Thesis, University of Melbourne, Australia, 1984.

Platinum, Johnson Matthey Prospectus, 1990.

Platinum, Johnson Matthey Prospectus, 1991.

Pratt, A.S., and Cains, J. A., Platinum Metals Review, vol. 21, p. 3, 1977.

Press, W. H., Flannery, B. P., Teukodsky, S. A., and Vetterting, W. T., "Numerical Recipes, the Art of Scientific Computing, Fortran Version", Cambridge University Press, 1989.

Prikop, J., "Motionless mixers", M.Sc. Thesis, Czech Tech. Univ., Prague, 1982, (in Czech).

Razon, L.F. and Schmitz, R.A., "Multiplicities and Instabilities in Chemically Reacting Systems- A Review", Chem. Eng. Science, vol. 42,no.5, pp.1005-1047, 1987.

Schlatter, J. C., Klimisch, R. L., and Taylor, K. C., Science, vol. 179, p.798, 1973.

Schlatter, J. C., and Taylor, K. C., "Platinum and Palladium Addition to Supported Rhodium Catalysts for Automotive Emission Control", J. Catalysis, vol. 49, p.42, 1977.

Seider, E.N., Tate, G.E., Ind. Eng. Chem., 28, p.1420, 1936.

Shah, R. K., and London, A. L., "Laminar Flow Forced Convection Heat Transfer and Flow Friction in Sraight and Curved Ducts- A Summary of Analytical Solutions", Technical Report no. 75, Department of Mechanical Engineering, Stanford University, Stanford, California, 1971.

Sheintuch, M, and Schmitz, R. A., "Oscillations in Catalytic Reactions ", Cata. Rev.-Sci. Eng., vol. 15 (1), pp.107-172, 1977.

Shishu, R. C., and Kowalczyk, L. S., "The Oxidation of Carbon Monoxide on Supported Platinum", A Study of Honeycomb Catalyst Reaction Kinetics", Platinum Metals Rev., vol. 18, pp. 58-64, 1974.

Sinkule, J, and Hlavacek, V. " Heat and Mass Transfer in Monolithic Honeycomb Catalysts-III Radiation Model" Chem. Eng. Sci., vol. 33, pp. 839-845, 1978.

Sir, J., "Pressure Drop and Homogenization Characteristics of Kenics Motionless Mixer", Ph.D. Thesis, Pardubice, 1980, (in Czech).

Sir, J., and Lecjaks, Z., " Pressure Drop and Homogenization Efficiency of a Motionless Mixer", Chem. Eng. Commun., vol. 16, pp. 325-334, 1982.

Sklyarov, A. V., Trt'yakov, I.I., Shab. B. R., Roginski, S. Z., Dokl. Phys. Chem., vol. 189, p.829, 1969.

Slin'ko, M. G. and Slin'ko, M. M.," Self-Oscillations of Heterogeneous Catalytic Reaction Rates", Cata. Rev.-Sci. Eng., vol. 17(1), pp.119-153, 1978.

Smith, J.M.,"Chemical Engineering Kinetics," 2nd ed, McGraw-Hill, New York, N. Y., 1970.

Smithberg, E., Landis, F., J. Heat Transfer, vol. 86, pp.39-45, 1964.

Socha, L.S., Day, Jr. J. P., and Barnett, E. H., "Impact of Catalyst Support Design Parameters on FTP Emissions", S.A.E. Trans., paper no. 892041, pp. 745-754, 1989.

Solov'eva, L.S., Russ. J. Phys. Chem., vol. 34, p.586, 1960.

Starkman, E. S., "Prospects for Attainment of the 1975-76 Vehicle Emission Standards", AIChE Symposium Series, vol. 70, no. 137, pp. 66-74, 1973.

Stevens, J. G., and Ziegler, E. N., " Effect of Momentum Transport on Conversion in Adiabatic Catalytic Tubular Reactors", Chem. Eng. Sci. , vol. 32, pp. 385-391, 1977.

Su, E.C., and Montreuil, C.N. and Rothschild, W.g., " Oxygen Storage Capacity of Monolithic Three Way Catalysts ", Applied Catalysis, vol. 17, p.75, 1985.

Su, E.C., and Shishu, R.C., (Private Communications with Voltz (1973)), 1972.

Sulzer— Mixing Process Equipment—Static mixing, dispersing, heat and mass transfer, reaction engineering, Sulzer Prospectus, Sulzer, CH-8401 Winterthur, 1987.

Summers, J. C. and Ansen, S. A., J. Catalysis, vol. 58, pp.131-143, 1979.

Summers, J. C. and Ausen, S. A., J. Catalysis, vol. 52., p. 445, 1978.

Summers, L. C., Williamson, W. B., and Henk, M. G.,"Uses of Palladium in automotive emission control catalysts", SAE Trans., vol. 97, paper no. 880281, 1988.

Sundaram, K. M. and Froment, G. F., "A Comparison of Simulation Models for Empty Tubular Reactors", Chem. Eng. Sci., vol. 34, pp. 117-124, 1979.

Tauscher, W., "Industrielle Anwendungen eines Statischer Mischers", Verfahrenstechnik, vol. 10, p.258, 1976.

Taylor, K. C., unpublished results (Volts (1973)), 1971.

Taylor, K. C., "The Catalytic Chemistry of Nitrogen oxides", Plenum: New York, p.173, 1975.

Taylor, K. C., "Catalysts in cars", Chemtech, pp. 551-555, 1990

Thomas, W. J., "The catalytic monolith", Chemistry and Industry, pp. 315-319, May 1987

Ullah, U., and Waldram, S.P., paper to be presented at IChemE Annual Research Meeting, January, 1992.

U.S. Patent 3, vol. 885, p. 977, Corning Glass Works, May 1975.

Voltz, S.E.,Morgan, C.R., Liederman,D., and Jacob, S.M., "Kinetic Study of Carbon Monoxide and Propylene Oxidation "on Platinum Catalysts", Ind. Eng. Chem. Prod. Res. Devel. , vol. 12, p. 294 (1973)

Votruba, J, Mikus ,O.,Hlavacek, V, Skrivanek, J, "A note on pressure drop in monolithic catalysts", Chem., Eng. , Science, vol. 29, pp. 2128-2130, 1974.

Votruba, J. ; Mikus, O., Nguen, K., Hlavacek, V. and Skrivanek, J., "Heat and Mass Transfer in Honeycomb Catalysts-II", Chem. Eng. Sci., vol. 30, pp. 201-206, 1975b.

Votruba, J., Nguen-Khue, H. V., Sinkule, J., Skrivanek, J., "Experimental Study and Mathematical Modeling of Monolithic Converters", ISCRE VI, p.240-249, 1976.

Votruba, J. ; Sinkule, J.; Hlavacek, V. and Skrivanek, J., "Heat and Mass Transfer in Monolithic Honeycomb Catalysts-I", Chem. Eng. Sci., vol. 30, pp. 117-123, 1975a.

Wagner, C., Chem. Tech. Berlin, 18, 28, (Refferred to by Pfefferle and Pfefferle), 1945.

Walas, S. M., "Reaction Kinetics for Chemical Engineers," McGraw-Hill, New York, N. Y., 1959.

Weaver, E.E., S.A.E., paper no. 690016, 1969.

Wei, J. , "Catalysis For Motor Vehicle Emissions", Advances in Catalysis, vol. 24, p.57, 1975.

Wei J., and Becker, E. R., "The Optimum Distribution of Catalytic Material on Support Layers in Automotive Catalysis", Adv. Chem. Ser., vol. 143, pp.116-132, 1975.

Wendland , D. W., "The Segmented Oxidizing Monolith Catalytic Converter-Theory and Performance", Transactions of the ASME, vol. 102, pp.194-198 May 1980.

Weyermuller, G. H., "Maintenance Slashed, Product Waste Reduced by Tubular Unit", Chem. Processing, p.69, 1969.

Wilkinson, W.L. and Cliff, M.J., "An investigation into the performance of a static in-line mixer", Proc. 2nd Europ. Conf. on Mixing, Cambridge, U.K., BHRA, Cranfield, U.K., pp. A2-15—A2-28, 1977.

Williamson, W. B., Gandhi, H. S., Heyde, M. E., and Zawacki, G. A., "Deactivation of 3-way catalysts by fuel contaminants- Lead, Phosphorous and Sulfur", SAE Trans., vol. 88, paper no. 790942, 1979.

Williamson, E. B., Summers, J. C., and Skowron, J. F., "Catalyst Technologies for Future Automotive Emission Systems", S.A.E., paper no. 880103, vol.97, pp. 3.41-3.51, 1988.

Winterbottom, W. L., Surf. Sci., vol. 36, p. 205, 1973.

Yao, H. C., Japer, S. and Shelef, M.,"Surface Interactions in the system Rh/Al_2O_3", J. Catalysis, vol. 50, p.407, 1977.

Yao, H. C., Stepien, H. K., and Gandhi, H. S., "Metal Support Interactions in Automotive Exhaust Catalysts: Rh-Washcoat Interactions", J. Catalysis, vol. 61, p. 547, 1980.

Young, L. C., Finlayson B.A., "Mathematical Modeling of the Monolith Converter", ISCRE , pp. 629-643, May 1974.

Young, L.C., and Finlayson, B.A, "Mathematical Models of the Monolith Catalytic Converter: Part I . Development of Model and Application of Orthogonal Collocation", AIChE J. , vol. 22, no. 2, pp. 331-342, 1976a.

Young, L.C., and Finlayson, B.A, "Mathematical Models of the Monolith Catalytic Converter: Part II . Application to Automobile Exhaust", AIChE J. , vol. 22, no. 2, pp. 343-353, 1976b.

Young, L.C., and Finlayson, B.A, "Mathematical Models of the Monolith Catalytic Converter: Part III. Hysteresis in Carbon Monoxide Reactor", AIChE J., vol. 25, no. 1, pp. 192-196, 1979.

Zygourakis, K., "Transient Operation of Monolithic Catalytic Converters: A Two-Dimensional Reactor Model and the Effecyts of Radially Nonuniform Flow Distributions", Chem. Eng. Sci., vol. 44, no.9, pp. 2075-2086,1989.

APPENDIX A

Legislation concerning auto-emissions

Over the last ten years legislation has continued to become more stringent throughout the developed world, and is likely to spread to the developing world as concern mounts over the pollution levels. The gases CO and NO_x and the HC's are found to be toxic and can cause acid rain and smog. This was the deciding factor for stringent emission control legislation first introduced in California in the 1950's, followed by the rest of the US in the 70's.

Legislation differs in varying parts of the world. However, the US took the lead with the most stringent emission standards, with Japan, Australia and the EC following suit but to lesser degrees. Table A.1 indicates the the US standards since the introduction of legislation. The standards are presented in grams/mile, this being more universal than grams/test since test cycles vary throughout the world.

Table A.1 US Auto Emission standard g/mile (Starkman,1973; Platinum, 1991; Taylor, 1990)

Year	CO	NOx	HC
Prior to control (1960)	90	5	15
1970	34	5	4.1
1975	15	3.1	1.5
1982	3.4	1.0	0.41
1990	3.4	1.0	0.41
1993-5	3.4	0.4	0.25
2004	1.7	0.2	0.125

The figures for the 1990 controls represent a 96% removal of CO and HC and an 80% removal of NO_x. Not only are the standards becoming stricter but also the manufacturers will become liable for warranty claims for lengthened durability requirements. This will compel automakers to use more pgm per catalyst probably to impact in mid-1993.

APPENDIX B

Table B.1 : Monolith Properties

Substrate	Cordierite
Catalyst	Pt/Rh (5 / 1 wt%)
Cell Shape	Square
Hydraulic diameter	1.04 mm
Wall thickness	0.25 mm
Cell density	62 cells/cm^2
Open fractional area	0.67
Surface to volume ratio	3846.15 m^{-1}
Wetted perimeter	0.62 m

Table B.2 : Nitrogen gas properties and reactant inlet concentrations at various temperatures

Property	T=273 K	T=523 K	T=644 K	T= 673 K
Density, ρ (kg/m^3)	1.25	0.65	0.53	0.51
Viscosity, ($\times 10^{-5}$) μ (kg/m s)	1.655	2.559	3.13	3.26
Specific heat capacity, c_p (kJ/kmol K)	29.14	29.72	30.41	30.60
Thermal conductivity, k_g (W/m K)	0.0241	0.0412	0.0482	0.0498
Diffusion Coefficient, ($\times 10^{-5}$) $D_{i\,(CO\ in\ N2)}$ (m^2/ s)	1.734	5.372	7.627	8.22
Prandtl number, $Pr = \frac{c_p \mu}{k_g}$	0.716	0.659	0.705	0.716
Schmidt number, $Sc = \frac{\mu}{\rho D_i}$	0.764	0.730	0.780	0.782
Heat of reaction, ΔH_r (kJ/kmol)	-283.00	-283.75	-283.73	-283.69
Concentration of CO at inlet, C_{COin} ($kmol/m^3$)	2.232×10^{-4}	1.165×10^{-4}	9.462×10^{-5}	9.054×10^{-5}
Total concentration of inlet gases, C_T ($kmol/m^3$)	0.0446	0.0233	0.0189	0.0181

APPENDIX C

RATE DATA

Table C.1 Rate data as a function of flow rate for sample 1:
L=1 mm, $S_A=2.91\times10^{-4}$ m^2, T_{Gin}=371°C, $[CO]_{in}$=0.5 %,
$[O_2]_{in}$=0.25%

F_t (L/min) S.T.P.	$[CO]_{in}$	$[CO]_{out}$	$[CO]_{av}$	X	$-r_{CO}$ (10^{-5})	$(T_s)_{Side}$	$(T_s)_{Centre}$
	(mol. fract. %)			(%)	kmol/m^2 s	(°C)	(°C)
5.0	0.50	0.320	0.410	36.0	2.301	387.92	394.1
7.5	0.50	0.355	0.428	29.0	2.781	386.57	393.06
10.0	0.51	0.410	0.460	20.0	2.557	382.8	391.2
15.0	0.52	0.440	0.480	15.15	2.906	382.7	387.9
17.5	0.52	0.455	0.488	13.4	3.007	380.0	386.5
19.5	0.50	0.440	0.470	12.0	2.991	378.7	385.0
23.0	0.48	0.430	0.445	10.4	3.058	377.0	382.11
25.0	0.51	0.462	0.486	9.38	2.997	376.47	382.06
28.0	0.48	0.440	0.460	8.4	3.007	375.6	381.0
30.0	0.51	0.470	0.490	7.87	3.018	375.01	380.09
35.0	0.49	0.450	0.470	7.84	3.512	374.75	380.0
40.0	0.47	0.435	0.452	7.45	3.809	374.43	379.06

Table C.2 Rate data as a function of flow rate for sample 1:
L=1 mm, S_A=2.91 (10^{-4} m^2), T_{Gin}=250°C, $[CO]_{in}$=0.5 %,
$[O_2]_{in}$=0.25%

F_t (L/min) S.T.P.	$[CO]_{in}$	$[CO]_{out}$	$[CO]_{av}$	X	$-r_{CO}$ (10^{-6})	$(T_s)_{Side}$	$(T_s)_{Centre}$
	(mol. fract. %)			(%)	kmol/m^{2}s	(°C)	(°C)
3.0	0.49	0.46	0.475	6.1	2.340	253.20	252.37
5.0	0.49	0.47	0.480	4.1	2.621	250.14	250.65
7.5	0.50	0.49	0.495	2.1	2.014	253.10	252.78
10.0	0.50	0.495	0.498	1.0	1.278	252.10	251.56

Table C.3 Sample I: Rate data, F_t=30 L/min (STP), S_A=2.912×10^{-4} m^2

T_{Gin} (°C)	$(T_s)_{av}$ (°C)	$[CO]_{in}$ (%)	$[O_2]_{in}$ (%)	Conversion (%)	$-r_{CO}$ (10^{-5}) (kmol/m^{2}s)
325.0	327.5	1.00	0.25	1.85	1.418
	328.0	0.70		2.86	1.535
	328.0	0.60		3.98	1.830
	329.2	0.50		5.77	2.2117
	330.1	0.40		8.04	2.465
	330.2	0.30		11.40	2.62
	333.9	0.50	1.63	14.70	5.6345
	333.9		1.30	14.00	5.3662
	333.9		1.00	13.70	5.2512
	334.0		0.67	11.76	4.5076
	332.9		0.33	8.80	3.3730
	328.4		0.17	3.92	1.5025
	327.0		0.083	1.96	0.7513
	325.8		0.042	0.98	0.3756
350.0	357.9	2.00	0.50	3.20	4.9056
	358.5	1.8		4.20	5.7947
	359.2	1.6		4.83	5.9235
	360.3	1.40		6.10	6.5459
	358.7	0.50		13.00	4.9823
	362.6	1.0		7.70	5.9021
	362.4	0.8		10.07	6.1749
	355.4	0.30		13.30	3.0583
	359.3	0.50	1.63	16.3	6.2478
	359.3		1.30	14.9	5.7112
	359.5		1.00	14.3	5.4812
	359.5		0.67	12.2	4.6763
	358.5		0.33	10.2	3.9097
	354.1		0.17	5.1	1.9548
	352.1		0.083	2.0	0.7666
	351.5		0.0417	1.0	0.3833
371.0	376.9	0.70	0.25	6.2	3.3266
	377.0	0.625		7.0	3.3534
	377.4	0.50		10.64	4.0778
	376.4	0.40		12.20	3.7405
	374.9	0.30		14.30	3.2883
	378.3	0.50	1.63	17.8	6.8227
	378.5		1.30	18.5	7.0911
	379.1		1.00	15.2	5.8262
	379.1		0.67	15.2	5.8262
	378.4		0.33	13.04	4.9982
	375.0		0.167	6.4	2.4531
	372.9		0.083	2.13	0.8164
	371.7		0.0417	1.06	0.4063

Table C.4: Sample 2, F_t=30 L/min (STP), S_A=2.3296×10^{-4}

T_{Gin} (°C)	$(T_s)_{av}$ (°C)	$[CO]_{in}$ (%)	$[O_2]_{in}$ (%)	Conversion (%)	$-r_{CO}$ (10^{-5}) (kmol/m^{2}s)
325.0	326.9	1.50	0.25	1.50	2.1559
	328.4	1.30		0.90	1.1211
	328.3	1.00		1.67	1.6001
	328.5	0.80		2.03	1.5561
	329.7	0.60		3.50	2.0121
	329.6	0.50		4.10	1.9642
	330.9	0.40		7.50	2.8745
	330.5	0.30		8.34	2.3973
	329.0	0.20		11.90	2.2804
	327.1	0.10		13.64	1.3069
	331.3	0.50	0.33	7.14	3.4206
	330.6		0.30	6.12	2.9320
	329.7		0.25	5.10	2.4433
	327.5		0.20	4.08	1.9546
	327.0		0.15	2.04	0.9773
	326.5		0.1	1.53	0.7330
350.0	353.0	1.50	0.25	1.91	2.7451
	353.8	1.30		1.80	2.2421
	353.8	1.00		2.22	2.1271
	354.5	0.80		3.79	2.9052
	355.4	0.70		3.38	2.2670
	355.3	0.60		4.39	2.5238
	356.0	0.50		8.75	4.1920
	356.0	0.40		10.00	3.8326
	355.5	0.30		9.68	2.7825
	354.2	0.20		9.52	1.8243
	352.3	0.10		13.64	1.3069
	358.2	0.50	0.33	9.18	4.3980
	358.0		0.30	8.16	3.9093
	354.8		0.20	5.10	2.4433
	353.5		0.15	4.08	1.9546
	352.2		0.10	2.55	1.2217
	351.4		0.05	2.04	0.9773
371.0	375.2	1.50	0.25	2.29	3.2913
	376.0	1.30		1.80	2.2421
	376.6	1.00		2.81	2.6924
	376.6	0.80		4.11	3.1504
	377.1	0.60		6.25	3.5931
	377.8	0.50		8.33	3.9908
	377.8	0.40		10.26	3.9323
	376.7	0.30		10.00	2.8745
	374.9	0.20		14.29	2.7384
	373.4	0.10		18.2	1.7439

Table C.4: (Sample 2) contd.

T_{Gin} (°C)	$(T_s)_{av}$ (°C)	$[CO]_{in}$ (%)	$[O_2]_{in}$ (%)	Conversion (%)	$-r_{CO}$ (10^{-5}) (kmol/m^{2}s)
371.0	379.9	0.5	0.33	10.42	4.9920
	379.1		0.30	9.38	4.4938
	376.1		0.20	6.25	2.9943
	374.7		0.15	4.17	1.9978
	373.4		0.10	2.60	1.2456
	372.6		0.05	1.56	0.7474
400.0	405.6	1.50	0.25	3.44	4.9441
	406.1	1.30		2.70	3.3632
	406.2	1.00		3.93	3.7656
	406.7	0.80		5.10	3.9093
	406.9	0.60		7.02	4.0358
	407.4	0.50		8.30	3.9764
	406.9	0.40		10.26	3.9323
	405.7	0.30		12.10	3.4750
	404.3	0.20		11.90	2.2804
	402.3	0.10		13.60	1.3031
400.0	409.0	0.5	0.33	11.46	5.4903
	408.7		0.30	10.42	4.9920
	405.6		0.20	7.29	3.4925
	404.3		0.15	5.21	2.4960
	403.0		0.10	4.17	1.9978
	401.7		0.05	2.08	0.9964
425.0	431.2	1.50	0.25	3.82	5.4903
	431.3	1.30		3.15	3.9237
	431.9	1.00		3.37	3.2290
	432.0	0.80		5.41	4.1469
	432.6	0.60		7.14	4.1047
	432.6	0.50		9.29	4.4500
	432.0	0.40		10.35	3.9640
	431.5	0.30		11.67	3.3545
	429.6	0.20		12.50	2.3954
	427.5	0.10		10.00	0.9582
	434.0	0.50	0.33	12.5	5.9885
	433.7		0.30	10.42	4.9920
	430.6		0.20	8.33	3.9907
	429.2		0.15	5.21	2.4960
	427.8		0.10	4.17	1.9978
	426.6		0.05	2.08	0.9965

Table C.5 : Sample 3, F_t=30 L/min (STP), S_A=2.3296×10^{-4}m^2

T_{Gin} (°C)	$(T_s)_{av}$ (°C)	$[CO]_{in}$ (%)	$[O_2]_{in}$ (%)	Conversion (%)	$-r_{CO}$ (10^{-5}) (kmol/m^{2}s)
275.0	275.4	1.00	0.25	0.52	0.5210
	275.9	0.80		0.61	0.4701
	275.3	0.50		2.00	0.7303
	276.3	0.30		2.87	0.8250
	276.2	0.50	0.30	0.78	0.3727
	276.1		0.25	0.90	0.4329
	275.6		0.20	0.58	0.2761
	275.5		0.10	0.36	0.1743
300.0	301.4	1.00	0.25	1.10	1.0540
	301.9	0.80		1.37	1.0502
	303.3	0.50		3.13	1.4995
	304.5	0.40		5.13	1.9662
	304.6	0.30		7.10	2.0410
	304.1	0.20		9.40	1.8014
	302.7	0.10		13.64	1.3069
	306.4	0.50	0.33	6.25	2.9943
	305.2		0.30	5.21	2.4960
	302.7		0.20	3.125	1.4971
	301.0		0.10	1.05	0.5030
350.0	355.1	1.00	0.25	2.78	2.6637
	355.3	0.80		4.00	3.0661
	356.5	0.60		5.70	3.2769
	357.1	0.55		6.70	3.5308
	357.1	0.50		8.20	3.9285
	356.4	0.40		10.00	3.8327
	356.0	0.30		13.00	3.7368
	355.5	0.20		14.60	2.7978
	352.6	0.10		20.00	1.9163
	357.7	0.50	0.33	10.20	4.8866
	357.5		0.30	10.20	4.8866
	356.2		0.25	7.14	3.4206
	354.3		0.20	6.12	2.9320
	353.0		0.15	4.08	1.9546
	352.2		0.10	2.04	0.9773
	351.2		0.05	1.02	0.4887

Table C.5: Sample 3 (Cont.)

T_{Gin} (°C)	$(T_s)_{av}$ (°C)	$[CO]_{in}$ (%)	$[O_2]_{in}$ (%)	Conversion (%)	$-r_{CO}$ (10^{-5}) (kmol/m^{2}s)
371.0	375.1	1.5	0.25	2.36	3.3919
	375.7	1.3		2.73	3.4005
	375.7	0.8		4.2	3.2194
	377.0	0.4		10.26	3.9323
	376.0	0.3		12.485	3.5888
	374.5	0.2		14.29	2.7384
	372.9	0.1		9.5	0.9103
	371.9	0.05		20.0	0.9582
	379.5	0.5	0.33	11.45	5.4855
	378.4		0.25	8.33	3.9908
	375.3		0.20	6.25	2.9943
	372.7		0.10	2.11	1.0109
400	405.82	1.0	0.25	3.37	3.2290
	406.81	0.8		5.48	4.2006
	406.76	0.7		6.59	4.4200
	406.71	0.6		7.35	4.2270
	407.23	0.5		9.54	4.5653
	406.79	0.4		11.28	4.3214
	404.98	0.3		13.30	3.8231
	404.29	0.2		15.00	2.8745
	402.29	0.1		15.00	1.4372
	408.13	0.5	0.33	12.50	5.9885
	407.98		0.30	11.98	5.7394
	407.17		0.25	10.42	4.9920
	405.39		0.20	7.29	3.4925
	404.06		0.15	5.21	2.4960
	402.20		0.10	3.13	1.4995
	401.53		0.05	2.08	0.9965
425	431.9	1.0	0.25	4.40	4.2159
	431.9	0.8		5.75	4.4037
	431.9	0.7		6.83	4.5860
	432.5	0.6		8.18	4.7010
	432.6	0.5		9.95	4.7650
	432.0	0.4		11.54	4.4229
	430.3	0.3		15.0	4.3117
	429.0	0.2		17.5	3.3536
	427.0	0.1		20.0	1.9163
	433.9	0.5	0.33	14.5	6.9467
	433.0		0.30	12.5	5.9885
	432.2		0.25	10.42	4.9920
	430.3		0.20	8.33	3.9908
	428.4		0.15	6.25	2.9942
	427.1		0.10	4.20	2.0121
	425.8		0.05	2.08	0.9965

Table C.6: Sample 4 , L=1.5cm, $S_A=2.7456\times10^{-4}m^2$

$F_{t\ in}$ (L/min) S.T.P	T_{Gin} (°C)	$(T_s)_{av}$ (°C)	$[CO]_{in}$ (%)	$[O_2]_{in}$ (%)	Conversion (%)	$-r_{CO}$ (10^{-5}) ($kmol/m^2s$)
5.0	225.0	226.2	1.00	0.25	0.52	7.05e-7
		225.2	0.82		0.63	6.91e-7
		225.2	0.64		0.76	6.59e-7
		226.2	0.50		0.98	6.64e-7
		226.2	0.43		2.25	1.31e-6
		225.2	0.30		3.15	1.28e-6
		226.2	0.20		6.09	1.65e-6
		225.8	0.05		14.04	9.51e-7
		225.5	0.10		8.84	1.198e-6
5.0	225.0	247.1	0.50	2.00	29.87	2.022e-5
		226.2		1.00	3.77	2.557e-6
		225.2		0.50	1.89	1.282e-6
		225.5		0.25	0.981	6.644e-7
		225.2		0.20	0.909	6.405e-7
		225.1		0.1	0.31	2.10e-7
5.0	250.0	251.2	2.00	0.25	0.767	2.071e-6
		251.1	1.50		0.870	1.765e-6
		251.2	1.00		1.06	1.4338e-6
		251.1	0.80		1.273	1.38e-6
		251.7	0.60		1.69	1.375e-6
		252.0	0.50		2.94	1.994e-6
		252.3	0.40		4.836	2.622e-6
		254.2	0.30		6.15	2.499e-6
		259.0	0.20		13.28	3.599e-6
		258.0	0.16		13.84	3.000e-6
		252.8	0.35		6.84	3.245e-6
		252.2	0.45		4.425	2.698e-6
		251.2	0.70		1.539	1.4599e-6
		251.2	0.55		1.811	1.35e-6
		250.6	1.5		0.697	1.416e-6
		251.2	2.0		0.512	1.3883e-6
5.0	250.0	276.1	0.50	1.00	33.99	2.303e-5
		275.0		0.80	32.00	2.168e-5
		272.0		0.70	32.00	2.168e-5
		270.9		0.60	30.00	2.032e-5
		254.2		0.50	13.48	9.134e-6
		253.2		0.40	6.00	4.065e-6
		251.2		0.30	2.95	2.00e-6
		251.2		0.25	2.94	1.994e-6
		251.2		0.20	1.99	1.353e-6
		250.7		0.15	1.95	1.3228e-6
		250.2		0.05	1.00	6.7746e-7
		254.2		0.50	13.48	9.134e-6

Table C.6: Sample 4 (contd.)

$F_{t\ in}$ (L/min) S.T.P	T_{Gin} (°C)	$(T_s)_{av}$ (°C)	$[CO]_{in}$ (%)	$[O_2]_{in}$ (%)	Conversion (%)	$-r_{CO}$ (10^{-5}) (kmol/m^{2}s)
10.0	275.0	277.6	1.00	0.25	1.096	2.972e-6
		277.2	0.80		1.996	4.340e-6
		277.1	0.60		3.03	4.931e-6
		277.3	0.50		3.99	5.4221e-6
		278.9	0.40		7.196	7.832e-6
		281.1	0.20		16.42	8.944e-6
		278.09	0.10		29.52	8.004e-6
		276.7	0.15		20.90	8.510e-6
		277.6	0.47		5.31	6.762e-6
		277.11	0.55		2.784	4.150e-6
		276.07	1.50		1.089	4.432e-6
		275.04	2.00		0.529	2.87e-6
		275.04	2.30		0.213	1.331e-6
		282.18	0.35		6.537	6.212e-6
		277.4	0.95		1.577	4.06e-6
10.0	275.0	290.2	0.50	1.00	22.00	2.980e-5
		290.2		0.90	22.00	2.980 e-5
		289.9		0.80	20.99	2.845e-5
		288.2		0.60	19.98	2.7099e-5
		283.0		0.40	9.36	1.268e-5
		276.1		0.20	2.58	3.531e-6
		275.1		0.10	1.845	2.521e-6
		277.1		0.25	5.00	6.775e-6
		287.7		0.50	18.97	2.570e-5
10.0	300.0	307.18	0.6	0.25	8.31	1.352e-5
		309.15	0.5		12.18	1.654e-5
		308.21	0.4		15.87	1.723e-5
		309.15	0.3		21.43	1.742e-5
		306.80	0.2		27.86	1.511e-5
		304.9	0.1		33.21	9.053e-6
		310.12	0.45		12.956	1.580e-5
		307.5	0.8		3.921	8.512e-6
		315.7	1.0		3.875	1.050e-5
10.0		316.9	0.50	1.00	24.56	3.326e-5
		316.6		0.80	24.52	3.3228e-5
		315.1		0.50	23.54	3.190e-5
		312.21		0.30	16.68	2.260e-5
		307.4		0.25	12.75	1.727e-5
		305.16		0.20	8.83	1.196e-5
		302.1		0.10	4.90	6.646e-6
		301.02		0.05	2.94	3.988e-6

APPENDIX D

i) Effect of temperature on nitrogen properties

Experimentally a maximum temperature rise of up to 35°C in the gas phase was experienced for the monolith reactor at 371°C and at a flowrate of 30 L/min (STP). The effect of this temperature rise on the properties of nitrogen are presented in table D.1 :

Table D.1 Effect of temperature rise along reactor on properties of nitrogen

Property	T=371 °C (a)	T= 406 °C (b)	Ratio (a)/(b)
ρ (kg/m^3)	0.53	0.503	1.054
μ (kg/m s)	3.13×10^{-5}	3.30×10^{-5}	0.948
c_p (kJ/kmolk)	30.41	30.59	1.007
k_g (W/m K)	0.0482	0.0509	1.039
D_i (m^2/s)	7.627×10^{-5}	8.352×10^{-5}	0.913

From table D.1 it can be seen that the deviation of the gas properties as a result of temperature increase is less than 9%. Thus the assumption that the properties remain constant at the inlet temperature of the gas over the total length of the reactor, is reasonable and does not lead to any significant errors.

ii) The properties of the mixture compared to that of nitrogen

The composition of the gas mixtures are designated as below:

Mixture A: [CO]=0.5 %, [O_2]=0.25 %, [N_2]=99.25 %
Mixture B: [CO]=1.0 %, [O_2]=2.0 %, [N_2]=97.0 %

These compositions are respresentative of the range of inlet mixture compositions used in the kinetic, monolith and ATCR experiments of chapters 5, 6 and 7.

The properties of mixtures were predicted using the techniques in Bird et al. (1960, p.25). The ratios are given in table D.2 for the mixture compositions A and B compared to those of nitrogen at 371°C:

Table D.2 Properties of the mixture compared to that of nitrogen at 371°C

Property	Property Mixture A / Property of N_2	Property Mixture B / Property of N_2
ρ	1.000	1.003
μ	1.000	1.002
c_p	0.999	0.999
k_g	1.003	1.008

Table D.2 shows that the properties of the mixture compared that of nitrogen deviate by up to 1%, and therefore for the conditions investigated in this study the properties of nitrogen may be taken to be representative of the inlet reactant gas mixture.

APPENDIX E

Table E.1 Experimental data for Set I, at T_{Gin} =371 ± 1°C

N	F_t S.T.P (L/min)	Re (entry conditions)	Conversion X (%)	Temp. rise in gas ΔT (°C)	Pressure drop , ΔP (N/m^2)
1	5.0	38.89	83.0	6.6	247.975
	7.5	58.34			
	10.0	77.79	51.0	13.2	538.613
	12.5	97.23			
	15.0	116.68	68.0	18.5	871.913
	17.5	136.13			
	20.0	155.58	72.0	21.7	1194.547
2	5.0	38.89	93.0	4.0	229.310
	7.5	58.34	57.0	9.5	399.960
	10.0	77.79	53.0	13.1	519.948
	12.5	97.23	47.0	15.4	719.928
	15.0	116.68	64.0	18.2	853.248
	17.5	136.13	73.0	20.8	1013.232
	20.0	155.58	77.0	21.8	1146.552
4	5.0	38.89	97.0	4.25	235.976
	7.5	58.34	71.0	9.84	355.964
	10.0	77.79	55.0	12.75	541.279
	12.5	97.23	52.0	14.85	699.930
	15.0	116.68	65.0	18.00	879.912
	17.5	136.13	70.0	22.30	1061.227
	20.0	155.58	77.0	20.00	1199.880
8	5.0	38.89	88.7	5.88	230.644
	7.5	58.34	72.0	12.26	351.298
	10.0	77.79	57.3	13.85	471.286
	12.5	97.23	54.7	15.14	589.274
	15.0	116.68	72.5	20.95	711.262
	17.5	136.13	94.0	24.87	818.585
	20.0	155.58	100.0	26.86	897.244
16	5.0	38.89	97.9	7.49	184.648
	7.5	58.34	76.0	12.50	307.969
	10.0	77.79	66.0	15.16	434.623
	12.5	97.23	61.5	19.47	598.740
	15.0	116.68	73.0	21.92	766.590
	17.5	136.13			
	20.0	155.58			

Table E.2 Experimental data for Set II, for T_{in} =371 ± 1°C

N	F_t S.T.P (L/min)	Re (entry conditions)	Conversion X (%)	Temp. rise in gas ΔT (°C)	Pressure drop, ΔP (N/m^2)
1	5.0	38.89	100.0		
	7.5	58.34	98.0	22.09	273.306
	10.0	77.79	94.0	23.95	361.297
	12.5	97.23	83.7	27.02	429.957
	15.0	116.68	89.4	28.75	512.615
	17.5	136.13	91.7	30.32	599.94
	19.5	151.68	91.7	30.9	661.267
	25.0	194.47	87.2	33.1	837.916
	30.0	233.36	82.97	35.04	993.901
4	5.0	38.89	97.96	15.54	212.645
	7.5	58.34	98.0	19.03	281.972
	10.0	77.79	98.0	22.70	370.630
	12.5	97.23	96.0	24.82	441.289
	15.0	116.68	98.0	27.11	526.614
	17.5	136.13	95.6	29.24	599.273
	19.5	151.68	93.9	30.60	671.537
	25.0	194.47	91.7	30.54	871.913
	30.0	233.36	86.0	34.31	1027.897
8	5.0	38.89	100.0	12.23	192.647
	7.5	58.34	98.0	19.45	262.640
	10.0	77.79	100.0	21.87	339.299
	12.5	97.23	98.0	25.2	416.625
	15.0	116.68	98.0	26.09	497.950
	17.5	136.13	96.0	27.5	579.942
	19.5	151.68	91.8	28.91	642.602
	25.0	194.47	89.8	32.06	849.248
	30.0	233.36	87.7	34.38	1022.564

Table E.3 Experimental data for Set II, at T_{Gin} =250 ± 1°C

N	F_t S.T.P (L/min)	Re (entry conditions)	Conversion X (%)	Temp. rise in gas ΔT (°C)	Pressure drop, ΔP (N/m^2)
1	5.0	47.62	100.0	24.00	184.648
	7.5	71.44	98.0	26.00	229.977
	10.0	95.25	82.0	29.47	292.637
	12.5	119.07	80.0	30.33	339.299
	15.0	142.88	87.8	31.29	403.960
	17.5	166.69	86.0	33.24	459.954
	19.5	185.74	84.0	34.63	506.616
	25.0	238.13	75.0	35.11	629.270
	30.0	285.76	72.34	35.29	747.259
8	5.0	47.62	98.0	21.64	176.649
	7.5	71.44	96.0	23.9	221.978
	10.0	95.25	98.0	27.4	282.638
	12.5	119.07	94.0	29.0	337.966
	15.0	142.88	90.0	30.4	399.960
	17.5	166.69	89.6	30.0	467.287
	19.5	185.74	83.6	31.85	503.950
	25.0	238.13	69.4	34.01	647.935
	30.0	285.76	65.3	33.2	781.255

Table E.4 Experimental data for Set II, for T_{Gin} =400 ± 1°C

N	F_t S.T.P (L/min)	Re (entry conditions)	Conversion X (%)	Temp. rise in gas ΔT (°C)	Pressure drop, ΔP (N/m^2)
1	5.0	37.36			
	7.5	56.04	98.0	20.0	277.306
	10.0	74.73	95.9	24.44	369.296
	12.5	93.41	85.42	25.89	461.955
	15.0	112.09	89.6	27.16	535.946
	17.5	130.77	92.0	29.57	611.939
	19.5	145.72	95.0	30.22	679.932
	25.0	186.82	89.0	33.0	864.580
	30.0	224.18	83.3	35.09	1019.898
8	5.0	37.36	100.0		
	7.5	56.04	100.0	17.47	261.974
	10.0	74.73	98.0	20.88	344.632
	12.5	93.41	96.0	23.18	432.090
	15.0	112.09	98.0	24.83	519.281
	17.5	130.77	95.6	25.7	612.605
	19.5	145.72	91.8	27.75	673.933
	25.0	186.82	91.84	31.41	880.579
	30.0	224.18	89.6	33.74	1080.559

Table E.5 Experimental data set II, for N=1, for T_{Gin} =371 ± 1°C

L_T (cm)	F_t S.T.P (L/min)	Re (entry conditions)	Conversion X (%)	Temp. rise in gas ΔT (°C)	Pressure drop, ΔP (N/m^2)
1.0	2.5		100.00	31.00	57.980
	5.0	38.89	90.74	30.05	70.650
	7.5	58.34	85.00	29.40	76.650
	10.0	77.79	77.89	26.00	101.318
	12.5	97.23	67.64	23.47	118.649
	15.0	116.68	61.00	23.40	137.981
	17.5	136.13	54.08	21.10	164.645
	20.0	155.57	52.10	18.37	184.640
	25.0	194.47	48.95	17.60	220.640
	30.0	233.36	42.71	16.30	287.966
	35.0	272.25	38.30	14.30	349.293
	40.0	311.15	35.87	13.11	411.954
0.1	5.0	38.89	36.00	9.31	—
	7.5	58.34	29.00	9.20	—
	10.0	77.79	20.00	7.50	—
	15.0	116.68	15.00	5.94	—
	17.5	136.13	14.00	5.20	—
	19.5	151.69	12.00	6.60	—
	25.0	194.47	9.60	6.21	—
	30.0	233.36	8.40	3.75	—
	35.0	272.25	8.17	3.30	—
	40.0	311.15	6.73	3.58	—
	23.0	178.91	10.4	6.42	—
	28.0	217.81	8.4	5.87	—

APPENDIX F

Table F.1 Empty tube reactor data for varying inlet temperature

T_{Gin} (°C)	F_t S.T.P (L/min)	Re (entry conditions)	Conversion X (%)	Temp. rise in gas ΔT (°C)	Pressure drop, ΔP (N/m^2)
250.0	1.5	84.76	90.5	6.7	1.333
	3.0	169.56	74.1	3.99	1.333
	5.0	282.6	63.89	1.09	1.333
	7.5	423.8	57.69	1.14	2.660
	10.0	564.9	53.85	0.76	3.400
	12.5	706.4	47.05	0.59	4.655
	15.0	847.6	52.0	0.87	5.720
	17.5	988.8	53.0	1.20	6.890
	20.0	1130.0	52.0	1.45	8.530
371.0	1.5	84.76	92.7	4.22	1.333
	2.5	141.3	82.1	3.40	1.333
	5.0	282.6	67.9	2.33	1.333
	7.5	423.8	60.4	1.05	3.399
	10.0	564.9	56.7	0.75	5.333
	12.5	706.4	54.8	0.98	6.666
	15.0	847.6	52.94	1.15	7.999
	17.5	988.8	53.10	1.70	9.999
	20.0	1130.0	52.1	2.60	13.332
400.0	1.5	84.76	94.2	4.10	1.333
	2.5	141.3	84.0	3.80	1.333
	5.0	282.6	68.0	2.54	1.985
	7.5	423.8	62.9	1.03	4.265
	10.0	564.9	58.0	0.65	5.566
	12.5	706.4	55.3	0.68	6.666
	15.0	847.6	54.1	0.75	8.436
	17.5	988.8	52.0	0.81	11.233
	20.0	1130.0	54.0	1.32	14.332

Table F.2 ATCR data with Sulzer Mixer inserts at T_{Gin}=371°C

N_E	F_t S.T.P (L/min)	Re (entry conditions)	Conversion X (%)	Temp. rise in gas ΔT (°C)	Pressure drop, ΔP (N/m^2)
1	1.5	84.76	98.21	12.70	1.333
	2.5	141.3	91.07	15.47	1.999
	5.0	282.6	77.8	10.78	4.666
	7.5	423.8	67.6	6.80	8.666
	10.0	564.9	62.5	8.72	9.999
	12.5	706.4	62.5	8.66	24.664
	15.0	847.6	51.0	8.55	33.996
	17.5	988.8	58.0	8.30	49.328
	20.0	1130.0	57.14	8.00	58.661
2	1.5	84.76	100.00	29.8	4.666
	2.5	141.3	94.54	31.20	5.999
	5.0	282.6	77.3	21.90	11.999
	7.5	423.8	67.9	10.20	22.664
	10.0	564.9	67.3	12.24	28.664
	12.5	706.4	59.6	19.67	46.753
	15.0	847.6	63.7	12.60	71.993
	17.5	988.8			
	20.0	1130.0	63.2	11.60	117.322
3	1.5	84.76	100.00		1.999
	2.5	141.3	92.3	17.37	3.999
	5.0	282.6	84.26	12.70	11.999
	7.5	423.8	76.0	10.30	27.331
	10.0	564.9	71.2	11.08	37.310
	12.5	706.4	68.63	11.20	59.994
	15.0	847.6	63.7	13.00	86.658
	17.5	988.8	62.0	15.40	117.322
	20.0	1130.0	59.2	12.97	147.319
5	1.5	84.76	100.0		6.266
	2.5	141.3	98.1	5.30	7.999
	5.0	282.6	90.74	6.22	23.331
	7.5	423.8	84.9	9.70	39.996
	10.0	564.9	78.8	11.07	53.328
	12.5	706.4	74.5	10.02	100.657
	15.0	847.6	68.00	14.40	137.320
	17.5	988.8	65.5	15.40	176.649
	20.0	1130.0	63.3	15.41	223.311
7	1.5	84.76	100.00	18.70	6.666
	2.5	141.3	99.5	23.20	11.999
	5.0	282.6	92.7	14.40	30.664
	7.5	423.8	86.8	11.42	54.661
	10.0	564.9	80.8	11.10	82.658
	12.5	706.4	77.9	11.30	121.321
	15.0	847.6	74.51	16.80	172.649
	17.5	988.8	71.00	17.25	227.977
	20.0	1130.0	68.5	17.50	287.971

Table F.3 ATCR data with Kenics mixer inserts at T_{Gin}=371°C

N_E	F_t S.T.P (L/min)	Re (entry conditions)	Conversion X (%)	Temp. rise in gas ΔT (°C)	Pressure drop, ΔP (N/m^2)
1	1.5	84.76	95.54	10.50	0.999
	2.5	141.3	89.00	20.20	0.667
	5.0	282.6	76.85	15.22	2.666
	7.5	423.8	66.7	6.30	5.333
	10.0	564.9	53.00	6.70	7.333
	12.5	706.4	50.00	5.86	12.665
	15.0	847.6	45.00	6.47	24.664
	17.5	988.8	43.00	8.10	29.997
	20.0	1130.0	42.00	7.20	35.996
3	1.5	84.76	100.00	8.30	3.333
	2.5	141.3	92.3	16.00	2.666
	5.0	282.6		17.00	9.332
	7.5	423.8	78.8		15.332
	10.0	564.9	69.5	9.90	25.997
	12.5	706.4			
	15.0	847.6	60.00	12.44	43.996
	17.5	988.8			
	20.0	1130.0	56.6	13.60	75.326
7	1.5	84.76	100.00	17.09	
	2.5	141.3	98.15	23.00	
	5.0	282.6	92.5	16.30	10.666
	7.5	423.8	84.91	10.30	29.997
	10.0	564.9	79.00	11.00	43.329
	12.5	706.4	75.00	11.10	77.992
	15.0	847.6	72.5	14.35	108.656
	17.5	988.8			
	20.0	1130.0	68.00	14.08	181.982

Table F.4 ATCR data with Star and Orifice mixer inserts at T_{Gin}=371°C

N_E	F_t S.T.P (L/min)	Re (entry conditions)	Conversion X (%)	Temp. rise in gas ΔT (°C)	Pressure drop, ΔP (N/m^2)
1	1.5	84.76			5.2
	2.5	141.3	88.8	21.75	12.5
	5.0	282.6	74.0	15.60	15.66
	7.5	423.8	62.0	11.20	24.00
	10.0	564.9	47.5	8.11	39.00
	12.5	706.4	49.0	8.44	66.8
	15.0	847.6	50.0	7.99	117.5
	17.5	988.8	55.1	7.50	
	20.0	1130.0	50.0	7.24	185.8
6	1.5	84.76	100.00	18.05	22.8
	2.5	141.3	98.00	22.95	35.3
	5.0	282.6	92.00	16.11	45.9
	7.5	423.8	83.00	10.71	74.5
	10.0	564.9	78.20	10.95	200.3
	12.5	706.4	73.00	11.00	260.76
	15.0	847.6	72.00	14.10	470.6
	17.5	988.8	69.00	14.30	
	20.0	1130.0	66.00	15.40	763.8

Table F.5 ATCR with Star element, N_E=1

N_E	F_t S.T.P (L/min)	Re (entry conditions)	Conversion X (%)	Temp. rise in gas ΔT (°C)	Pressure drop, ΔP (N/m^2)
1	1.5	84.76			
	2.5	141.3	88.4	22.00	0.650
	5.0	282.6	72.00	12.00	5.323
	7.5	423.8	58.3	5.89	11.322
	10.0	564.9	46.2	7.90	17.322
	12.5	706.4	45.2	8.35	39.319
	15.0	847.6	47.1	8.24	61.984
	17.5	988.8	49.00	8.23	88.648
	20.0	1130.0	47.00	8.19	113.312

APPENDIX G

Mass balance on CO in the gas phase

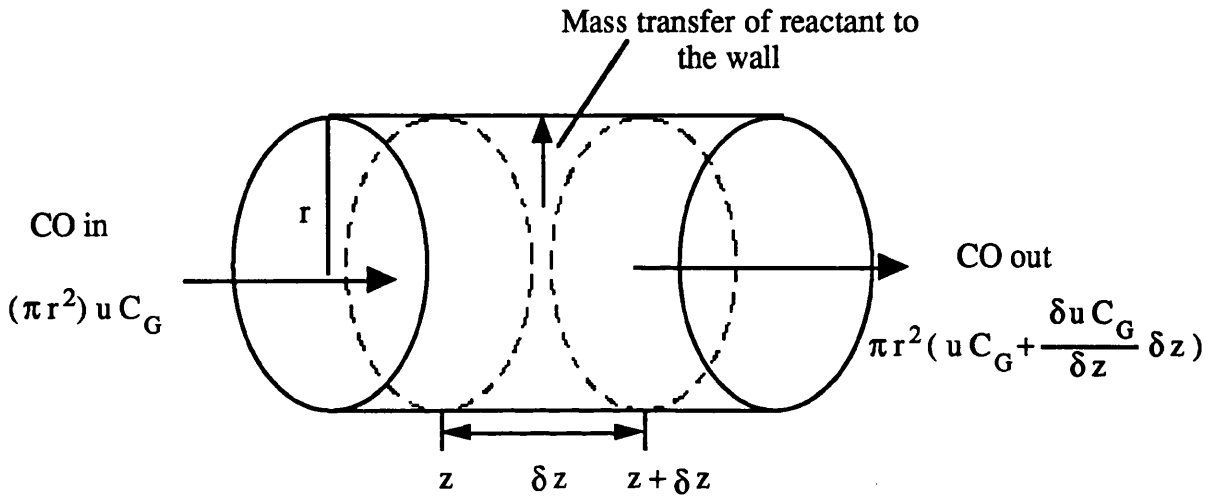

Reactant in = Reactant out + Reactant lost to heterogeneous reaction at the wall

$$(\pi r^2)\, u\, C_G = \pi r^2 (u C_G + \frac{\delta u C_G}{\delta z} \delta z) + 2\pi r \delta z\, k_m (C_G - C_S)$$

$$\pi r^2 \frac{\delta (u C_G)}{\delta z} + 2\pi r \delta z\, k_m (C_G - C_S) = 0$$

In the limit as $\delta z \rightarrow 0$

$$\pi r^2 \frac{d (u C_G)}{dz} = - 2\pi r\, k_m (C_G - C_S)$$

For constant u

$$\boxed{- u \frac{dC_G}{dz} = S\, k_m (C_G - C_S)}$$

Mass balance of CO on the solid phase

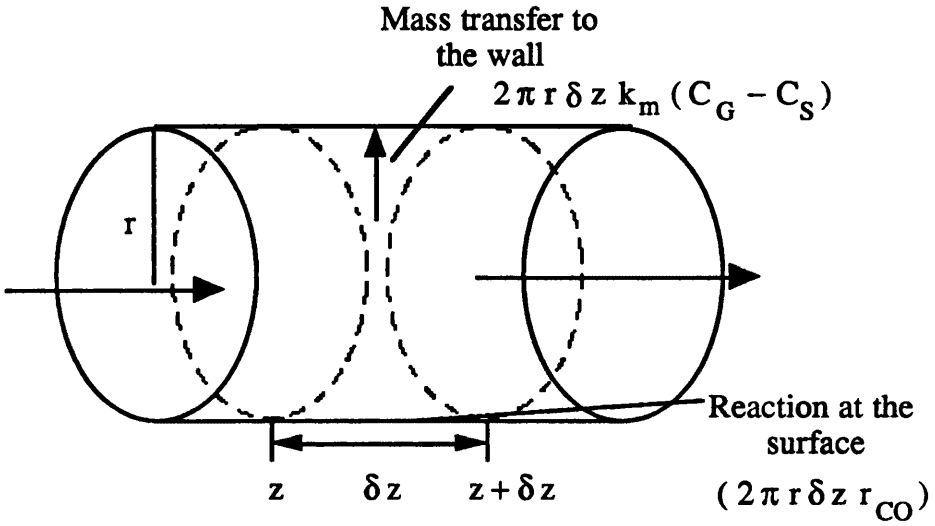

Mass transfer of CO to the surface = Reaction of CO at the surface

$$2\pi r \delta z k_m (C_G - C_S) = (2\pi r \delta z r_{CO})$$

$$\boxed{k_m (C_G - C_S) = r_{CO}}$$

Energy balance on the gas phase

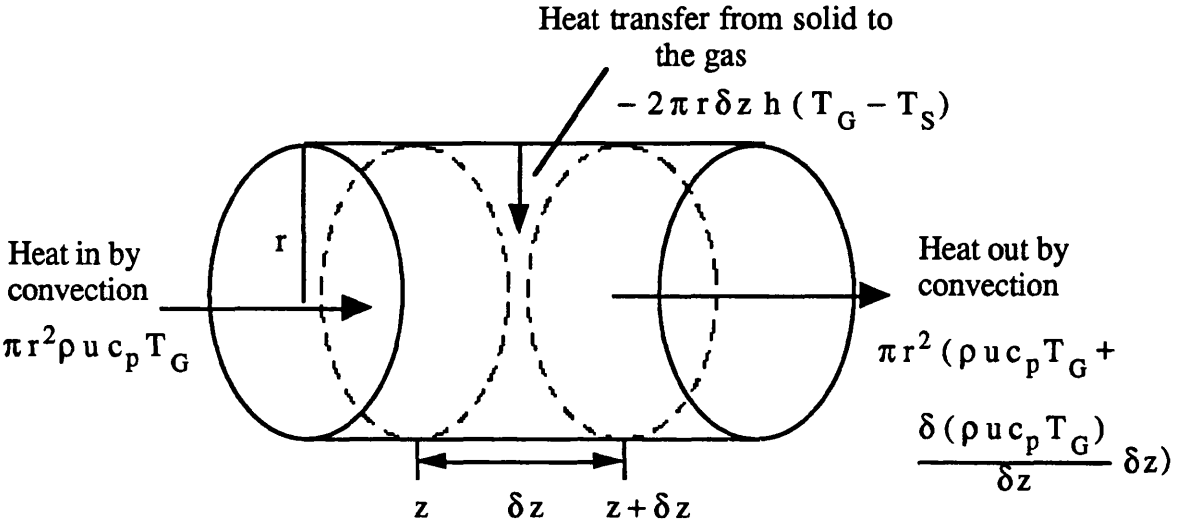

Heat in = Heat out + Heat transferred from heterogeneous reaction at the wall to the gas phase

$$\pi r^2 \rho u c_p T_G = \pi r^2 (\rho u c_p T_G + \frac{\delta(\rho u c_p T_G)}{\delta z}\delta z) - 2\pi r\delta z\, h\,(T_G - T_S)$$

If u= constant, c_p= constant and in the limit as $\delta z \rightarrow 0$

$$\boxed{\rho u c_p \frac{dT_G}{dz} = -h S (T_G - T_S)}$$

Energy balance on the solid phase

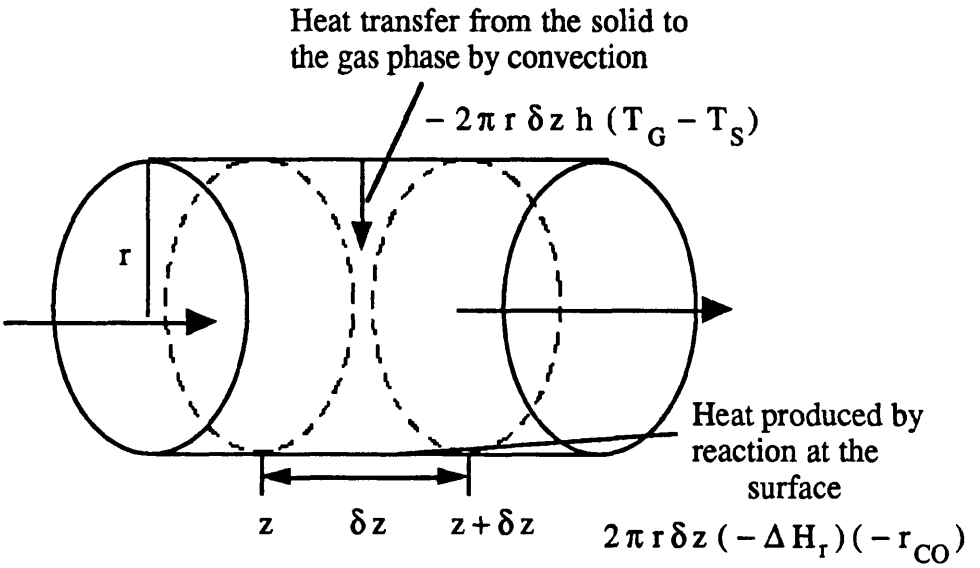

Heat produced by reaction of CO at the surface = Heat transfered to the gas phase

$$2\pi r\,\delta z\,(-\Delta H_r)(-r_{CO}) = -2\pi r\,\delta z\,h\,(T_G - T_S)$$

In the limit as $\delta z \rightarrow 0$

$$\boxed{(\Delta H_r)\,(r_{CO}) = -\,h\,(T_G - T_S)}$$

Computer Flowchart